RAI Responses 33-41

RESPONSE TO RAI COMMENT 33
ROADMAP TO REFERENCES

REFERENCED DOCUMENT	*EXCERPT LOCATION	REMARK
Cook et al. 2002		General reference, Executive Summary enclosed following response.
Cook et al. 2005 Table A-4	Excerpt enclosed following response.	
Malek et al. 1985 Pages 13 and 20	Excerpt enclosed following response.	
Saltstone PA 1992 Table 3.3-1	Excerpt enclosed following response.	
Saltstone Addendum 1998 Table 3	Excerpt enclosed following response.	
Yu et al. 1993	Excerpt enclosed following response.	Summary of Permeability to Liquid Test Results Table.

*Excerpt Locations:

1. Excerpt included in response: The excerpt is included within the text of the response or is appended to the response.
2. Excerpt enclosed following response: The excerpt is enclosed on a separate sheet or sheets following the response.
3. Representative excerpt(s) enclosed following response: Representative excerpts from a document that is wholly or largely applicable are enclosed following the response.
4. Other

WSRC-TR-2002-00456
Revision 0

KEY WORDS:
Vault
LLW Disposal
Disposal Authorization Statement

SPECIAL ANALYSIS:

REEVALUATION OF THE INADVERTENT INTRUDER, GROUNDWATER, AIR, and RADON ANALYSES FOR THE SALTSTONE DISPOSAL FACILITY

Authors

James R. Cook
Westinghouse Savannah River Company

David C. Kocher
SENES Oak Ridge, Inc.

Laura McDowell-Boyer
Alara Environmental Analysis, Inc.

Elmer L. Wilhite
Westinghouse Savannah River Company

October 23, 2002

Westinghouse Savannah River Company
Savannah River Site
Aiken, SC 29808

Prepared for the U.S. Department of Energy
under Contract No. DE-AC09-96SR18500

1. EXECUTIVE SUMMARY

This Special Analysis updates the inadvertent intruder analysis conducted in 1992 in support of the SDF RPA, extends the groundwater analysis to consider additional radionuclides, and provides an assessment of the air and radon emanation pathways. The results of the RPA were originally published in the WSRC report (WSRC-RP-92-1360) entitled *Radiological Performance Assessment for the Z-Area Saltstone Disposal Facility* (MMES et al., 1992). The present reevaluation considers new requirements and guidance of the USDOE Order 435.1 (USDOE, 1999), expands the list of radionuclides considered, incorporates an increase in design thickness of the roof on a disposal vault, and produces results in terms of interim limits on radionuclide-specific concentration and inventory rather than dose resulting from a projected inventory. The limits derived herein will be updated when the Saltstone PA is revised (currently planned for fiscal years 2003/2004).

The SDF is located within a 650,000 m^2 area of SRS designated as Z Area. The SDF together with the SPF are part of an integrated waste treatment and disposal system at the SRS. Saltstone is a solid waste form that is the product of chemical reactions between a salt solution and a blend of cementitious materials (slag, flyash, and cement). Based on the present projected site layout of the SDF, up to 730-million L (192 million gal) of wastewater can be treated for subsequent disposal as saltstone. The SPF and SDF are regulated by the State of South Carolina, USDOE Orders, and other Federal regulations that are applicable to disposal of solid waste.

As part of the RPA process, USDOE Order 435.1 requires an assessment of the dose to a potential member of the general public to limit doses from all pathways to no more than 25 mrem in a year and, from the air pathway alone, to no more than 10 mrem in a year. The Order also requires an assessment of radon release to ensure that the radon flux does not exceed 20 $pCi/m^2/s$. Additionally, for purposes of establishing limits on concentrations of radionuclides for disposal, the Order requires that an assessment be made of impacts to hypothetical persons assumed to inadvertently intrude into the low-level waste disposal facility and an assessment of the impacts to water resources. For the intruder analysis, the pertinent performance measure specifies that dose to such hypothetical individuals may not exceed 100 mrem EDE per year for chronic exposure, and may not exceed 500 (EDE) mrem from a single event. To meet the assessment requirement addressing impact on water resources in the Order, SRS uses the Safe Drinking Water Act Maximum Contaminant Levels (USEPA, 2000) as the pertinent performance measure.

To limit the number of radionuclides for which analyses are needed, the half-lives of radionuclides and physical processes by which low-level waste destined for the SDF is generated were considered. Such considerations led to selection of 75 radionuclides for analysis. Potentially significant contributions by radioactive decay products of these 75 radionuclides were also assessed.

Two time frames for the analyses are considered in this Special Analysis. The USDOE Order 435.1 specifies a time frame of 1,000 years after facility closure for establishing limits on allowable disposals. Here, both the 1,000-y time frame and a longer time frame of 10,000

years after facility closure are also considered, to be consistent with both the USDOE Order and the Disposal Authorization Statement (DAS) for SRS (Fiori and Frei, 1999).

In the intruder analysis, the only credible scenario within 10,000 years is the resident scenario, based on the current design of the SDF. The 0.4 m of grout directly above the saltstone, 0.1-m concrete roof over the vaults, and 1 m of grout on top of the roof combine to provide at least 0.5-m of shielding up to 10,000 years, assuring that excavation into the waste during this time period is not a credible occurrence (Fig. 1-1). The resident scenario is evaluated at 100, 1,000, and 10,000 years after disposal. In the resident scenario, the intruder is assumed to excavate no more than 3 meters in building a home. Evaluation of the scenario at 100 years, when the engineered barriers (i.e., the grout above the saltstone, the vault roof, and the grout above the roof) are assumed to be intact, resulting in the intruder's home being constructed on top of the uppermost layer of grout, is used to determine limits on allowable disposals of shorter-lived photon-emitting radionuclides in the waste. Evaluation of the resident scenario at 1,000 and 10,000 years, when the engineered barriers are assumed to have failed (i.e., have lost their physical integrity) and are no longer a deterrent to intrusion, resulting in a lesser thickness of shielding above the waste, is used to determine limits on allowable disposals of longer-lived photon-emitting radionuclides. The thickness of uncontaminated material above the waste is the same at these two later times because the upper 0.9 m of the closure has eroded (Fig. 1-1) and the depth of the intruder's excavation is limited to 3 m. The resident scenario at 1,000 years may be important for radionuclides having longer-lived photon-emitting decay products. The resident scenario at 10,000 years is important only when a longer-lived radionuclide has long-lived photon-emitting decay products whose activities increase with time beyond 1,000 years.

For the groundwater, air, and radon emanation pathways, results from the previous SDF PA and applicable portions of the E-Area LLWF PA were used to derive limits on allowable disposals based on analyses for time frames of 1,000 years and 10,000 years after facility closure. For the groundwater pathway, it was necessary to extend the previous analysis in the SDF PA to radionuclides not previously considered, using the PATHRAE code.

The results of this Special Analysis indicate that, for the 10,000-year time frame, 41 radionuclides, of the 75 selected, require limits on disposal. Of the 41 radionuclides for which disposal limits were derived, 34 are limited by the intruder analysis, four by the groundwater pathway analysis, two by the air pathway analysis, and one by the radon emanation analysis. The radionuclide disposal limits were compared with the currently estimated radionuclide concentrations in low curie salt. The greatest fraction of a limit is 0.038 for ^{126}Sn and the total sum-of-fractions of all the limits is 0.084. This provides assurance that low curie salt can be disposed in the saltstone disposal facility without exceeding any of the USDOE performance objectives.

For the 1,000-year time frame, 37 of the 75 radionuclides would require disposal limits. Of these, 35 would be limited by the intruder analysis, none by the groundwater analysis, two by the air pathway analysis, and none by the radon emanation analysis. The greatest fraction of a limit would remain 0.038 for ^{126}Sn and the total sum-of-fractions would decrease to 0.048.

The 10,000-year time frame limits should be used to develop WAC for the SDF.

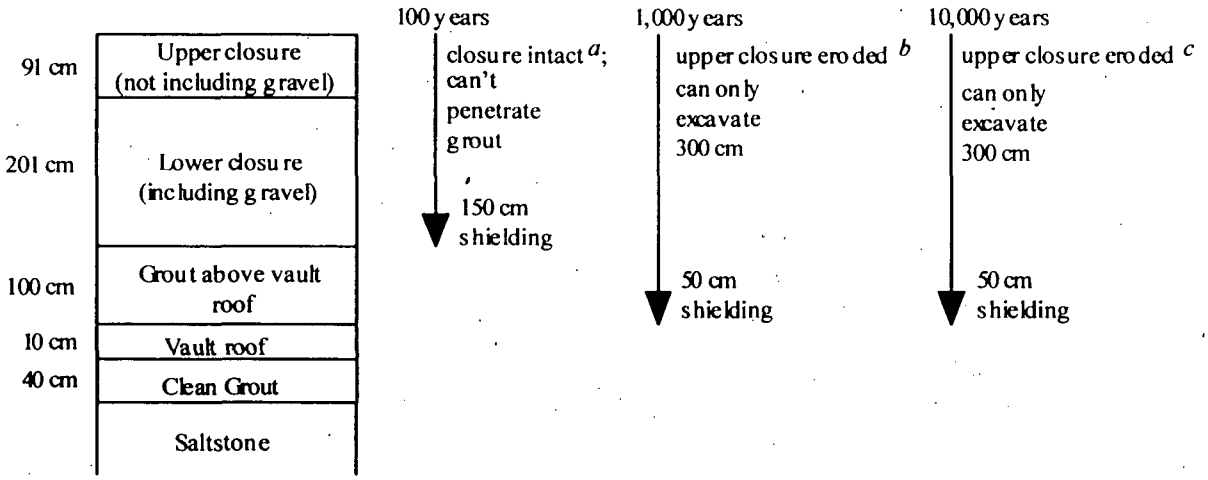

[a] At 100 years after closure, there has been no erosion and the grout and vault roof have not deteriorated so that they effectively prevent excavation. Therefore, the intruder constructs his residence atop the grout above the vault roof, resulting in a total of 150 cm of shielding between the residence and the saltstone.

[b] At 1,000 years after closure, erosion has removed the upper 91 cm of the closure. However, the gravel, which is the uppermost portion of the lower closure, prevents further erosion. The grout and vault roof have deteriorated to soil equivalent material so that they no longer can prevent excavation. Since the intruder's excavation is limited to 300 cm, the residence is constructed on top of the vault roof, resulting in a total of 50 cm of shielding between the residence and the saltstone.

[c] At 10,000 years after closure, erosion has not penetrated further than at 1,000 years (i.e., 91 cm), because of the gravel layer. Since the intruder's excavation is limited to 300 cm, the residence is constructed on top of the vault roof, resulting in a total of 50 cm of shielding between the residence and the saltstone.

Fig. 1-1. Resident Scenario Conceptual Model

APPROVED for Release for
Unlimited (Release to Public)
6/6/2005

WSRC-TR-2005-00074
Revision 0

KEY WORDS: Performance Assessment
Low-level Radioactive Waste Disposal

SPECIAL ANALYSIS: REVISION OF SALTSTONE VAULT 4 DISPOSAL LIMITS (U)

PREPARED BY:
James R. Cook
Elmer L. Wilhite
Robert A. Hiergesell
Gregory P. Flach

MAY 26, 2005

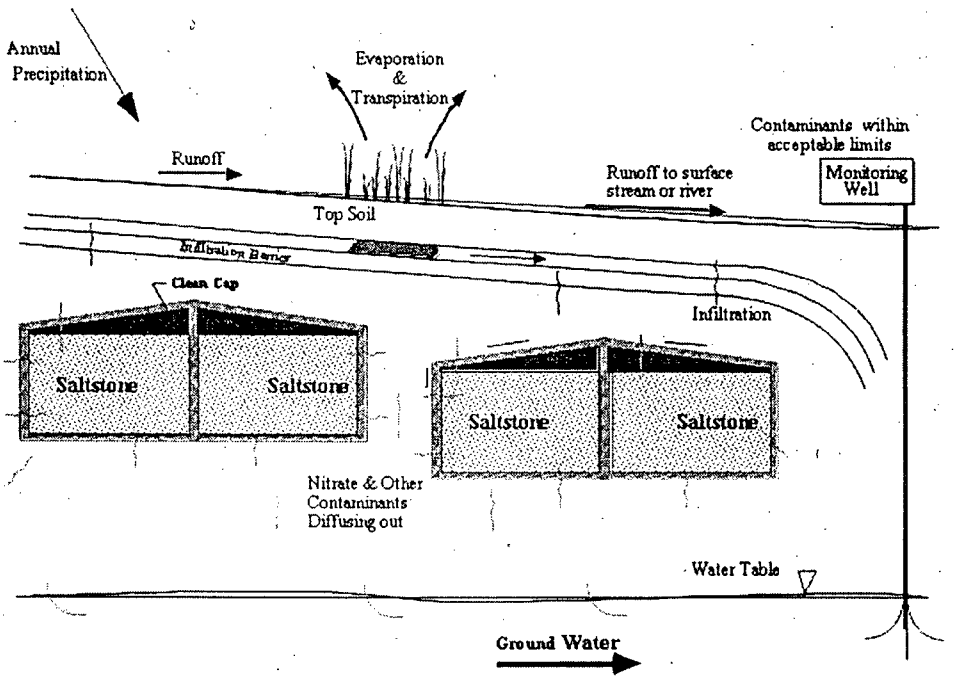

Westinghouse Savannah River Company
Savannah River Site
Aiken, SC 29808

Prepared for the U.S. Department of Energy Under Contract Number DE-AC09-96SR18500

SRNL
SAVANNAH RIVER NATIONAL LABORATORY

A.2.2 Time of Compliance and Simulation Time Intervals

The DOE time of compliance is 1,000 years (Wilhite 2003). However, the total time used for groundwater modeling is extended to 10,000 years to assess the impact of a longer period of compliance. The eight time intervals (Phifer 2004) used for groundwater modeling are shown in Table A-3.

Table A-3. Simulation Time Intervals

INTERVAL	TIME (YEARS)		
TI01	0	to	100
TI02	100	to	300
TI03	300	to	550
TI04	550	to	1,000
TI05	1,000	to	1,800
TI06	1,800	to	3,400
TI07	3,400	to	5,600
TI08	5,600	to	10,000

A.2.3 Flow Modeling

A.2.3.1 Flow Properties

The fundamental concept of the SDF (wasteform and facility features) is controlled contaminant release. Due to the low hydraulic conductivity and low molecular diffusion in cementitious materials, contaminant leaching from the SDF is very slow. This makes transformation into Saltstone an effective method for liquid waste disposal. Among all the factors affecting the SDF performance, the most important factor is hydraulic conductivity. The saturated hydraulic conductivities of the engineered porous media (Saltstone, concrete and gravel drain layers) were measured by Core Lab as described in 1993 (Yu 1993). These intact values are used for the first 100 years of simulation under the column heading TI01 in Table A-4.

Table A-4. Saturated Hydraulic Conductivities (cm/sec)

	TI01	TI02	TI03	TI04	TI05	TI06	TI07	TI08
			Horizontal conductivity:					
Nati/Back	1.00E-04	1.00E-04	1.00E-04	1.00E-04	1.00E-04	1.00E-04	1.00E-04	1.00E-04
Drain Bot	1.00E-01	9.99E-02	9.97E-02	9.90E-02	9.71E-02	9.30E-02	8.63E-02	7.46E-02
Drain Ver	1.00E-01	1.00E-01	1.00E-01	1.00E-01	1.00E-01	1.00E-01	1.00E-01	1.00E-01
Drain Top	1.00E-01	9.99E-02	9.93E-02	9.75E-02	9.28E-02	8.25E-02	6.58E-02	3.66E-02
Concrete	1.00E-12	5.20E-12	1.29E-11	3.16E-11	7.64E-11	1.98E-10	4.19E-10	1.00E-09
Saltstone	1.00E-11	3.00E-11	5.50E-11	1.00E-10	1.80E-10	3.40E-10	5.60E-10	1.00E-09
			Vertical conductivity:					
Drain Bot	9.52E-02	6.45E-02	2.70E-02	8.94E-03	3.34E-03	1.41E-03	7.25E-04	3.93E-04
Drain Top	8.89E-02	4.21E-02	1.29E-02	3.78E-03	1.36E-03	5.69E-04	2.91E-04	1.57E-04

In this SA, it is assumed the hydraulic conductivities of Saltstone and concrete will increase as time proceeds. As a result, water percolation will gradually increase through the vault. It is also assumed that the conductivities of the top and bottom drains will decrease with time due to plugging in the lower part of these drains resulting in the engineered drains becoming less effective in shedding perched water above the concrete roof. It is assumed that the effective

DP-MS-85-9

SLAG CEMENT — LOW-LEVEL WASTE FORMS AT THE SAVANNAH RIVER PLANT

by

R. I. A. Malek, D. M. Roy, and M. W. Barnes

Materials Research Laboratory,
The Pennsylvania State University
University Park, PA 16802

and

C. A. Langton

E. I. du Pont de Nemours and Company
Savannah River Laboratory
Aiken, South Carolina 29808

A paper proposed for presentation at the
87th Annual American Ceramic Society Meeting
Cincinnati, OH
May 5-9, 1985

This paper was prepared in connection with work done under Contract No. DE-AC09-76SR00001 with the U.S. Department of Energy.

Table VIII. Summary of X-Ray Phase Identification - 84-45.

Phase	Age (Days) 7	28	56	90	180
unreacted cement	*	decrease with time ——————————>			
unreacted fly ash (quartz + mullite)	*	*	*	*	*
unreacted slag	*	*	*	*	*
lime	**	**	**	**	**
bonding compound	substituted C-S-H	*	*	*	*
$Al(NO_3)_2 \cdot 9H_2O$	large quantity	**	**	**	**
$Ca(NO_3)_2 \cdot 2H_2O$	**	**	*	increase ———>	
Others:					
C_3AH_6, C_3FH_6	**	**	*	*	*
$Na_2CO_3 \cdot 10H_2O$	*	*	*	*	*
$CaCO_3$	**	**	*	increase ———>	

*Identified. **Unidentified.

appreciable reaction of the fly ash spheres and buildup of CSH structure. Some reticular network C-S-H is still apparent at this age. Figure 7 is a micrograph of 84-40 cured for 180 days. Again the overall integrity of the structure is evident. A plerosphere (spheres within fly ash spheres) appears very well reacted externally and bound into the surrounding matrix.

84-41. Figure 8 illustrates the morphology of 84-41 at 7 days. Micrograph 8(a) is a secondary electron image whereas 8(b) is a back-scattered image, which gives better contrast. These images show an area where an agglomerate has occurred (on the right hand side of the micrograph). Figure 8(c,d) are elemental maps for Ca and Si, respectively. It is evident from this series of micrographs that the agglomerated parts are cement (high Ca, low Si). Figures 8(e,f) are successively higher magnifications to the cement

side (right side) of micrographs (a,b). It shows precipitated crystals embedded in the hydrated matrix. EDXA of selected parts of that micrograph are shown. Curve a is for some area outside the crystalline part. It shows the C–S–H structure besides the precipitation of some other salts including Al and Na. Curve b is for a crystalline part. It shows the lime including C–S–H and sulphur-containing compounds. Such agglomerations can lead to a very low early strength (since early strength should be totally dependent on the cement portion) and a very slow strength development. Figure 9 is a series of micrographs at variable magnifications to 84–41 at 90 days. The poor integrity and high porosity of the structure is evident from micrographs 9(a,b). Micrograph 9(c) shows some characteristic features of the dissolution of low-calcium fly ash. Figure 9(c) shows a dissolved glassy surface with residual Fe oxide (magnetite or hematite) (low solubility) remaining attached to the surface of the ash sphere. Figure 10 is a series of micrographs at successively increasing magnifications of 84–41 cured for 180 days. Poor integrity and high porosity despite more gel formation are the common features.

84–45. Figure 11 shows low and high magnifications (backscatter images) of 84–45 cured for 7 days. Integrity and low porosity are apparent with some cenosphere peaks attached to the matrix. Figure 12 gives micrographs of a 28-day-old sample. Features similar to those in Fig. 11 (7 days) are evident. A glassy irregular slag fragmentation seen (left center, b). Figure 13 represents a 56-day-old sample, showing a dense structure. Some of the same common features as in Figs. 11 and 12 are evident, together with the inside of a (hemi-) sphere which remained attached to the matrix after sawing the sample. This indicates a good bond strength between fly ashes and matrix. Analysis of this hemisphere is shown in the EDXA result represented in Fig. 14. Figures 15 and 16 represent backscattered electron images for the mix 84–45 at 90 and 180 days, respectively. The same features of that mix at previous ages are evident; namely, integrity and low porosity. The latter indicates the very high degree of integrity obtained with this composition at 180 days.

4) Contaminant Release Rates

A modified Paige leach test (2) was used in evaluating formulations 84–40, 84–41, and 84–45. The leachant used was a natural spring water

4/10/98

WSRC-RP-92-1360

APPROVED for Release for
Unlimited (Release to Public)
6/23/2005

RADIOLOGICAL PERFORMANCE ASSESSMENT FOR THE Z-AREA SALTSTONE DISPOSAL FACILITY (U)

JRC 2/4/93

Prepared for the
WESTINGHOUSE SAVANNAH RIVER COMPANY
Aiken, South Carolina

by

MARTIN MARIETTA ENERGY SYSTEMS, INC.
EG&G IDAHO, INC.
WESTINGHOUSE HANFORD COMPANY
WESTINGHOUSE SAVANNAH RIVER COMPANY

December 18, 1992

Rev. 0

Table 3.3-1 Summary of hydraulic properties assumed in the near-field model

Material	K_s (cm s^{-1})	Effective porosity, θ_s	Residual moisture content, θ_r	α $(cm^{-1})^a$	n^a
Backfill	1.0×10^{-5}	0.44	na[b]	na[b]	na[b]
Clay	7.6×10^{-9}	0.39	0.115	8.2×10^{-4}	1.33
Gravel	0.5	0.38	0.010	8.2×10^{-2}	3.70
Concrete	1.0×10^{-10}	0.08	0.064	7.5×10^{-7}	1.57
Saltstone	1.0×10^{-11}	0.46	0.368	7.4×10^{-6}	4.41

[a] Fitting parameter for van Genuchten and Mualem expressions for moisture characteristic curves.

[b] A Stone's correlation curve was used to describe the moisture characteristic curve for the backfill.

[c] Saltstone, concrete, gravel, and backfill properties not required for fractured saltstone case.

ADDENDUM TO THE RADIOLOGICAL PERFORMANCE ASSESSMENT FOR THE Z-AREA SALTSTONE DISPOSAL FACILITY AT THE SAVANNAH RIVER SITE

Additional Information Supplied to the
DOE Performance Assessment Peer Review Panel and
DOE Headquarters in Support of Review, 1993-1997

Prepared by

WESTINGHOUSE SAVANNAH RIVER COMPANY
Aiken, South Carolina

April 1998

R.O

WSRC-RP-98-00156 pg. 81

Table 3. Sensitivity analysis results for degraded material properties of unfractured saltstone and concrete.

	Peak Groundwater Concentration							
	Z-Area RPA Intact[a]		Z-Area RPA Fracture[b]		Run 1[c]		Run 2[d]	
	pCi/L	Time (yr)	pCi/L	Time (yr)	pCi/L	Time (yr)	pCi/L	Time (yr)
^{79}Se	1.2×10^{-2}	2.1×10^{5}	4.4	1.5×10^{4}	2.0×10^{1}	8.0×10^{4}	2.1×10^{1}	8.0×10^{4}
^{99}Tc	6.7×10^{-7}	1.6×10^{6}	1.1×10^{1}	2.4×10^{3}	1.1×10^{2}	2.8×10^{5}	1.1×10^{2}	2.8×10^{5}
^{126}Sn	4.0×10^{-11}	9.2×10^{5}	2.2×10^{-3}	2.2×10^{5}	9.1×10^{-2}	3.0×10^{5}	9.1×10^{-2}	3.0×10^{5}
^{129}I	7.2×10^{-3}	$>2.5\times10^{6}$	7.5×10^{-2}	3.2×10^{3}	1.6×10^{-2}	2.8×10^{5}	1.6×10^{-2}	2.8×10^{5}

[a] Intact saltstone and concrete; $K_{sat} = 10^{-11}$ cm/s for saltstone and 10^{-10} cm/s for concrete; $D_{eff} = 5\times10^{-9}$ cm^2/s. See RPA, p. 4-8.

[b] Fractured saltstone and concrete; $K_{sat} = 10^{-11}$ cm/s for saltstone and 10^{-10} cm/s for concrete; $D_{eff} = 5\times10^{-9}$ cm^2/s. See RPA, p. 4-9.

[c] $K_{sat} = 10^{-8}$ cm/s for saltstone and 10^{-8} cm/s for concrete; $D_{eff} = 5\times10^{-9}$ cm^2/s.

[d] $K_{sat} = 10^{-8}$ cm/s for saltstone and 10^{-8} cm/s for concrete; $D_{eff} = 10^{-7}$ cm^2/s.

WESTINGHOUSE SAVANNAH RIVER COMPANY
SAVANNAH RIVER TECHNOLOGY CENTER

Keywords: Hydraulic Property
Mechanical Property
Performance Assessment

WSRC-RP-93-894

DATE: JUNE 30, 1993

TO: R. H. HSU, 773-43A
R. S. AYLWARD, 992-4W

FROM: A. D. YU, 773-43A
C. A. LANGTON, 773-43A
M. G. SERRATO, 992-4W

PHYSICAL PROPERTIES MEASUREMENT PROGRAM (U)

SUMMARY

This report summarizes the work performed by Core Laboratories (Carrollton, Texas) under subcontract No. AA46362N for the measurement of hydraulic and mechanical properties of the materials used for Environmental Restoration and Waste Management facilities at the Savannah River Site (SRS). The scope of the work includes the measurement of porosity, permeability to water (saturated hydraulic conductivity), capillary pressure, relative permeability, and mechanical properties of ten field samples. The samples are top soil, gravel, Dixie clay, Grace clay, sand, Burma Road backfill, Turner Road backfill, concrete for E-Area vault, concrete for Saltstone vault, and Saltstone. The Core Lab final report detailing sample preparation, test procedures, results, and QA is attached.

An analysis of the Core Lab results was made by WSRC personnel. The water-air two-phase flow properties (capillary pressure and relative permeability) are curve-fitted to analytical expressions. The calculated versus experimental characteristic curves and the parameters used for the curve fitting and are also included. The analytical expressions are used for groundwater modeling.

File: DRES-92119

SUMMARY OF PERMEABILITY TO LIQUID TEST RESULTS

Westinghouse Savannah River Company

Sample I.D.	Cumulative Test Time, days	Length, cm	Area, cm^2	Viscosity, cp	Delta Pressure, psi	Incremental Flow Rate, cc/sec	Permeability to Liquid, millidarcies	Hydraulic Conductivity, cm/sec (Q/A)	Porosity, percent
Turner Road Backfill - 1	36.8	7.59	11.76	0.988	50.0	1.6e-03	3.1e-01	3.0e-07	45.5
Turner Road Backfill - 2*	35.8	7.59	11.76	0.988	50.0	2.6e-03	4.8e-01	4.7e-07	42.7
Concrete from Saltstone Vault-1B	24.0	6.24	11.05	2.39	50.0	5.3e-07	2.1e-04	1.1e-10	17.4
Concrete from Saltstone Vault-5B	37.7	5.77	11.13	0.988	50.0	1.6e-05	2.4e-03	2.3e-09	18.9
Concrete from Saltst. Vault-7B*	38.0	5.05	11.10	0.988	50.0	9.9e-06	1.3e-03	1.3e-09	16.8
Concrete from E-Area Vault-2E	36.9	5.46	10.76	0.988	50.0	5.0e-09	7.4e-07	7.2e-13	18.1
Concrete from E-Area Vault-4E	37.5	5.35	10.68	0.988	50.0	8.3e-09	1.2e-06	1.2e-12	19.3
Concrete from E-Area Vault-7E*	37.5	4.44	10.72	0.988	50.0	1.0e-08	1.3e-06	1.2e-12	18.6
Saltstone - 1	16.0	4.29	11.07	2.39	50.0	2.4e-08	6.6e-06	3.4e-12	44.6
Saltstone - 3A	16.0	4.35	11.26	2.39	50.0	2.0e-08	5.4e-06	2.8e-12	41.6
Saltstone - 4*	12.0	4.74	11.30	2.39	50.0	1.3e-08	3.7e-06	1.9e-12	40.6

*Sample selected for Gas-Water Relative Permeability Tests

RESPONSE TO RAI COMMENT 34
ROADMAP TO REFERENCES

REFERENCED DOCUMENT	*EXCERPT LOCATION	REMARK
Core Laboratories Report attached to WSRC-RP-93-894	Values of water saturated hydraulic conductivity (from Project Summary) are included in response (Table 34-1).	Section 1, pages 1-6 enclosed following response.
Core Laboratories Report attached to WSRC-RP-93-894	Section 3 (Gas-Water, Water-Gas Relative Permeability). Results of tests included in response (Table 34-3).	
Core Laboratories Report attached to WSRC-RP-93-894	Data from pages 3-83, 3-93 and 3-103 are enclosed following response.	Table of data compiled from pages 3-83, 3-93, and 3-103 also enclosed following response
Domenico and Schwartz, 1990	Excerpt included in response (Table 34-2)	

*Excerpt Locations:

1. Excerpt included within response: The excerpt is included within the text of the response or is appended to the response.
2. Excerpt enclosed following response: The excerpt is enclosed on a separate sheet or sheets following the response.
3. Representative excerpt(s) enclosed following response: Representative excerpts from a document that is wholly or largely applicable are enclosed following the response.
4. Other

RESPONSE TO RAI COMMENT 34
ROADMAP TO REFERENCES

Compiled from three tables in Section 3 of Core Laboratories Report (contained in WSRC-RP-98-00156)

Sample	Time (min)	Cum. Vol. Injected (pore vols)	Cum. Vol. Injected (cc)	Inflow Rate (cc/min)
Saltstone #4	0.99	4.60E-05	1.00E-03	
	1.88	9.20E-05	2.00E-03	1.13E-03
	3.08	1.40E-04	3.05E-03	8.71E-04
	3.8	1.80E-04	3.92E-03	1.21E-03
	7.81	2.30E-04	5.01E-03	2.72E-04
	8.79	2.80E-04	6.10E-03	1.11E-03
	9.82	3.20E-04	6.97E-03	8.46E-04
	11.1	3.70E-04	8.06E-03	8.51E-04
	14.8	2.50E-02	5.45E-01	1.45E-01
	15.9	1.76E-01	3.83E+00	2.99E+00
	16.9	9.82E+01	2.14E+03	2.13E+03
	17	1.18E+02	2.57E+03	4.31E+03
	17.1	1.39E+02	3.03E+03	4.57E+03
	17.2	1.61E+02	3.51E+03	4.79E+03
	17.3	1.83E+02	3.99E+03	4.79E+03
Concrete (from Saltstone)	0.99	7.90E-02	7.44E-01	
	1.51	1.06E-01	9.99E-01	4.89E-01
	2.31	1.25E-01	1.18E+00	2.24E-01
	3.21	1.35E-01	1.27E+00	1.05E-01
	7.22	1.46E-01	1.38E+00	2.58E-02
	9.5	1.68E-01	1.58E+00	9.09E-02
	10.5	1.83E-01	1.72E+00	1.41E-01
	14.5	2.87E-01	2.70E+00	2.45E-01
	15.5	3.13E-01	2.95E+00	2.45E-01
	23.3	5.48E-01	5.16E+00	2.84E-01
	24.2	5.75E-01	5.42E+00	2.83E-01
	24.4	5.83E-01	5.49E+00	3.77E-01
Concrete (from E-Area)	1.13	5.60E-05	4.48E-04	
	2.08	1.10E-04	8.80E-04	4.55E-04
	2.8	1.70E-04	1.36E-03	6.67E-04
	6.81	2.20E-04	1.76E-03	9.98E-05
	8.11	2.80E-04	2.24E-03	3.69E-04
	9.09	3.40E-04	2.72E-03	4.90E-04
	11.1	3.90E-04	3.12E-03	1.99E-04
	14.1	4.50E-04	3.60E-03	1.60E-04
	15.1	5.10E-04	4.08E-03	4.80E-04
	15.8	5.60E-04	4.48E-03	5.71E-04
	22	6.20E-04	4.96E-03	7.74E-05
	37	6.70E-04	5.36E-03	2.67E-05

ADDENDUM TO THE RADIOLOGICAL PERFORMANCE ASSESSMENT FOR THE Z-AREA SALTSTONE DISPOSAL FACILITY AT THE SAVANNAH RIVER SITE

Additional Information Supplied to the
DOE Performance Assessment Peer Review Panel and
DOE Headquarters in Support of Review, 1993-1997

Prepared by

WESTINGHOUSE SAVANNAH RIVER COMPANY
Aiken, South Carolina

April 1998

Western Atlas International
A Litton/Dresser Company

CORE LABORATORIES

PHYSICAL PROPERTIES MEASUREMENT PROGRAM

COMPLETION OF ALL TASKS

SUBCONTRACT NO. AA46362-N

FINAL REPORT

Performed for:
WESTINGHOUSE SAVANNAH RIVER COMPANY
Savannah River Technology Center
Interim Waste Technology Section

March 31, 1993

Performed by:
Core Laboratories
Dallas Advanced Technology Center
Reservoir Flow Studies Laboratory
1875 Monetary Lane
Carrollton, Texas 75006

File: DRES-92119

PROJECT SUMMARY

Background

The testing program was designed to measure the fluid flow and mechanical properties of various materials utilized in the construction of waste containment vaults. All testing was performed at the minimum confining stress possible to model the field conditions. The ten supplied materials were as follows:

Unconsolidated Materials

- Top Soil
- Gravel
- Dixie Clay
- Grace Clay
- Sand
- Burma Road Backfill
- Turner Road Backfill

Consolidated Materials

- Concrete from the Saltstone Vault
- Concrete from the E-Area Vault
- Saltstone

The first seven materials, which are unconsolidated, were provided to Core Laboratories in labeled one gallon metal containers. The Concrete from the E-Area vault material was a 1ft x 1ft x 1ft block, the Concrete from the Saltstone Vault was supplied as a formed cylinder, and the Saltstone was contained in several one liter plastic jugs. Test samples of each material were prepared as described in the test protocols for each type of measurement.

Specific Permeability to Liquid and Effective Porosity

Specific permeability to liquid and effective porosity were determined for two samples of each unconsolidated material and three for each of the consolidated materials using the procedures described in Section 2. The tests were performed with no confining pressure to model the field conditions of the materials as closely as possible. The unconsolidated materials were tightly packed in stainless steel tubes with screens on each end. The consolidated materials were mounted in an epoxy coating. A test concrete sample, whose specific permeability to liquid had been previously determined at minimal confining stress in a coreholder, was mounted in epoxy and permeability remeasured, as a quality control check of the epoxy seal. The pre- and post-mounting permeability to liquid for this sample were equivalent, confirming the sealing of the epoxy to the sample.

Specific permeability to liquid and effective porosity test results are presented in summary form on Pages 1 and 2, and in detailed format in Section 2. The duplicate measurements were in excellent agreement for all materials. The calculated hydraulic conductivity was in the expected range for samples of this type.

Unsteady-State Gas-Water Water-Gas Relative Permeability

Unsteady-state tests were performed to determine the gas-water and water-gas relative permeability relationships on one sample of each material following the specific permeability to brine determinations using the procedures described in Section 3. The unsteady-state method was utilized due to the nature of the samples and the low permeability values of the consolidated samples.

The displacements were generally piston-like in both directions, resulting in end-point determinations only for the majority of the tests (gas-water curves were determined for only the Top Soil, Sand, Burma Road Backfill, and Turner Road Backfill samples). Gas-Water Water-Gas relative permeability test results are presented in summary form on Pages 3 and 4, and in graphical and tabular formats in Section 3. Where incremental two-phase data was not available, curves were extrapolated from the end-points.

The Top Soil, Gravel, and Sand samples demonstrated gas-water relative permeability characteristics typical of clean water-wet unconsolidated materials. The Dixie Clay, Grace Clay, Burma Road Backfill, and Turner Road Backfill samples showed evidence of drying during the gas injection, which apparently caused cracking or shrinkage of the clay materials in these samples. The effective permeabilities to gas at residual water saturation and to water at trapped gas saturation were higher for each of these five samples than the corresponding specific permeability to brine.

The Concrete samples demonstrated expected behavior, however, the throughputs on these samples were less than a pore volume due to their low permeability. The Saltstone sample exhibited an effective permeability to gas at residual water saturation 32400 times higher than the specific permeability to brine and an effective permeability to water at trapped gas saturation 157 times higher. These data can be explained by drying of the Saltstone during the gas injection, or the presence of a trapped gas saturation in the original preparation of the material. The observed increase in permeability is not due to bypassing around the epoxy seal as the absolute permeability measurements are low (effective permeability to gas at residual water saturation - 1.2e-01 md, effective permeability to water at trapped gas saturation - 5.8e-04 md).

Air-Brine Capillary Pressure

Air-brine drainage capillary pressure curves were determined on two samples of each of the unconsolidated materials using the procedures described in Section 4. The water saturation at a capillary pressure of 35 psi for the Top Soil, Sand and Gravel, ranged from 8.4 to 21.8 percent pore space. These values are in the expected range for samples of this type. The clay containing samples (Dixie Clay, Grace Clay, Burma Road Backfill, and Turner Road Backfill) ranged from 71.2 to 94.1 percent pore space water saturation at 35 psi capillary pressure.

Air-brine imbibition capillary pressure curves were determined on one sample of each of the consolidated materials using the procedures described in Section 4. The samples were first desaturated with air at 35 psi capillary pressure, then allowed to imbibe water at pressures up to 35 psi. These tests indicated that less than while ten percent pore space water will be removed by air at 35 psi capillary pressure, the displaced fluid will re-imbibe to resaturate the pore space.

The end-point saturations for all materials are in good agreement with those determined in the gas-water relative permeability tests. The duplicate measurements were in good agreement for all materials. Air-Brine Capillary Pressure test results are presented in summary form on Pages 5 and 6, and in graphical and tabular format in Section 4.

Acoustic Velocity

Dynamic Moduli and Poisson's Ratio were determined on two samples of each material by measuring acoustic velocity as outlined in Section 5. Gravel, Burma Road Backfill, and Turner Road Backfill were retested for quality control purposes. An Ottowa Sand sample was prepared and tested as a check plug in addition to the normal aluminum standard. These samples were tested at three overburden pressures in 500 psi increments beginning with 300 psi. Net stress was held constant by increasing the overburden and pore pressures on the samples at the same rate. Overburden pressure variation was used to determine if improper transducer seating was occurring at low pressures causing inaccurate travel times. A saltstone vault concrete sample (2-B), was also re-tested for confirmation of the data.

The data demonstrate that measured travel time increases gradually with increasing overburden pressure. The lack of erratic or excessive changes in travel times indicates that transducer seating at low pressures is effective. Retested backfill samples are in close agreement to the original data as is the saltstone vault concrete sample.

The gravel samples, however, show a significantly higher shear velocity over the original test data. In order to verify this finding, another set of gravel samples was prepared and tested with similar results. The original data files were reviewed in an attempt determine a reason for the variance. Original data acquisition work sheets indicate that first arrival times for the shear waves were very difficult to determine

which resulted in a reported shear velocity which was too low. The cause of this weak shear signal in the original test was probably due to loose screens on the samples. The original data has been revised for the final presentation.

Acoustic velocity test results are presented in summary form on Pages 7 and 8, and in graphical and tabular format in Section 5.

Pore Volume Compressibility

Pore Volume Compressibility was measured on two samples of each material using the procedures described in Section 6. The pore volume reduction at 200 psi applied stress for the unconsolidated materials ranged from 23.95 to 38.53 percent. The consolidated materials demonstrated much lower reductions in pore volume, ranging from 0.98 to 5.21 percent. These test results are as expected for these materials. The duplicate measurements were in good agreement for all samples. Pore Volume Compressibility test results are presented in summary form on Page 9, and in graphical and tabular format in Section 6.

Quality Control

All equipment was calibrated and standards evaluated as described in the individual test protocols. Copies of all records of pertinent information regarding the performance of each type of test are included at the end of each Section. The main tool for assessing the quality of the data set was duplicate measurements. In all cases, the duplicate measurements were in good agreement. In general, the data was within the expected ranges for the types of materials tested.

File: DRES-92119

SUMMARY OF PERMEABILITY TO LIQUID TEST RESULTS

Westinghouse Savannah River Company

Sample I.D.	Cumulative Test Time, days	Length, cm	Area, cm^2	Viscosity, cp	Delta Pressure, psi	Incremental Flow Rate, cc/sec	Permeability to Liquid, millidarcies	Hydraulic Conductivity, cm/sec	Porosity, percent
Top Soil - 1	3.0	7.59	11.76	0.988	0.050	0.017	3120	3.06e-03	40.5
Top Soil - 2*	3.0	7.59	11.76	0.988	0.049	0.017	3190	3.13e-03	38.8
Gravel - 1	3.0	30.48	5.07	0.988	0.029	0.050	151000	1.48e-01	38.0
Gravel - 2*	3.0	30.48	5.07	0.988	0.027	0.050	162000	1.59e-01	38.6
Dixie Clay - 1	11.0	7.59	11.76	0.988	50.0	5.1e-05	9.5e-03	9.4e-09	54.1
Dixie Clay - 2*	11.0	7.59	11.76	0.988	50.0	3.9e-05	7.3e-03	7.1e-09	57.7
Grace Clay - 1	17.8	7.59	11.76	0.988	50.0	3.4e-05	6.4e-03	6.3e-09	54.8
Grace Clay - 2*	17.8	7.59	11.76	0.988	50.0	4.2e-05	7.9e-03	7.7e-09	57.6
Sand - 1	2.5	7.59	11.76	0.988	0.100	0.033	3120	3.06e-03	39.9
Sand - 2*	2.5	7.59	11.76	0.988	0.055	0.017	2840	2.79e-03	34.8
Burma Road Backfill - 1	36.8	7.59	11.76	0.988	50.0	2.1e-03	4.0e-01	3.9e-07	47.5
Burma Road Backfill - 2*	35.8	7.59	11.76	0.988	50.0	4.3e-03	8.1e-01	8.0e-07	51.6

*Sample selected for Gas-Water Relative Permeability Tests

File: DRES-92119

SUMMARY OF PERMEABILITY TO LIQUID TEST RESULTS

Westinghouse Savannah River Company

Sample I.D.	Cumulative Test Time, days	Length, cm	Area, cm^2	Viscosity, cp	Delta Pressure, psi	Incremental Flow Rate, cc/sec	Permeability to Liquid, millidarcies	Hydraulic Conductivity, cm/sec	Porosity, percent
Turner Road Backfill - 1	36.8	7.59	11.76	0.988	50.0	1.6e-03	3.1e-01	3.0e-07	45.5
Turner Road Backfill - 2*	35.8	7.59	11.76	0.988	50.0	2.6e-03	4.8e-01	4.7e-07	42.7
Concrete from Saltstone Vault-1B	24.0	6.24	11.05	2.39	50.0	5.3e-07	2.1e-04	1.1e-10	17.4
Concrete from Saltstone Vault-5B	37.7	5.77	11.13	0.988	50.0	1.6e-05	2.4e-03	2.3e-09	18.9
Concrete from Saltst. Vault-7B*	38.0	5.05	11.10	0.988	50.0	9.9e-06	1.3e-03	1.3e-09	16.8
Concrete from E-Area Vault-2E	36.9	5.46	10.76	0.988	50.0	5.0e-09	7.4e-07	7.2e-13	18.1
Concrete from E-Area Vault-4E	37.5	5.35	10.68	0.988	50.0	8.3e-09	1.2e-06	1.2e-12	19.3
Concrete from E-Area Vault-7E*	37.5	4.44	10.72	0.988	50.0	1.0e-08	1.3e-06	1.2e-12	18.6
Saltstone - 1	16.0	4.29	11.07	2.39	50.0	2.4e-08	6.6e-06	3.4e-12	44.6
Saltstone - 3A	16.0	4.35	11.26	2.39	50.0	2.0e-08	5.4e-06	2.8e-12	41.6
Saltstone - 4*	12.0	4.74	11.30	2.39	50.0	1.3e-08	3.7e-06	1.9e-12	40.6

*Sample selected for Gas-Water Relative Permeability Tests

File: DRES-9211

SUMMARY OF GAS-WATER RELATIVE PERMEABILITY TEST RESULTS

Westinghouse Savannah River Company

Sample I.D.	Porosity, percent	Initial Conditions: Water Saturation, percent pore space	Initial Conditions: Specific Permeability to Water, millidarcies	Terminal Conditions: Water Saturation, percent pore space	Terminal Conditions: Effective Permeability to Fluid, millidarcies	Terminal Conditions: Relative Permeability to Fluid,+ millidarcies	Fluid Recovered: percent pore space	Fluid Recovered: percent flui in place
Turner Road	42.7	100.0	0.478	75.2	1.30	2.70*	24.8	24.8
Backfill 2		-	-	86.0	1.90	4.02**	10.8	43.6
Concrete from the	16.8	100.0	1.3e-03	85.4	7.9e-06	0.0061*	14.6	14.6
Saltstone Vault 7B		--	--	87.0	2.0e-04	0.154**	1.5	10.3
Concrete from the	18.6	100.0	1.3e-06	100.0	4.6e-08	0.035**	--	--
E-Area Valt 7E		--	--	98.7	5.4e-07	0.415**	1.3	--
Saltstone 4	40.6	100.0	3.7e-06	99.3	1.2e-01	32400*	0.7	0.7
		--	--	99.3	5.8e-04	157**	--	--

* to Gas .
** to Water
\+ Relative to the specific permeability to water

RESPONSE TO RAI COMMENT 34
ROADMAP TO REFERENCES

Compiled from three tables in Section 3 of Core Laboratories Report (contained in WSRC-RP-98-00156)

Sample	Time (min)	Cum. Vol. Injected (pore vols)	Cum. Vol. Injected (cc)	Inflow Rate (cc/min)
Saltstone #4	0.99	4.60E-05	1.00E-03	
	1.88	9.20E-05	2.00E-03	1.13E-03
	3.08	1.40E-04	3.05E-03	8.71E-04
	3.8	1.80E-04	3.92E-03	1.21E-03
	7.81	2.30E-04	5.01E-03	2.72E-04
	8.79	2.80E-04	6.10E-03	1.11E-03
	9.82	3.20E-04	6.97E-03	8.46E-04
	11.1	3.70E-04	8.06E-03	8.51E-04
	14.8	2.50E-02	5.45E-01	1.45E-01
	15.9	1.76E-01	3.83E+00	2.99E+00
	16.9	9.82E+01	2.14E+03	2.13E+03
	17	1.18E+02	2.57E+03	4.31E+03
	17.1	1.39E+02	3.03E+03	4.57E+03
	17.2	1.61E+02	3.51E+03	4.79E+03
	17.3	1.83E+02	3.99E+03	4.79E+03
Concrete (from Saltstone)	0.99	7.90E-02	7.44E-01	
	1.51	1.06E-01	9.99E-01	4.89E-01
	2.31	1.25E-01	1.18E+00	2.24E-01
	3.21	1.35E-01	1.27E+00	1.05E-01
	7.22	1.46E-01	1.38E+00	2.58E-02
	9.5	1.68E-01	1.58E+00	9.09E-02
	10.5	1.83E-01	1.72E+00	1.41E-01
	14.5	2.87E-01	2.70E+00	2.45E-01
	15.5	3.13E-01	2.95E+00	2.45E-01
	23.3	5.48E-01	5.16E+00	2.84E-01
	24.2	5.75E-01	5.42E+00	2.83E-01
	24.4	5.83E-01	5.49E+00	3.77E-01
Concrete (from E-Area)	1.13	5.60E-05	4.48E-04	
	2.08	1.10E-04	8.80E-04	4.55E-04
	2.8	1.70E-04	1.36E-03	6.67E-04
	6.81	2.20E-04	1.76E-03	9.98E-05
	8.11	2.80E-04	2.24E-03	3.69E-04
	9.09	3.40E-04	2.72E-03	4.90E-04
	11.1	3.90E-04	3.12E-03	1.99E-04
	14.1	4.50E-04	3.60E-03	1.60E-04
	15.1	5.10E-04	4.08E-03	4.80E-04
	15.8	5.60E-04	4.48E-03	5.71E-04
	22	6.20E-04	4.96E-03	7.74E-05
	37	6.70E-04	5.36E-03	2.67E-05

File: DRES-92119

GAS-WATER RELATIVE PERMEABILITY TEST RESULTS

Unsteady-State Method
Temperature: 72° F

Westinghouse Savannah River Company
Sample I.D.: Concrete Saltstone 7B
Porosity: 16.8 percent
Specific Permeability to Water: 1.3e-03 md

Length: 5.05 cm
Area: 11.10 cm2
Viscosity of Water: 0.988 cp
Viscosity of Gas: 0.018 cp
Differential Pressure GF: 50.0 psi
Differential Pressure WF: 50.0 psi

Cumulative Time, minutes	Cumulative Fluid Injected pore volumes	Cumulative Gas Produced, pore volumes	Effective Water Produced, pore volumes	Effective Permeability to Gas, millidarcies	Effective Permeability to Water, millidarcies
			Gas Displacing Water		
0.990	0.079	-	0.079	-	1.1e-03
1.51	0.106	-	0.106	-	7.5e-04
2.31	0.125	-	0.125	-	3.4e-04
3.21	0.135	-	0.135	-	1.7e-04
7.22	0.146	-	0.146	-	3.8e-05
9.50	0.168	0.022	0.146	2.5e-06	-
10.5	0.183	0.038	0.146	4.0e-06	-
14.5	0.287	0.141	0.146	6.8e-06	-
15.5	0.313	0.167	0.146	7.2e-06	-
23.3	0.548	0.402	0.146	7.9e-06	-
24.2	0.575	0.429	0.146	7.9e-06	-
24.4	0.583	0.437	0.146	7.9e-06	-
			Water Displacing Gas		
0.035	0.0016	0.0016	-	1.2e-05	-
1.05	0.008	0.0080	-	1.6e-06	-
1.99	0.011	0.011	-	8.9e-07	-
3.04	0.013	0.013	-	4.5e-07	-
4.03	0.014	0.014	-	2.8e-07	-
4.92	0.015	0.015	-	1.6e-07	-
6.05	0.015	0.015	-	2.5e-09	-
6.86	0.019	0.015	4.3e-03	-	7.5e-05
7.95	0.029	0.015	1.5e-02	-	1.4e-04
8.71	0.039	0.015	2.4e-02	-	1.8e-04
11.8	0.082	0.015	6.8e-02	-	2.0e-04
15.0	0.128	0.015	1.1e-01	-	2.0e-04
16.0	0.142	0.015	1.3e-01	-	2.0e-04

File: DRES-92119

GAS-WATER RELATIVE PERMEABILITY TEST RESULTS

Unsteady-State Method
Temperature: 72° F

Westinghouse Savannah River Company
Sample I.D.: Concrete E-Area 7E
Porosity: 18.6 percent
Specific Permeability to Water: 1.3e-06 md

Length: 4.44 cm
Area: 10.72 cm2
Viscosity of Water: 0.988 cp
Viscosity of Gas: 0.018 cp
Differential Pressure GF: 50.0 psi
Differential Pressure WF: 50.0 psi

Cumulative Time, minutes	Cumulative Fluid Injected pore volumes	Cumulative Gas Produced, pore volumes	Effective Water Produced, pore volumes	Effective Permeability to Gas, millidarcies	Effective Permeability to Water, millidarcies
			Gas Displacing Water		
1.13	5.6e-05	-	5.6e-05	-	6.2e-07
2.08	1.1e-04	-	1.1e-04	-	7.3e-07
2.80	1.7e-04	-	1.7e-04	-	9.7e-07
6.81	2.2e-04	-	2.2e-04	-	1.7e-07
8.11	2.8e-04	-	2.8e-04	-	5.4e-07
9.09	3.4e-04	-	3.4e-04	-	7.1e-07
11.1	3.9e-04	-	3.9e-04	-	3.4e-07
14.1	4.5e-04	-	4.5e-04	-	2.3e-07
15.1	5.1e-04	-	5.1e-04	-	7.3e-07
15.8	5.6e-04	-	5.6e-04	-	9.7e-07
22.0	6.2e-04	-	6.2e-04	-	1.1e-07
37.0	6.7e-04	-	6.7e-04	-	4.6e-08
			Water Displacing Gas		
0.347	1.1e-04	-	1.1e-04	-	4.0e-06
1.30	1.7e-04	-	1.7e-04	-	7.3e-07
4.02	2.2e-04	-	2.2e-04	-	2.6e-07
8.03	2.8e-04	-	2.8e-04	-	1.7e-07
9.33	3.4e-04	-	3.4e-04	-	5.4e-07
10.3	3.9e-04	-	3.9e-04	-	6.8e-07
11.3	4.5e-04	-	4.5e-04	-	7.3e-07
12.0	5.1e-04	-	5.1e-04	-	9.7e-07
13.0	5.6e-04	-	5.6e-04	-	6.9e-07
14.3	6.2e-04	-	6.2e-04	-	5.4e-07

File: DRES-92119

GAS-WATER RELATIVE PERMEABILITY TEST RESULTS

Unsteady-State Method
Temperature: 72° F

Westinghouse Savannah River Company		Length:	4.74 cm
Sample I.D.:	Saltstone 4	Area:	11.32 cm2
Porosity:	40.6 percent	Viscosity of Water:	2.39 cp
Specific Permeability to Water:	3.7e-06 md	Viscosity of Gas:	0.018 cp
		Differential Pressure GF:	51.7 psi
		Differential Pressure WF:	50.0 psi

Cumulative Time, minutes	Cumulative Fluid Injected pore volumes	Cumulative Gas Produced, pore volumes	Effective Water Produced, pore volumes	Effective Permeability to Gas, millidarcies	Effective Permeability to Water, millidarcies
		Gas Displacing Water			
0.990	4.6e-05	-	4.6e-05	-	3.3e-06
1.88	9.2e-05	-	9.2e-05	-	3.7e-06
3.08	1.4e-04	-	1.4e-04	-	2.8e-06
3.80	1.8e-04	-	1.8e-04	-	4.6e-06
7.81	2.3e-04	-	2.3e-04	-	8.2e-07
8.79	2.8e-04	-	2.8e-04	-	3.4e-06
9.82	3.2e-04	-	3.2e-04	-	3.2e-06
11.1	3.7e-04	-	3.7e-04	-	2.5e-06
14.8	2.5e-02	0.025	3.7e-04	3.7e-06	-
15.9	0.176	0.176	3.7e-04	7.9e-05	-
16.9	98.2	98.2	3.7e-04	5.3e-02	-
17.0	118	118	3.7e-04	1.1e-01	-
17.1	139	139	3.7e-04	1.2e-01	-
17.2	161	161	3.7e-04	1.2e-01	-
17.3	183	183	3.7e-04	1.2e-01	-
		Water Displacing Gas			
0.0	96	0.045	-		3.5e-02
0.240	0.084	-	0.084		2.0e-02
0.287	0.095	-	0.095		1.8e-02
1.08	0.131	-	0.131		3.3e-03
1.66	0.146	-	0.146		1.9e-03
3.30	0.159	-	0.159		6.3e-04
5.00	0.173	-	0.173		6.0e-04
7.21	0.192	-	0.192		6.2e-04
12.0	0.231	-	0.231		6.0e-04
13.3	0.241	-	0.241		5.9e-04
17.2	0.271	-	0.271		5.8e-04
19.1	0.286	-	0.286		5.8e-04
26.2	0.342	-	0.342		5.8e-04

→ 3-103

RESPONSE TO RAI COMMENT 35
ROADMAP TO REFERENCES

REFERENCED DOCUMENT	*EXCERPT LOCATION	REMARK
Cook et al. 2005	Excerpt enclosed following response.	Executive Summary attached.
Saltstone PA 1992	Excerpt enclosed following response	Section 5.3.

*Excerpt Locations:

1. Excerpt included in response: The excerpt is included within the text of the response or is appended to the response.
2. Excerpt enclosed following response: The excerpt is enclosed on a separate sheet or sheets following the response.
3. Representative excerpt(s) enclosed following response: Representative excerpts from a document that is wholly or largely applicable are enclosed following the response.
4. Other

WSRC-TR-2005-00074
Revision 0

KEY WORDS: **Performance Assessment**
Low-level Radioactive Waste Disposal

SPECIAL ANALYSIS: REVISION OF SALTSTONE VAULT 4 DISPOSAL LIMITS (U)

PREPARED BY:
James R. Cook
Elmer L. Wilhite
Robert A. Hiergesell
Gregory P. Flach

MAY 26, 2005

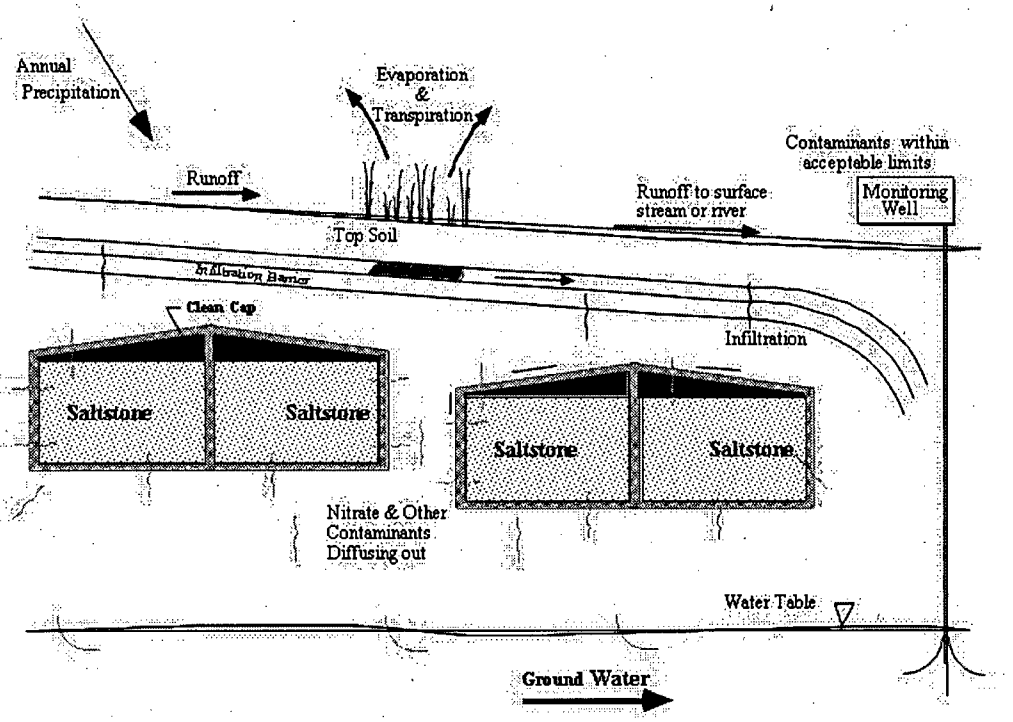

Westinghouse Savannah River Company
Savannah River Site
Aiken, SC 29808

Prepared for the U.S. Department of Energy Under Contract Number DE-AC09-96SR18500

SRNL
SAVANNAH RIVER NATIONAL LABORATORY

EXECUTIVE SUMMARY

New disposal limits have been computed for Vault 4 of the Saltstone Disposal Facility based on several revisions to the models in the existing Performance Assessment and the Special Analysis issued in 2002. The most important changes are the use of a more rigorous groundwater flow and transport model, and consideration of radon emanation. Other revisions include refinement of the aquifer mesh to more accurately model the footprint of the vault, a new plutonium chemistry model accounting for the different transport properties of oxidation states III/IV and V/VI, use of variable infiltration rates to simulate degradation of the closure system, explicit calculation of gaseous releases and consideration of the effects of settlement and seismic activity on the vault structure. The disposal limits have been compared with the projected total inventory expected to be disposed in Vault 4. The resulting sum-of-fractions of the 1000-year disposal limits is 0.2, which indicates that the performance objectives and requirements of DOE 435.1 will not be exceeded. This SA has not altered the conceptual model (i.e., migration of radionuclides from the Saltstone waste form and Vault 4 to the environment via the processes of diffusion and advection) of the Saltstone PA (MMES 1992) nor has it altered the conclusions of the PA (i.e., disposal of the proposed waste in the SDF will meet DOE performance measures). Thus a PA revision is not required and this SA serves to update the disposal limits for Vault 4. In addition, projected doses have been calculated for comparison with the performance objectives laid out in 10 CFR 61. These doses are 0.05 mrem/year to a member of the public and 21.5 mrem/year to an inadvertent intruder in the resident scenario over a 10,000-year time-frame, which demonstrates that the 10 CFR 61 performance objectives will not be exceeded. This SA supplements the Saltstone PA and supersedes the two previous SAs (Cook et al. 2002; Cook and Kaplan 2003).

4/10980

WSRC-RP-92-1360

RADIOLOGICAL PERFORMANCE ASSESSMENT FOR THE Z-AREA SALTSTONE DISPOSAL FACILITY (U)

JRC 2/4/93

Prepared for the
WESTINGHOUSE SAVANNAH RIVER COMPANY
Aiken, South Carolina

by

MARTIN MARIETTA ENERGY SYSTEMS, INC.
EG&G IDAHO, INC.
WESTINGHOUSE HANFORD COMPANY
WESTINGHOUSE SAVANNAH RIVER COMPANY

December 18, 1992

Rev. 0

A few recommendations pertinent to the closure concept are in order. Although degradation of the facility over time was addressed and the performance of a degraded facility was evaluated, degradation of the clay/gravel drain overlying the vaults was not considered. Because of the uncertainty associated with the functional life of this drain, it is preferable from the standpoint of providing reasonable assurance to not have to rely on its continued function as conceptualized. The primary function of this drain system is to reduce potential perching of water on the vaults, and perched water has the most impact analytically on the degraded vault/saltstone scenarios. Therefore, a program of research is recommended to investigate alternatives to this system that would serve a similar purpose. One alternative that has been identified is placing a permeable material on the top of and around the sides of the vaults, for the purpose of enhancing drainage of any perched water. Any changes must be fully investigated in terms of constructibility and possible adverse affects on performance.

Another consideration regarding the closure concept assumed for this RPA is the possibility that the concept may be overdesigned. The results of the RPA indicated that the presence or absence of the upper moisture barrier was not a significant factor in the analysis. This observation in part arises from the fact that the clay/gravel drain directly on top of the vaults was assumed to function indefinitely. There is preliminary evidence from model simulations that indicate normal infiltration into the facility does not necessarily significantly increase releases from the SDF. Furthermore, more dilution water in the near field can lower concentrations of contaminants in water reaching the aquifer beneath the site. Because the hydraulic conductivity of concrete and saltstone is the limiting factor on flow through the wasteform in the intact scenarios, the importance of reducing infiltration through the site is reduced.

One final observation regarding the possibility of overdesign of the SDF is that the waterproof polymer coating applied to the interior walls of the vaults may not be necessary. Credit was not taken for this design feature of the SDF because of the large uncertainty in the effectiveness and the lifetime of this material. However, the analytical results do not indicate a need for this coating since releases from the vaults are predicted to peak thousands of years in the future, even without considering any retardation of release by this coating. The waterproof polymer coating may be superfluous for this facility.

5.3 DATA AND RESEARCH NEEDS

A number of data and research needs have been identified in the course of performing the RPA for the SDF. These needs are directed at improving the confidence in the results of the RPA. Because the RPA is to be maintained through time, and thus is a living document, further iterations of the RPA process will benefit greatly if these needs are satisfied.

Research and testing to improve the quality of data in the area of hydraulic properties of slag saltstone are needed. The models used in this RPA to simulate releases of contaminants from saltstone are very sensitive to the value of the saturated hydraulic conductivity assumed, and there is a large amount of uncertainty associated with the value that was used. The addition of slag to saltstone resulted in reduced leaching of Tc-99 and chromium, leading to the hypothesis that hydraulic characteristics may be altered in addition to chemical characteristics. The saturated hydraulic conductivity of slag saltstone should be measured experimentally for use in modeling the release from the SDF.

Field measurement over time to determine the degree of saturation of slag saltstone in the field should also be done to further reduce uncertainties related to long-term acceptability of performance. The simulations performed in this RPA assumed that saltstone was near to saturation at steady state. However, if the degree of saturation of the monoliths after curing is even a few percent less than saturation, it may take a considerable amount of time to achieve near-saturation, thus, affecting the time-history profiles of releases. The release rate of saltstone constituents is very sensitive to the degree of saturation, because the unsaturated hydraulic conductivity is orders of magnitude less than the saturated conductivity, even for small reductions in saturation. A modeling investigation is also recommended to establish the sensitivity of model results to initial saturation assumed for saltstone. More sophisticated modeling techniques for the saltstone/concrete/soil system should also be investigated to provide additional insight into the long-term performance of the saltstone wasteform.

A further evaluation of the uncertainties in the degraded vaults scenario is indicated, based on the importance of this analysis to peak groundwater concentrations. Although multiple conservatisms are built into the analysis of this scenario in this RPA, a quantitative evaluation of the effects of these conservatisms is recommended for future iterations of the RPA.

With respect to estimates of dose to inadvertent intruders, confidence in the results would be increased if root uptake of Tc-99 were measure from mix of crushed saltstone and soil. The results of the agriculture scenario involving intrusion into saltstone are the highest values obtained in this RPA for inadvertent intruders, and the analysis supporting the results is quite sensitive to the plant-to-soil concentration ratio for Tc-99. Technetium-99 is believed to be less available from the saltstone-soil mix, but direct experimental evidence is lacking. Furthermore, the time history of root uptake should be measured for such a mix, to evaluate whether the Tc-99 becomes more or less available over time.

To evaluate the accuracy of the estimated inventory of nitrate and radionuclides in the SDF, multiple measurements of key radionuclides in different batches of LLW streams are recommended. The sensitivity of intruder dose estimates to the inventory of Sn-126 indicates the desirability of such measurements to confirm experimentally whether the estimated inventory is accurate, and the projected variability.

Finally, detailed engineering plans for closure of the SDF must be completed. These plans will establish the ability to construct the closure as presently conceived, and will also provide a basis for the cost of final closure. As noted in the previous section, the results of this RPA were inconclusive regarding the need for the upper moisture barrier, but suggested the possibility that this barrier may represent an overdesign of the facility. Further evaluation of the impact of closure design on the results should be undertaken.

RESPONSE TO RAI COMMENT 36
ROADMAP TO REFERENCES

REFERENCED DOCUMENT	*EXCERPT LOCATION	REMARK
Cook et al. 2005 (WSRC-TR-2005-00074)	Representative excerpt(s) enclosed following response	Section A.4 and Section 7.5.5

*Excerpt Locations:

1. Excerpt included within response: The excerpt is included within the text of the response or is appended to the response.
2. Excerpt enclosed following response: The excerpt is enclosed on a separate sheet or sheets following the response.
3. Representative excerpt(s) enclosed following response: Representative excerpts from a document that is wholly or largely applicable are enclosed following the response.
4. Other

7/14/2005

WSRC-TR-2005-00074
Revision 0

KEY WORDS: **Performance Assessment**
Low-level Radioactive Waste Disposal

SPECIAL ANALYSIS: REVISION OF SALTSTONE VAULT 4 DISPOSAL LIMITS (U)

PREPARED BY:
James R. Cook
Elmer L. Wilhite
Robert A. Hiergesell
Gregory P. Flach

MAY 26, 2005

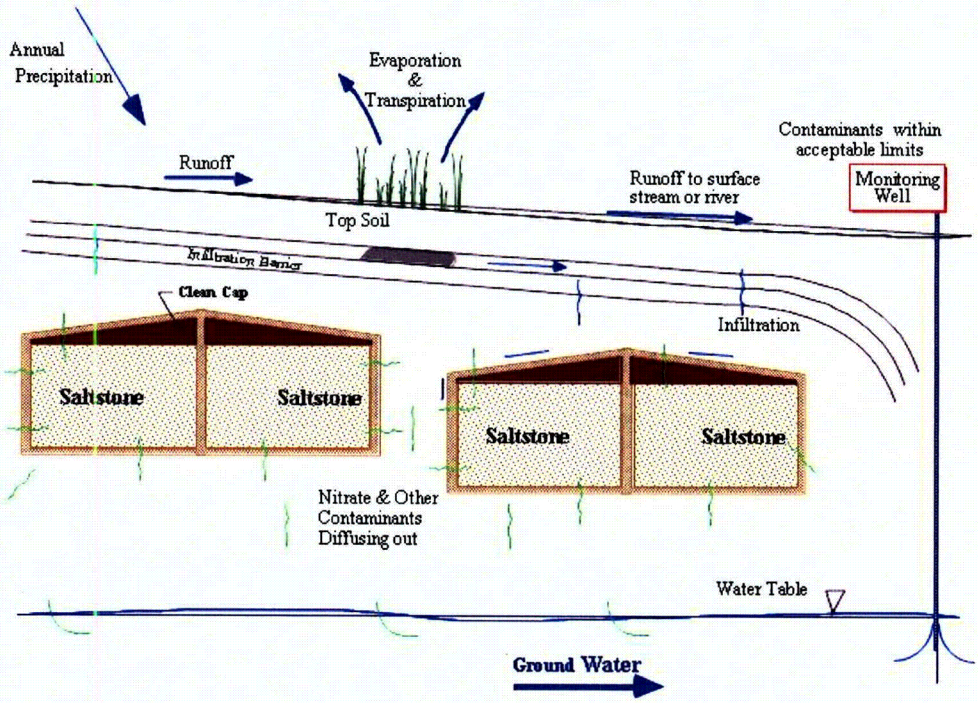

Westinghouse Savannah River Company
Savannah River Site
Aiken, SC 29808

Prepared for the U.S. Department of Energy Under
Contract Number DE-AC09-96SR18500

SRNL
SAVANNAH RIVER NATIONAL LABORATORY

7.5.5 Impact of Cover and Vault Degradation Beyond 10,000 Years

The fractional flux of I-129 at the water table at 10,000 years is 1.29E-07 mole/yr/mole and rising as shown in Table A-11 and Figure 7-16. To capture the peak of the flux transient, assuming hydrologic conditions at 10,000 years persist indefinitely, the simulation run time was extended to 70,000 years as shown in Figure 7-17 and discussed in Section 7.5.2. Additional simulations were performed considering continued degradation of the cover system, vault, and Saltstone contents beyond 10,000 years, with and without consideration of large-scale cracks in Saltstone due to differential settlement and earthquakes. Table 7-11 summarizes the assumed changes in hydraulic conductivities and infiltration between 10,000 and 100,000 years for these sensitivity runs.

From 10,000 to about 12,000 years, the gravel drainage layer overlying the vault roof is predicted to completely silt up with fines (Phifer 2004b), producing a significantly lower hydraulic conductivity. The lower hydraulic conductivity estimate is conservatively assumed to apply over the entire 10,000 to 25,000 year period in model simulations. Compared to the 5600 to 10,000 year period, the horizontal conductivity for this layer and time period abruptly decreases approximately 2.5 orders of magnitude, as indicated by Tables A-4 and 7-11. The change drastically reduces the ability of the layer to drain water off the top of the vault. Without macroscopic cracks in Saltstone, water ponds over the vault roof from 10,000 to 50,000 years in PORFLOW flow simulations. The increased hydraulic head gradient driving flow through Saltstone, coupled with moderately increased Saltstone and concrete conductivities compared to earlier times, produces a higher fractional flux shown in Figure 7-18 (No Crack curve) due to post-10,000 year degradation. Flux peaks occur shortly after 10,000 and 25,000 years in response to step changes in the modeled properties for Saltstone and concrete.

However, under ponded water or positive pressure conditions, large-scale cracks are expected to preferentially transmit water compared to the surrounding matrix, as discussed in section A-4. The additional effect of cracks on flow and water table flux was considered in a second sensitivity run. The physical cracks are predicted to occur at a 30 ft spacing within the plane of the 2D PORFLOW vadose zone model, which is a typical cross-section of the long axis of the vault. To approximately estimate the impact of transverse physical cracks, three longitudinal cracks at a nominal 30 ft spacing were placed in the half-width 2D model as surrogates (Figure 7-19), and assigned the properties of the vertical drain. Each crack was assigned to one column of grids with a width of 2 feet and given a porosity of 0.08 to represent the flow properties of a crack with a width of 2 inches. The presence of cracks in the model prevents water from ponding on the vault roof, but provides sudden pathways for water to infiltrate the core of the Saltstone waste. The resulting flux transient for I-129 is shown in Figure 7-18 (Crack curve). A very sharp peak in flux is observed immediately following 10,000 years, when the cracks suddenly become active in the simulations. The flux is diffusion-limited, and stabilizes to a much lower value after I-129 is leached from Saltstone near the crack faces. A second peak occurs at 25,000 years in response to increased Saltstone conductivity, similar to the no-crack sensitivity run. At 50,000 years, the conductivity of Saltstone is assumed to increase by 2 orders of magnitude, and the remaining inventory flushes from the vault by advection.

To a large extent, the abrupt changes in flux observed in the simulations including cracks are an artifact of simulating transport using a sequence of steady-state flow fields. In reality, the flow conditions would change gradually over time, and the flux transient would be much smoother than depicted in Figure 7-18. In particular, flux peaks are expected to be lower in peak magnitude, but broader in duration.

This study demonstrates the importance of the drainage layer at the top of the vault. The time over which the layer continues to function could be increased by making the layer thicker.

Table 7-11. Material Properties and Infiltration Beyond 10,000 Years.

Hydraulic Conductivity and Infiltration (cm/yr)	TI09 10,000 to 25,000 years	TI10 25,000 to 50,000 years	TI11 50,000 to 100,000 years
Horizontal conductivity			
Native and backfilled soil	3.15E+03	3.15E+03	3.15E+03
Drain, bottom	1.77E+06	3.15E+03	3.15E+03
Drain, vertical	3.15E+06	1.06E+06	1.81E+04
Drain, top	3.15E+03	3.15E+03	3.15E+03
Concrete	9.46E-02	3.15E-01	3.15E+01
Saltstone	9.46E-02	3.15E-01	3.15E+01
Vertical conductivity			
Drain, bottom	7.16E+03	3.15E+03	3.15E+03
Drain, top	3.15E+03	3.15E+03	3.15E+03
Infiltration	35.81	35.81	40.93

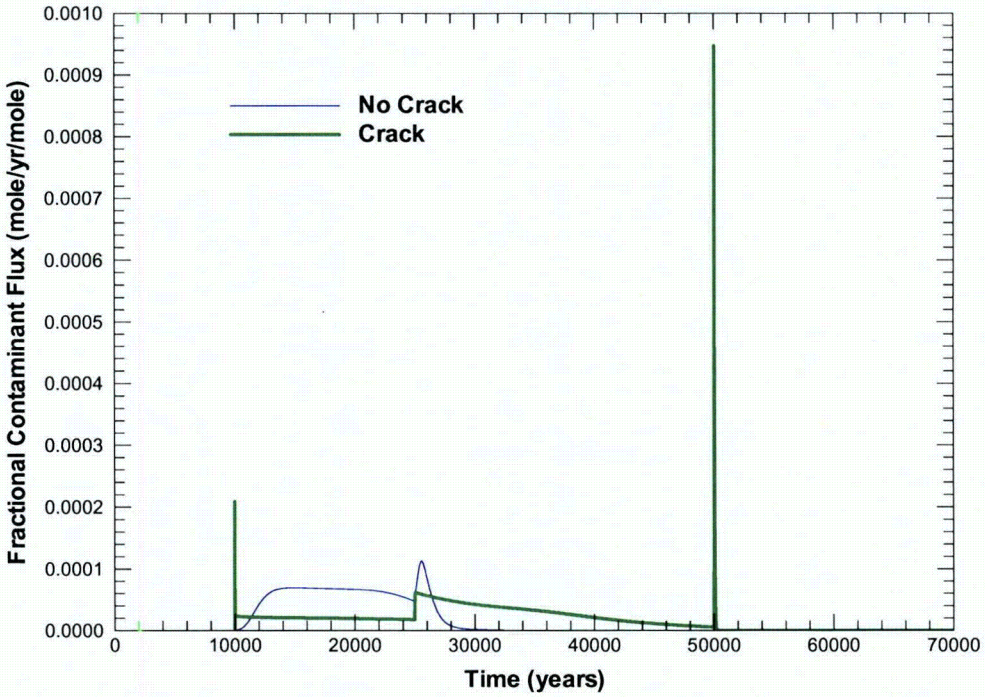

Figure 7-18. Instantaneous I-129 Fractional Contaminant Flux to the Water Table (10,000 to 70,000 yrs) Assuming Cover and Vault Degradation, With and Without Cracks.

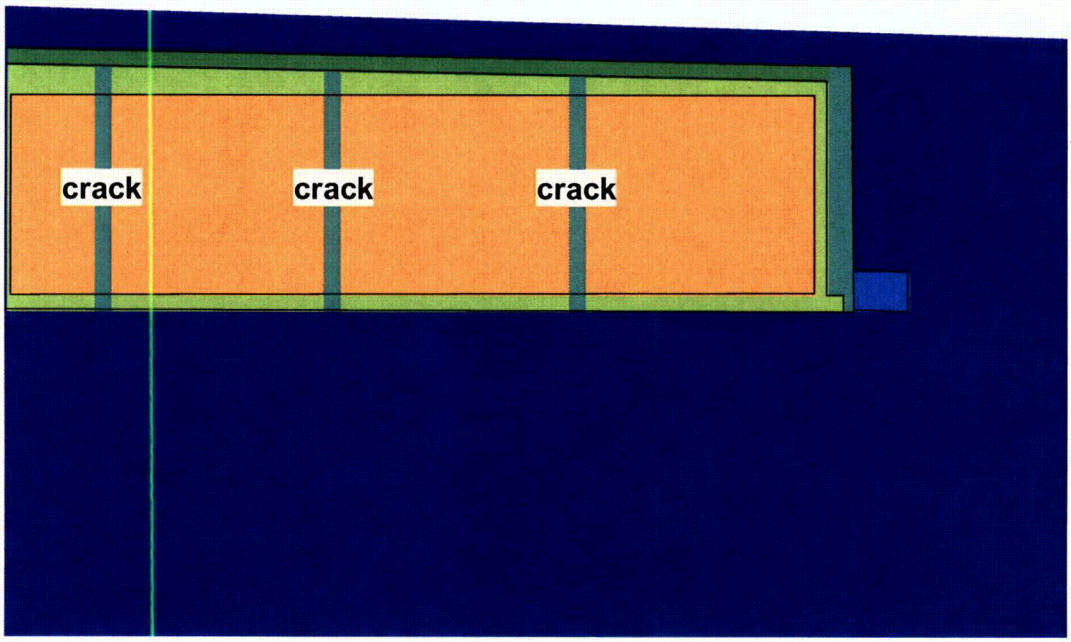

Figure 7-19. Surrogate Longitudinal Cracks in Two-Dimensional PORFLOW Model Representing Transverse Physical Cracks.

A.4 Impact of Macroscopic Cracks on Saltstone Vault 4 Performance

Vertical cracks or fractures spanning the entire Saltstone Vault 4 width and height are predicted to occur at 30 ft intervals, coinciding with construction joints, in response to static settlement and earthquakes. For the assumed properties of saltstone (10^{-11} cm/s conductivity), the literature indicates cracks can be neglected when the suction head exceeds approximately 200 cm in saltstone. Such conditions are predicted to occur during the 0-10,000 year period. This conclusion applies regardless of crack geometry, i.e., open at top, open at bottom, or through-crack.

A.4.1 Introduction

Peregoy (2003) analyzed the structural behavior of Saltstone Vault 4 in response to forecast static settlement and earthquakes. Approximately vertical cracks or fractures spanning the entire Vault 4 width and height were predicted to occur at 30 ft intervals, coinciding with construction joints. In the structural simulations, these macroscopic cracks were observed to open at either the top or bottom, while remaining in close contact at the opposite end of the fracture face, the latter forming a "hinge" of sorts. The cracks developed gradually over time (Peregoy 2003, Figure 9, Figure 10 and Table 2). Predicted mean crack sizes are summarized in Table A-20.

Table A-20. Summary of mean crack sizes at specific times.

Cracks open at bottom

Time (yr)	Crack width at open end (in)	Average width (in)
100	0.06	0.03
500	0.18	0.09
1000	0.30	0.15
2500	0.63	0.31
5000	1.15	0.58
10000	2.18	1.09

Cracks open at top

Time (yr)	Crack width at open end (in)	Average width (in)
100	0.01	0.004
500	0.03	0.015
1000	0.06	0.03
2500	0.16	0.08
5000	0.31	0.16
10000	0.62	0.31

Under a positive pressure condition, cracks or fractures in the saltstone monolith would be liquid-filled and form preferential pathways for infiltrating water compared to the surrounding low permeability matrix (10^{-11} cm/s). Under negative pressure or suction, the impact of cracks on saltstone performance is not immediately clear. The purpose of this Section is to assess the effect of macroscopic cracks on moisture movement through Saltstone Vault 4 under a range of hydraulic conditions and crack dimensions.

A.4.2 Flow Regimes

Water flow through a rough walled crack in a porous medium occurs in at least three distinct regimes:

1. Saturated flow, that is, liquid completely filling the aperture.
2. "Thick" film flow on each crack wall, where water is present as a film completely filling surface pits and grooves and the air-water interface is relatively flat.
3. "Thin" film flow, where water recedes into surface pits/grooves by capillary forces and adheres to flat surfaces by adsorption.

The saturated flow regime occurs at positive or very slightly negative pressures. The "thick" and "thin" film flow regimes occur at increasing negative pressures or suction in the surrounding porous medium. Each flow regime is analyzed separately below in the context of a uniform crack width.

An implicit assumption in these analyses is that the source of liquid to the crack is steady rather than episodic/transient, and that the resulting fracture flow is steady. Unsteady fracture flow has been observed at laboratory scale and inferred at field scale (Persoff and Pruess 1995; Su et al. 2001; Nativ et al. 1995; Fabryka-Martin et al. 1996; Pruess 1999). At laboratory scale, unsteady flow appears to be associated with relatively low suctions in a variable aperture setting. Under these conditions, water fills the smaller apertures while larger apertures are desaturated. At field scale (e.g. Yucca Mountain), unsteady flow has been inferred under high matrix suction. Temporal and spatial variations in infiltration and physical heterogeneity are thought to be factors leading to episodic flow.

The planned Saltstone closure cover system is expected to insulate cracks from episodic rainfall and lead to a relatively steady influx of water. Saltstone itself is expected to exhibit uniform properties in comparison with fractured geologic media. Cracks forming from differential settlement and seismic events are expected to be unsaturated. All of these conditions favor steady flow in Saltstone Vault 4.

A.4.3 Saturated Flow

The height of capillary liquid rise H between two parallel surfaces of aperture b is given by (e.g. Looney and Falta 2000)

$$H = \frac{2\sigma}{\rho g b} \tag{A-20}$$

where σ is surface tension, ρ is liquid density, and g is gravitational acceleration. In the context of a fracture subject to a given pressure P in the surrounding matrix, the aperture will be liquid filled under the condition

$$P > -\frac{2\sigma}{b} \tag{A-21}$$

where suction is indicated by a negative pressure value (e.g. Wang and Narasimhan 1985). The equivalent permeability of the fracture is

$$k = \frac{b^2}{12} \tag{A-22}$$

and the hydraulic conductivity is

$$K = \frac{\rho g k}{\eta} = \frac{\rho g b^2}{12\eta} \tag{A-23}$$

where η is liquid viscosity. Figure 1 shows hydraulic conductivity as a function of aperture for water at 20°C. Note that even narrow cracks have a high conductivity compared to cementitious materials.

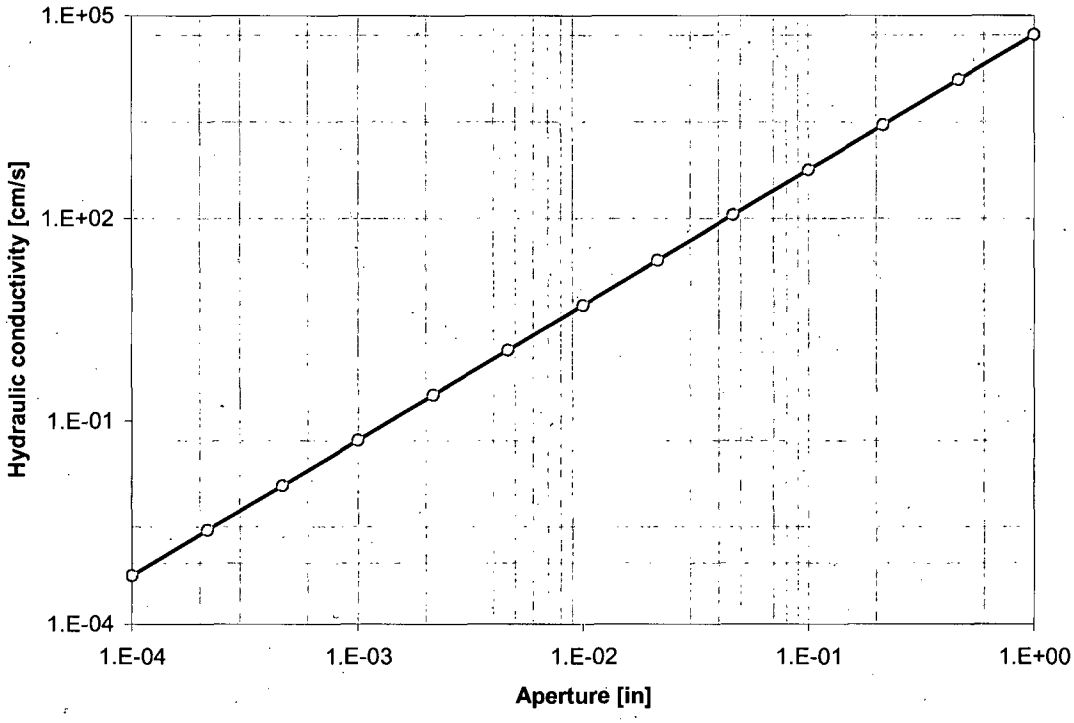

Figure A-77. Hydraulic conductivity of saturated cracks as a function of aperture.

A.4.4 Film Flow

When $P < -2\sigma/b$, liquid can no longer span an aperture and the crack will desaturate. For this condition, a rough fracture face can be conceptually simplified as a repeating series of vertical flat surfaces and V-shaped grooves to facilitate further analysis, following Or and Tuller (2000, Figure 1). At pressures slightly below $-2\sigma/b$, liquid will completely fill a groove and form a flat liquid-vapor interface. At a sufficiently low pressure, liquid will recede into the corner of the groove and be retained by capillary forces. Under this condition, the matric potential

$$\mu = \frac{P}{\rho} = gH \tag{A-24}$$

determines the radius of the liquid vapor interface in a groove (Or and Tuller 2000, Figure 2):

$$r(\mu) = -\frac{\sigma}{\rho\mu} \tag{A-25}$$

For a groove of depth L and angle γ, the maximum radius accommodated by the groove geometry is

$$r_c = \frac{L\tan(\gamma/2)}{\cos(\gamma/2)} \tag{A-26}$$

The critical pressure defining the transition between flat and curved interfaces is

$$P_c = -\frac{\sigma}{r_c} \tag{A-27}$$

and is the result of combining equations (A-24) through (A-26). Thus the three flow regimes identified earlier occur over the following pressure ranges for the assumed geometry of the fracture face:

1. Saturated flow: $P > -\frac{2\sigma}{b}$
2. "Thick" film flow: $-\frac{\sigma}{r_c} < P < -\frac{2\sigma}{b}$
3. "Thin" film flow: $P < -\frac{\sigma}{r_c}$

Liquid not being held by capillary suction will adhere to the remaining surfaces of the fracture face as a thin film. Considering only van der Waal forces, liquid adsorption on solid surfaces can be characterized by

$$h(\mu) = \left[\frac{A_{svl}}{6\pi\rho\mu}\right]^{1/3} \tag{A-28}$$

where h is film thickness and A_{svl} is a Hamaker constant.

Liquid held in groove corners by capillary suction and adhering as a thin film to remaining surfaces flows downward under the force of gravity. Or and Tuller (2000) present a detailed analysis of the liquid area and average velocity associated with corner and film flows, which is summarized in the Appendix. Figures A-78a and A-78b illustrate equivalent film thickness and average hydraulic conductivity for a representative "rough" fracture surface (Or and Tuller 2000, Figure 6a). The critical matric potential defining the transition between "thick" and "thin" film flow is μ_c = -0.22 J/kg or approximately 2 cm of suction head. A discontinuity in film thickness is observed in Figure 6a at this matric potential.

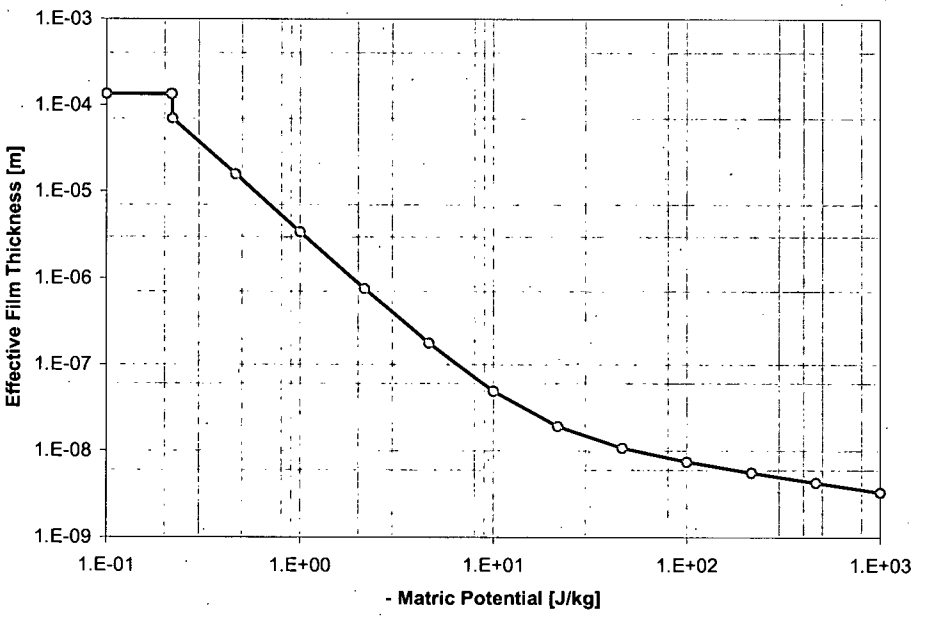

(a)

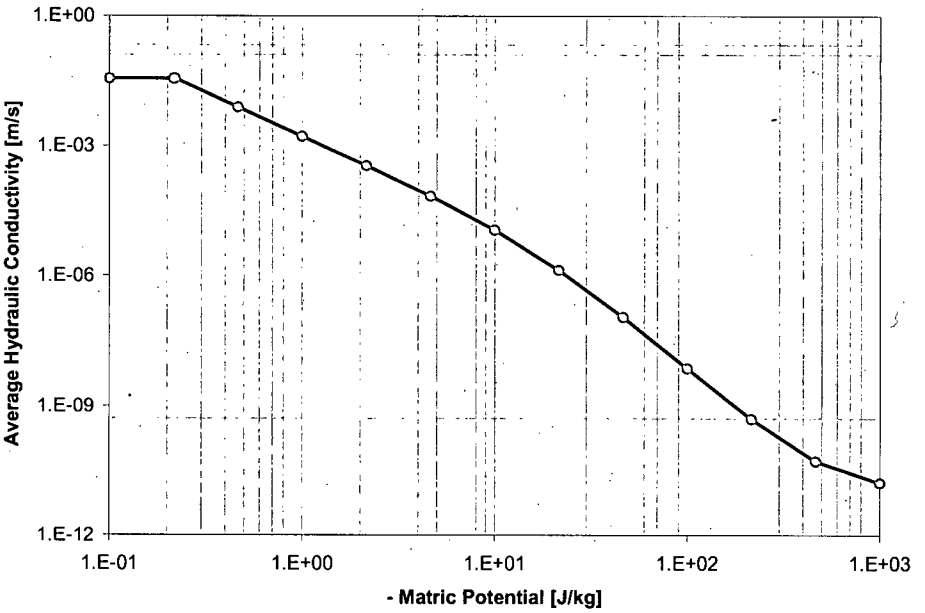

(b)

Figure A-78. Predicted film flow behavior for a representative "rough" fracture face with $L = 5 \times 10^{-4}$ m and $\gamma = 60°$: a) equivalent film thickness, and b) average hydraulic conductivity.

A.4.5 Application to Saltstone Vault 4

Under saturated flow conditions, the thickness of saltstone transmitting the same flow as a saturated crack under the same hydraulic gradient is

$$D_{saltstone} = \frac{K_{crack} b}{K_{saltstone}} \tag{A-29}$$

where b is the aperture and K_{crack} is defined by Figure A-77. For the assumed Saltstone Vault 4 hydraulic conductivity of 10^{-11} cm/s, even a small crack is significant because of the extreme conductivity contrast. During the 10,000-50,000 year period, Saltstone Vault 4 is predicted to experience ponding on the upper surface. Cracks should be considered under these positive pressure conditions.

Similarly, the equivalent thickness of saltstone for unsaturated flow is

$$D_{saltstone} = \frac{2K_A D_A}{K_{saltstone}} \tag{A-30}$$

where the factor of two results from consideration of flow down both sides of the crack, D_A the average film thickness (e.g. Figure A-78a), and K_A is average conductivity (e.g. Figure 2b). Figure 3 defines the suction head required to desaturate a fixed width crack and the equivalent saltstone thickness, for the aperture conditions assumed in Figure A-78.

For example, at a suction of 100 cm, cracks larger than 6×10^{-4} inches will be unsaturated according to equation (A-27). Therefore the exact geometry of the crack, i.e. open at top or bottom, has little impact on the end result. The equivalent saltstone thickness, assuming a conductivity of 10^{-11} cm/s, would be about 3 ft. At lower suctions, the equivalent thickness increases rapidly. Conversely, thickness rapidly decreases at higher suction. During the 0-10,000 year period, Saltstone Vault 4 is predicted to experience a suction of around 1200 cm. At this suction, unsaturated crack flow is predicted to be negligible ($D_{saltstone} \approx 10^{-3}$ ft from Figure A-79). An informal sensitivity study that varied groove depth (L), angle (γ), and spacing (β in Or and Tuller (2000)) indicates this conclusion is not sensitive to the particular values assumed in Figure A-79.

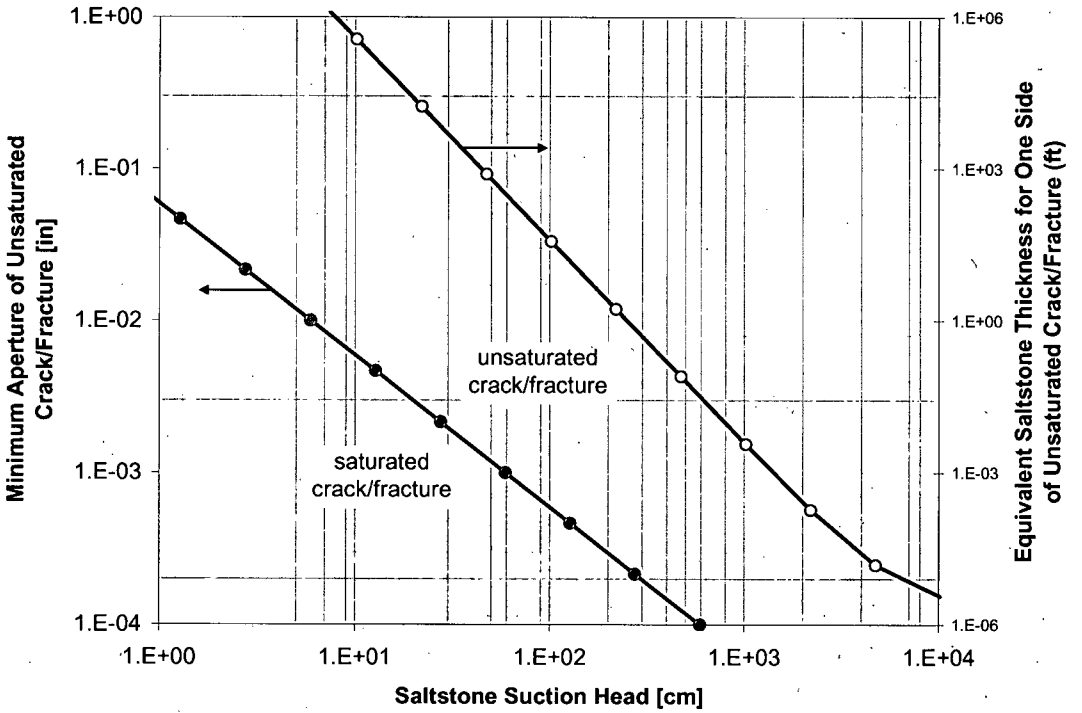

Figure A-79. Minimum unsaturated aperture and equivalent saltstone thickness for film flow down crack faces.

A.4.6 Conclusions

Macroscopic cracks forming in Saltstone Vault 4, whether pinched at top or bottom or through-wall, can be neglected when the suction head exceeds approximately 200 cm. Such conditions are predicted to occur during the 0-10,000 year period. At lower suction or positive pressure conditions, crack flow may be significant.

A.4.7 Details from Or and Teller Reference

The key equations and relationships needed to reproduce Figure 6a in Or and Tuller (2000) are summarized below:

Matric potential

$$\mu = \frac{P}{\rho} = gH \tag{A-31}$$

Film thickness adsorbed to surface under tension

$$h(\mu) = \left[\frac{A_{svl}}{6\pi\rho\mu}\right]^{1/3} \tag{A-32}$$

Corner radius under capillary retention

$$r(\mu) = -\frac{\sigma}{\rho\mu} \tag{A-33}$$

Critical matric potential

$$\mu_c = -\frac{\sigma\cos(\gamma/2)}{\rho L\tan(\gamma/2)} \tag{A-34}$$

Critical radius of curvature ($r < r_c$)

$$r_c = \frac{L\tan(\gamma/2)}{\cos(\gamma/2)} \tag{A-35}$$

Corner area for $\mu < \mu_c$

$$A_{C1}(\mu) = r(\mu)^2\left[\frac{1}{\tan(\gamma/2)} - \frac{\pi(180-\gamma)}{360}\right] \tag{A-36}$$

Corner area for $\mu \geq \mu_c$

$$A_{C2} = L^2\tan(\gamma/2) \tag{A-37}$$

Film area for $\mu < \mu_c$

$$A_{F1}(\mu) = h(\mu)\left\{\beta L + 2\left[\frac{L}{\cos(\gamma/2)} - \frac{r(\mu)}{\tan(\gamma/2)}\right]\right\} \tag{A-38}$$

Film area for $\mu \geq \mu_c$

$$A_{F2}(\mu) = h(\mu)\{\beta L + 2(1-\delta)L\tan(\gamma/2)\} \tag{A-39}$$

Smooth vertical surface film flow (Tokunaga and Wan 1997; Or and Tuller 2000)

$$\bar{v} = \frac{\rho g}{3\eta}h^2 \tag{A-40}$$

Corner vertical flow (Or and Tuller 2000)

$$\bar{v} = \frac{\rho g}{\varepsilon\eta}r^2 \tag{A-41}$$

where

$$\varepsilon = \exp\left[\frac{b + d\gamma}{1 + c\gamma}\right] \tag{A-42}$$

and $b = 2.124$, $c = -0.00415$ and $d = 0.00783$ for $10° < \gamma < 150°$.

Hydraulic conductivity

$$K \equiv \bar{v} \tag{A-43}$$

Average hydraulic conductivity (velocity) for $\mu < \mu_c$

$$K_{A1} = \frac{K_F A_{F1} + K_C A_{C1} \delta}{A_{F1} + A_{C1}} \tag{A-44}$$

Average hydraulic conductivity (velocity) for $\mu \geq \mu_c$

$$K_{A1} = \frac{K_F A_{F2} + K_C A_{C2} \delta}{A_{F2} + A_{C2}} \tag{A-45}$$

Width of representative surface element

$$W = \beta L + 2L \tan(\gamma / 2) \tag{A-46}$$

Effective film thickness

$$D = \frac{A_F + A_C}{W} \tag{A-47}$$

RESPONSE TO RAI COMMENT 37
ROADMAP TO REFERENCES

REFERENCED DOCUMENT	EXCERPT LOCATION	REMARK
Chandler 2004	X-SD-Z-00001, Revision 2 Attachment 8.1 enclosed following response.	This attachment shows both the limits mentioned as well as documents their bases.
Cook, et al. 2005	WSRC-TR-2005-00074, Revision 0, Table A-9 enclosed following response.	
Cozzi, 2004	WSRC-TR-2004-00477, Revision 0, Section 4.0 enclosed following response.	This test report concludes that Saltstone containing Tank 48 material passes TCLP tests.
Cozzi and Zamencnik 2004	WSRC-TR-2004-00749, Revision 0.	The Task Technical and QA Plan identifies benzene as a known decomposition product of TPB salts.
Cozzi, et al. 2005	WSRC-TR-2005-00180, Revision 0, Executive Summary enclosed following response.	The highlighted text indicates the decomposition of the KTPB in the Tank 48 simulant as well as the decomposition rate dependence on temperature.
DOE 2005	DOE-WD-2005-001 dated February 28, 2005, Section 7.2.3.14 enclosed following response.	The indicated paragraph demonstrates that the first step in performing a safety analysis is the CHA Process.
Mahoney, et al. 2004	CBU-PED-2004-00027, Revision 0, Sections 9.4, 10.1, and 10.2 enclosed following response.	These sections demonstrate the variability of options (and consequently schedule) for Tank 48 material processing. Regardless of the option selected, however, the establishment of limits for Saltstone will be completed prior.

RESPONSE TO RAI COMMENT 37
ROADMAP TO REFERENCES

WSRC 2004	WSRC-SA-2003-00001, Revision 2, Section 3.4 and 3.4.1 enclosed following response	This section of the DSA states that the CHAP only identified an explosion in the SFT as a high-risk event. The basis of that CHA was the Time-to-LFL calculation for the SFT, which is also the basis for the Tank 48 organic limits referenced in (Chandler 2004).
WSRC 2005	ENG.08, Revision 2 Sections 5.2-5.3 and Attachment 7 enclosed following response.	These attachments detail the process of WAC revisions including the review and approval by the receiving facility's management.

CBU BUSINESS MANAGEMENT

CBU-PED-2004-00027
REVISION: 0

APPROVED for Release for
Unlimited (Release to Public)

KEYWORDS:
Tank Farm, Salt Program,
DWPF, Liquid Waste,
ETP, Sludge Washing,
Waste Solidification,
ARP, CSSX, SWPF

RETENTION: PERMANENT
CLASSIFICATION: U
Does not contain UCNI

Paul D. d'Entremont
ADC/RO 8/27/04

Interim Salt Processing Strategy Planning Baseline

M. J. Mahoney, 766-H
P. D. d'Entremont, 766-H

Contributors:
S. S. Cathey, 766-H
M. D. Drumm, 766-H
D. C. Sherburne, 704-S
T. R. Reynolds, 704-S
D. T. Conrad, 766-H
J. S. Ledbetter, 766-H
K. A. Hauer, 703-H
J. T. Carter, 703-H
S. J. Robertson, 766-H
H. H. Elder, 766-H
D. P. Chew, 766-H
S. C. Shah, 766-H
T. B. Caldwell, 766-H

Issued: August 27, 2004

9.3.2 Risks

The risks associated with salt tank characterization are as follows:

- The model has a number of assumptions about how supernate behaves when it is drained. To date, the draining process has been successfully completed on only one tank, Tank 41. There is some limited data available from Tank 3, but the Tank 3 draining process was not completed. Based on data obtained from Tank 41, the model assumptions have been adjusted. However, how well the assumptions will work for other tanks is unknown at this time. A model uncertainty evaluation is in progress.
- The model does not predict the concentration of constituents other than Cs-137. These must be determined or estimated from other data. There is a risk that some other constituent will exceed Saltstone WAC limits. These risks will be mitigated by the enhanced characterization program.[7]

9.4 Tank 48 Disposition by Aggregation

The Recommended Case assumes the disposition path for Tank 48 is to aggregate this waste along with other waste going to Saltstone such that the radionuclides meet Saltstone limits. The main radionuclides of concern are Cs-137 and actinides.

The risks of aggregation of Tank 48 waste are as follows:

- A new permit with considerably higher limits is required. The Cs-137 concentration in Tank 48 waste is currently 1.7 Ci/gal Cs-137.[13] Plans are to aggregate this waste with other wastes so that the combined concentration is less than 0.2 Ci/gal Cs-137, with an alpha emitter concentration of less than Class C (100 nCi/gm in the grout). However, this is well in excess of the current Saltstone permit and also in excess of Class A for alpha emitters. SCDHEC has previously stated they are reluctant to approve a permit with greater than Class A limits. Although the focus of the SCDHEC statements was total curies, not alpha concentrations, there is a risk that SCDHEC will not grant a permit that allows Cs-137 or alpha concentrations high enough. For example, if Saltstone is limited to Class A limits for alpha emitters (10 nCi/gm), aggregation of Tank 48 waste in a reasonable period of time is not feasible.
- The tetraphenylborate and other constituents in Tank 48 waste may cause unacceptable releases from Saltstone. Toxicity Characteristic Leach Procedure (TCLP) tests have already been conducted for benzene releases from Tank 48 waste. Preliminary results indicate that all benzene TCLP results are well below regulatory limits. Measurements for nitrobenzene and mercury continue.[8] There is a risk these tests will be unacceptable. There is also a risk that benzene releases will cause flammability or toxicity concerns in the area of the vault. When test results are available, a safety basis review of aggregating Tank 48 waste in Saltstone will be conducted to identify any modifications required.
- A revision to the Tank Farm Documented Safety Analysis (DSA) will be required. There is a risk that flammability concerns will lead to modifications being required for Tank 50, Low Point Pump Pit and associated transfer paths

evaluation is currently in progress to assess the impact of the DSA revision for trapped gas retention in slurried sludge on the overall sludge processing life-cycle.

10. Opportunities

There are a number of opportunities for improving the schedule or recovering from schedule problems, which are described in this section.

10.1 Tank 48 Disposition by Thermal and Chemical Degradation

The Planning Baseline for Salt Processing, which was described above, is to aggregate Tank 48 waste with other wastes going to Saltstone so that the resulting waste meets revised Saltstone WAC, DSA and permit requirements. However, there are a number of risks to this approach.

The backup case is to degrade the tetraphenylborate in Tank 48 using a combination of a catalyst (most likely palladium) and elevated temperatures. The degradation products from this operation, mostly benzene, are released into the vapor space and purged from the tank by the tank's ventilation system. The goal of the process is to reduce the tetraphenylborate inventory to a level that is acceptable for the Tank Farm DSA, about 400 grams.[13] Once the inventory is reduced to this level, the waste in Tank 48 can be treated as normal Tank Farm waste, i.e. it can be evaporated or mixed with other wastes. (Note that degradation may be beneficial even if it is not possible to reduce the tetraphenylborate inventory to less than 400 grams because it could be used to reduce the amount of tetraphenylborate being sent to Saltstone).

Research and development to support this case is currently underway. Preliminary results have not yet identified a combination of palladium catalyst and elevated temperature that will be sufficient to degrade the tetraphenylborate. There are a number of risks.

The risks of thermal and chemical degradation are as follows:

- It might not be possible to find conditions that will cause degradation at a rate high enough to adequately degrade the tetraphenylborate in a reasonable amount of time but not exceed safety limits in Tank 48. The desired rate is about 2 – 7 mg/L/hr. Research is currently ongoing to determine a method for achieving this degradation rate.
- Purposely raising the degradation rate in Tank 48 presents safety hazards. If the reaction were to get out of control, it could cause flammable vapors in Tank 48. The plan currently assumes that the costs of controls to mitigate this hazard are minimal. There is a risk that controls would be prohibitively expensive or burdensome.
- The implementation of this option would result in an estimated 750,000 gallons of waste in Tank 48 that must be transferred to an evaporator system for processing. Though it is expected that the space recovery from evaporation will be high, there is still a risk on the tank space impact on the Planning Baseline.

10.2 Other Opportunities for Dispositioning Tank 48 Waste

Even if it is not possible to reduce the tetraphenylborate inventory in Tank 48 to less than 400 grams, thermal and chemical degradation could be beneficially used. Depending on the results of the ongoing research on degradation, there are a number of possible ways that degradation could be used to enhance the program:

- Degradation could be performed on Tank 48 before aggregation, reducing the concentration of tetraphenylborate in the material being sent to Saltstone. This would mitigate the risks of tetraphenylborate in Tank 50 and Saltstone.
- After most of Tank 48 has been emptied by aggregation, the current plan is to flush the tank to further reduce the inventory of tetraphenylborate. There is a risk that more flushing than currently planned might be needed. Degradation could be used at this point to reduce the inventory of tetraphenylborate and reduce the difficulty of returning this tank to Tank Farm service.
- It may be possible to raise the DSA limit for the tetraphenylborate inventory in Tank 48 as more data on degradation becomes available.

10.3 Acceleration of MCU Startup

The recommended and back-up strategies show a need for the start-up of MCU operation in August 2007. This is based upon the need to start-up the MCU to decontaminate higher activity salt solutions on a schedule that supports several of the program objectives that are described in Section 5. Specifically, the program objectives supported by MCU start-up in August 2007 are:

- Maintain sufficient space in the Tank Farms to allow continued DWPF Operations
- Support Sludge Batch preparation for DWPF
- Provide tank space to support staging of salt solution adequate to feed 5 Mgal of salt solution to SWPF during the initial year of operation starting in April 2009.
- Ensure that the curies to Saltstone during the Interim Salt program are acceptably low (less than 5 MCi total).

MCU start-up in August 2007 is also supportive of the following key assumption described in Section 6. :

- Process adequate salt solution as LCS and eventually by the ARP/MCU process to support Tanks 41, 42, 48, 49, 50, and 28 as SWPF feed staging tanks.

Acceleration of MCU startup before August 2007 would benefit the Salt Program in the following ways:

- It would reduce the number of curies sent to Saltstone as outlined in the Planning Baseline. Earlier operation of MCU would allow additional Salt batches to be processed through the MCU instead of being sent directly to Saltstone. The resulting decontaminated salt solution would then be sent to Saltstone.
- It would provide experience with operating a solvent extraction process on a production scale prior to operation of SWPF. Application of lessons learned during the operation of MCU provides risk reduction for SWPF startup and initial operations (The information will probably be received too late to have a significant impact on SWPF design).

WSRC-TR-2005-00180
Revision 0

MEASUREMENTS OF FLAMMABLE GAS GENERATION FROM SALTSTONE CONTAINING SIMULATED TANK 48H WASTE (INTERIM REPORT)

A.D. Cozzi, D.A. Crowley, J.M. Duffey, R.E. Eibling, T.M. Jones, A.R. Marinik, J.C. Marra, and J.R. Zamecnik

April 2005

Immobilization Technology Section
Savannah River National Laboratory
Aiken, SC 29808

Prepared for the U.S. Department of Energy Under Contract Number DEAC09-96SR18500

SRNL
SAVANNAH RIVER NATIONAL LABORATORY

EXECUTIVE SUMMARY

The Savannah River National Laboratory was tasked with determining the benzene generation rates in Saltstone prepared with tetraphenylborate (TPB) concentrations ranging from 30 mg/L to 3000 mg/L in the salt fraction and with test temperatures ranging from ambient to 95 °C.[1] Defense Waste Processing Facility Engineering (DWPF-E) provided a rate of benzene evolution from saltstone of 2.5 µg/L /h saltstone (0.9 µg/kg saltstone/h) to use as a target rate of concern (TRC).[2]

The generation of benzene, toluene, and xylenes from saltstone containing a simulant of Tank 48H salt solution has been measured as a function of time at several temperatures and concentrations of TPB. The Tank 48H simulant contained potassium tetraphenylborate (KTPB), the decomposition products (phenol, biphenyl, and benzene), and diphenylmercury in addition to inorganic salts. The saltstone slurries were prepared from blends of the Tank 48H simulant and DWPF recycle simulant.

The purpose of this interim report is to provide DWPF-E with a brief description of the methodology and an indication of the trends of benzene evolution. The data presented are to be used by DWPF-E for preliminary calculations with the knowledge that more data are being collected and may alter the final results. A more complete description of the methods and materials will be included in the final report. The benzene evolution rates approximately follow an increasing trend with both increasing temperature and TPB concentration. The benzene generation rates at 95 °C from 1000 mg/L and 3000 mg/L TPB simulant exceeded the recovery-adjusted 0.9 µg/kg saltstone/h TRC (2.5 µg/L saltstone/h), while all other conditions resulted in benzene generation rates below this TRC (except for the initial rate from tests at 75 °C and 3000 mg/L). The toluene evolution rates for at least one sample at each temperature exceeded the TRC initially, but all dropped below the TRC within 2-5 days. The toluene emissions appear to be mainly dependent on the fly ash and are independent of the TPB level, indicating that toluene is not generated from TPB.

. WSRC-TR-2005-00074
Revision 0

KEY WORDS: Performance Assessment
Low-level Radioactive Waste Disposal

SPECIAL ANALYSIS:
REVISION OF SALTSTONE VAULT 4 DISPOSAL LIMITS (U)

PREPARED BY:
James R. Cook
Elmer L. Wilhite
Robert A. Hiergesell
Gregory P. Flach

MAY 26, 2005

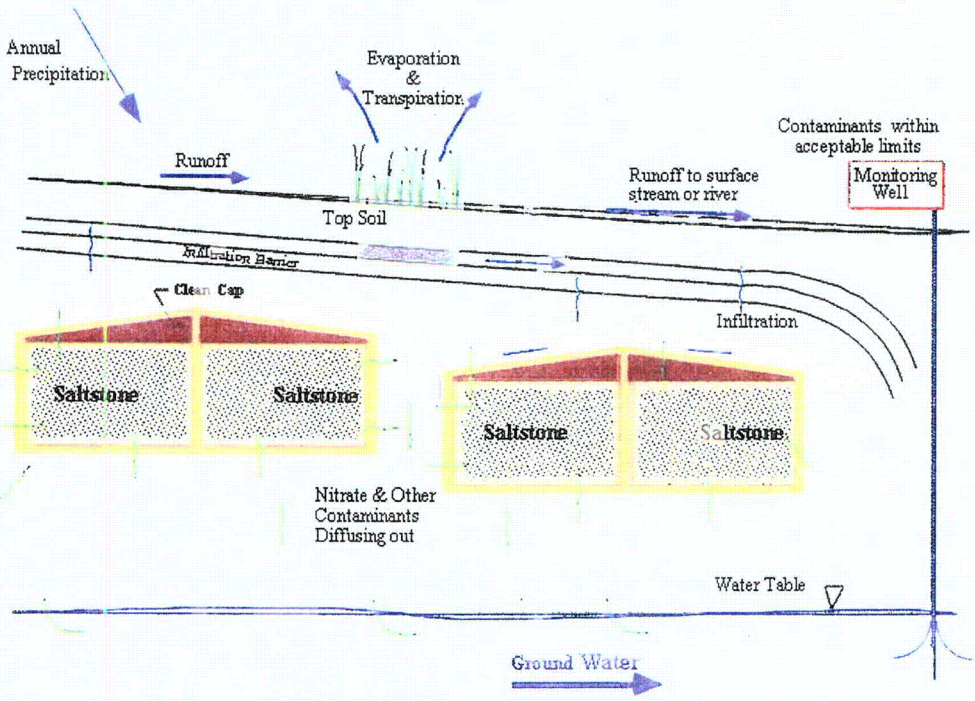

Westinghouse Savannah River Company
Savannah River Site
Aiken, SC 29808

Prepared for the U.S. Department of Energy Under
Contract Number DE-AC09-96SR18500

SRNL
SAVANNAH RIVER NATIONAL LABORATORY

A.2.6 Molecular Diffusion

The molecular diffusion coefficients selected for use in this investigation were established by material type, and are listed below in Table A-9. These values are not expected to vary significantly as the material hydraulic properties in some zones and no attempt was made to re-define them as such changes occurred. The selected values are consistent within the range of diffusion coefficients reported for ionic solutes in porous media (Domenico and Schwartz, 1990). The values selected for Saltstone and concrete are near the lower end of this range, as one would expect.

Table A-9. Molecular Diffusion Coefficients

Porous Media	Molecular Diffusion Coefficients	
	cm^2/sec	$cm^2/year$
Native/Backfill Soil	5.E-05	1.58E+02
Drainage Layer	5.E-05	1.58E+02
Saltstone	5.E-09	1.58E-01
Concrete	1.E-08	3.15E-01

A.2.7 Initial and Boundary Conditions

For the first time period (0 to 100 years), an initial amount of 1,000,000 moles of the parent radionuclide is placed in the Saltstone, from NX = 4 to 64 (0.75 to 99.25 ft) and NY = 33 to 61 (42.0 to 65.75 ft). The height from 65.75 to 66.75 ft is clean pour (i.e., concrete containing no waste). The thickness of the third dimension is 1.0 cm. The porosity of Saltstone is 0.42. PORFLOW sets the initial concentration in the pore water at every node of the "waste" zone to be equal. From PORFLOW output, this concentration for nitrate is 1.1138 mol/cm^3. Since $Q = C \times V \times \phi \times S = 10^6$ moles and $V = 98.5 \times 23.75 \times 30.48^2 = 2.1734 \times 10^6$ cm^3, then S = 0.9836. This is in good agreement with the average Saltstone saturation predicted by the TI01 steady-state flow field.

No-flux boundary conditions for contaminant transport are assumed for the top and both sides of the modeling domain. No boundary condition is specified for the bottom of the modeling domain. PORFLOW 5.97.0 has a default algorithm to calculate convective and diffusive fluxes to the water table.

A.2.8 PORFLOW Transport Runs

Under the initial and boundary conditions, contaminant transport is simulated for the first time interval (0 to 100 years). The steady-state flow field is used for the transient-state transport simulations. Contaminant migration is generally in a downward direction from Saltstone to the water table. The time-history of the contaminant release to the water table is saved for post processing. In the post-processing program, the predicted quantity of contaminant release in mole/yr is divided by the initial amount of 1,000,000 moles to get a fractional release rate (unit = mole/year/mole parent).

For the second time interval (100 to 300 years), the flow field is represented by a new set of saturations and velocities. Because the infiltration rate is higher, the saturation at each of the

MAJOR REWRITE

APPROVED for Release for Unlimited (Release to Public)

1.0 PURPOSE

This procedure documents the requirements for the creation, revision, and use of Waste Acceptance Criteria (WAC), Waste Compliance Plans (WCP), and Special Waste Compliance Plans (SWCP), and the responsibilities of each organization when sending waste streams across the interfaces of Liquid Waste Disposition Projects, Waste Solidification Projects, and supporting organizations.

2.0 SCOPE

This procedure applies to the departments and facilities in Liquid Waste Disposition Projects, Waste Solidification Projects, and supporting organizations.

3.0 TERMS AND DEFINITIONS

A. High Level Waste (HLW) – "The highly radioactive waste material that results from the reprocessing of spent nuclear fuel, including liquid waste produced directly in reprocessing and any solid waste derived from the liquid, that contains a combination of transuranic waste and fission products in concentrations requiring permanent isolation." (DOE Order 435.1) Most of the wastes received into the Tank Farms are high-level wastes. However, if the material meets certain criteria, it can be sent to a non-high-level waste treatment facility, e.g. Saltstone or Wastewater Treatment.

B. Salt – The soluble fraction of Tank Farm precipitated waste.

C. Sludge – The insoluble fraction of Tank Farm precipitated waste.

D. Waste Acceptance Criteria (WAC) – Document describing the requirements necessary to accept the transfer of waste streams between facilities such as the Canyons, Tank Farms, Saltstone, Effluent Treatment, Salt Waste Processing (Future), and DWPF, whose processes have external interfaces. Each facility typically has a WAC (shown in Attachment 1) or a document containing the equivalent information to a WAC associated with it.

E. Waste Compliance Plan (WCP) – Document describing the methods used to meet the WAC for the transfer of waste streams between facilities such as the Canyons, Tank Farms, Saltstone, Effluent Treatment, Salt Waste Processing (Future), and DWPF, whose processes have external interfaces. Each facility typically has a WCP (shown in Attachment 1) or a document containing the equivalent information to a WCP associated with it.

F. Special Waste Compliance Plan (SWCP) – Document with the same function of a WCP but required for the transfer of a Special Waste.

G. Regular Waste (RW) – Waste that has a consistent composition – both the species present, and their concentrations, are relatively constant over time.

5.0 PROCEDURE

5.1 USE OF WACS, WCPS, AND SWCPS

WACs, WCPs, and SWCPs satisfy the requirements of Department of Energy (DOE) Order 435.1 as shown in Attachment 6. The DWPF Waste Form Compliance Plan and the DWPF Waste Form Qualification Report are also included in Attachment 6 as the basis documents for waste certification as defined in DOE Order 435.1 and implemented through the DOE EM-Waste Acceptance Product Specifications (WAPS). WACs, WCPs, and SWCPs are used to implement feed acceptance criteria from a facility's Safety Basis documents. The sending facility's WCP/SWCP shall control parameters so they meet the WAC. The WCP/SWCP for the sending facility may also need to control other parameters that are not safety or regulatory related (e.g., parameters that affect product quality).

5.2 REVISION OF WACS, WCPS, AND SWCPS

WACs, WCPs, and SWCPs will comply with the guidelines of Attachment 7, WAC/WCP/SWCP Development Guidelines. The Engineering Manager for the facility owning the WAC, WCP, or SWCP is responsible for making sure revisions to the WAC, WCP, or SWCP, with guidance from the FE&D group, are appropriately developed per Attachment 7. Steps to revise a WAC are described in 5.3 [2].

5.3 STEPS IN WAC PROCESS

This section describes the formal process for creating and revising WACs and identifies the organizations responsible for each step. The steps are outlined in a functional flow diagram shown in Attachment 2. The following subsections describe each step in the diagram of Attachment 2 and should be used together to complete the process.

[1] New WAC Development/Initial Flowsheet Development

A new WAC development coincides with a new facility or process. A new WAC will be developed for Salt Processing (ARP, MCU, and SWPF) as shown in Attachment 1.

[a] Receiving Facility and FE&D group develop the initial flowsheet or revise the existing flowsheet for the new facility or process (Step 1).

[b] Savannah River National Laboratory (SRNL) performs the appropriate technical studies, presenting the results of completed evaluations and develops a schedule and/or provides status updates for future evaluations (Step 2).

[c] Receiving Facility and FE&D group perform initial impact reviews as described in Section 5.5 and Attachment 4 to determine if and how the composition of the transferred material from the new process will impact both the Receiving Facility and downstream facilities. The FE&D group documents the impacted facility's SSCs including the receipt tank(s) and transfer path(s) and the results of the impact analyses (Step 3).

[d] Receiving Facility and FE&D group informs all organizations listed in Table 1, including the impacted facilities' Facility Manager(s) (FM), of the upcoming transfers (Step 4). Not all organizations are affected and it will be decided at the initial strategy meeting which organizations are the stakeholders, i.e, which organizations should continue with the planning of the new process and resulting waste stream.

5.3 **STEPS IN WAC PROCESS** - continued

[1] **New WAC** - continued

Table 1 - Organizations to Inform for Initial Meetings

H-Canyon Systems Engineering
F-Canyon Systems Engineering
DWPF Process Cognizant Engineering
DWPF Programs Engineering
Saltstone Engineering
Effluent Treatment Project – Process Support
H&F Tank Farms Process Support
Waste Characterization/Program Support (Field Support Services Business Unit)
Program Development and Optimization
Savannah River National Laboratory (SRNL)
Salt Engineering
H-Disposition
F-Disposition

[e] Receiving Facility and FE&D group initiates strategy meeting(s) (Step 5).

[f] Receiving Facility, FE&D group, and all organizations listed in Table 1 identify the downstream facilities (stakeholders) that will be impacted by the new process and resulting waste stream (Step 6).

[g] FE&D group ensures that all of the stakeholders are informed of and are adequately represented during the strategy meeting(s) (Step 7).

[h] During the strategy meeting(s), the Receiving Facility and FE&D group determine the impacts of the new process and resulting waste stream, impacted SSCs, potential material composition impacts, and potential schedule impacts (Step 8).

[i] Receiving Facility and FE&D group review the initial flowsheet for the new process and revise it as necessary (Step 9).

[j] Receiving Facility and FE&D group finalize the flowsheet for the new process and potential new waste streams (Step 10).

[k] Receiving Facility and the appropriate safety group develop and document a new basis for the DSA/Safety Basis for the new process (Step 11).

[2] **WAC Revision**

[a] As the safety basis is developed, the Receiving Facility begins drafting the WAC (Step 12). (Note: Attachment 8 shows an example WAC cover sheet as described by the Implementation Checklist development in Section 5.6. The next revision of all WACs shall include this WAC cover sheet as well as the Implementation Checklist.)

[b] During the WAC draft development and review, the Receiving Facility and Stakeholders develop the Implementation Checklist (Section 5.6, Attachment 9, Step 13).

5.3 STEPS IN WAC PROCESS - continued

[2] WAC Revision - continued

[c] Receiving Facility, FE&D group, and stakeholders review the draft WAC (Step 14).

[d] LWDP Scheduling Integration Group determines if the schedule inputs provided during the Strategy Meetings meet the qualification of a formal schedule change input form (SCIF) (Step 15). The guidelines for a SCIF are found in Reference 7.0 G. If so, the Receiving Facility and LW Scheduling Integration Group prepare (Step 16) and obtain approval of the SCIF (Step 17). If not, the Receiving Facility and LW Scheduling Integration Group obtain approval of the schedule (Step 18) and insert it into the appropriate Plan of the Week (POW) or Plan of the Day (POD) schedules (Step 19).

[e] Receiving Facility incorporates comments on draft WAC and Implementation Checklist (Step 20).

[f] Waste Generator determines if the new process, waste stream, or WAC requirements will affect the existing WCPs (Step 21). If the existing WCPs are affected, refer to Section 5.4 and Attachment 3 for WCP/SWCP development (Step 22). If the existing WCPs are not affected, no change in the WCP is necessary. If a deviation was identified (Section 5.10), the deviation is approved.

[g] Approves the DSA/Safety Basis, if necessary, for new process WACs or changes to the safety basis (Step 23).

[h] Receiving Facility (DAE) performs a USQ on the new/revised WAC (Step 24).

[i] Receiving Facility (DAE) Managers approve new/revised WAC (Step 25).

[j] Receiving Facility (DAE) and all stakeholders complete and approve the Implementation Checklist by approving the appropriate WCPs, procedures, etc. (Step 26).

[k] Receiving Facility implements WAC and approves waste stream to new/revised process or facility (Step 27).

[l] Receiving Facility approves or disapproves the transfer of waste stream(s) by revising the appropriate controlling document (the ERD is the controlling document for the Tank Farms – Step 29).

5.4 STEPS IN WCP/SWCP PROCESS

This section describes the formal process for creating and revising the WCPs and SWCPs and identifies the organizations responsible for each step. The steps are outlined in a functional flow diagram shown in Attachment 3. The following subsections describe each step in the diagram of Attachment 3 and should be used together to complete the process.

ATTACHMENT 7 (Page 1 of 2)
WAC/WCP/SWCP DEVELOPMENT GUIDELINES

- These guidelines document format and content suggestions for WACs, WCPs, and SWCPs.
- The information below should be included in WACs, WCPs, or SWCPs to ensure development is based on sound and defensible data.
- The review cycle for the document should include the appropriate review as specified in Sections 5.4[4] and 5.5.
- All WAC revisions in LWDP require FOSC review. WSP does not require FOSC review but can provide FOSC review for WAC revisions, if necessary.
- The originator, technical reviewer, Chief Engineer, and facility manager, at a minimum, must approve the WAC.
- Approval of WCPs/SWCPs for LWDP must include FOSC review if there is a deviation. WSP does not require FOSC review but can provide FOSC review for deviations, if necessary.
- To be consistent with liquid waste and waste solidification documents, the format of the WAC/WCP/SWCP should include eight major sections, labeled:

  1.0 PURPOSE
  2.0 SCOPE
  3.0 TERMS, DEFINITIONS, ACRONYMS
  4.0 RESPONSIBILITIES
  5.0 PROGRAM CRITERIA
  6.0 RECORDS
  7.0 REFERENCES
  8.0 ATTACHMENTS

- Section 5.0 PROGRAM CRITERIA should contain the major document content and may include subsections unique to the specific WAC/WCP/SWCP.
- An example of Section 5.0 subsections for a WAC is as follows:

  5.1 General Information
  5.1.1 Introduction
  5.1.2 Background
  5.2 Prerequisite Programmatic Criteria
  5.3 Acceptance Criteria
  5.3.1 Physical/Chemical Criteria
  5.3.2 Radionuclide Criteria
  5.3.3 Nuclear Safety Criteria
  5.3.4 Heat Load
  5.4 Administrative Controls
  5.4.1 General Documentation
  5.4.2 Nonconformances

ATTACHMENT 7 (Page 2 of 2)
WAC/WCP/SWCP DEVELOPMENT GUIDELINES

5.4.3 Deviations

- An example of Section 5.0 subsections for a WCP/SWCP is as follows:

5.1 General Information
- 5.1.1 Introduction
- 5.1.2 Background

5.2 Prerequisite Programmatic Criteria

5.3 Compliance Plan
- 5.3.1 Physical/Chemical
- 5.3.2 Radionuclide
- 5.3.3 Nuclear Safety
- 5.3.4 Heat Load

5.4 Administrative Controls
- 5.4.1 General Documentation
- 5.4.2 Nonconformances
- 5.4.3 Deviations

The Acceptance Criteria and Compliance subsections should include specific information on scope, specification, and basis. Criteria which must be met in order to satisfy Safety Basis requirements must be clearly noted within the WAC/WCP/SWCP. Section 5.3 should specify how the generator plans to meet the WAC (e.g. process knowledge, sampling, etc.)

WASTE SOLIDIFICATION ENGINEERING

X-SD-Z-00001
Revision: 2

KEYWORDS:
Saltstone, WAC,
Waste Acceptance Criteria,

WASTE ACCEPTANCE CRITERIA FOR AQUEOUS WASTE SENT TO THE Z-AREA SALTSTONE PRODUCTION FACILITY (U)

RETENTION: Permanent
Disposal Auth: DOE/ADM 17-32.a
Track Number: 10080

September 2004

CLASSIFICATION: U
Does not contain UCNI

APPROVED for Release for
Unlimited (Release to Public)

Paul D. d'Entremont
ADC/RO 9/7/04

Approval:

Timothy E. Chandler, Author, Waste Solidification Engineering — Date: 9-7-04

Thomas D. Lokabill, Reviewer, Waste Solidification Engineering — Date: 9-7-04

Keith R. Liner, CBU Environmental Engineering — Date: 9/7/04

Patrick D. Schneider, Saltstone Operations Manager — Date: 9/7/04

Marshall S. Miller, Waste Solidification Chief Engineer — Date: 9-9-04

Dennis G. Thompson, Saltstone Facility Project Manager — Date: 9.7.04

Implementation:

Dennis G. Thompson, Saltstone Facility Project Manager — Effective Date: 12.16.04

NOTE:

These waste acceptance criteria reflect new limits based on ESH-EPG-2004-00194, Notification of Changes to Waste Influent Concentrations at the Z-Area Saltstone Industrial Wastewater Treatment Facility and Industrial Solid Waste Landfill, G. Laska, EPG-WSRC, to B. Mullinax, SCDHEC, August 18, 2004, which describes plans to transfer H-Canyon Low Level Waste to Tank 50H for subsequent processing in the Saltstone Facility.

Attachment 8.1: Acceptance Limits for Chemical Contaminants in Aqueous Waste Transferred to Z-Area (page 2 of 2)

Chemical Name	Chemical Formula	Molecular Weight (grams/mole)	WAC Limit (mg/L)	Basis
Organic Compounds				
Total Organic Carbon			5.00E+03	83% of Permit Max
Butanol & Isobutanol	C_4H_9OH	74.12	2.25E+03	75% of DSA value (See Note 3)
Isopropanol	C_3H_7OH	60.09	2.25E+03	75% of DSA value (See Note 3)
Methanol	CH_3OH	32.04	2.25E+02	75% of DSA value (See Note 3)
Phenol	C_6H_5OH	94.11	7.50E+02	75% of DSA value (See Note 3)
Tetraphenylborate (See Note 1)	$B(C_6H_5)_4^-$	319.22	3.00E+01	Protects assumptions made concerning benzene concentrations in Time-to-LFL calculation for the SFT (S-CLC-Z-00012)
Toluene	$C_6H_5CH_3$	92.13	3.75E+02	75% of DSA value (See Note 3)
Tributylphosphate	$(C_4H_9)_3PO$	218.31	3.00E+02	75% of DSA value (See Note 3)
EDTA	(See Note 2)	292.25	3.75E+02	75% of DSA value (See Note 3)

Note 1: The rate of benzene generation from TPB and TPB degradation products shall be less than 0.092 milligrams per liter per hour at 40°C. This is an acceptance limit.

Note 2: EDTA (ethylene-diamine-tetraacetic acid) formula: $(HOCOCH_2)_2NCH_2CH_2N(CH_2COOH)_2$. EDTA is assigned CAS No. 60-00-4, and is a CERCLA Hazardous Substance.

Note 3: The DSA values referenced in Attachment 8.1 are those concentrations evaluated in USQ-SSF-2004-0016. These values will be incorporated into Revision 2 of WSRC-SA-2003-00001, the "Saltstone Facility Documented Safety Analysis."

WSRC-SA-2003-00001
REV. 2

SALTSTONE FACILITY

DOCUMENTED SAFETY ANALYSIS

Revision 2

November 2004

APPROVED for Release for
Unlimited (Release to Public)

Westinghouse Savannah River Company
Aiken, SC 29808

SAFETY • RESPONSIBILITY • SECURITY
SRS
SAVANNAH RIVER SITE

PREPARED FOR THE U.S. DEPARTMENT OF ENERGY UNDER CONTRACT NO. DE-AC09-96SR18500

- In the PVVS, the offgases from the SFT and the exhaust from the SHT Ventilation System are sent through a HEPA filter.
- The venturi scrubber in the SHT Ventilation System removes particles and certain gases from the vented offgases.

No Z-Area liquid effluents are discharged directly to the environment without passing a radiological screening. Design features designed to minimize effluent releases to the environment include the following:

- Liquid process waste from flushing activities and facility drains is collected in the SFT and returned to the process stream at the saltstone mixer.
- Rainwater can drain into the SFT sump. The sump is analyzed to determine if it is radioactively contaminated. If the contents are contaminated, they are transferred to the SFT for subsequent processing into saltstone.
- For the saltstone vaults, leaching and migration of chemicals and radionuclides from the saltstone monoliths are minimized through design and material selection so that groundwater at the landfill boundary will not exceed Environmental Protection Agency drinking water standards.
- Groundwater monitoring wells are installed and monitored to detect contamination.

3.3.2.3.5 ACCIDENT SELECTION

DOE-STD-3009-94 (Ref. 2), Section 3.3.2.3.5 requires at least one bounding accident from each of the major types determined from the hazard analysis should be selected unless the bounding consequences are Low.

Since the consequences for the SFT explosion event were qualitatively determined to be High, this event was selected for quantitative analysis.

3.4 ACCIDENT ANALYSIS

Section 3.3 discusses the process by which potential events are screened in order to identify those that require further, quantitative accident analysis. This section describes the methodology used to analyze these accidents, and presents the final results of the analysis. As a result of the initial CHA performed for the Saltstone Facility, only one postulated event, Explosion in the SFT, was binned as a high-risk event for radiological and chemical hazards (Region A). Per DOE-STD-3009-94, this event was selected for a more formal, quantitative accident analysis. The bounding accident scenario addresses a detonation of the SFT due to the presence of benzene in the vapor space. The resulting explosion fails the tank, and hazardous material is released to the environment.

Based on the results of the CHA, this accident analysis conservatively bounds the consequences of any credible event that could occur at the Saltstone Facility. Prior to it being processed into grout and pumped to the vaults for permanent disposal, salt solution is the only hazardous material stored in Z-Area. The largest inventory of salt solution in Z-Area is

contained in the SFT. Once formed into saltstone, the radionuclides and toxic chemicals in the salt solution are immobilized and isolated from the environment by the stability of the material and the design of the disposal vaults. Saltstone grout is not considered a hazardous material and is not subject to rapid dispersion in case of a catastrophic failure of a vault. Therefore, the highest consequence accident involving the contents of the SFT is considered the bounding accident scenario for the Saltstone Facility.

3.4.1 Methodology/Scenario Development

Accident analysis for the Saltstone Facility began with the development of the bounding accident scenario. A source term was then determined using phenomenological calculations. Once the source term was developed, the radiological and toxicological consequences were determined using computer programs. Finally, the consequences were compared to the EGs to determine if safety-related SSCs and Administrative Controls are required. Per DOE-STD-3009-94, detailed accident quantification is not required for HC-3 facilities. Therefore, a graded-approach was taken during the development of the bounding accident analysis, which simplified the development of the source term and consequence analysis.

A detonation of the SFT is postulated to occur due to the presence of benzene vapor in the tank's vapor space. During the processing of high-level waste in the In-Tank Precipitation Facility, sodium tetraphenylborate was used to remove cesium from the waste. Operation of this facility and the ensuing recovery of Tank 49H resulted in the accumulation of tetraphenylborate (TPB) solids (primarily potassium TPB) in Tank 50H, which is the feed tank to the Saltstone Facility. Therefore, measurable quantities of TPB are present in the salt solution that is transferred to the Saltstone Facility for treatment and disposal. TPB (both soluble and insoluble) slowly undergoes hydrolysis in the salt solution to produce benzene. For the bounding accident scenario, it is assumed that sufficient benzene can be generated in the waste such that the Lower Flammability Limit for benzene is exceeded in the SFT vapor space. The flammable vapor composition subsequently leads to an explosion that serves as the initiator for the bounding accident, which involves the release of salt solution stored in the SFT to the environment.

The bounding accident scenario makes the following assumptions:

- An explosion occurs in the SFT to initiate the event.
- The SFT explosion is conservatively assumed to occur once in the lifetime of the facility (i.e., event frequency is Anticipated).
- Bounding radionuclide concentrations shown in Table 3.6-6 and bounding chemical concentrations shown in Table 3.6-7 were used to establish source term and consequence analysis for the bounding accident scenario. All radionuclides and chemicals are assumed to be at their bounding concentrations simultaneously. The concentrations of radionuclides and chemicals in the actual salt solution that will be treated in the Saltstone Facility are much less than the concentrations used in the accident analysis.

- No credit is taken for operator intervention to prevent the explosion or mitigate the resulting spill of hazardous material.

- No credit is taken for secondary containment provided by the concrete dike surrounding the SFT.

- No credit is taken for any installed equipment or procedures that could prevent the explosion or mitigate the consequences of the explosion.

- The density of the salt solution in the SFT is assumed to be 1000 kg/m^3, which is the density of water. Using a lower than normal density for the salt solution results in a slight over prediction of the source term and consequence.

- In order to produce the maximum source term, it is assumed that a stoichiometric benzene concentration exists in the SFT vapor space at the time of the explosion.

- The predominant flammable vapor in the SFT is benzene. Other flammable vapors may be present, but their quantities are considered insignificant. Although hydrogen will be present in the vapor space due to radiolysis of water, the explosion of stoichiometric benzene bounds the hydrogen explosion.

- The height of the sloped bottom on the SFT is combined with the height of the right-circular cylinder portion of the tank to maximize the calculated tank vapor space. By doing this, the maximum volume of the SFT is assumed to be 29 m^3.

- Any flammable vapors located in the vapor space of the SSHT do not contribute to the amount of energy released by the SFT explosion.

- For the radiological source term and consequence analysis, a 3-minute plume duration is assumed for the explosion event.

- For the chemical source term and consequence analysis, a 15-minute plume duration is assumed for the explosion event.

- Onsite dispersion factor (χ/Q) at 100 meters is 1.0×10^{-3} sec/m^3.

- Offsite χ/Q at 10.9 km is 2.63×10^{-6} sec/m^3.

3.4.2 Source Term Analysis

The source term (ST) is a measure of the amount of material released to the environment during a postulated event. Thus, the source term units are typically units of mass or volume (grams, gallons, etc.). The release of radioactive material due to a tank explosion occurs in two cumulative phases. The initial phase considers the result from the explosion of the tank itself. The second phase is the aerodynamic entrainment of material as ambient wind conditions resuspend the released radioactive material pooled outdoors.

DOE-WD-2005-001
February 28, 2005

Draft Section 3116 Determination

Salt Waste Disposal

Savannah River Site

Pursuant to Part 835, activities at SRS, including disposal operations at SDF, must be conducted in compliance with the documented RPP for SRS as approved by DOE. The key elements of the RPP include monitoring of individuals and work areas, control of access to areas containing radiation and radioactive materials, use of warning signs and labels, methods to control the spread of radioactive contamination, radiation safety training, objectives for the design of facilities, criteria for levels of radiation and radioactive material in the workplace, and continually updated records to document compliance with the provisions of Part 835. The RPP also includes formal plans and measures for applying the ALARA process.

The requirements of Part 835 as contained in the approved RPP are incorporated in the WSRC's Standards and Requirements Implementing Document system. The Standards and Requirements Implementing Document system links the requirements of Part 835 to the site-level and lower-level implementing policies and procedures that control radiological work activities conducted across the site. These requirements are primarily contained in the WSRC 5Q Manual, *Radiological Control*, and its lower tier manuals, e.g., WSRC 5Q1.1, *Radiation and Contamination Control Procedures Manual,* and WSRC 5Q1.2, *Radiation Monitoring Procedures Manual.* These procedures control the planning of radiological work, the use of radiation monitoring devices by employees, the bioassay program, the air monitoring program, the contamination control program, the ALARA program, the training of general employees, radiological workers, Radiological Control Inspectors, and health physics professionals and technicians, and the other aspects of an occupational radiation protection program as required by Part 835.

7.2.3.14 Documented Safety Analysis

A DSA [43] has been approved by DOE for operation of SPF and SDF in accordance with 10 CFR Part 830. As the first step in the development of the DSA, a formal Consolidated Hazards Analysis (CHA) [44] was performed at the Saltstone Facility to evaluate the potential risk of operations to the workers and the public. The CHA was performed by a group of approximately 20 subject matter experts, with expertise in the fields of operations, engineering, industrial hygiene, radiological protection, environmental compliance, and maintenance.

The CHA consisted of three basis phases: hazard identification; hazard classification; and hazard evaluation. During the hazard identification phase, all possible radiological and chemical hazardous materials associated with the normal and abnormal operations of the facility were identified, along with all potential energy sources available to disperse the hazardous materials to the environment.

During the hazard classification phase, the maximum quantities of hazardous materials possible in the Saltstone Facility are evaluated against the criterion listed in DOE-STD-1027-92, *Hazard Categorization and Accident Analysis Techniques for Compliance with DOE Order 5480.23, Nuclear Safety Analysis Reports*, to determine the overall hazard classification of the facility. It was determined by the CHA team that the hazard classification of the Saltstone Facility was Hazard Category 3, which is the lowest hazard classification and denotes a potential for only

localized consequences to workers at the facility and no potential for significant consequences to other workers at the site or to members of the public.

During the third and final phase of the CHA, all possible normal and abnormal operational events that could result in exposing facility workers or the public to hazardous material were evaluated to determine the magnitude of the risk. During this hazard evaluation phase, the consequence and frequency of each operational event was qualitatively determined, and the resulting level of risk was identified. The purpose of identifying the level of risk was to determine which operational events posed some level of risk (and thus required additional evaluation) and those events which presented negligible risk to the facility workers and public. As a result of the hazard evaluation for the Saltstone Facility, all normal operational events were determined to present negligible risk to the workers and public (i.e., exposure < 5 rem to facility workers), and were thus removed from further evaluation. For purposes of this CHA, the waste inventory and curie concentrations were assumed to be greater than currently planned for the DDA, ARP/MCU, and SWPF streams.

The DSA analyzed the hazards that were identified in the CHA that could impact facility workers during normal operations and accident conditions, and specifically included radiation exposure hazards. The DSA identified the basis for derivation of the Saltstone Facility Technical Safety Requirements (TSR) [45] and also discussed summary descriptions of the key features of safety management programs at SRS as they pertain to SDF.

The Saltstone Facility TSR document identified the administrative controls that are necessary to achieve safe operations at SDF. In part, these TSR administrative controls require: (1) that a facility manager be assigned who is accountable for safe operation and in command of activities necessary to maintain safe operation; (2) that personnel who carry out radiological controls functions for SDF have sufficient organizational freedom to ensure independence from operating pressures; (3) that SDF personnel receive initial and continuing training including radiological control training; and (4) that an RPP shall be prepared consistent with 10 CFR Part 835. The DSA determined that the administrative controls identified in the TSR are sufficient to ensure worker protection in accordance with 10 CFR Part 835.

In addition, the design requirements for SPF and SDF implemented 10 CFR Part 835 [46] and, in particular, implemented ALARA principles. The design is currently being upgraded to reflect the radionuclide concentrations in the low-activity waste streams to be received at SPF and SDF from planned Interim Salt Processing facilities and SWPF. While the upgraded design is not yet complete, based on the current SPF and SDF design, it is estimated that occupational exposures for SPF and SDF workers will be at least an order of magnitude lower than the 10 CFR Part 835 dose limit of 5 rem per year during both Interim Salt Processing and SWPF operation.

7.2.3.15 Radiological Design for Protection of Occupational Workers and the Public

New SRS radiological facilities and facility modifications including the ongoing Saltstone Facility modifications are designed to meet the requirements of 10 CFR 835 Subpart K, *Design and Control* [47]. SRS Engineering Standard 01064, *Radiological Design Requirements* [40],

provides the requirements necessary to ensure compliance with 10 CFR Part 835. The standard refers to 10 CFR Part 835, DOE orders, DOE standards, DOE handbooks, national consensus standards, SRS manuals, SRS engineering standards, SRS engineering guides, and site operating experience in order to meet the 10 CFR Part 835 specific requirements and additional requirements to ensure the design provides for protection of the worker and the environment.

The standard covers the full spectrum of radiological design requirements and not just radiation exposure limits. The following are the specific areas addressed in the standard: radiation exposure limits; facility and equipment layout; area radiation levels; radiation shielding; internal radiation exposure; radiological monitoring; confinement; and ventilation.

The design requirements for several of the important sections of the standard are highlighted in order to understand the design limits and philosophy for SRS designs. The first area of interest is the radiation exposure limits. The following is an excerpt of the standard which presents the exposure limits and philosophy for both external and internal radiation exposure.

> "During the design of new facilities or modification of existing facilities, the design objective for controlling personnel exposure from external sources of radiation in areas of continuous occupancy (2000 hours per year) shall be to maintain exposure levels below an average of 0.5 mrem per hour and as far below this average as is reasonably achievable. The design objectives for exposure rates for potential exposure to a radiological worker where occupancy differs from the above shall be As Low As Reasonably Achievable (ALARA) and shall not exceed the external limits in Table 5-1. Regarding the control of airborne radioactive material, the design objective shall be, under normal conditions, to avoid releases to the workplace atmosphere and in any situation, to control the inhalation of such material by workers to levels that are ALARA; confinement and ventilation shall normally be used [6.3, 6.12]. Table 5-1 summarizes the design basis external radiation exposure limits.

Design Basis Annual Occupational Radiation Exposure Limits

Type of Exposure	Limit (rem)
Whole Body TEDE	1.0
Internal CEDE	0.5
Lens of Eye	3
Extremity	10
Any Organ (other than eye) or Tissue	10

> To meet the Site's no deliberate intake policy, engineered controls will be evaluated and implemented to ensure that, under normal operating conditions, no worker will receive a deliberate intake of radionuclides (i.e., CEDE=0 rem). As a result, the TEDE limit will be independent of the CEDE limit. The 0.5 rem CEDE limit in Table 5.1 is to be applied to potential intakes from anticipated

potential releases or anticipated off-normal maintenance. Under these anticipated potential conditions, engineered controls will be evaluated and implemented to minimize the potential for workers to receive intakes that will exceed the 0.5 rem CEDE. This evaluation will not take credit for the use of respiratory protection.

The dose to any member of the public or a minor exposed to radiation at a DOE facility shall not exceed 0.1 rem TEDE in a year."

The facility design also incorporates radiation zoning criteria in order to ensure the exposure limits presented above are met by providing adequate radiation shielding. Areas in which non-radiological workers are present are assumed to have continuous occupancy (2,000 hours per year) and are designed to a dose rate less than 0.05 mrem per hour to ensure that the annual dose is less than 100 mrem. Other zoning criteria are established to ensure radiological worker doses are ALARA and less than 1,000 mrem per year to meet the 10 CFR 835.1002 design requirements.

The design is also required to provide necessary radiological monitoring or sampling for airborne and surface contamination to ensure the engineered controls are performing their function and, in the event of a failure or upset condition, workers are warned and exposures avoided.

Radiological protection personnel ensure the requirements of the standard are addressed and presented in design summary documentation. The incorporation of all the radiological design criteria in the engineering standard ensures the requirements of 10 CFR Part 835 are met and the design provides for the radiological safety of the workers and environment.

7.2.3.16 Regulatory and Contractual Enforcement

Any violation of the requirements in 10 CFR Part 835 is subject to civil penalties pursuant to section 234A of the Atomic Energy Act of 1954, as amended, 42 USC 2011 et seq., as implemented by DOE regulations in 10 CFR Part 820. In addition, the requirements in 10 CFR Part 835 and all applicable DOE Orders are incorporated into all contracts with DOE contractors, including WSRC, the DOE contractor for disposal operations at SDF as well as other operations at SRS. DOE enforces these contractual requirements through contract enforcement measures, including the reduction of contract fees.

7.2.3.17 Access Controls, Training, Dosimetry, and Monitoring

Training or an escort is required for individual members of the public for entry into controlled areas. In addition, use of dosimetry is required if a member of the public is expected to enter a controlled area and exceed 0.05 rem per year to ensure no member of the public exceeds radiation exposure limits [48].

In addition, worker radiation exposure monitoring is performed for all workers expected to receive 100 mrem per year from internal and external sources of radiation to provide assurance

FORMULATION DEVELOPMENT FOR PROCESSING TANK 48H IN SALTSTONE

A.D. Cozzi

October 2004

SAVANNAH RIVER NATIONAL LABORATORY

Immobilization Technology Section
Savannah River National Laboratory
Aiken, SC 29808

Prepared for the U.S. Department of Energy Under Contract Number DEAC09-96SR18500

4.0 CONCLUSIONS AND RECOMMENDATIONS

- Aggregates were prepared with Tank 48H material and either DWPF recycle simulant or inhibited water with concentrations of 1500, 3500, and 5500 mg/L TPB.
- Air entrainment caused by the mixing of the aggregate in the slurry preparation method used produced a stable structure the led to premature gelation of the slurries that required admixtures for remediation.
- Processable Saltstone slurry formulations were demonstrated with Tank 48H material and both DWPF recycle simulant and inhibited water with concentrations of 3500, and 5500 mg/L TPB. It is expected that acceptable formulation can be prepared with aggregates of 1500 mg/L TPB. Table 4-1 is the recommended initial processing parameters for the six aggregates tested.

Table 4-1. Recommended Initial Processing Parameters for Tank 48H Aggregates.

TPB (mg/L)	Water/Premix	Set Retarder (Wt %)	Antifoam (Wt %)
1500	0.60-0.63	0.1-0.2	0.1
3500	0.65	0.2	0.15
5500	0.65	0.30	0.15-0.2

- Analysis of the TCLP extracts of the Saltstone prepared from the six aggregates indicates that the resulting Saltstone is not hazardous for benzene, nitrobenzene, or mercury.
- Testing of the fresh Saltstone slurry and cured Saltstone prepared with simulants indicate that the neither the fresh nor cured Saltstone is hazardous for ignitability.
- After transferring Tank 48H material to Tank 50 and prior to processing through the SPF, Tank 50 should be sampled to verify processability with the recommended processing parameters in Table 4-1.

APPROVED for Release for Unlimited (Release to Public) 6/23/2005

Task Title Tetraphenylborate Decomposition in Saltstone		TTR Number: SP-TTR-2004-0005	TTR Date: 11/17/2004
Task Leader A.D. Cozzi	Signature:	Organization: SRNL/ITS	Date: 12/17/04
Task Leader J.R. Zamecnik	Signature:	Organization: SRNL/ITS	Date: 12/17/04
Technical Reviewer (if required): M.S. Hay	Signature:	Organization: SRNL/WPT	Date: 1/4/05
Level 3 Manager (or designee): D.A. Crowley	Signature:	Organization: SRNL/ITS	Date: 1/4/05
Waste Solidification Engineering: J.E. Occhipinti	Signature:	Organization: CBU/WSE	Date: 1/11/05
ITS QA Coordinator: T.K. Snyder	Signature:	Organization: SRNL/ITS	Date: 1-3-05
SRNL QA Representative: J.P. Vaughan	Signature:	Organization: SRNL-QA	Date: 1/3/05

Distribution:

T.E.	Chandler,	704-Z	D.	Maxwell,	766-H
D.T.	Conrad,	766-H	J.E.	Occhipinti,	704-S
A.D.	Cozzi,	773-43A	L.M.	Papouchado,	773-A
D.A.	Crowley,	773-A	M.A.	Rios-Armstrong,	766-H
W.B.	Dean,	766-H	S.J.	Robertson,	766-H
R.E.	Eibling,	999-W	B.C.	Rogers,	766-H
R.	Dunn,	773-A	S.C.	Shah,	766-H
S.D.	Fink,	773-A	D.C.	Sherburne,	704-S
R.C.	Fowler,	703-H	J.A.	Smith,	704-29S
J.	Griffin,	773-A	T.K.	Snyder,	999-W
J.R.	Harbour,	773-42A	R.H.	Spires,	766-H
M.S.	Hay,	773-42A	A.V.	Staub,	704-28S
E.W.	Holtzscheiter,	773-A	P.C.	Suggs,	766-H
D.P.	Lambert,	773-A	D.G.	Thompson,	704-Z
C.A.	Langton,	773-43A	J.P.	Vaughan,	773-41A
T.D.	Lookabill,	704-Z	W.R.	Wilmarth,	773-42A
S.L.	Marra,	999-W	J.R.	Zamecnik,	773-41A

Task Title Tetraphenylborate Decomposition in Saltstone		TTR Number: SP-TTR-2004-0005	TTR Date: 11/17/2004
Task Leader A.D. Cozzi	Signature:	Organization: SRNL/ITS	Date: 12/17/04
Task Leader J.R. Zamecnik	Signature:	Organization: SRNL/ITS	Date: 12/17/04
Technical Reviewer (if required): M.S. Hay	Signature:	Organization: SRNL/WPT	Date: 1/4/05
Level 3 Manager (or designee): D.A. Crowley	Signature:	Organization: SRNL/ITS	Date: 1/4/05
Waste Solidification Engineering: J.E. Occhipinti	Signature:	Organization: CBU/WSE	Date: 1/4/05
ITS QA Coordinator: T.K. Snyder	Signature:	Organization: SRNL/ITS	Date: 1-3-05
SRNL QA Representative: J.P. Vaughan	Signature:	Organization: SRNL-QA	Date: 1/3/05

Distribution:

T.E.	Chandler,	704-Z	D.	Maxwell,	766-H
D.T.	Conrad,	766-H	J.E.	Occhipinti,	704-S
A.D.	Cozzi,	773-43A	L.M.	Papouchado,	773-A
D.A.	Crowley,	773-A	M.A.	Rios-Armstrong,	766-H
W.B.	Dean,	766-H	S.J.	Robertson,	766-H
R.E.	Eibling,	999-W	B.C.	Rogers,	766-H
R.	Dunn,	773-A	S.C.	Shah,	766-H
S.D.	Fink,	773-A	D.C.	Sherburne,	704-S
R.C.	Fowler,	703-H	J.A.	Smith,	704-29S
J.	Griffin,	773-A	T.K.	Snyder,	999-W
J.R.	Harbour,	773-42A	R.H.	Spires,	766-H
M.S.	Hay,	773-42A	A.V.	Staub,	704-28S
E.W.	Holtzscheiter,	773-A	P.C.	Suggs,	766-H
D.P.	Lambert,	773-A	D.G.	Thompson,	704-Z
C.A.	Langton,	773-43A	J.P.	Vaughan,	773-41A
T.D.	Lookabill,	704-Z	W.R.	Wilmarth,	773-42A
S.L.	Marra,	999-W	J.R.	Zamecnik,	773-41A

I. INTRODUCTION

A. Task Definition

The operating strategy for processing at Saltstone is projected to result in elevated temperatures in the Saltstone vaults over a period of months. The review for this strategy resulted in a review of documentation for the production of benzene via the decomposition of potassium tetraphenylborate (KTPB) solids at elevated temperatures for an extended period of time. Initial results of this review indicate that benzene could potentially accumulate in the vault vapor space under the strategy. The current Z-Area Safety Basis does not postulate an explosion in the vaults, and therefore, the Safety Basis does not restrict vault temperatures or TPB concentrations relative to a vault explosion.

An evaluation of prior Saltstone production confirmed that previous facility operation has not resulted in elevated grout temperatures for extended periods of time (no temperature higher than 51°C and these peaks lasted for days rather than months). This review combined with previous sampling for benzene in vault cells provides the basis for the position that there is no imminent hazard at the vaults.

The Savannah River National Laboratory (SRNL) was requested to determine benzene generation rates in Saltstone prepared with TPB concentrations ranging from 30 mg/L to 3000 mg/L in the salt fraction and test temperatures ranging from ambient to 95°C[1]. The request included determination of the effect of surface area to volume ratio on the benzene generation rate.

A three stage approach will be used to meet these objectives. In the first stage, testing will be performed to select one of several potential methodologies for the collection, recovery and analysis of benzene. The second stage will entail demonstrating the methodology selected in Stage I in testing with surrogate materials. Testing of saltstone prepared with actual Tank 48H waste as the source of TPB will take place in Stage III.

Materials and Mixes

The salt solutions to be tested in Stage II will consist of Tank 48H simulant (as the source of TPB) blended with a simulant of DWPF recycle material, inhibited water, or other salt solution specified by the customer and documented in the Laboratory Notebook*. Table 1 is the properties for the materials to be blended. The Tank 48H simulant[2] is based on samples of Tank 48H taken in 2003[3]. The DWPF recycle simulant will target the average sodium and the maximum anion and mercury content of the Tank 23 and Tank 24 samples taken 100 inches from the tank bottom as reported by Swingle[4]. Table 2 is the composition of the DWPF Recycle simulant based on the major components in Reference 4. Any additional constituents will be specified by the customer and documented in the Laboratory Notebook*. The salt solutions will target three TPB concentrations, 30 mg/L, the estimated concentration of TPB currently in Tank 50H, 1000 mg/L, the concentration limit of TPB in the Saltstone Processing Facility Documented Safety Analysis (SPF-DSA), and 3000 mg/L, the expected maximum or bounding TPB concentration in batches made with Tank 48H waste. Table 3 is the make up of each of the salt solutions.

Table 1. Composition and Properties of Materials for Simulant Makeup.

Material	TPB	Wt. % Solids		Density	Mercury
	(mg/L)	Undissolved	Total†	(g/ml)	(mg/L)
Tank 48H[3]	18,800	2.18	18.42	1.144	10.3
DWPF Recycle simulant (s)	0	<1	5.09	1.039	14.5[4] (Tank 24)
Inhibited Water (IW)	0	0	0.1	~1	0

† Total solids is used to determine the water:premix ratio used for Saltstone processing.

Table 2. Composition of DWPF Recycle Simulant.

* WSRC-NB-2004-00180 "Benzene Generation in Saltstone"

RESPONSE TO RAI COMMENT 38
ROADMAP TO REFERENCES

REFERENCED DOCUMENT	*EXCERPT LOCATION	REMARK
Chandler 2005	Excerpt enclosed following response.	Email from Timothy Chandler to Christine Langton and forwarded to D. Chew.
Cook et al. 2002		General reference, Executive Summary enclosed following response.
Cook et al. 2005	Excerpt enclosed following response.	Table A-4
Langton 1985	Excerpt enclosed following response.	DPST-85-528, Tables I, II, and III
Langton 1985	Excerpt enclosed following response.	DPST-85-982
Langton 1987	Excerpt enclosed following response.	Entire document. DPST-87-673
Langton 1987	Excerpt enclosed following response.	DPST-87-530, Tables V and IX
Langton 1987	Excerpt enclosed following response.	Entire document. DPST-87-869
Langton 1998	Excerpt enclosed following response.	Entire document.
Malek et al. 1985	Excerpt enclosed following response.	
Phifer 2004		General reference, no excerpt included with this response.
MMES 1992 (Saltstone PA)	Excerpt enclosed following response.	Tables 2.3-1 and 3.3.1
Yu et al. 1993	Excerpt enclosed following response.	Summary of Permeability to Liquid Test Results Table.

*Excerpt Locations:

1. Excerpt included in response: The excerpt is included within the text of the response or is appended to the response.
2. Excerpt enclosed following response: The excerpt is enclosed on a separate sheet or sheets following the response.
3. Representative excerpt(s) enclosed following response: Representative excerpts from a document that is wholly or largely applicable are enclosed following the response.
4. Other

7/15/2005

TECHNICAL DIVISION
SAVANNAH RIVER LABORATORY

Keywords: Slag Saltstone Physical Properties
Slag Saltstone Processing
Cold Run-In Formulation
F Fly Ash Variability

M E M O R A N D U M

DPST-87-673 ←

cc: G. T. Wright, 773-A
E. S. Occhipinti, 704-S
R. L. Hooker, 704-S
G. W. Oakes, 704-S
E. L. Wilhite, 773-43A
E. G. Orebaugh, 773-43A
P. F. McIntyre, 773-43A
B. G. Kitchen, 773-41A
SRL Records (4), 773-A

October 26, 1987

TO: H. F. STURM, JR., 773-43A

FROM: C. A. LANGTON, 773-43A CAL

PHYSICAL PROPERTIES OF SLAG SALTSTONE

SUMMARY

Physical properties of two slag saltstone mixes were measured and a formulation for cold run-in of the saltstone equipment has been recommended. In addition, the effects of fly ash variability (ashes from three different power plants) were evaluated with respect to saltstone processing.

Compressive strength, rheological properties and thermal properties are comparable or improved with respect to the former reference mix (C fly ash and H cement). Fly ash source does not significantly affect processing.

Formulations for cold run-in of the saltstone facility can be made from the slag saltstone dry solids blend plus water (water to solids ratio of about 0.5). Rheological properties of this grout are similar to mixes containing salt solution.

RESULTS

Compressive Strength

Compressive strength measurements were made on 2-inch cubes of slag mixes I and II (ingredients listed in Table I) after 7, 14, and 28 days curing at room temperature. Samples were tested in triplicate. Plant Bowen Class F fly ash, slag from Blue Circle, Atlantic Cement Company and Type II Giant Cement or $Ca(OH)_2$ from Augusta Lime and Fertilizer were used in these mixes.

Data are tabulated in Table II and average values are plotted in Figure 1. After 7 days curing, both mixes exceeded 500 psi which confirms that the grout set. The average strength after 28 days curing was 2113 psi for the mix containing $Ca(OH)_2$ as the lime source versus 1926 for the mix containing portland cement. The lower value for the cement mix is attributed to a higher solution loading and also slower reaction rates in this formulation.

Rheology

Plastic viscosities, yield points, and 10 minute gel strengths were evaluated using a 6 speed Fann 35A rotoviscometer. Each mix was prepared and tested 5 times to evaluate rheological behavior as a function of batch. Plant Bowen Class F fly ash, slag from Blue Circle, Atlantic Cement Company and Type II Giant Cement or $Ca(OH)_2$ from Augusta Lime and Fertilizer were used in these mixes. Data are tabulated in Appendix I and rheological properties are summarized in Table III. Average readings for shear stress at various shear rates are plotted in Figures 2 and 3.

These grouts can be characterized as Bingham plastics which undergo irreversible reactions as a function of time that ultimately result in setting of rigid solid. Both mixes are pumpable/pourable slurries after mixing. Mix I containing $Ca(OH)_2$ had an average plastic viscosity of 27 cp and a yield point of 175 dynes/cm^2. Mix II containing portland cement had values of 21 cp and 31 dynes/cm^2, respectively. The higher values for the $Ca(OH)_2$ mix are attributed to the higher surface area (finer particle size) of the $Ca(OH)_2$ compared to the cement. Initial rapid hydration of the cement, in particular, the tricalcium aluminate, may account for the faster gelation of the cement mix.

The cement containing grout had an average 10 min gel strength of 2945 dynes/cm^2 compared to 791 dynes/cm^2 for the $Ca(OH)_2$ mix. From these measurements and physical appearance of the grouts, the cement mix is probably not pumpable after

10 minutes under static conditions. The $Ca(OH)_2$ mix was pourable and, therefore, probably pumpable after 10 minutes under static conditions. For comparison, the former cement-based reference mix prepared in a Waring Blender routinely exceeded a 10 minute gel strength of 600 lbs/100 ft^2 (3000 dynes/cm^2) and was not pourable.[1] Other rheological data for cement-based saltstone grouts are reported in references 2 and 3.

All grouts tested in this evaluation of rheology set within 2 days and had no free water or phase separation.

Thickening Time

The effect of fly ash variability on grout processing was evaluated by measuring differences in thickening times with an LSD/SRL designed gel strength tester.

This instrument measures the force exerted by grout on a paddle rotating at a very slow speed, 0.01 inches/sec or less. The sensitivity of this instrument is greater than that of the Fann viscometer and gel strength is measured and recorded as a function of time rather than at a given time, ie., 10 minutes.

Results for fly ashes from Plant Bowen, the Marshall Plant and the Belews Creek Plant are summarized in Table IV. Data for these ashes in slag mixes I and II are plotted in Figure 4. For comparison, data for the slag mix II with 3 rather than 5% cement, a mix with no lime source, and the former Class H cement-Class C fly ash are plotted in Figure 5.

Slag mix I containing $Ca(OH)_2$ as the lime source gels slowly and reaches a gel strength of 6 lbs/ft^2 in 8-40 minutes depending on the fly ash source.* Marshall ash produced the

* Grouts which result in measurements of 60 lbs/ft^2 in the gel strength tester are not pourable. A paddle pressure of 40 lbs/ft^2 (0.3 psi) for the gel strength tester was used here as a tentative guide for estimating the maximum shear stress which may be broken back to reinitiate grout flow after the material has been static. However, correlations must be made between the gel strength tester results and actual operating conditions and equipment. Also 6 lbs/ft^2 measured on the gel strength tester does not correspond to 6 lb/ft^2 measured on the Fann viscometer even though both instruments have been calibrated. (A grout with a gel strength of 6 lbs/ft^2 measured on the Fann Viscometer is not pourable.) This is attributed to fresh material being sheared in the first case versus shearing in a region of disturbed material for the second case.

fastest gelling grout. Mix I containing plant Bowen ash resulted in the slowest gelling grout. The maximum reading on the gel strength tester which can be related to a marginally pourable material is 40 lbs/ft^2 (0.3 psi). This value is measured after more than 60 minutes at near static conditions for slag mix I.

Slag mix II containing portland cement as the lime source gels in 3 to 5 minutes. The more rapid thickening is attributed to hydration of tricalcium aluminate in the cement. Thickening to 40 lbs/ft^2 occurred in 9 to 12 min for this mix. A modified slag mix II containing 3 wt% cement gelled slower than the mix containing 5 wt% cement (11 min to develop 6 lbs/ft^2 shear stress).

A slag mix containing no lime source reached 6 lbs/ft^2 gel strength in 35 min. It reached 30 lbs/ft^2 after 400 min and was still pourable at the end of this run.

For comparison, the gel strength development of the class H cement-Class C fly ash mix (former reference) is shown in Figure 5. This mix gelled to 6 lbs/ft^2 in 2 min. and to 40 lbs/ft^2 in 8.5 min. It was not pourable after termination of the run.

Thermal Properties

The effects of fly ash source on the adiabatic temperature rise and set time are summarized in Table V and Figure 6. In mix I, ashes from the Bowen and Belews Creek Plants have similar temperature rises (54 and 52°C) and set in 3 and 7 hrs., respectively. A lower temperature rise of 37°C was obtained for the grout containing ash from the Marshall Plant. In the $Ca(OH)_2$ system, Marshall ash is probably less reactive than the other two fly ashes.

The average set time of slag mix II is 32 hr. compared to 5 hr. for slag mix I. This longer set time is attributed to delayed hydration of the tri- and dicalcium silicates in the cement which release Ca^{+2}, thereby activating the slag hydration. The adiabatic temperature rise for mix II is similar to that of mix I. The Marshall ash again resulted in the lowest temperature rise of 42°C. Mixes containing Bowen and Belews Creek ashes had temperature rises of 48 and 53°C, respectively.

Ambient temperature of starting materials in all of these tests was 26°C. Consequently, the maximum adiabatic temperature measured was 26°C + the adiabatic temperature rise.

Cold Run-In Formulations

Water and 50 wt% caustic solution were substituted for 29 wt% salt solution in slag mixes I and II. A water to cementitious solids ratio of 0.49 was used. Rheological properties of the resulting grouts were measured and are summarized in Table VI. Cold run-in formulations made with potable water have rheological properties similar to mixes made with salt solution and are suitable for cold run-in of the saltstone facility. Mixes made with 50% caustic solution did not set for at least 60 days and are consequently unacceptable.

Lack of set is attributed to the very high pH of this solution which probably resulted in dissolution rather than hydration of the cementitious solids.

Fly Ash Variability

As discussed earlier in this report, fly ashes from three different sources, Bowen, Marshall, and Belews Creek power plants were evaluated for processing. (SRP D-Area ash was also tested, DPST-86-864.) Although the resulting grouts had different set times, temperature rises and rheological properties, the ranges measured were within the limits of processability as defined by comparison to properties of the saltstone processed at the full scale Halliburton demonstration.

Fly ashes from these sources were also used to prepare leach samples. Effective diffusivities for NO_3^- and Cr are summarized in Table VII. Leach data are tabulated and cumulative fractions leached versus time are plotted in Appendix II. Effective NO_3^- diffusion coefficients range from 3.5×10^{-9} to 4.2×1^{-10} for slag mixes I and II made with the various fly ashes. The chromium effective diffusion coefficient ranges from 4.0×10^{-13} to 6.2×10^{-14} for the same mixes. Mix II (containing cement as the lime source) has higher D_{eff} NO_3 but lower D_{eff} Cr than Mix I (containing $Ca(OH)_2$ as the lime source). Additional data are needed for a statistical correlation of performance with fly ash source and for detailed interpretation of results. However, all slag mixes tested in this study have improved leaching properties relative to the former cement-based mix.

Vendor analyses of these ashes are attached in Appendix III. Ashes which have chemical and physical properties similar to these ashes are expected to perform similarly in the saltstone formulation.

CONCLUSIONS

- Slag-Class F fly ash mixes have comparable or improved physical properties (compressive strength, rheology, thickening time, and thermal properties) compared to the Class H cement-Class C fly ash saltstone mix.

- Fly ashes from three different power plants resulted in some variability in rheological and thermal properties. However, processing will not be significantly impacted by the amount of variation seen in this study. The variability in fly ash properties are typical of commercially available Class F fly ash. Other Class F fly ashes which are within the range of ASTM 618 chemical and physical properties as were the three ashes tested are expected to result in acceptable saltstone.

- The use of $Ca(OH)_2$ as a lime source has some advantages over use of portland cement, ie., slower gelation but faster setting. However, set time and gelation of the cement mix was improved relative to the former reference mix and is therefore considered acceptable.

- Water can be used in the slag saltstone formulation instead of salt solution for cold run in. A water to cementitious solids ratio of 0.5 is recommended.

REFERENCES

1. C. A. Langton, unpublished data.

2. C. A. Langton, "Halliburton Laboratory Report - Saltstone Slurry Properties", DPST-85-875, October 28, 1985.

3. C. A. Langton and E. L. Wilhite, "Trip Report, Slurry Property Evaluation at Halliburton, February 1985", DPST-85-469, April 23, 1985.

CAL/tyb
87-673

TABLE I

INGREDIENTS IN SLAG MIXES I AND II

Component	Slag Mix I wt%	Slag Mix II wt%
Slag	26	24
Class F fly ash	26	24
Lime source	3 ($Ca(OH)_2$)	5 (Type II cement)
Simulated DWPF salt solution (29 wt% salt)	45	47

TABLE 2. Compressive Strength Measurements for Slag Saltstones

TIME (days)	COMPRESSIVE STRENGTH SLAG 1 (kg/sqcm)	(lbs/sqin)	COMPRESSIVE STRENGTH SLAG 2 (kg/sqcm)	(lbs/sqin)
7	115	1632	118	1679
	91	1295	64	911
	93	1323	118	1679
AVE =	100	1423	100	1423
STD =	11	149	25	356
14	117	1665	101	1437
	130	1850	116	1651
	130	1850	86	1224
AVE =	126	1793	101	1437
STD =	6	90	12	174
28	132	1878	138	1964
	147	2092	138	1964
	166	2362	130	1850
AVE =	149	2113	135	1926
STD =	14	199	4	54

FIGURE 1. Averaged Compressive Strength As a Function of Curing Time

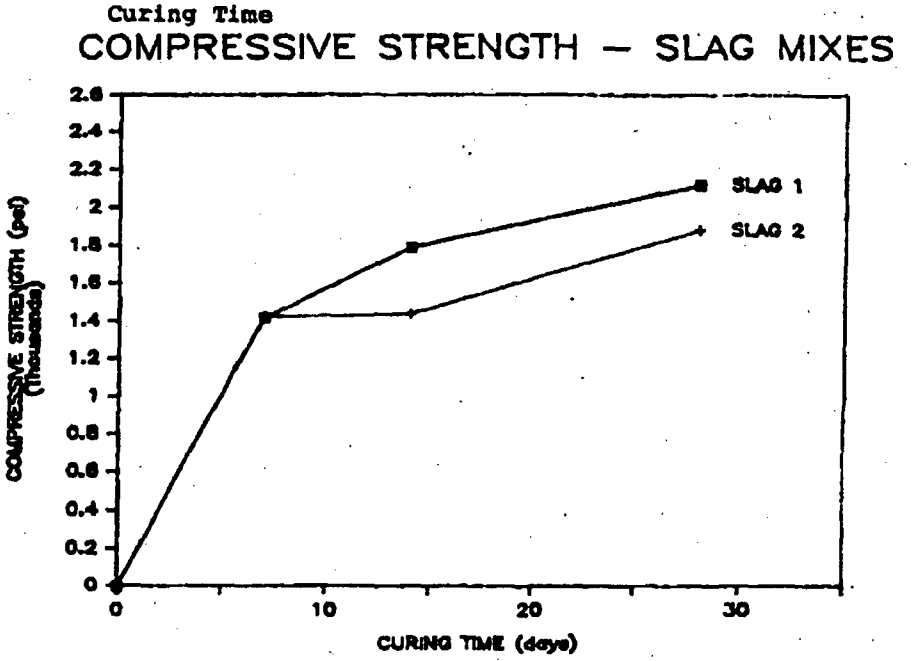

TABLE 3. Rheological Properties of Slag Saltstone.

MIX	PLASTIC VISCOSITY (cp)	YIELD POINT (lb/100ft2)	YIELD POINT (dynes/cm2)	10 MIN. GEL STRENGTH (lb/100ft2)	10 MIN. GEL STRENGTH (dynes/cm2)
SLAG 1-1	19	47	225	170	814
2	21	48	230	180	862
3	32	33	158	170	814
4	31	31	148	140	670
5	32	24	115	166	795
AVE.	27	36.6	175	165.2	791
STD. DEV.	5.8	9.4	45	13.4	64
SLAG 2-1	21	6	29	620	2969
2	20	8	38	620	2969
3	22	7	34	615	2945
4	21	6	29	600	2873
5	20	5	24	620	2969
AVE.	20.8	6.4	31	615	2945
STD. DEV.	0.7	1.0	5	7.7	37

FIGURE 2. Shear Stress vs. Shear Rate for Slag Mix I.

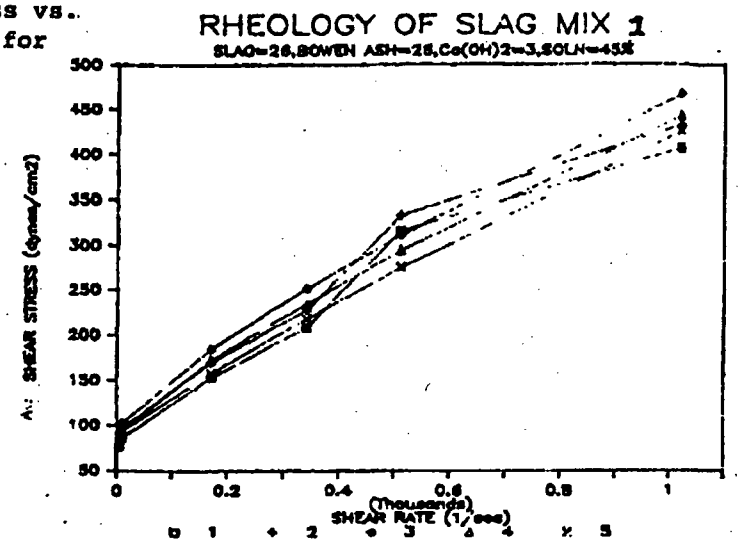

FIGURE 3. Shear Stress vs. Shear Rate for Slag Mix II.

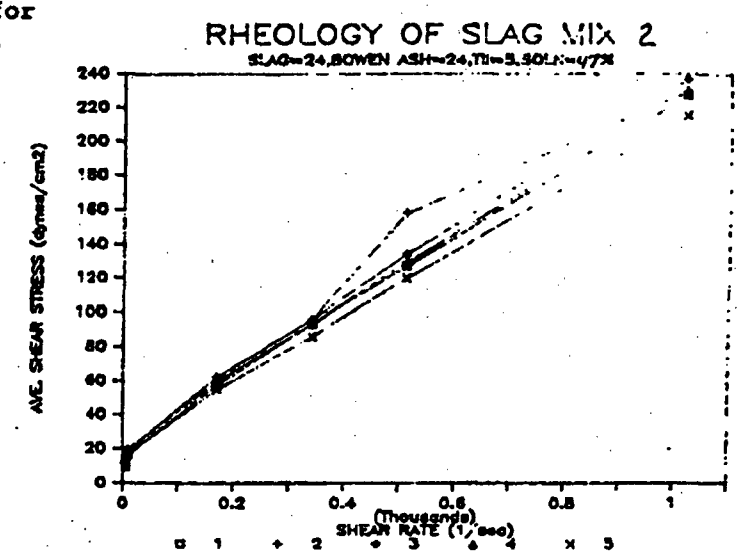

TABLE IV

THICKENING TIME OF SLAG SALTSTONES AS A FUNCTION OF FLY ASH SOURCE

Mix No.	Ingredients wt%		Time to Gel 6 lbs/ft2* min	Time to Gel 40 lbs/ft2* min
Slag I	26	Slag	40	>60
	26	Bowen Fly Ash		
	3	$Ca(OH)_2$		
	45	Salt Solution		
	26	Slag	8	85
	26	Marshall Fly Ash		
	3	$Ca(OH)_2$		
	45	Salt Solution		
	26	Slag	8	200^+
	26	Belews Creek Fly Ash		
	3	$Ca(OH)_2$		
	45	Salt Solution		
Slag II	24	Slag	3	11
	24	Bowen Fly Ash		
	5	Type II Cement		
	47	Salt Solution		
	24	Slag	5	12
	24	Marshall Fly Ash		
	5	Type II Cement		
	47	Salt Solution		
	24	Slag	4	9
	24	Belews Creek Fly Ash		
	5	Type II Cement		
	47	Salt Solution		
Slag II Modified	24	Slag	11	26
	24	Bowen Fly Ash		
	3	Type II Cement		
	49	Salt Solution		
Slag CaO	27	Slag	35	400^+
	27	Bowen		
	46	Salt Solution		
Cement-C Ash Former Reference	11.5	Class H Cement	2	8.5
	46	Class C Fly Ash		
	42.5	Salt Solution		

* 1 lb/ft^2 = 478 $dynes/cm^2$

TABLE V

ADIABATIC TEMPERATURE RISES AND SET TIMES OF SLAG SALTSTONES I AND II MADE FROM DIFFERENT CLASS F FLY ASHES

Adiabatic Temperature Rise, °C		Set Time, Hr.
Slag Mix I		
Bowen	54	3
Marshall	37	5
Belews Creek	52	7
Slag Mix II		
Bowen	48	28
Marshall	42	32
Belews Creek	53	35

TABLE VI

RHEOLOGICAL PROPERTIES OF FORMULATIONS TESTED AS CANDIDATES FOR THE COLD RUN IN STARTUP OF Z-AREA

Mix No.	Ingredients (wt%)	Plastic Viscosity (cp)	Yield Point (lbs/100 ft^2)	Yield Point ($dynes/cm^2$)	10 min Gel Strength (lbs/100 ft^2)	10 min Gel Strength ($dynes/cm^2$)	Set Time (days)	Free H_2O
1-727	Slag = 32.1 F Fly Ash = 32.1 $Ca(OH)_2$ = 3.8 H_2O = 32	46	75		30		<5	5 ml/125 ml
3-777	Slag = 30.3 F Fly Ash = 30.3 Type II Cement = 6.4 H_2O = 33	33	34	163	40	192	1	1 ml/125 ml
2-727	Slag = 17 F Fly Ash = 17 $Ca(OH)_2$ = 2 $Na(OH)_2$ = 64 50% Solution	162	13		190		Unset after 60 days	None
4-777	Slag = 15.4 F Fly Ash = 15.4 Type II Cement = 3.2 Na(OH) 50% = 66 Solution	150	12		190		Unset after 60 days	None

TABLE VII

EFFECTIVE DIFFUSION COEFFICIENTS FOR SLAG MIXES I AND II MADE FROM VARIOUS FLY ASHES

Fly Ash Source	Slag Mix I D_{eff} (cm^2/sec) NO_3	Slag Mix I D_{eff} (cm^2/sec) Cr	Slag Mix II D_{eff} (cm^2/sec) NO_3	Slag Mix II D_{eff} (cm^2/sec) Cr
Bowen	8.5×10^{-10}	---	Test in Progress	
Marshall	7.2×10^{-10}	4.0×10^{-13}	3.5×10^{-9}	1.3×10^{-13}
Belews Creek	4.2×10^{-10}	1.2×10^{-13}	2.6×10^{-9}	6.2×10^{-14}
D-Area	1.9×10^{-9}	---	---	---

FIGURE 4. Thickening (Blade Pressure) vs. Time at Near Static Conditions for Slag Saltstones I and II As a Function of Fly Ash Source

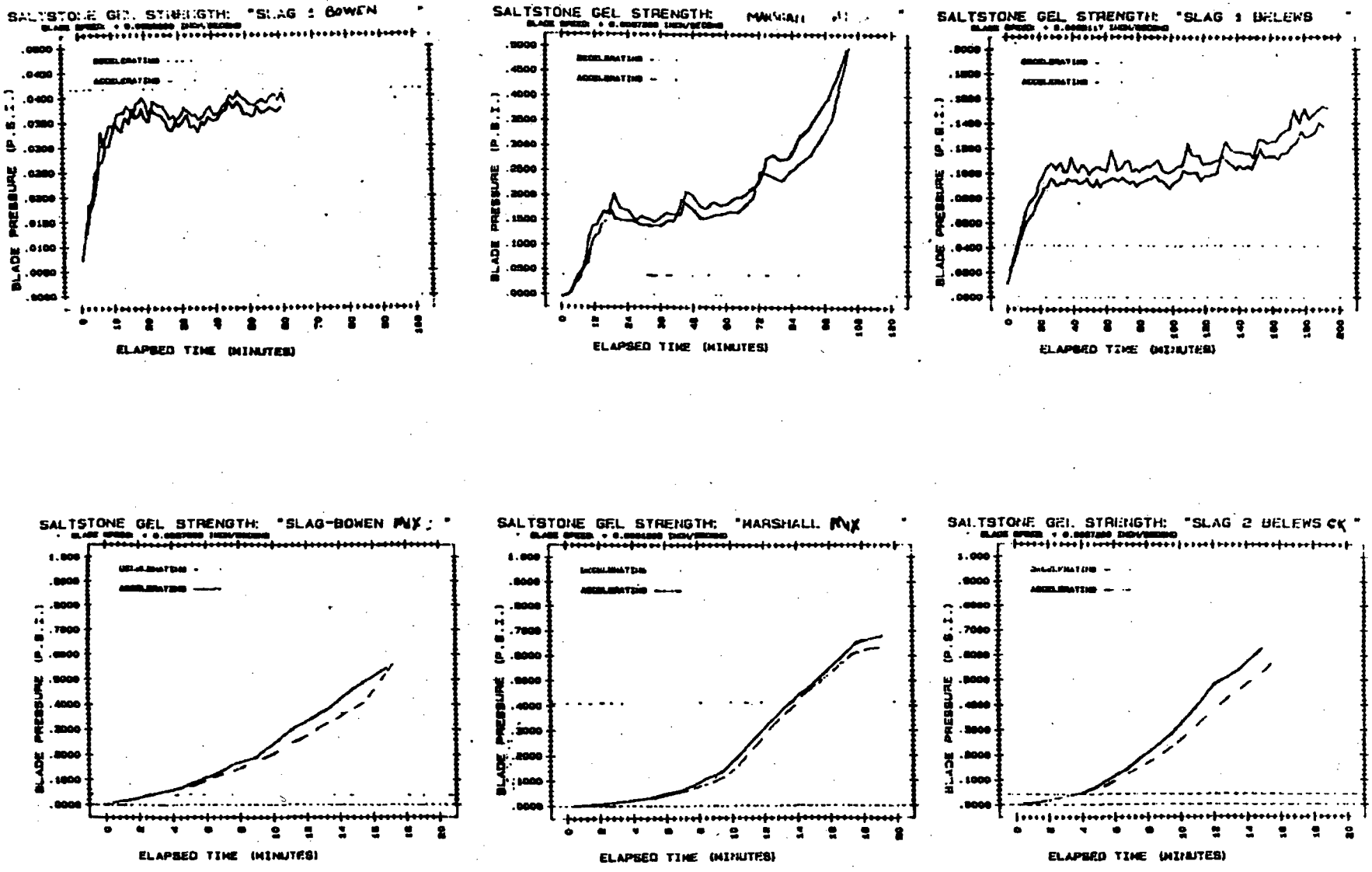

FIGURE 5. Thickening (Blade Pressure) vs. Time of Modified Slag Saltstones and the Former Reference Mix

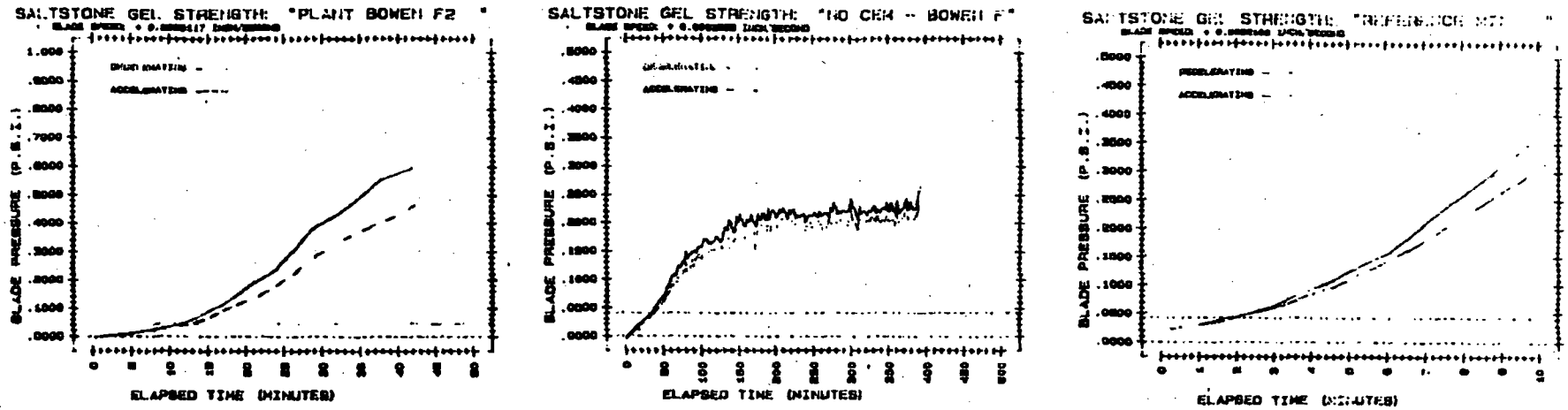

FIGURE 6. Adiabatic Temperature Rise vs. Time for Slag Mixes I and II

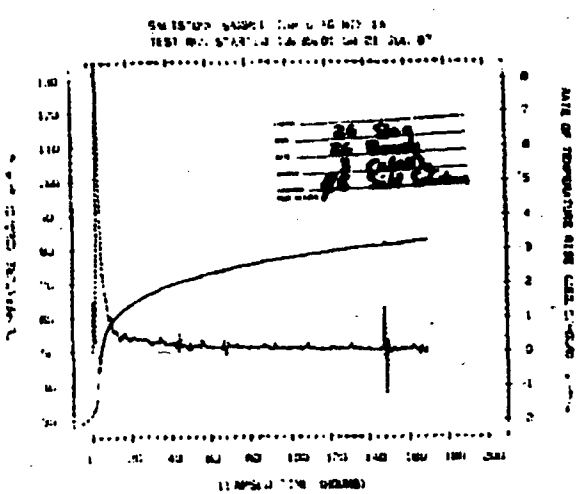

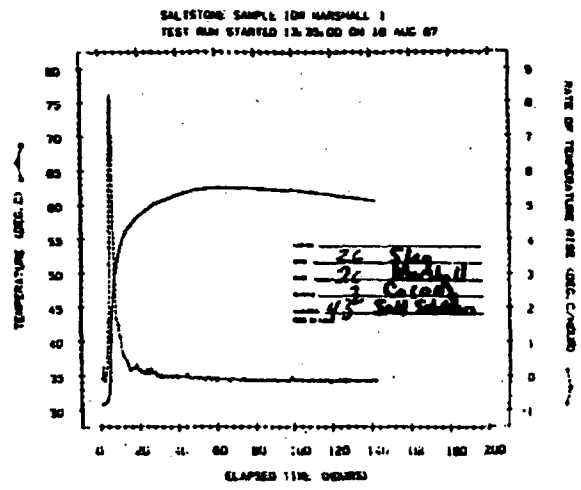

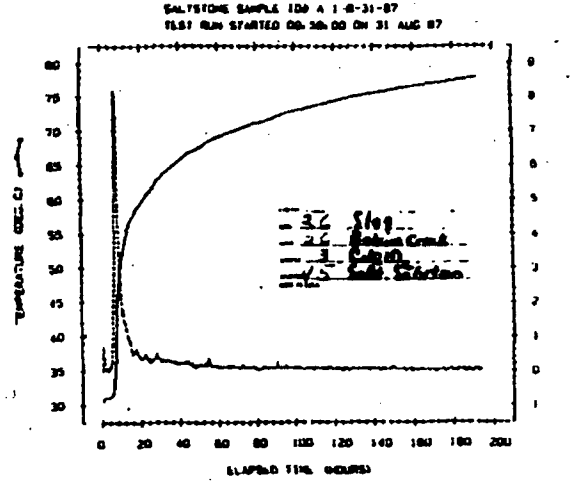

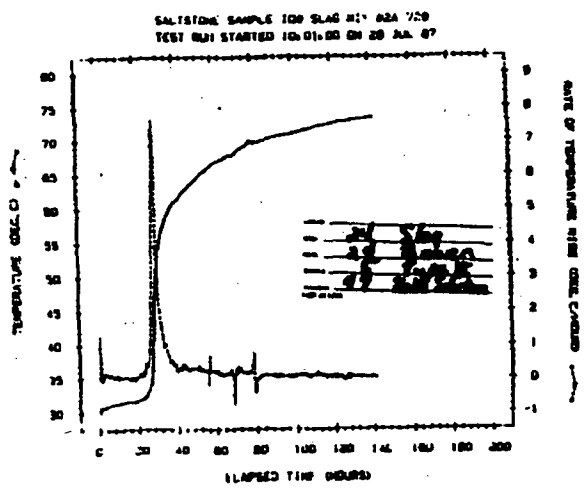

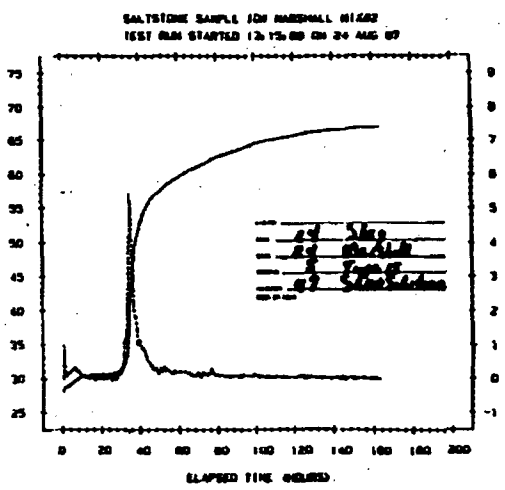

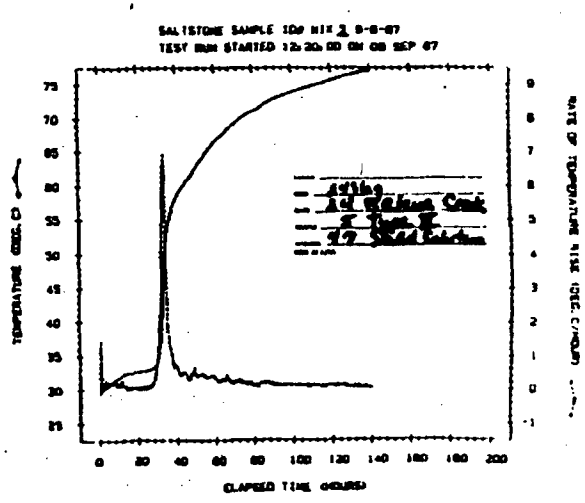

APPENDIX I

RAW DATA - RHEOLOGICAL PROPERTIES

SLAG 1 -1 (5-29-87)

SHEAR RATE	SHEAR STRESS lbs/100ft2			SHEAR RATE	SHEAR STRESS dynes/cm2		
rpm	1-h	h-1	ave.	(1/sec)	1-h	h-1	ave.
3	16	16	16	5.1	77	77	77
6	18	18	18	10.2	86	86	86
100	33	31	32	170	158	148	153
200	45	42	44	340	215	201	208
300	60	72	66	511	287	345	316
600	88	82	85	1021	421	393	407

SLAG 1 -2 (6-10-87)

SHEAR RATE	SHEAR STRESS lbs/100ft2			SHEAR RATE	SHEAR STRESS dynes/cm2		
rpm		h-1	ave.	(1/sec)	1-h	h-1	ave.
3	18	18	18	5.1	86	86	86
6	21	20	21	10.2	101	96	98
100	37	34	36	170	177	163	170
200	50	45	48	340	239	215	227
300	63	76	70	511	302	364	333
600	94	87	91	1021	450	417	433

SLAG 1-3 (5-29-87)

SHEAR RATE	SHEAR STRESS lbs/100ft2			SHEAR RATE	SHEAR STRESS dynes/cm2		
rpm	1-h	h-1	ave.	(1/sec)	1-h	h-1	ave.
3	19	19	19	5.1	91	91	91
6	22	21	22	10.2	105	101	103
100	40	37	39	170	192	177	184
200	55	50	53	340	263	239	251
300	68	62	65	511	326	297	311
600	100	95	98	1021	479	455	467

SLAG 1 -4 (5-29-87)

SHEAR RATE	SHEAR STRESS lbs/100ft2			SHEAR RATE	SHEAR STRESS dynes/cm2		
rpm	1-h	h-1	ave.	(1/sec)	1-h	h-1	ave.
3	18	18	18	5.1	86	86	86
6	20	19	20	10.2	96	91	93
100	37	35	36	170	177	168	172
200	51	47	49	340	244	225	235
300	65	58	62	511	311	278	294
600	96	89	93	1021	460	426	443

SLAG 1 -5 (5-29-87)

SHEAR RATE	SHEAR STRESS lbs/100ft2			SHEAR RATE	SHEAR STRESS dynes/cm2		
rpm	1-h	h-1	ave.	(1/sec)	1-h	h-1	ave.
3	18	18	18	5.1	86	86	86
6	20	19	20	10.2	96	91	93
100	34	32	33	170	163	153	158
200	47	44	46	340	225	211	218
300	60	55	58	511	287	263	275
600	92	86	89	1021	440	412	426

SLAG -1 (6-10-87)

SHEAR RATE	SHEAR STRESS lbs/100ft2			SHEAR RATE	SHEAR STRESS dynes/cm2		
rpm	1-h	h-1	ave.	(1/sec)	1-h	h-1	ave.
3	2	2	2	5.1	10	10	10
6	4	3	4	10.2	19	14	17
100	13	11	12	170	62	53	57
200	21	18	20	340	101	86	93
300	30	23	27	511	144	110	127
600	53	42	48	1021	254	201	227

SLAG 2 -2 (6-10-87)

SHEAR RATE	SHEAR STRESS lbs/100ft2			SHEAR RATE	SHEAR STRESS dynes/cm2		
rpm	1-h	h-1	ave.	(1/sec)	1-h	h-1	ave.
3	3	3	3	5.1	14	14	14
6	4	4	4	10.2	19	19	19
100	14	12	13	170	67	57	62
200	22	18	20	340	105	86	96
300	32	34	33	511	153	163	158
600	52	44	48	1021	249	211	230

SLAG 2 -3 (6-9-87)

SHEAR RATE	SHEAR STRESS lbs/100ft2			SHEAR RATE	SHEAR STRESS dynes/cm2		
rpm	1-h	h-1	ave.	(1/sec)	1-h	h-1	ave.
3	3	3	3	5.1	14	14	14
6	4	4	4	10.2	19	19	19
100	14	12	13	170	67	57	62
200	22	18	20	340	105	86	96
300	32	24	28	511	153	115	134
600	56	43	50	1021	268	206	237

SLAG 3 -4 (6-9-87)

SHEAR RATE	SHEAR STRESS lbs/100ft2			SHEAR RATE	SHEAR STRESS dynes/cm2		
rpm	1-h	h-1	ave.	(1/sec)	1-h	h-1	ave.
3	2	2	2	5.1	10	10	10
6	4	4	4	10.2	19	19	19
100	14	11	13	170	67	53	60
200	22	17	20	340	105	81	93
300	31	23	27	511	148	110	129
600	54	42	48	1021	259	201	230

SLAG 2 -5 (6-9-87)

SHEAR RATE	SHEAR STRESS lbs/100ft2			SHEAR RATE	SHEAR STRESS dynes/cm2		
rpm	1-h	h-1	ave.	(1/sec)	1-h	h-1	ave.
3	3	3	3	5.1	14	14	14
6	4	3	4	10.2	19	14	17
100	13	10	12	170	62	48	55
200	20	16	18	340	96	77	86
300	28	22	25	511	134	105	120
600	48	42	45	1021	230	201	215

APPENDIX II

LEACH DATA FOR SLAG SALTSTONE AS A FUNCTION OF FLY ASH SOURCE AND TYPE OF LIME SOURCE

NO3 LEACHING VERSUS MIX INGREDIENTS

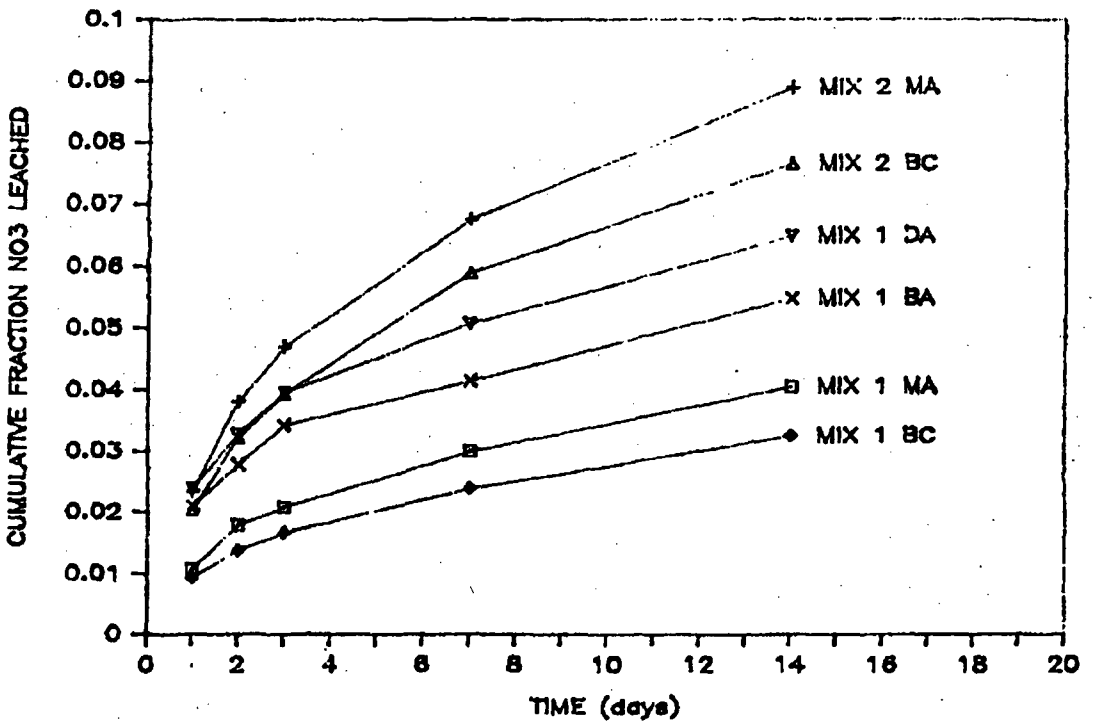

Mix 1
- 26 Slag
- 26 Class F fly ash
- 3 $Ca(OH)_2$
- 45 DWPF Salt Solution

Mix 2
- 24 Slag
- 24 Class F fly ash
- 5 Type II cement
- 47 DWPF salt solution

LEACH INTERVAL (days)	NO3 CUMULATIVE FRACTION LEACHED ---------- SERIES 723 ---------- 1A&B	2A&B	3A&B	4A&B	815 2E	826 2A&B
1	0.0106	0.0234	0.0094	0.0203	0.021	0.024
2	0.0178	0.0381	0.0137	0.0322	0.0278	0.0327
3	0.0208	0.0469	0.0165	0.0394	0.0342	0.0396
7	0.0299	0.0674	0.0239	0.0589	0.0415	0.0507
14	0.0405	0.0898	0.0324	0.0764	0.0547	0.0648

BA = Bowen Ash
BC = Belews Creek Ash
DA = SRP D-Area Precipitator Ash
MA = Marshall Ash

Cr LEACHING VERSUS MIX INGREDIENTS

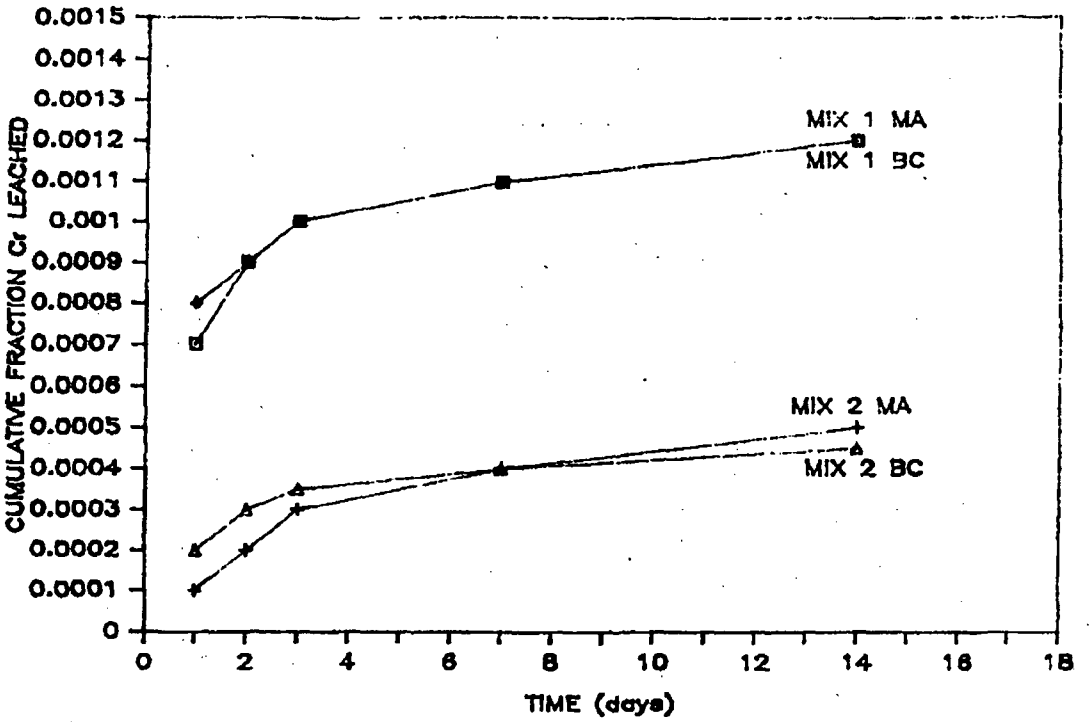

	Cr CUMULATIVE FRACTION LEACHED SERIES 723			
Leach Time Days	1A&B	2A&B	3A&B	4A&B
1	0.0007	0.0001	0.0008	0.0002
2	0.0009	0.0002	0.0009	0.0003
3	0.001	0.003	0.001	0.00035
7	0.0011	0.0004	0.0011	0.0004
14	0.0012	0.0005	0.0012	0.00045

Sample No.	Sample Comp (wt %)	Sample Mass (gm)	NO3 Waste Form (wt %)	NO3 Waste Form Mo (gm)	NO3 Mass Fraction	Sample Surface Area S (cm2)	Sample Volume V (cm3)	Sample Aspect Ratio V/S (cm)	Leachate Volume (ml)	Leach Time (days)	Leach Interval (days)	NO3 Leached #1 (mg/l)	NO3 Leached #2 (mg/l)	NO3 Leached Ave. (mg/l)	NO3 Leached Ave Mass Mi (gm)	NO3 BLR Bulk Leach Rate gm/cm2-d	NO3 NLR Norm Leach Rate gm/cm2-d	Cumulative NO3 Leached (g)	Cumulative Fract. NO3 Leached Sum Mi/Mo	Eff. D cm2/sec
1A 723	26% SLAG 260 MARSHALL ASH	178.00	4.72	8.41	0.0472	126.53	106.56	0.84	500.00	0										
1B 723	3% Ca(OH) 45% DMPP SOLN (29%SALT)	175.00	4.73	8.27	0.0473	123.70	103.38	0.84	500.00	1	1	197	152	174.5	0.09	6.97E-04	1.48E-02	0.09	0.0106	7.07E-10
										2	1	84	160	122	0.06	4.88E-04	1.03E-02	0.15	0.0178	1.92E-09
	source NO3 129.284 g/l				radius A=	2.25	6.70	=height A		3	1	56	50	53	0.03	2.12E-04	4.48E-03	0.17	0.0208	5.97E-10
					radius B=	2.25	6.50	=height B		7	4	168	143	151.5	0.08	2.42E-03	3.20E-03	0.25	0.0299	6.31E-10
										14	7	181	172	176.5	0.09	4.94E-03	2.13E-03	0.34	0.0405	5.85E-10

Sample No.	Sample Comp (wt %)	Sample Mass (gm)	NO3 Waste Form (wt %)	NO3 Waste Form Mo (gm)	NO3 Mass Fraction	Sample Surface Area S (cm2)	Sample Volume V (cm3)	Sample Aspect Ratio V/S (cm)	Leachate Volume (ml)	Leach Time (days)	Leach Interval (days)	NO3 Leached #1 (mg/l)	NO3 Leached #2 (mg/l)	NO3 Leached Ave. (mg/l)	NO3 Leached Ave Mass Mi (gm)	NO3 BLR Bulk Leach Rate gm/cm2-d	NO3 NLR Norm Leach Rate gm/cm2-d	Cumulative NO3 Leached (g)	Cumulative Fract. NO3 Leached Sum Mi/Mo	Eff. D cm2/sec
2A 723	26% SLAG 260 MARSHALL ASH	189.00	4.94	9.33	0.0494	127.94	108.15	0.85	500.00	0										
2B 723	5% TII 47% DMPP SOLN (29%SALT)	192.00	4.94	9.48	0.0494	129.36	109.74	0.85	500.00	1	1	437	456	446.5	0.22	1.74E-03	3.51E-02	0.22	0.0235	3.63E-09
										2	1	284	252	268	0.13	1.04E-03	2.11E-02	0.36	0.0381	8.03E-09
	source NO3 129.184 g/l				radius A=	2.25	6.80	=height A		3	1	166	159	162.5	0.08	6.32E-04	1.28E-02	0.44	0.0469	5.01E-09
					radius B=	2.25	6.90	=height B		7	4	388	395	387.5	0.19	6.02E-03	7.63E-03	0.63	0.0674	3.32E-09
										14	7	401	396	398.5	0.20	1.08E-02	4.48E-03	0.83	0.0888	2.48E-09

Sample No.	Sample Comp (wt %)	Sample Mass (gm)	NO3 Waste Form (wt %)	NO3 Waste Form Mo (gm)	NO3 Mass Fraction	Sample Surface Area S (cm2)	Sample Volume V (cm3)	Sample Aspect Ratio V/S (cm)	Leachate Volume (ml)	Leach Time (days)	Leach Interval (days)	NO3 Leached #1 (mg/l)	NO3 Leached #2 (mg/l)	NO3 Leached Ave. (mg/l)	NO3 Leached Ave Mass Mi (gm)	NO3 BLR Bulk Leach Rate gm/cm2-d	NO3 NLR Norm Leach Rate gm/cm2-d	Cumulative NO3 Leached (g)	Cumulative Fract. NO3 Leached Sum Mi/Mo	Eff. D cm2/sec
3A 723	26% SLAG 26% BELENS CREEK ASH	164.00	4.73	7.75	0.0473	118.85	97.02	0.82	500.00	0										
3B 723	3% Ca(OH) 45% DMPP SOLN (29%SALT)	170.00	4.72	8.03	0.0472	120.87	100.20	0.83	500.00	1	1	137	164	150.5	0.08	6.38E-04	1.33E-02	0.08	0.0094	5.49E-10
										2	1	63	65	64	0.03	2.68E-04	5.67E-03	0.11	0.0137	6.81E-10
	source NO3 129.184 g/l				radius A=	2.25	6.10	=height A		3	1	43	44	43.5	0.02	1.82E-04	3.85E-03	0.13	0.0165	5.03E-10
					radius B=	2.25	6.30	=height B		7	4	112	122	117	0.06	1.96E-03	2.59E-03	0.19	0.0239	4.08E-10
										14	7	133	129	131	0.07	3.84E-03	1.66E-03	0.25	0.0324	3.69E-10

Sample No.	Sample Comp (wt %)	Sample Mass (gm)	NO3 Waste Form (wt %)	NO3 Waste Form Mo (gm)	NO3 Mass Fraction	Sample Surface Area S (cm2)	Sample Volume V (cm3)	Sample Aspect Ratio V/S (cm)	Leachate Volume (ml)	Leach Time (days)	Leach Interval (days)	NO3 Leached #1 (mg/l)	NO3 Leached #2 (mg/l)	NO3 Leached Ave. (mg/l)	NO3 Leached Ave Mass Mi (gm)	NO3 BLR Bulk Leach Rate gm/cm2-d	NO3 NLR Norm Leach Rate gm/cm2-d	Cumulative NO3 Leached (g)	Cumulative Fract. NO3 Leached Sum Mi/Mo	Eff. D cm2/sec
4A 723	26% SLAG 26%BELENS CREEK ASH	179.00	4.94	8.86	0.0494	123.78	103.38	0.84	500.00	0										
4B 723	5% TII 47% DMPP SOLN (29%SALT)	180.00	4.93	8.88	0.0493	125.11	104.97	0.84	500.00	1	1	325	395	360	0.18	1.45E-03	2.93E-02	0.18	0.0207	2.63E-09
										2	1	217	204	210.5	0.11	8.46E-04	1.71E-02	0.29	0.0323	5.32E-09
	source NO3 129.184 g/l				radius A=	2.25	6.50	=height A		3	1	132	122	127	0.06	5.10E-04	1.03E-02	0.35	0.0394	3.29E-09
					radius B=	2.25	6.60	=height B		7	4	345	346	345.5	0.17	5.55E-03	7.04E-03	0.52	0.0589	2.91E-09
										14	7	303	314	308.5	0.15	8.68E-03	3.59E-03	0.68	0.0764	1.62E-09

Cr Leaching

Sample No.	Sample Comp (wt %)	Sample Mass (gm)	Cr+6 Waste Solution (ppm)	Cr+6 Waste Form No (mg)	Sample Surface Area S (cm2)	Sample Volume V (cm3)	Sample Aspect Ratio V/S (cm)	Leachate Volume (ml)	Leach Time (days)	Leach Interval (days)	Cr+6 Leached A (mg/l)	Cr+6 Leached B (mg/l)	Cr+6 Leached Ave. (mg/l)	Cr+6 Leached Ave Mass (mg)	Cr+6 Bulk Leach Rate mg/cm2-d	Cumulative Cr+6 Leached (mg)	Fract. Cr+6 Leached Sum mg1/mgo	Eff. D Cr+6 (cm2/sec)
1A 723	26% SLAG 26% MARSHALL ASH	178	2430	158	126.53	106.56	0.84	500.00	0									
1B 723	38 Ca(OH) 45% DMPP SOLN (29%SALT)	175	2430	156	123.78	103.38	0.84	500.00	1	1	0.241	0.201	0.222	0.11	8.87E-04	0.11	0.0007	1.17E-12
									2	1	0.0571	0.057	0.05705	0.03	3.28E-04	0.14	0.0009	1.22E-12
					2.25	6.70	=height A		3	1	0.03	0.0238	0.0269	0.01	1.08E-04	0.15	0.0010	4.61E-13
					2.25	6.50	=height B		7	4	0.0315	0.0282	0.02985	0.01	4.77E-04	0.17	0.0011	6.87E-14
									14	7	0.0503	0.0282	0.03925	0.02	1.10E-03	0.19	0.0013	8.26E-14

Sample No.	Sample Comp (wt %)	Sample Mass (gm)	Cr+6 Waste Solution (ppm)	Cr+6 Waste Form No (mg)	Sample Surface Area S (cm2)	Sample Volume V (cm3)	Sample Aspect Ratio V/S (cm)	Leachate Volume (ml)	Leach Time (days)	Leach Interval (days)	Cr+6 Leached A (mg/l)	Cr+6 Leached B (mg/l)	Cr+6 Leached Ave. (mg/l)	Cr+6 Leached Ave Mass (mg)	Cr+6 Bulk Leach Rate mg/cm2-d	Cumulative Cr+6 Leached (mg)	Fract. Cr+6 Leached Sum mg1/mgo	Eff. D Cr+6 (cm2/sec)
2A 723	24% SLAG 24% MARSHALL ASH	189	2430	175	127.96	108.15	0.85	500.00	0									
2B 723	5% TII 47% DMPP SOLN (29%SALT)	192	2430	178	129.36	109.74	0.85	500.00	1	1	0.0314	0.036	0.0337	0.02	1.33E-04	0.02	0.0001	5.96E-14
									2	1	0.0354	0.0294	0.0324	0.02	1.28E-04	0.03	0.0002	3.21E-13
			radius		2.25	6.80	=height A		3	1	0.0262	0.0252	0.0257	0.01	9.99E-05	0.05	0.0003	3.41E-13
			radius		2.25	6.90	=height B		7	4	0.037	0.0387	0.03385	0.02	5.26E-04	0.06	0.0004	7.21E-14
									14	7	0.0655	0.0554	0.06045	0.03	1.64E-03	0.09	0.0005	1.60E-13

Sample No.	Sample Comp (wt %)	Sample Mass (gm)	Cr+6 Waste Solution (ppm)	Cr+6 Waste Form No (mg)	Sample Surface Area S (cm2)	Sample Volume V (cm3)	Sample Aspect Ratio V/S (cm)	Leachate Volume (ml)	Leach Time (days)	Leach Interval (days)	Cr+6 Leached A (mg/l)	Cr+6 Leached B (mg/l)	Cr+6 Leached Ave. (mg/l)	Cr+6 Leached Ave Mass (mg)	Cr+6 Bulk Leach Rate mg/cm2-d	Cumulative Cr+6 Leached (mg)	Fract. Cr+6 Leached Sum mg1/mgo	Eff. D Cr+6 (cm2/sec)
3A 723	26% SLAG 26% BELENS CREEK ASH	164	2430	165	126.05	97.02	0.82	500.00	0									
3B 723	38 Ca(OH) 45% DMPP SOLN (29%SALT)	170	2430	151	120.87	100.20	0.83	500.00	1	1	0.218	0.231	0.2245	0.11	9.40E-04	0.11	0.0008	1.57E-12
									2	1	0.051	0.0432	0.0471	0.02	1.97E-04	0.14	0.0009	9.36E-13
			radius		2.25	6.10	=height A		3	1	0.0222	0.0225	0.02235	0.01	9.35E-05	0.15	0.0010	3.50E-13
			radius		2.25	6.30	=height B		7	4	0.0263	0.0321	0.0292	0.01	4.89E-04	0.16	0.0011	7.23E-14
									14	7	0.0445	0.0396	0.04205	0.02	1.21E-03	0.18	0.0012	1.04E-13

Sample No.	Sample Comp (wt %)	Sample Mass (gm)	Cr+6 Waste Solution (ppm)	Cr+6 Waste Form No (mg)	Sample Surface Area S (cm2)	Sample Volume V (cm3)	Sample Aspect Ratio V/S (cm)	Leachate Volume (ml)	Leach Time (days)	Leach Interval (days)	Cr+6 Leached A (mg/l)	Cr+6 Leached B (mg/l)	Cr+6 Leached Ave. (mg/l)	Cr+6 Leached Ave Mass (mg)	Cr+6 Bulk Leach Rate mg/cm2-d	Cumulative Cr+6 Leached (mg)	Fract. Cr+6 Leached Sum mg1/mgo	Eff. D Cr+6 (cm2/sec)
4A 723	24% SLAG 24% BELENS CREEK ASH	179	2430	166	123.78	103.38	0.84	500.00	0									
4B 723	5% TII 47% DMPP SOLN (29%SALT)	188	2430	167	125.11	104.97	0.84	500.00	1	1	0.0454	0.0586	0.052	0.03	2.09E-04	0.03	0.0002	1.56E-13
									2	1	0.0388	0.0321	0.03545	0.02	1.26E-04	0.04	0.0003	3.33E-13
			radius		2.25	6.50	=height A		3	1	0.0168	0.0185	0.01765	0.01	7.09E-05	0.05	0.0003	1.78E-13
			radius		2.25	6.60	=height B		7	4	0.0302	0.0282	0.0292	0.01	4.69E-04	0.07	0.0004	5.89E-14
									14	7	0.0184	0.0113	0.01885	0.01	3.05E-04	0.07	0.0004	5.66E-15

APPENDIX III

VENDOR ANALYSIS OF FLY ASHES
ASTM 618-80

Report of Fly Ash Analysis

Consulting Geotechnical, Materials and Environmental Engineers
Geologists, Scientists and Chemists

Raba-Kistner
Consultants, Inc.
P.O. Box 690287, San Antonio, TX 78269-0287
12821 W. Golden Lane, San Antonio, TX 78249
(512) 699-9090

Monier Resources, Inc.
Attn: Mr. Buddy Briscoe

Report No: SA0879-1004

Date: 3/9/87

Laboratory No: 8-9527

Project: Bowen Plant No. 1 Fly Ash Quality Assurance

Sample: 4th Quarter - 1986

Chemical Analysis	Results	Spec* Class F/C
Silicon Dioxide (SiO_2), %	48.5	
Aluminum Oxide (Al_2O_3), %	26.2	
Iron Oxide (Fe_2O_3), %	10.8	
Sum of SiO_2, Al_2O_3, Fe_2O_3, %	85.5	70.0/50.0 min.
Calcium Oxide (CaO), %	1.8	
Magnesium Oxide (MgO), %	0.9	5.0 max.
Sodium Oxide (Na_2O), %	0.32	
Potassium Oxide (K_2O), %	2.53	
Sulfur Trioxide (SO_3), %	0.7	5.0 max.
Moisture Content, %	0.1	3.0 max.
Loss on Ignition, %	1.5	12.0/6.0 max.
Available Alkalies (as Na_2O), %		1.50 max.
Available Sodium (as Na_2O), %		
Available Potassium (as K_2O), %		

Physical Analysis	Results	Spec*
Amount Retained on 325 Sieve, %	15.0	34 max.
Pozzolanic Activity Index with portland cement at 28 days, % of control	88.3	75 min.
with lime at 7 days, psi	1100	800 min.
Water Required, % of Control	93.4	105 max.
Autoclave Soundness, %	-.01	0.8 max.
Specific Gravity	2.37	
Multiple Factor, %		255 max.
Drying Shrinkage, %		0.03 max.
Reactivity with Cement Alkalies		
Reduction of expansion, %		75 min.
Mortar expansion, %		0.020 max.
Fineness		
Blaine air permeability, cm^2/cm^3		
Wagner turbidimetric, cm^2/g		

*ANSI/ASTM C618-80

Copies To: Above (1)
dgr 3/9

RABA-KISTNER CONSULTANTS, INC.

By Donald T. Fetzer
Donald T. Fetzer

7

1 1/2 D

Report of Fly Ash Analysis

Consulting Geotechnical, Materials and Environmental Engineers
Geologists, Scientists and Chemists

Raba-Kistner Consultants, Inc.

P.O. Box 690287, San Antonio, TX 78269-0287
12821 W. Golden Lane, San Antonio, TX 78249
(512) 699-9090

Monier Resources, Inc.
Attn: Mr. Buddy Briscoe

Report No: SA0879-1004

Date: 6/2/87

Laboratory No: 8-9671

Project: Bowen Plant No. 1 Fly Ash Quality Assurance

Sample: April, 1987 Monthly Composite

Chemical Analysis	Results	Spec* Class F/C
Silicon Dioxide (SiO_2), %	48.0	
Aluminum Oxide (Al_2O_3), %	27.1	
Iron Oxide (Fe_2O_3), %	10.4	
Sum of SiO_2, Al_2O_3, Fe_2O_3, %	85.5	70.0/50.0 min.
Sulfur Trioxide (SO_3), %	0.6	5.0 max.
Moisture Content, %	0.4	3.0 max.
Loss on Ignition, %	1.9	12.0/6.0 max.

Physical Analysis	Results	Spec*
Amount Retained on 325 Sieve, %	13.1	34 max.
Pozzolanic Activity Index with portland cement at 28 days, % of control		75 min.
with lime at 7 days, psi		800 min.
Water Required, % of Control		105 max.
Autoclave Expansion, %		0.8 max.
Specific Gravity	2.42	

*ANSI/ASTM C618-80

Copies To: Above (1)
jgr 6/2

Raba-Kistner Consultants, Inc.

By David P. Donnell

Donald T. Fetzer

Report of Fly Ash Analysis

DLN)

Consulting Geotechnical, Materials and Environmental Engineers
Geologists, Scientists and Chemists

Raba-Kistner
Consultants, Inc.
P.O. Box 690287, San Antonio, TX 78269-0287
12821 W. Golden Lane, San Antonio, TX 78249
(512) 699-9090

Monier Resources, Inc.
Attn: Mr. Buddy Briscoe

Report No: SA0879-1004

Date: 5/28/87

Laboratory No: 8-9629

Project: Bowen Plant No. 1 Fly Ash Quality Assurance

Sample: 1st Quarter - 1987 Composite

Chemical Analysis	Results	Spec* Class F/C
Silicon Dioxide (SiO_2), %		
Aluminum Oxide (Al_2O_3), %		
Iron Oxide (Fe_2O_3), %		
Sum of SiO_2, Al_2O_3, Fe_2O_3, %		70.0/50.0 min.
Sulfur Trioxide (SO_3), %		5.0 max.
Moisture Content, %		3.0 max.
Loss on Ignition, %		12.0/6.0 max.

Physical Analysis	Results	Spec*
Amount Retained on 325 Sieve, %		34 max.
Pozzolanic Activity Index - with portland cement at 28 days, % of control	96.0	75 min.
with lime at 7 days, psi	940	800 min.
Water Required, % of Control	90.5	105 max.
Autoclave Expansion, %	+.01	0.8 max.
Specific Gravity		

*ANSI/ASTM C618-80

Copies To: Above (1)
dgr 5/28

Raba-Kistner Consultants, Inc.

By Donald T. Fetzer
Donald T. Fetzer

1005

Report of Fly Ash Analysis

Consulting Geotechnical, Materials and Environmental Engineers
Geologists, Scientists and Chemists

Raba-Kistner Consultants, Inc

P O. Box 690287. San Antonio, TX 78269-0287
12821 W. Golden Lane. San Antonio, TX 78249
(512) 699-9090

Monier Resources, Inc.
Attn: Mr. Buddy Briscoe

Report No: SA0879-1009

Date: 6/2/87

Laboratory No: 8-9658

Project: Marshall Plant Fly Ash Quality Assurance

Sample: April, 1987 Monthly Composite

Chemical Analysis	Results	Spec* Class F/C
Silicon Dioxide (SiO_2), %	46.4	
Aluminum Oxide (Al_2O_3), %	30.6	
Iron Oxide (Fe_2O_3), %	8.9	
Sum of SiO_2, Al_2O_3, Fe_2O_3, %	85.9	70.0/50.0 min.
Sulfur Trioxide (SO_3), %	0.6	5.0 max.
Moisture Content, %	0.1	3.0 max.
Loss on Ignition, %	1.4	12.0/6.0 max.

Physical Analysis	Results	Spec*
Amount Retained on 325 Sieve, %	15.2	34 max.
Pozzolanic Activity Index with portland cement at 28 days, % of control	*89 6-18	75 min.
with lime at 7 days, psi	1050	800 min.
Water Required, % of Control	95.6	105 max.
Autoclave Expansion, %	+.02	0.8 max.
Specific Gravity	2.29	

*ANSI/ASTM C618-80

Copies To: Above (1)
dgr 6/2

* DATE DUE

Raba-Kistner Consultants, Inc.
By David P Donnell
Donald T. Fetzer

7

DNB

Report of Fly Ash Analysis

Consulting Geotechnical, Materials and Environmental Engineers
Geologists, Scientists and Chemists

Raba-Kistner
Consultants, Inc.
P.O. Box 690287, San Antonio, TX 78269-0287
12821 W. Golden Lane, San Antonio, TX 78249
(512) 699-9090

Monier Resources, Inc.
Attn: Mr. Buddy Briscoe

Report No: SA0880-1015

Date: 3/9/97

Laboratory No: 8-9531

Project: Belews Creek Plant Fly Ash Quality Assurance

Sample: 4th Quarter - 1986

Chemical Analysis	Results	Spec* Class F/C
Silicon Dioxide (SiO_2), %	50.5	
Aluminum Oxide (Al_2O_3), %	27.9	
Iron Oxide (Fe_2O_3), %	6.7	
Sum of SiO_2, Al_2O_3, Fe_2O_3, %	85.1	70.0/50.0 min.
Calcium Oxide (CaO), %	1.7	
Magnesium Oxide (MgO), %	0.9	5.0 max.
Sodium Oxide (Na_2O), %	0.37	
Potassium Oxide (K_2O), %	1.38	
Sulfur Trioxide (SO_3), %	0.6	5.0 max.
Moisture Content, %	0.2	3.0 max.
Loss on Ignition, %	2.1	12.0/6.0 max.
Available Alkalies (as Na_2O), %		1.50 max.
Available Sodium (as Na_2O), %		
Available Potassium (as K_2O), %		

Physical Analysis	Results	Spec*
Amount Retained on 325 Sieve, %	21.8	34 max.
Pozzolanic Activity Index with portland cement at 28 days, % of control	87.4	75 min.
with lime at 7 days, psi	1100	800 min.
Water Required, % of Control	95.1	105 max.
Autoclave Soundness, %	-.03	0.8 max.
Specific Gravity	2.31	
Multiple Factor, %		255 max.
Drying Shrinkage, %		0.03 max.
Reactivity with Cement Alkalies		
Reduction of expansion, %		75 min.
Mortar expansion, %		0.020 max.
Fineness		
Blaine air permeability, cm^2/cm^3		
Wagner turbidimetric, cm^2/g		

*ANSI/ASTM C618-80

Copies To: Above (1)
dgr 3/9

RABA-KISTNER CONSULTANTS, INC.

By Donald T. Fetzer
Donald T. Fetzer

Report of Fly Ash Analysis

Consulting Geotechnical, Materials and Environmental Engineers
Geologists, Scientists and Chemists

Raba-Kistner Consultants, Inc
P O. Box 690287, San Antonio, TX 78269-0287
12821 W. Golden Lane, San Antonio, TX 78249
(512) 699-9090

Monier Resources, Inc.
Attn: Mr. Buddy Briscoe

Report No: SA0880-1015

Date: 6/2/87

Laboratory No: 8-9667

Project: Belews Creek Plant Fly Ash Quality Assurance

Sample: April, 1987 Monthly Composite

Chemical Analysis	Results	Spec* Class F/C
Silicon Dioxide (SiO_2), %	53.7	
Aluminum Oxide (Al_2O_3), %	33.2	
Iron Oxide (Fe_2O_3), %	6.2	
Sum of SiO_2, Al_2O_3, Fe_2O_3, %	93.1	70.0/50.0 min.
Sulfur Trioxide (SO_3), %	0.5	5.0 max.
Moisture Content, %	0.3	3.0 max.
Loss on Ignition, %	3.1	12.0/6.0 max.

Physical Analysis	Results	Spec*
Amount Retained on 325 Sieve, %	22.7	34 max.
Pozzolanic Activity Index with portland cement at 28 days, % of control		75 min.
with lime at 7 days, psi		800 min.
Water Required, % of Control		105 max.
Autoclave Expansion, %		0.8 max.
Specific Gravity	2.25	

*ANSI/ASTM C618-80

Copies To: Above (1)
dgr 6/2

Raba-Kistner Consultants, Inc.

By David P. Darnell
AA Donald T. Fetzer

Report of Fly Ash Analysis

Consulting Geotechnical, Materials and Environmental Engineers
Geologists, Scientists and Chemists

Raba-Kistner
Consultants, Inc.
P.O. Box 690287, San Antonio, TX 78269-0287
12821 W. Golden Lane, San Antonio, TX 78249
(512) 699-9090

Monier Resources, Inc.
Attn: Mr. Buddy Briscoe

Report No: SA0880-1015

Date: 5/28/87

Laboratory No: 8-9635

Project: Belews Creek Plant Fly Ash Quality Assurance

Sample: 1st Quarter - 1987 Composite

Chemical Analysis	Results	Spec* Class F/C
Silicon Dioxide (SiO_2), %		
Aluminum Oxide (Al_2O_3), %		
Iron Oxide (Fe_2O_3), %		
Sum of SiO_2, Al_2O_3, Fe_2O_3, %		70.0/50.0 min.
Sulfur Trioxide (SO_3), %		5.0 max.
Moisture Content, %		3.0 max.
Loss on Ignition, %		12.0/6.0 max.

Physical Analysis	Results	Spec*
Amount Retained on 325 Sieve, %		34 max.
Pozzolanic Activity Index with portland cement at 28 days, % of control	91.7	75 min.
with lime at 7 days, psi	840	800 min.
Water Required, % of Control	92.9	105 max.
Autoclave Expansion, %	-.01	0.8 max.
Specific Gravity		

*ANSI/ASTM C618-80

Copies To: Above (1)
dgr 5/28

Raba-Kistner Consultants, Inc.

By Donald T. Fetzer

Donald T. Fetzer

OSR 14-357
(Rev 10-86)

SAVANNAH RIVER
DOCUMENT APPROVAL SHEET
(See SRP Procedures Manual Item 101)

Document Number DPST-87-673
UC or C Number

1. DESCRIPTION OF DOCUMENT (to be completed by author)

TITLE Physical Properties of Slag Saltstone

AUTHOR(S) C. A. Langton, 773-43A PHONE NO. 5-5806

TYPE: ☒ INTERNAL DOCUMENT ☐ EXTERNAL DOCUMENT
☐ DP Report
☐ Paper (see below)
☐ Other

Additional Information for External Papers

PAPER FOR: Presentation Only _____ Publication Only _____ Both _____

MEETING NAME _____

CITY _____ DATES _____

CHAIRMAN & ADDRESS _____

JOURNAL NAME _____

DEADLINES FOR PUBLICATION: Abstract _____ No. of Copies _____
Paper _____ No. of Copies _____

I understand that for the information in this paper for external distribution:
A. Approvals by both Du Pont and DOE-SR managements are required.
B. Distribution verbally, or by publication, must be in accordance with policies set forth in DOE-SR orders.
C. Content of the external distribution must be limited to that actually approved by DOE-SR.

AUTHOR'S SIGNATURE Christine A Langton

2. APPROVAL BY AUTHOR'S ORGANIZATION (required for all technical documents)

SRP/SRL ORGANIZATION IWT/SRL

DERIVATIVE CLASSIFIER H F Thurmond

Classification U Topic Saltstone

DISTRIBUTION
X Limit to List Attached. Reason: INTERNAL DOCUMENT
_____ Limit to SRP & SRL. Reason: _____
_____ Limit to DOE-SR & Du Pont Contractual Family. Reason: _____
_____ Site-Specific Procedure, Data Sheet, TA, etc.
_____ Unlimited To General Public

APPROVED BY RESEARCH MANAGER/SUPERINTENDENT M W Wright DATE 1/26/88

3. CLASSIFICATION & PATENT INFORMATION (to be completed by Patent & Classification Reviewer)

CLASSIFICATION (circle one for each)		CLASSIFICATION GUIDE TOPICS	PATENT CONSIDERATIONS
Overall	S C UCNI U		Possible Novel Features
Abstract	S C UCNI U		
Title	S C UCNI U		Closest Prior Art
Cover Letter	S C UCNI U		

APPROVED BY AED PATENT & CLASSIFICATION OFFICER _____ DATE _____

4. PUBLICATIONS DIVISION PROCESSING

DATE RECEIVED _____ PUBLICATIONS SUPERVISOR _____

EDITOR _____ DATE ASSIGNED _____

DATE COPIES SUBMITTED FOR RELEASE _____

DOE-SR RELEASE DATES: Patent Branch _____ Tech. Info. Office _____

DATE COMPLETED _____ DATE SUBMITTED TO OSTI _____

TECHNICAL DIVISION
SAVANNAH RIVER LABORATORY

M E M O R A N D U M

Keywords: Saltstone Pore Solution Analyses
Pennsylvania State Univ. Saltstone Progress Report

DPST-87-530 ←

cc: E. S. Occhipinti, 704-S
H. D. Harmon, 773-A
E. L. Wilhite, 773-43A
E. G. Orebaugh, 773-43A
P. F. McIntyre, 773-43A
J. P. Harley, 773-43A
SRL Records, (4), 773-A

July 7, 1987

TO: H. F. STURM, JR., 773-43A

FROM: C. A. LANGTON, 773-43A CAL

ANALYSIS OF SALTSTONE PORE SOLUTIONS PSU PROGRESS REPORT IV

SUMMARY

Pore solutions were extracted from the cement-Class C fly ash mix (former reference mix) and three slag-containing saltstones. The purpose of this work was to: 1) quantify waste ion source terms in the pore solution for modeling studies; 2) identify precipitated phases incorporating waste ions; and 3) provide data for interpreting cement, fly ash, and slag hydration rates and reaction products.

The concentrations of the various ions in the waste solution approximate the concentrations in the pore solutions, although the pore solution analyses for NO_3^-, NO_2^-, Na^+ vary by about 40% compared to the original waste analyses. This is attributed to the opposing effects of removing water from solution by hydration reactions versus removing salts from solution as precipitates.

Nitrate, nitrite, and sodium appear to be removed from solution to some extent as the samples age. Nitrate and nitrite are probably precipitated as soluble salts which can redissolve as the composition of the pore solution changes. Sodium is probably incorporated in the hydrated silicate phases.

TABLE V

RESULTS OF CHEMICAL ANALYSES OF PORE FLUIDS EXPRESSED FROM MIX 84-48 AT VARIOUS AGES (mg/L)

	7d	28d	56d	90d
AlO_2^-	17.7	6.3	26.9	1.33
Ca^{+2}	9.0	29	94.6	92.05
Fe^{+3}*	1.6	3.5	1.74	2.21
K^+	6,000	7,000	7,400	6,500
Mg^{+2}*	0.1	1.2	11.5	1.96
Na^+	77,000	85,000	91,000	60,000
SiO_3^{-2}*	203.6	230.7	169.6	76.6
CO_3^{-2}	800	1,000	675	736.5
Cl^-	1170	1380	661	739
NO_2^-	42,000	43,000	33,800	27,000
PO_4^{-3}	<150	<150	<150	<150
NO_3^-	175,000	205,000	177,000	122,700
SO_4^{-2}	26,000	25,000	25,500	24,000
OH^-[a]	14,258	16,315	227	3,794
pH	13.8	13.98	12.13	13.3

a = Calculated values.

Error estimated to be ±5% except where indicated (*) the error was estimated to be ±20%.

TABLE IX

SUMMARY OF COMPOUNDS IDENTIFIED BY XRD FORMED FROM IONIC SPECIES IN PORE FLUIDS OF THE REFERENCE MIX AND SLAG-CONTAINING MIXES

Reference Mix	Slag-Containing Mixes
C-S-H*	
N-C-S-H*	N-C-S-H* Substituted C-S-H*
$Ca(NO_3)_2 \cdot 2H_2O$	$Ca(NO_3)_2 \cdot 2H_2O$ $Al(NO_3)_3 \cdot 9H_2O$ $C_4A\bar{S}H_{12}$*
$C_4A\bar{C}H_{11}$*	$C_4A\bar{C}H_{11}$* $C_4A\bar{C}_{0.25-0.5}H_{12}$*
$C_3A \cdot Ca(NO_3)_2 \cdot 9H_2O$	$Mg_6Al_2(CO_3,NO_3)(OH)_6 \cdot 4H_2O$
$C_3A_{0.2}F_{0.8}H_6$-C_3FS_3*	$C_3A_{0.2}F_{0.8}H_6$-C_3FS_3*
C_3AH_6*	C_3AH_6*
$CaCO_3$	$CaCO_3$
$Na_2CO_3 \cdot 10H_2O$	$Na_2CO_3 \cdot 10H_2O$

*Cement chemistry notations were used in these formulae; A = Al_2O_3, C = CaO, $\bar{C}$ = CO_2, F = Fe_2O_3, H = H_2O, K = K_2O, N = Na_2O, S = SiO_2, and $\bar{S}$ = SO_3.

TECHNICAL DIVISION
SAVANNAH RIVER LABORATORY

Keywords: Saltstone EP and TCLP Results
Saltstone Toxicity
Saltstone Nonhazardous Waste Form
Saltstone Compositional Range

M E M O R A N D U M

DPST-87-869

cc: G. T. Wright, 773-A
E. S. Occhipinti, 704-S
R. L. Hooker, 704-S
G. W. Oakes, 704-S
E. L. Wilhite, 773-43A
E. G. Orebaugh, 773-43A
P. F. McIntyre, 773-43A
SRL Records (4), 773-A

December 10, 1987

TO: H. F. STURM, JR., 773-43A

FROM: C. A. LANGTON, 773-43A CAL

EP TEST RESULTS FOR SLAG SALTSTONE

SUMMARY

Twenty-one slag saltstone mixes covering a range of dry solids and waste solution proportions passed the EP test for toxic metals leachability. Consequently, they qualify as nonhazardous waste forms. (The highest Cr concentration in any extract was 0.6 mg/l compared to the guideline value of 5 mg/l.)

Based on test results, the range of acceptable mixes, i.e., those mixes which qualify as nonhazardous based on EP criteria, is shown below.

Slag	10 - 40 wt%	
Fly ash	10 - 40 wt%	Σ components = 100%
Cement or $Ca(OH)_2$	0 - 10 wt%	
Salt solution	40 - 55 wt%	

OSR 24-A118
(REV 2-83)

E. I. DU PONT DE NEMOURS & COMPANY
INCORPORATED
SAVANNAH RIVER LABORATORY
AIKEN, SOUTH CAROLINA 29808-0001
(TWX 810-771-2670 TEL 803-725-6211, WU AUGUSTA GA)

cc: R. Maher, 703-A
L. M. Papouchado, 703-A
D. L. McIntosh, 773-A
E. S. Occhipinti, 704-S
H. F. Sturm, Jr., 773-43A

December 18, 1987

SRL
RECORD COPY

J. T. GRANAGHAN, PLANT MANAGER
SAVANNAH RIVER PLANT

ATTENTION: D. C. NICHOLS, 704-S

SALTSTONE FORMULATION VARIABILITY LIMITATIONS

(Ref: Letter D. C. Nichols to G. T. Wright, 10/21/87)

As requested in the reference letter, testing to identify the acceptable variability in saltstone formulation ingredients has been completed.

Any variation within the ranges listed in the attached document, DPST-87-869, will produce a non-toxic saltstone meeting all state and local performance criteria.

G. T. Wright
Research Manager
Interim Waste Technology Division

GTW/HFS/tyb
Attachment
7293

Cr leaching results showed some sensitivity to cement content. Consequently, the cement content for the target mix in the cement system has been reduced from 5 to 3 wt%. No sensitivity was discernable based on $Ca(OH)_2$ contents between 0 - 10 wt%. DWPF saltstone target mix proportions are specified as follows.

Grade 120 slag	25 wt%
Class F fly ash	25 wt%
Type II cement or $Ca(OH)_2$	3 wt%
Salt solution (29 wt% salt)	47 wt%

(Additional work is in progress to determine if further reduction in cement content of the target mix is beneficial. However, data is not yet available.)

SAMPLE PREPARATION

Salt Solution

Salt solution containing 29 wt% dissolved sodium salts was doped with 100 ppm Ag, As, Ba, Cd, Hg, Pb, Se and 2000 ppm Cr. A comparison of the expected average salt solution[2] composition and the doped solution used in these samples is shown in Table I. Except for Cr and Ba, the metal concentrations in the doped solution were at least 1000x the expected values.

The solution was also doped with the long-term average concentrations of organics from the in-tank precipitation and acid hydrolysis processes.[1] These organics were added to evaluate their effect on metals leaching.

The impact of the F and H Areas Effluent Treatment Facility waste on salt solution composition was not taken into account. Tributyl phosphate will be added to salt solution as the result of the ETF but this is not expected to affect leaching or setting of the saltstone.

Saltstone Samples

Twenty-one saltstone mixes were selected from a test matrix originally set up to establish operating limits for raw materials proportioning. Ingredients for these mixes are listed in Table 2.

Samples were prepared in a Waring blender and cast into polypropylene bottles which were sealed during curing. After curing for 28 days at room temperature the samples were sent to Environmental and Chemical Sciences, Inc., New Ellenton, SC, and extracted according to the EP procedure. Metals in the extracts were analyzed by ICP (EPA Method 200.7).

RESULTS AND DISCUSSION

Analyses of the EP leachates are attached. EPA Guideline concentrations for these metals and the maximum concentrations observed in these leachates are listed in Table 3. The maximum extract concentration divided by the guideline concentration factor was also calculated for each metal and is shown in Table 3. This factor reflects the amount by which the extract concentration is below the guideline value. This factor is very conservative since the metals in the solution were doped at greater than 1000X the expected values (except for Ba and Cr).

In order to identify the most limiting indicator of EP performance, the highest extraction value divided by guideline value factor was multiplied by the metal doping factor (doped divided by expected concentration). Such a calculation indicates that only Cr leaching needs to be considered for any further discrimination of the mix design.

R. L. Postles was requested to derive discriminants for stricter Cr leaching criteria and to derive imperical equations which bound the entire experimental design point-set. A detailed report is attached. Results are summarized for the two compositional systems in Table IV.

The mix design was separated into two systems, one containing cement, the other $Ca(OH)_2$, both of which were added to the waste form to provide a source of Ca ions to activate the slag hydration and enhance hydrate precipitation. Only one source of Ca ions is needed in the mix design to accelerate final set and based on EP results no lime source is needed to stabilize Cr.

Since all mixes containing 0 wt% cement or $Ca(OH)_2$ and all mixes containing up to 10 wt% $Ca(OH)_2$ had EP Cr level <0.05 mg/l, it was impossible to derive further compositional discrimination in these systems. These mixes are insensitive to proportioning of ingredients over the range tested. However, the cement system does show a variation between extracted Cr concentration and cement content. The lowest Cr extraction values, i.e., Cr $\leq$ 0.113 mg/l are characteristic of mixes containing <5 wt% cement. (See attached R. L. Postles memo for additional discriminants.)

Qualitative examination of the EP Cr data for the cement system suggests that Cr leaching is optimized (lowered) by using low cement, high slag, and low solution loading in the mix design. However, all mixes tested had Cr values much less than (<8.5x) the guideline value.

CONCLUSIONS

- All of the slag mixes tested passed the EP test which qualifies them as non-hazardous waste forms.
- Based on reported test data, saltstone mixes containing salt solution with metal concentrations equal or less than those used in this study and with compositions bounded by the following constraints will pass the EP test criteria and qualify as nonhazardous waste forms:

Grade 120 slag	25 (±15) wt%
Class F fly ash	25 (±15) wt%
Type II portland cement or $Ca(OH)_2$	3 (-3 + 7) wt%
Salt Solution	47 (-7 + 8) wt%

(components = 100 wt%)

- Since the actual salt solution will contain lower concentration of metals than the solution used in this study, slag saltstones with compositions within the range tested will be nonhazardous.
- Organics added to the solution in the long-term average concentrations did not result in excessive metals leaching from the samples.
- Cr leaching was somewhat sensitive to cement content over the range of proportions tested. Consequently, the cement content in the target formulation was lowered from 5 to 3 wt%.

REFERENCES

1. John R. Fowler, DPST-87-818, Saltstone Material Balance for Blended Waste with Recycle.

2. DPSP-85-1142, Rev. 1, Industrial Solid Waste Permit Application for the Proposed Z-Area Saltstone Disposal Facility.

3. Federal Register, Friday, June 13, 1986, p. 21685, Part II, Environmental Protection Agency, 40 CFR Parts 261, 271, and 302, Hazardous Waste Management Systems; Identification and Listing of Hazardous Waste; Notification Requirements; Reportable Quantity Adjustments; Proposed Rule.

CAL/tyb
87-869

TABLE 1

Comparison of the Expected[2] Salt Solution Composition and the Composition of the Solution Used in the EP Samples

	Expected Long-Term Average Salt Solution	Experimental Salt Solution
H_2O	71 wt%	71 wt%
$NaNO_3$	14.1	14.2
$NaNO_2$	3.5	3.5
NaOH	3.8	3.8
Na_2CO_3	1.5	1.5
$NaAl(OH)_4$	3.3	3.3
Na_2SO_4	1.7	1.7
NaCl	0.11	0.1
Na_3PO_4	0.12	0.1
$Na_2C_2O_4$	0.28	0.3
Ag	8.5×10^{-4} ppm	96 ppm
As	3×10^{-4}	85
Ba	11	110
Cd	5×10^{-2}	101
Cr	161*	1790
Hg	1.2×10^{-2}	94
Pb	2×10^{-8}	102
Se	7.9×10^{-1}	103
Methanol	-- ** wt%	3×10^{-2} wt%
Isopropanol	--	2×10^{-3}
NaB_4	0.05	8×10^{-2}
Phenol	--	4×10^{-2}
Phenylboric acid	--	5×10^{-3}
Benzene	--	6×10^{-3}
Biphenyl	--	***
Diphenyl amine	--	***
Terphenyl	--	***

*Increased to 1400 ppm max

**Not listed

**Not included because expected concentrations are less than 10^{-4} wt%

TABLE 2

Ingredients in Slag Saltstone Samples Extracted by EP Test

Mix No.	Slag	Class F Fly Ash	Ca(OH)2	Type II Cement	Solution (29% Salt)
1	26 wt%	26 wt%	3 wt%	0 wt%	45 wt%
2	24	24	0	5	47
3	10	27	10	0	53
4	10	27	0	10	53
5	27	10	10	0	53
6	10	40	0	10	40
7	27	10	0	10	53
8	40	10	0	10	40
9	37	10	0	0	53
10	40	10	0	0	53
11	24	24	0	10	42
12	24	24	10	0	42
13	25	25	0	10	40
14	18.5	18.5	0	8	55
15	10	33.5	0	10	46.5
16	33.5	10	0	10	46.5
17	10	33.5	10	0	46.5
18	33.5	10	10	0	46.5
19	18.5	18.5	8	0	55
20	<10	18.5	0	0	41.5
21	38.5	10	0	0	51.5

TABLE 3

Comparison of Guideline Values for EP Toxic Metals and Extract to Guideline

	Maximum Observed In EP Leachate (mg/L)	Guideline[3] Value for EP Leachate	Guideline to Extract Ratio	Doping Factor	Composite Factor
Arsenic	<0.5	5.0	>10*	1000X	$>10^4$
Barium	0.137	100.0	>30	10X	$\geq 7 \times 10^3$
Cadmium	<0.02	1.0	>50*	1000X	$\geq 5 \times 10^4$
Chromium	0.588	5.0	8.5	1X	8.5
Lead	<0.5	5.0	>10	1000X	10^4
Mercury	0.00929	0.2	21	1000X	3×10^4
Selenium	<0.5	1.0	>2	1000X	2×10^3
Silver	<0.5	5.0	>10*	1000X	10^4

*EP leachate analysis reported as less than values. Consequently, guideline value divided by extraction value may be larger than indicated.

TABLE 4. Summary of EP extract results for the cement system (above) and the $Ca(OH)_2$ systems.

MIX NO.	SLAG %	FLYASH %	CEMENT %	SALT %	EP Cr ppm
20	40	18.5	0	41.5	<0.05
21	38.5	10	0	51.5	<0.05
9	37	10	0	53	<0.05
10	40	10	0	50	<0.05
2	24	24	5	47	0.113
8	40	10	10	40	0.160
4	10	27	10	53	0.223
11	24	24	10	42	0.238
16	33.5	10	10	46.5	0.286
15	10	33.5	10	46.5	0.288
13	25	25	10	40	0.307
7	27	10	10	53	0.353
14	18.5	18.5	8	55	0.389
6	10	40	10	40	0.588
Avg.	27.0	19.3	6.6	47.1	
Std. Dev.	11.58	9.95	4.57	5.57	

(Cement-containing): the boundary of the intersection of the asymmetric ellipsoid given by:

$$\{ [(SLAG-27.0)/11.58]^2 + [(FLYASH-19.3)/9.95]^2 + [(CEMENT-6.6)/4.57]^2 + [(SALT-47.1)/5.57]^2 \} \leq 8.7$$

MIX NO.	SLAG %	FLYASH %	$Ca(OH)_2$ %	SALT %	EP Cr ppm
1	26	26	3	45	<0.05
5	27	10	10	53	<0.05
12	24	24	10	42	<0.05
17	10	33.5	10	46.5	<0.05
18	33.5	10	10	46.5	<0.05
19	18.5	18.5	8	55	<0.05
20	40	18.5	0	41.5	<0.05
21	38.5	10	0	51.5	<0.05
9	37	10	0	53	<0.05
10	40	10	0	50	<0.05
3	10	27	10	53	0.067
Avg.	27.7	18.0	5.5	48.8	
Std. Dev.	11.26	8.61	4.84	4.74	

($Ca(OH)_2$-containing): the containing ellipsoid is:

$$\{ [(SLAG-27.0)/11.26]^2 + [(FLYASH-18.0)/8.61]^2 + [(CAOH-5.5)/4.84]^2 + [(SALT-48.8)/4.74]^2 \} \leq 6.8$$

ATTACHMENT I

EP RESULTS

ENVIRONMENTAL & CHEMICAL SCIENCES, INC.
P.O. Box 1393 • Aiken, South Carolina 29802 • (803) 652-7450 • (803) 652-2206

CLIENT: Savannah River Plant - C. Langton
DATE: October 16, 1987
JOB NO: 7292

SAMPLE TYPE: Saltstone
COLLECTED BY: Client
DATE RECEIVED: 9/21/87

EP TOXICITY:

	ECS I.D.	SAMPLE I.D.	As mg/L	Ba mg/L	Cd mg/L	Cr mg/L	Hg mg/L	Pb mg/L	Se mg/L	Ag mg/L
D	12700	1 812	<0.5	<0.05	<0.02	<0.05	0.00147	<0.5	<0.5	<0.5
D	12701	2 812	<0.5	<0.05	<0.02	0.113	0.00127	<0.5	<0.5	<0.5
D	12702	3 812	<0.5	<0.05	<0.02	0.067	0.00134	<0.5	<0.5	<0.5
D	12703	4 812	<0.5	<0.05	<0.02	0.223	0.00536	<0.5	<0.5	<0.5
D	12704	5 812	<0.5	0.077	<0.02	<0.05	0.00108	<0.5	<0.5	<0.5
D	12705	6 812	<0.5	<0.05	<0.02	0.588	0.00280	<0.5	<0.5	<0.5
D	12706	7 812	<0.5	<0.05	<0.02	0.353	0.00602	<0.5	<0.5	<0.5
D	12707	8 812	<0.5	<0.05	<0.02	0.160	0.00139	<0.5	<0.5	<0.5
D	12708	9 812	<0.5	<0.05	<0.02	<0.05	0.00300	<0.5	<0.5	<0.5
D	12709	10 812	<0.5	<0.05	<0.02	<0.05	0.00168	<0.5	<0.5	<0.5
D	12710	11 812	<0.5	<0.05	<0.02	0.238	0.00167	<0.5	<0.5	<0.5
D	12711	12 812	<0.5	<0.05	<0.02	<0.05	0.00085	<0.5	<0.5	<0.5
D	12712	13 812	<0.5	<0.05	<0.02	0.307	0.00208	<0.5	<0.5	<0.5
D	12713	14 812	<0.5	<0.05	<0.02	0.389	0.00929	<0.5	<0.5	<0.5
D	12714	15 812	<0.5	<0.05	<0.02	0.288	0.00225	<0.5	<0.5	<0.5
D	12715	16 812	<0.5	0.073	<0.02	0.286	0.00544	<0.5	<0.5	<0.5
D	12716	17 812	<0.5	0.137	<0.02	<0.05	0.00300	<0.5	<0.5	<0.5
D	12717	18 812	<0.5	0.051	<0.02	<0.05	0.00122	<0.5	<0.5	<0.5
D	12718	19 812	<0.5	<0.05	<0.02	<0.05	0.00137	<0.5	<0.5	<0.5
D	12719	20 812	<0.5	<0.05	<0.02	<0.05	0.00089	<0.5	<0.5	<0.5
D	12720	21 812	<0.5	<0.05	<0.02	<0.05	0.00644	<0.5	<0.5	<0.5

Approved by: Henry J. Kania Laboratory Director
Henry J. Kania, Ph.D.

HJK/kr

ATTACHMENT II

Derivation of equations bounding the entire experimental design point-set and derivataion of discriminants which impose stricter criteria on Cr leaching. Memo from R. L. Postles to C. A. Langton, November 25, 1987.

cc: R. J. Pryor
G. T. Wright
R. R. Beckmeyer
H. F. Sturm

November 25, 1987

TO: CHRIS LANGTON

FROM: DICK POSTLES Dick Postles

RE: Cr CONTENT OF SALTCRETE FORMULATIONS

You all have measured the Cr content (by the EP method) of some formulations of saltcrete chosen according to an experimental design.

Your intent was to delineate a range of composition for which Cr ≤ 5 ppm. However, all 14 Cement-containing and all 11 $Ca(OH)_2$-containing compositions met this criterion "easily" (maximum Cr ~0.6 ppm). Hence, the descriptive work reduced to:

i. Deriving the expression for a 3-dimensional solid which bounds the entire experimental design point-set, and/or

ii. Deriving discriminants which impose stricter criteria on Cr.

For i. (Cement-containing): the boundary of the intersection of the asymmetric ellipsoid given by:

$$\{ [(SLAG-27.0)/11.58]^2 + [(FLYASH-19.3)/9.95]^2 +$$

$$[(CEMENT-6.6)/4.57]^2 + [(SALT-47.1)/5.57]^2 \} \leq 8.7$$

and the region bounded by the basic constraints:

$$10 \leq SLAG \leq 40\%$$
$$10 \leq FLYASH \leq 40\%$$
$$0 \leq CEMENT \leq 10\%$$
$$40 \leq SALT \leq 55\%$$

and the region of processibility:

$$(1.31*CEMENT + 0.26*SLAG) \geq 8\%$$

is an approximate bound to the experimental compositions. It is approximate, in that it extends beyond the convex hull of the experimental design point set. So: although we know that all the good formulations are contained within it, we do not know that all contained within it are good. [Only one of the experimental points (Mix No. 6: 10, 40, 10, 40) requires the upper bound to be as large as 8.7. The remaining 13 are bounded by ≤~5.]

For i. ($Ca(OH)_2$-containing): the containing ellipsoid is:

$$\{ [(SLAG-27.0)/11.26]^2 + [(FLYASH-18.0)/8.61]^2 + [(CAOH-5.5)/4.84]^2 + [(SALT-48.8)/4.74]^2 \} \leq 6.8$$

with the basic constraints as above except: $0 \leq Ca(OH)_2 \leq 10\%$

and the corresponding processibility constraint:

$$(-0.3255 * Ca(OH)_2 + 0.7935 * SALT) \geq 30\%.$$

The same type of approximation is involved as above.

The higher-order discriminants germane to lower levels of Cr are described in the attachment.

ATTACHMENT

1. Generalities:

The data attached in Table 1 show that there is essentially no discrimination power in the $Ca(OH)_2$ data; all but one datum show EP Cr levels < 0.05 ppm. Hence, it remains only to bound the entire composition point set for this case.

However, the Cement data show a reasonable variation of Cr with composition; and so higher-order discriminants are derivable, in addition to the "global" bound.

2. Higher-Order Discriminants - Cement Data:

Cr ≤ 0.113 ppm: By inspection, CEMENT≤5% is sufficient to discriminate.

Cr ≤ 0.160 ppm: CEMENT by itself is no longer sufficient; but 0.3*(SLAG) > CEMENT does effect perfect separation. (See Table 3.)

Cr ≤ 0.30 ppm: No linear discriminant exists which will effect perfect separation.

Note: The discriminant analysis above was effected by the same technique described in:

Memo, R. L. Postles to C. A. Langton, "Experimental Design for Flyash/Slag Mixtures - Revisited", September 8, 1986

3. Global Discriminants:

Expressions of the form "$\Sigma_i[(x_i-a_i)/b_i]^2 = c^2$" generate an ellipsoid in the "centered" variables "x_i-a_i" with intercepts on the coordinate axes "$\pm b_i/c$". Setting the "a_i" equal to the observed component centroids and the "b_i" equal to the observed standard deviations gives the left-hand side of the expression:

$$\{ [(SLAG-27.0)/11.58]^2 + [(FLYASH-19.3)/9.95]^2 +$$

$$[(CEMENT-6.6)/4.57]^2 + [(SALT-47.1)/5.57]^2 \} \leq 8.7.$$

The right-hand "c^2" was determined empirically such that every experimental formulation was contained therein. See Table 2.

TABLE 1

THE CEMENT DATA

MIX NO.	SLAG %	FLYASH %	CEMENT %	SALT %	EP Cr ppm
20	40	18.5	0	41.5	<0.05
21	38.5	10	0	51.5	<0.05
9	37	10	0	53	<0.05
10	40	10	0	50	<0.05
2	24	24	5	47	0.113
8	40	10	10	40	0.160
4	10	27	10	53	0.223
11	24	24	10	42	0.238
16	33.5	10	10	46.5	0.286
15	10	33.5	10	46.5	0.288
13	25	25	10	40	0.307
7	27	10	10	53	0.353
14	18.5	18.5	8	55	0.389
6	10	40	10	40	0.588
Avg.	27.0	19.3	6.6	47.1	
Std. Dev.	11.58	9.95	4.57	5.57	

THE $CA(OH)_2$ DATA

MIX NO.	SLAG %	FLYASH %	$Ca(OH)_2$%	SALT %	EP Cr ppm
1	26	26	3	45	<0.05
5	27	10	10	53	<0.05
12	24	24	10	42	<0.05
17	10	33.5	10	46.5	<0.05
18	33.5	10	10	46.5	<0.05
19	18.5	18.5	8	55	<0.05
20	40	18.5	0	41.5	<0.05
21	38.5	10	0	51.5	<0.05
9	37	10	0	53	<0.05
10	40	10	0	50	<0.05
3	10	27	10	53	0.067
Avg.	27.7	18.0	5.5	48.8	
Std. Dev.	11.26	8.61	4.84	4.74	

```
        SAS(R) LOG   OS SAS 5.16          MVS/XA JOB T6476SA@ STEP STEP     PROC SAS              13:33 MONDAY, NOVEMBER 23, 198

NOTE: COPYRIGHT (C) 1984,1986 SAS INSTITUTE INC., CARY, N.C.  27511, U.S.A.
NOTE: THE JOB T6476SA@ HAS BEEN RUN UNDER RELEASE 5.16 OF SAS AT E. I. DU PONT DE NEMOURS & COMPANY (02398001).

NOTE: CPUID   VERSION = FF  SERIAL = 171474  MODEL = 3090 .

NOTE: SAS OPTIONS SPECIFIED ARE:
      NEWS SORT=7 LEAVE=600K

        ****************  SAS NEWS ********************

        PROBLEMS ENCOUNTERED EXECUTING THIS VERSION OF
        SAS SOFTWARE SHOULD BE DIRECTED TO PAIGE RABINN
        (EXTENSION 51244).


1          DATA ;  INPUT  SLAG  FLYASH  CEMENT  SALT ;
2                  CSQ = ((SLAG-27.0)/11.58)**2 + ((FLYASH-19.3)/9.95)**2 ;
3                  CSQ = CSQ + ((CEMENT-6.6)/4.57)**2 + ((SALT-47.1)/5.57)**2 ;
4                  CARDS ;

NOTE: DATA SET WORK.DATA1 HAS 14 OBSERVATIONS AND 5 VARIABLES. 433 OBS/TRK.
NOTE: THE DATA STATEMENT USED 0.04 SECONDS AND 332K.

19                             ;
20         PROC PRINT ;
NOTE: THE PROCEDURE PRINT USED 0.08 SECONDS AND 464K AND PRINTED PAGE 1.
NOTE: SAS USED 464K MEMORY.

NOTE: SAS INSTITUTE INC.
      SAS CIRCLE
      PO BOX 8000
      CARY, N.C. 27511-8000
```

TABLE 2

CEMENT - CONTAINING

SAS

OBS	SLAG	FLYASH	CEMENT	SALT	CSQ
1	24.0	24.0	5	47.0	0.41314
2	10.0	27.0	10	53.0	4.42955
3	40.0	10.0	10	40.0	4.31224
4	24.0	24.0	10	42.0	1.68211
5	10.0	33.5	10	46.5	4.75700
6	33.5	10.0	10	46.5	1.75380
7	40.0	18.5	0	41.5	4.36327
8	38.5	10.0	0	51.5	4.56958
9	37.0	10.0	0	53.0	4.82707
10	40.0	10.0	0	50.0	4.49069
11	10.0	40.0	10	40.0	3.46157
12	27.0	10.0	10	53.0	2.54913
13	25.0	25.0	10	40.0	2.53634
14	18.5	18.5	8	55.0	2.65071

```
1          SAS(R) LOG   OS SAS 5.16          MVS/XA JOB T6476SA2 STEP STEP     PROC SAS          10:37 WEDNESDAY, NOVEMBER 25, 198

NOTE: COPYRIGHT (C) 1984,1986 SAS INSTITUTE INC., CARY, N.C.  27511, U.S.A.
NOTE: THE JOB T6476SA2 HAS BEEN RUN UNDER RELEASE 5.16 OF SAS AT E. I. DU PONT DE NEMOURS & COMPANY (02398001).

NOTE: CPUID   VERSION = FF  SERIAL = 171474  MODEL = 3090 .

NOTE: SAS OPTIONS SPECIFIED ARE:
      NEWS SORT=7 LEAVE=600K

        ****************  SAS NEWS ********************

        PROBLEMS ENCOUNTERED EXECUTING THIS VERSION OF
        SAS SOFTWARE SHOULD BE DIRECTED TO PAIGE RABON
        (EXTENSION 51244).


1          DATA ;  INPUT  SLAG  FLYASH  CAOH  SALT ;
2                  CSQ = ((SLAG-27.7)/11.26)**2 + ((FLYASH-18.0)/8.61)**2 ;
3                  CSQ = CSQ + ((CAOH-5.5)/4.84)**2 + ((SALT-48.8)/4.74)**2 ;
4                  CARDS ;

NOTE: DATA SET WORK.DATA1 HAS 11 OBSERVATIONS AND 5 VARIABLES. 433 OBS/TRK.
NOTE: THE DATA STATEMENT USED 0.04 SECONDS AND 332K.

16                                ;
17         PROC PRINT ;
NOTE: THE PROCEDURE PRINT USED 0.08 SECONDS AND 464K AND PRINTED PAGE 1.
NOTE: SAS USED 464K MEMORY.

NOTE: SAS INSTITUTE INC.
      SAS CIRCLE
      PO BOX 8000
      CARY, N.C. 27511-8000
```

TABLE 2

$Ca(OH)_2$-CONTAINING

SAS

OBS	SLAG	FLYASH	CAOH	SALT	CSQ
1	26.0	26.0	3	45.0	1.79562
2	10.0	27.0	10	53.0	5.21320
3	27.0	10.0	10	53.0	2.51676
4	24.0	24.0	10	42.0	3.51611
5	10.0	33.5	10	46.5	6.81171
6	33.5	10.0	10	46.5	2.22854
7	18.5	18.5	8	55.0	2.64866
8	40.0	18.5	0	41.5	4.85981
9	38.5	10.0	0	51.5	3.39908
10	37.0	10.0	0	53.0	3.62194
11	40.0	10.0	0	50.0	3.41199

```
1          SAS(R) LOG   OS SAS 5.16          MVS/XA JOB T6476SA@ STEP STEP     PROC SAS          8:55 WEDNESDAY, NOVEMBER 18, 198
NOTE: COPYRIGHT (C) 1984,1986 SAS INSTITUTE INC., CARY, N.C.  27511, U.S.A.
NOTE: THE JOB T6476SA@ HAS BEEN RUN UNDER RELEASE 5.16 OF SAS AT E. I. DU PONT DE NEMOURS & COMPANY (02398001).

NOTE: CPUID   VERSION = FF  SERIAL = 171474  MODEL = 3090 .

NOTE: SAS OPTIONS SPECIFIED ARE:
      NEWS SORT=7 LEAVE=600K

        ****************  SAS NEWS ********************

        PROBLEMS ENCOUNTERED EXECUTING THIS VERSION OF
        SAS SOFTWARE SHOULD BE DIRECTED TO PAIGE RABON
        (EXTENSION 51244).

1           PROC MATRIX ;
2                        NOTE  ENTER MATRIX X1 OF GOOD POINTS (EP CR<=0.160)  ;
3                        X1 =  24     5    /
4                              40    10    /
5                              40     0    /
6                              38.5   0    /
7                              37     0    /
8                              40     0    ;  PRINT X1 ;
9                        NOTE  ENTER MATRIX X2 OF BAD POINTS ;
10                       X2 =  10    10    /
11                             10    10    /
12                             27    10    /
13                             24    10    /
14                             25    10    /
15                             18.5   8    /
16                             10    10    /
17                             33.5  10    ;  PRINT X2 ;
18          NOTE  COMPUTE MEANS X_BAR,  NORMALIZED CROSSPRODUCTS S_, COVARIANCES S;
19                COL1 = NCOL(X1) ;  ROW1 = NROW(X1) ;  ROW2 = NROW(X2) ;
20                X1BAR = J(ROW1, COL1, 1) ;
21                        DO L=1 TO ROW1 ;  DO K=1 TO COL1 ;
22                           X1BAR(L,K) = SUM(X1(,K))#/ROW1 ;
23                        END ; END ;  PRINT X1BAR ;
24                X2BAR = J(ROW2, COL1, 1) ;
25                        DO L=1 TO ROW2 ;  DO K=1 TO COL1 ;
26                           X2BAR(L,K) = SUM(X2(,K))#/ROW2 ;
27                        END ; END ;  PRINT X2BAR ;
28                S1    = (X1-X1BAR)'*(X1-X1BAR) ;  PRINT S1 ;
29                S2    = (X2-X2BAR)'*(X2-X2BAR) ;  PRINT S2 ;
30                S     = (S1+S2)#/(ROW1+ROW2)   ;  PRINT S  ;
31                SDET  = DET(S) ;                  PRINT SDET ;
32                B     = INV(S) ;                  PRINT B ;
33                CHECK= B*S-I(COL1) ;              PRINT CHECK ;
34          NOTE  GET COEFFICIENTS OF AXIS WHICH PROVIDES MAXIMAL SEPARATION ;
35                A = B*((X1BAR(1,))'-(X2BAR(1,)')) ; PRINT A ;
36          NOTE  COMPUTE VALUES FOR EACH POINT ALONG THIS AXIS ;
37                D1 = X1*A ;  PRINT D1 ;
38                D2 = X2*A ;  PRINT D2 ;

NOTE: PROC IML WILL REPLACE PROC MATRIX AFTER VERSION 5.
NOTE: THE PROCEDURE MATRIX USED 0.19 SECONDS AND 854K AND PRINTED PAGES 1 TO 3.
NOTE: SAS USED 854K MEMORY.
```

TABLE 3

0.3#SLAG > CEMENT

TABLE 3
(CONT'D)

ENTER MATRIX X1 OF GOOD POINTS (EP CR<=0.160)

X1	COL1	COL2
ROW1	24	5
ROW2	40	10
ROW3	40	0
ROW4	38.5	0
ROW5	37	0
ROW6	40	0

ENTER MATRIX X2 OF BAD POINTS

X2	COL1	COL2
ROW1	10	10
ROW2	10	10
ROW3	27	10
ROW4	24	10
ROW5	25	10
ROW6	18.5	8
ROW7	10	10
ROW8	33.5	10

COMPUTE MEANS X_BAR, NORMALIZED CROSSPRODUCTS S_, COVARIANCES S

X1BAR	COL1	COL2
ROW1	36.5833	2.5
ROW2	36.5833	2.5
ROW3	36.5833	2.5
ROW4	36.5833	2.5
ROW5	36.5833	2.5
ROW6	36.5833	2.5

X2BAR	COL1	COL2
ROW1	19.75	9.75
ROW2	19.75	9.75
ROW3	19.75	9.75
ROW4	19.75	9.75
ROW5	19.75	9.75
ROW6	19.75	9.75
ROW7	19.75	9.75
ROW8	19.75	9.75

TABLE 3
(CONT'D)

S1	COL1	COL2
ROW1	197.208	-28.75
ROW2	-28.75	87.5

S2	COL1	COL2
ROW1	574	2.5
ROW2	2.5	3.5

S	COL1	COL2
ROW1	55.0863	-1.875
ROW2	-1.875	6.5

SDET	COL1
ROW1	354.545

B	COL1	COL2
ROW1	0.0183333	0.00528846
ROW2	0.00528846	0.155372

CHECK	COL1	COL2
ROW1	-4.3021E-16	4.3368E-18
ROW2	-2.7756E-17	-2.0817E-16

GET COEFFICIENTS OF AXIS WHICH PROVIDES MAXIMAL SEPARATION

A	COL1
ROW1	0.27027
ROW2	-1.03742

COMPUTE VALUES FOR EACH POINT ALONG THIS AXIS

TABLE 3
(CONT'D)

D1	COL1
ROW1	1.29936
ROW2	0.436571
ROW3	10.8108
ROW4	10.4054
ROW5	9.99998
ROW6	10.8108

D2	COL1
ROW1	-7.67152
ROW2	-7.67152
ROW3	-3.07694
ROW4	-3.88775
ROW5	-3.61748
ROW6	-3.29939
ROW7	-7.67152
ROW8	-1.32018

WSRC-TR-98-00337
REV. 0

KEY WORDS: Saltstone
Cesium
Salt Waste Treatment

RETENTION: Permanent

DIRECT GROUT STABILIZATION OF HIGH CESIUM SALT WASTE: SALT WASTE ALTERNATIVE PHASE III FEASIBILITY STUDY (U)

Author

Christine A. Langton,
Westinghouse Savannah River Company
Savannah River Technology Center,
Aiken, SC 29808

Date: September 30, 1998

Westinghouse Savannah River Company
Savannah River Site
Aiken, SC 29808

WSRC-TR-98-00337
REV. 0

KEY WORDS: Saltstone
Cesium
Salt Waste Treatment

RETENTION: Permanent

DIRECT GROUT STABILIZATION OF HIGH CESIUM SALT WASTE: SALT WASTE ALTERNATIVE PHASE III FEASIBILITY STUDY (U)

Author

Christine A. Langton,
Westinghouse Savannah River Company
Savannah River Technology Center,
Aiken, SC 29808

Date: September 30, 1998

Westinghouse Savannah River Company
Savannah River Site
Aiken, SC 29808

REVIEWS and APPROVALS

Author

C. A. Langton, Author
Waste Processing Technology — Date: 10-2-98

Approvals/Review

J. R. Fowler,
Salt Disposition Flowsheet Team — Date: 10/4/98

B. T. Butcher, Level 4
Waste Processing Technology — Date: 10/2/98

W. L. Tamosaitis, Level 3 Manager
Waste Processing Technology — Date: 10/2/98

J. T. Carter
Salt Disposition Flowsheet Team — Date: 10/3/98

K. J. Rueter
Salt Disposition System Engineering Team — Date: 10/4/98

WSRC-TR-98-00337
Revision: 0
September 30, 1998

DIRECT GROUT STABILIZATION OF HIGH CESIUM SALT WASTE: SALT WASTE ALTERNATIVE PHASE III FEASIBILITY STUDY (U)

Christine A. Langton,
Westinghouse Savannah River Company
Savannah River Technology Center,
Aiken, SC 29808

SUMMARY

The direct grout alternative is a viable option for treatment/stabilization and disposal of salt waste containing Cs-137 concentrations of 1-3 Ci/gal.

The composition of the direct grout salt solution is higher in sodium salts and contains up to a few hundred ppm Cs-137 more than the current reference salt solution. However it is still similar to the composition of the current reference salt solution. Consequently, the processing, setting, and leaching properties (including TCLP for Cr and Hg) of the direct grout and current saltstone waste forms are very similar.

The significant difference between these waste solutions is that the high cesium salt solution will contain between 1 and 3 Curies of Cs-137 per gallon compared to a negligible amount in the current salt solution. This difference will require special engineering and shielding for a direct grout processing facility and disposal units to achieve acceptable radiation exposure conditions. The Cs-137 concentration in the direct grout salt solution will also affect the long-term curing temperature of the waste form since 4.84 Watts of energy are generated per 1000 Ci of Cs-137. The temperature rise of the direct grout during long-term curing has been calculated by A. Shaddy, SRTC.[1]

The effect of curing temperature on the strength, leaching and physical durability of the direct grout saltstone is described in this report. At the present time, long term curing at 90°C appears to be unacceptable because of cracking which will affect the structural integrity as evaluated in the immersion test. (The experiments conducted in this feasibility study do not address the effect of cracking on leaching of contaminants other than Cr, Hg, and Cs.) No cracking of the direct grout or reference saltstone waste forms was observed for samples cured at 70°C.

At the present time the implications of waste form cracking at elevated curing temperatures has not been fully addressed. The direct grout falls within the definition of NRC Class C waste. NRC requires that Class C waste forms or their containers demonstrate structural integrity to qualify for disposal. Direct grout cured at 90° C will not meet the integrity requirement. However, the disposal vault may meet this requirement.

BACKGROUND

Direct disposal of the cesium in grout is one of the alternatives identified in WSRC-RP-98-00166.[2] In this proposed process, Cs-137 is not separated from the salt waste or concentrated supernate. It is instead sent to the new shielded Saltstone Facility. The resulting waste form would be classified as Class C low-level waste if disposal was regulated by the NRC. A new grout production facility is needed for this option. The new facility requires remote maintenance capabilities and a shielded cell for the grout production equipment. The test plan for this effort is presented elsewhere.[3]

Comparison of Reference Z-Area Salt Solution and High-Cesium salt Solution

The average composition of the direct grout salt solution is listed in Table 1 and compared to the current reference salt solution composition. The average cesium concentration in the direct grout waste stream is estimated to be 1.65E-4M (1.5 Ci/gal).[4] This waste and the resulting direct grout waste form which has about 40 % less curies per volume (about 250 Ci/cubic meter of saltstone) due to dilution with the cementing reagents fall within the NRC Class C waste category. The Cs-137 concentration limit for Class C waste is 4600 curies per cubic meter.[5]

Table 1. Compositions of the Reference Salt Solution and the Direct Grout, High Cesium Salt Solution.[4,6]

Component	Reference Salt Solution (Molar)	Direct Grout High Cesium Salt Solution (Molar)
NO_3^-	2.04	2.49
NO_2^-	0.62	0.581
OH^-	1.17	2.181
CO_3^{-2}	0.15	0.181
AlO^{-2}	0.41	0.355
SO_4^{-2}	0.15	0.169
F^-	0.0015	0.0361
Cl^-	0.023	0.0282
$C_2O_4^{-2}$	0.025	0.0136
PO_4^{-2}	0.01	0.009
Na+	4.94	6.44
K^+	-	0.0168
Cs^+	20 n Ci/g	0.000165
Hg	0.012 mg/L	33 mg/L
Cr	161 mg/L	161 mg/L

Class C Requirements for Low-Level Waste Disposal[7]

In addition to the minimum requirements for Class A, B, and C wastes, NRC has structural stability requirements for Class B and C waste.[7] Stability requires that the waste form maintains its structural integrity under the expected disposal conditions. Structural stability is necessary to inhibit a) slumping, collapse, or other structural failure of the disposal unit if an engineered structure is not used and b) radionuclide release from the waste form that might ensue due to increases in leaching that could be caused by premature disintegration of the waste form. Stability is also considered in the intruder pathways where it is assumed that wastes are recognizable after the active control period. To the extent practical, Class B and C waste forms should maintain gross physical properties and identity over a 300 year period. To ensure that Class B and C wastes maintain stability the following conditions should be met:

- The waste should be a solid form or in a container or structure that provides stability after disposal.
- The waste should not contain free standing and/or corrosive liquids.
- The waste or container should be resistant to degradation caused by radiation effects.
- The waste or container should be resistant to biodegradation.
- The waste or container should remain stable under the compressive loads inherent in the disposal environment.
- The waste or container should remain stable if exposed to moisture or water after disposal.
- The as-generated waste should be compatible with the solidification medium or container.

NRC identifies the following tests, which can be used to demonstrate waste form stability:

- Compressive strength; ASTM C-39 (60 psi minimum).
- Resistance to thermal cycling degradation; ASTM B-553.
- Radiation stability at 10E+8 Rads in gamma irradiator or equivalent.
- Resistance to biodegradation; ASTM G-21 and G-22.
- Leach testing; ANS 16.1 (Cs leach index minimum of 6).
- Immersion testing, i. e., compressive strength after 90 day immersion period should be 500 psi minimum and not less than 75 % of the pre-immersion compressive strength.
- Free standing liquids (less than 0.5 volume per cent per Method described in Appendix 2 of ANSI/ANS 55.1).
- Full-scale testing.

EXPERIMENTAL METHOD

Preparation of the Reference Salt Solution and Direct Grout, High Cesium Salt Solution[8]
Simulated salt solution was made according to the following recipes. Cesium, mercury and chromium were spiked in amounts greater than the concentrations listed in Table 1 in order to determine differences between leaching performance in the various leaching tests. This was necessary given the detection level for non radioactive cesium used in these experiments.

Table 2. Ingredients in the Reference Salt Solution and the Direct Grout, High Cesium Salt Solution.

Ingredient	Reference Salt Solution (g/L)	Direct Grout High Cesium Salt Solution (g/L)
$NaNO_3$	173.4	211.6
$NaNO_2$	43.1	40.09
NaOH	46.7	87.24
$Na_2CO_3H_2O$	18.5	22.44
$NaAlO_2H_2O$	40.6	34.48
Na_2SO_4	20.9	24.00
NaF	0.62	1.52
NaCl	1.35	1.65
$Na_2C_2O_4$	3.44	1.82
Na_3PO_4	2.9	-
$Na_2PO_412H_20$	-	3.42
KNO_3	-	1.69
$CsNO_3$	-	0.643*
$HgCl_2$	0.338**	0.338**
Na_2CrO_4	0.623 ***	0.623***

* Cs spiked at 0.0033 M Cs using $CsNO_3$. This is 20 times more than the concentration projected for the direct grout case.
** Hg spiked at 250 ppm as $HgCl_2$ in direct grout solution prepared for this feasibility study.
*** Cr spiked at 1830 mg/L as Na2CrO4.

Preparation of Reference Saltstone and High Cesium, Direct Grout
The ingredients and proportions in the reference saltstone are shown below:

Cement Type I/II	4	wt %
Fly ash Class F	25	wt %
Slag Grade 120	25	wt %
Salt solution (containing 71 wt % water)	46	wt %

The water to total cementitious solids of this mixture is 0.6048.

The ingredients and proportions used in the direct grout saltstone containing the high cesium loading are shown below. The water to the total cementitious solids ratio is 0.6092 and is similar to that of the reference saltstone.

Cement Type I	4	wt %
Fly ash Class F	24	wt %
Slag Grade 120	24	wt %
Salt solution (containing 66 wt. % water)	48	wt %

The dry cementitious reagents were premixed to simulate the Z-Area process and then added to the salt solution. Mixing was carried out in a Waring blender for one minute at low speed. Samples were immediately cast into the appropriate containers for the various tests.

Testing

The approach was to compare the high-cesium, direct grout to reference saltstone with respect to the following properties:

- Set time
- Bleed water
- Processing (flowability of grout –subjective evaluation)
- Compressive strength (28 days)
- Leaching
  - TCLP for Cr, Hg, Cs
- Radiolytic gas generation
- Durability Evaluation (limited testing modified ANS 16.1 soak test).

Curing

The curing was conducted at ambient temperature, 45°, 70° and 90° C +/-5° C and 100 % relative humidity. This curing range is representative of the range of initial and long-term curing temperatures which could be encountered under actual field conditions.

Irradiation Experiments

Two samples of direct grout were cast in cylindrical containers approximately 1 x 4 inches in size. These containers were sealed during the 28-day cure period. One sample was cured a 24.5° C and the other at 90° C. The moisture contents of these samples were measured to be 24 and 27 wt. %, respectively. The porosity of each sample was estimated to be 30 to 40 volume percent. These two samples were irradiated simultaneously at a dose rate of 4.2 E+5 rad/hour for 185 hours in a Co-60 source. The dose accumulated in the 185 hr irradiation experiment is equivalent to an approximate 34 year dose at a nominal Cs-137 curie loading of 250 Ci/m^3. Given the nominal density of the direct grout, 1617 kg/m^3, this corresponds to 7.242 E-4 Watts/kg, or a dose rate of 261 rad/hr. Experimental details pertaining to the Co-60 irradiation, gas analyses, and dose calculations are given elsewhere.[9]

(grout plus moisture). Given a nominal moisture content of about 25 wt. %, a $G(H_2)$ based on water alone was calculated to be in the range of 0.08 to 0.12. These G values are significantly lower than the maximum value obtained from pure water, 0.45. Similar results were obtained for dry CST powder irradiation experiments.[8]

Hydrogen concentrations in air of 4 % or more constitute a flammable mixture. Assuming that the direct grout disposed of in the new saltstone vaults will not constitute a closed system (the grout and the concrete vault have open, interconnected porosity), the radiolytic gas production is not expected to result in accumulation of hydrogen in the pores of the saltstone or the air void spaces in the vault.

In addition, visual observation of the samples after irradiation to a 34 year dose indicated no degradation or cracking. However, a difference in the gas pressure versus irradiation time profiles was observed for the direct grout samples cured at 24° and 90° C. Direct grout cured at 24°.C showed a linear increase in pressure as a function of irradiation time. A G value for the total gas produced was similar to the G value for hydrogen (0.01 and 0.02, respectively). Direct grout cured at 90°C showed an initial depressurization followed by a linear increase in pressure. This is similar to the profile observed with CST irradiation.[9] Although the $G(H_2)$ was similar for the two samples, the sample cured at 90° C resulted in more total gas generation. A G value for the total gas produced was higher than the G value for hydrogen (0.07 and 0.03, respectively). This indicates that there was radiolytic production of gas other than hydrogen in the direct grout sample cured at 90° C.

Phase Determination

X-ray diffraction analyses of specimens cured over the entire temperature range indicate the presence of poorly crystalline hydrotalcite, a hydrated magnesium silicate phase characteristic of hydrated slag systems. Gypsum, a hydrated calcium sulfate phase was also detected in all of the samples. The current analysis did not indicate any phase differences over the temperature range studied.

Immersion Test (Durability/Integrity Evaluation)

An immersion test to evaluate structural integrity is in progress. Samples cured at 24.5, 45, 70 and 90°C are currently immersed in deionized water. These samples will be soaked for 90 days and then the compressive strength will be measured. To date, the only type of data available are the result of visual observations. Cracking was observed in the samples cured at 90°C at the time the samples were removed from the molds. Samples cured at 70°C and lower did not show any signs of cracking. See Figure 2. All of these samples were cured in sealed containers and did not experience significant drying. Consequently, the cracking observed in the direct grout and reference saltstone samples cured at 90°C is probably caused by a mechanism other than external drying. Crystallization of soluble or insoluble phases within the matricies of these samples is one possible explanation. However, additional studies are required to understand the cause of the cracking.

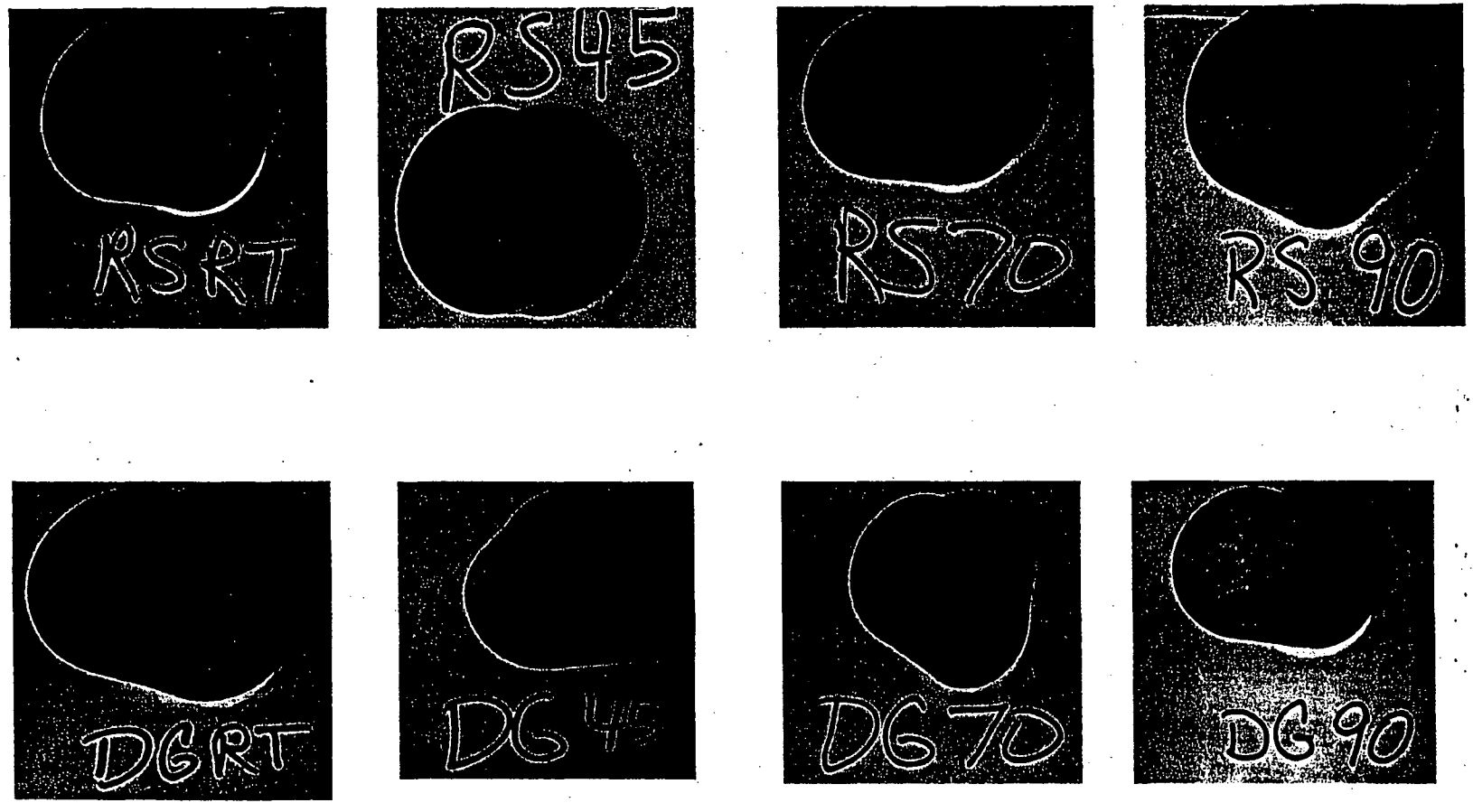

Figure 2. Effect of Curing Temperature on the Reference Saltstone and Direct-Grout Samples Prepared for Immersion Testing (All Samples Were Cured in Sealed Containers). Cracks Were Observed in the 90 C Samples at the Time of De-Molding. No Cracks Were Observed in the Other Samples.

RECOMMENDATIONS

Long-term curing experiments of reference saltstone and direct grout as a function of curing temperature are recommended if direct disposal of grout is selected as the preferred or backup technology to replace the current ITP process. This recommendation is consistent with the direct grout feasibility evaluation and the SRTC technical program evaluation conducted by BNFL. (See Attachment for the BNFL comments.)

Leaching experiments on direct grout cured over the temperature range 24 to 90° C is also recommended.

Additional irradiation and gas collection/analysis experiments should be conducted to further investigate the affect of curing temperature on the direct grout performance.

Regulatory and performance requirements for direct grout should be determined.

Production and pouring strategies should be developed to meet the regulatory and performance requirements.

Tests should be conducted to determine the effect of changes in the salt composition on the properties of the direct grout in order to establish acceptable operating ranges.

Based on the results of this feasibility study, the current saltstone formulation range is adequate for the direct grout. However, if the short term curing temperature cannot be managed by applying a multi-cell pour strategy, then substituting granulated slag for Grade 120 slag should be evaluated. The simplest way to control the long term curing temperature is to adjust the curie content of the waste/waste form if long-term curing is an issue.

QUALITY ASSURANCE

Results are recorded in WSRC-NB-98-00204. Testing was conducted in accordance with SRTC procedures.

REFERENCES

1. A. Shadday, "Thermal Modeling of the Saltstone Pouring and Curing Process," (U), M-CLC-A-00144, 9-22-98.

2. P. L. Rutland, et al., "Bases, Assumptions, and Results of the Flowsheet Calculations for the Initial Eighteen Salt Disposition Alternatives," WSRC-RP-98-00166, June 15, 1998.

3. C. A. Langton, "Phase IV Test Plan for Direct Grout" (U), SRT-WED-98-0114, 8-31-98.

4. D. D. Walker, E-Mail correspondence, 7-27-98.

5. CFR Part 61.55.

6. D. D. Walker, E-Mail correspondence, 7-29-98.

7. CFR Part 61.56.

8. D. D. Walker, E-Mail correspondence, 9-24-98.

9. N. E. Bibler and C. L. Crawford, and C. R. Biddle, "Results of Scoping Studies for Determining Radiolytic Hydrogen Production form Moist CST and CST Slurries," WSRC-RP-98-01143, 10-2-98.

10. Martin Marietta Energy Systems, Inc., "Radiological Performance Assessment for the Z-Area Saltstone Disposal Facility" (U), WSRC-RP-92-1360, 12-18-92.

ACKNOWLEDGEMENTS

D. D. Walker, SRTC, and J. R. Fowler provided the high-cesium salt waste composition used to prepare the direct grout formulation.

C. Crawford and N. Bibler, and C. Biddle, SRTC/ITS, conducted irradiation experiments and provided the analysis to the gas generation rate.

L. Tovo, SRTC/ADS, and B. T. Butcher, SRTC/WPT expedited analytical analyses.

ATTACHMENT I

BNFL Response to Questions and SRTC Program Review

BNFL

Memorandum

To: SRTC

Date: 22 September 1998

From: Graham Jonsson
Ext: +44 19467 72477
Fax: +44 19467 72490

Your ref:
Our ref: CEM/98/S/065

Subject: **Saltstone Immobilisation Programme**

To all at SRTC

SALTSTONE IMMOBILISATION PROGRAMME

This note details comments made by BNFL regarding initial questions raised by SRTC. With respect to the Saltstone immobilisation programme (Section 1), and then in Section 2 a review of the proposed SRTC development programme is given.

SECTION 1

Q1:Does the Saltstone formulation require changing based on the inclusion of the Cs in order to meet TCLP requirements ?

A1:The inclusion of Cs into the wasteform on it's own should not affect the leachability of the metals in the TCLP test. Given that the TCLP test would be performed after 28 days , it is very unlikely that the higher overall temperature of the Saltstone monolith will have any effect on metal solubilities. However the longer term effects of the elevated temperatures on metal retention within the system should be part of the forward programme as it is outside of the current scope of experience.

Although this is different to the TCLP test (i.e. a test that is undertaken after 28 days) it is none the less important that the chemistry of the system is understood to predict longer term behaviour. It is also important to realise that in the TCLP test , the sample is actually ground and therefore monolithicity is not a factor. It is the actual effects of heat upon the overall cement system that is the major point to establish.

Q2:If the formulation does need changing to meet TCLP would this be adequate , or would an alternative additive be required ?

A2 : As stated in Answer 1 it is not certain how the microstructure will be affected by being exposed to high temperatures (greater than 80°C)over extended periods of time. It is not considered that the ability to comply with the TCLP requirements will be affected. If overall radiogenic heat is seen as problematic the simplest alternative may be to just limit the amount of Cs present in the waste. Alternatively different cement systems can be evaluated for suitability.

Q3:What would the bulk temperature rise to based on the heat of hydration ,and would the pouring volume need to be limited because of this ?

A3:Information provided by SRTC is now being used by modellers to predict the bulk temperature rise.

Q4:What effect will the higher Cs loading have on the bulk temperatures in the long term ?

A4 : The Cs loading will govern the bulk temperature within the matrix , with overall tempertaure increasing as the Cs loading increases. Initial results from modelling experiments at SRTC indicate that the bulk temperatures will be around 90°C . This can be substantiated by additional modelling studies in the U.K.

Q5:If curing heat or radiolytic heat is a concern how would we address ?

A5:This can be done by limiting the amount of Cs within the product ,changing the cement formulation or considering an alternative matrix.

Q6:Will gas generation be a concern and if so how will it be addressed ?

A6: The porosity and permeability of the cement microstructure will be sufficient to deal with gas generated from any associated reactions. However this will need to be checked during the development programme to establish the effects at the elevated temperatures.

Q7:What tests would be required to demonstrate short and longer term gas generation will not be a problem ?

A7: The sample will need to be exposed to the expected radiation dose that it would need to withstand in order to retain product integrity. Whereas in the U.K. wasteforms are exposed to the cumulative dose that they would experience during up to 100 years' storage and disposal, the actual dose that the Saltstone wasteform will need to withstand will be specific to the waste acceptance criteria (WAC) governing disposal.

Section 2 : Proposed SRTC development programme

Set :

This is normally undertaken to establish throughput requirements for batch plants. As the proposed process is continuous mixing followed by pumping and placement ,setting is only important if severe retardation is observed , or if set is achieved too quickly. The latter point may be particularly important if the mix were to be delayed on line to the disposal facility. This could result in blocked pipework and the inherent problems of dealing with remediation where the radiation levels will be significantly higher for manual intervention.
Time of set will also need to be established during the pouring stage to establish the effects of pouring additional cemented products on material that may have only undergone partial setting. This can lead to cracking and loss of product integrity.

Bleed water :

Again bleed water is normally associated with plant throughput requirements , although the avoidance of the generation of secondary wastes is also of major importance. Ideally the formulation should provide a bleed free product , however at what time bleed water must not be present will be very specific to this particular project.

Processing :

The proposal is to have a subjective test. Experience in the U.K. indicates that this kind of evaluation is not suitable ,and it is suggested that actual methods to evaluate grout processability / fluidity are established.

Compressive strength :

While the test indicates that the test will be undertaken after 28 days, it is recommended that a strength development profile is undertaken. This will allow a prediction to be made of any potential interactions taking place within the matrix. It may also be beneficial to undertake these measurements over longer periods so that the longer term strength development profile can be monitored.

There are also non-destructive tests that can be performed to monitor strength development as opposed to compressive strength.

Leaching :

The standard test is to undertake the TCLP test after 28 days. It is recommended that additional testing is undertaken to establish any likely affects of the higher heat loading on the overall cement microstructure.

Radiolytic gas\generation:

The wasteform needs to be exposed to the cumulative radiation dose that the wasteform will experience during the evaluation period. This will not only establish the effects of radiation on the wasteform stability , but can also be used to establish the effects (if any) of dealing with any gas generated upon the cement microstructure.

The curing temperatures will need to reflect the actual core temperatures which the matrix will experience and therefore any tests will need to be able to reflect these temperatures as opposed to simply curing at the temperature under assessment.

General comments:

The overall programme is focussed mainly on passing the necessary WAC. However as this wastestream composition is now fundamentally different to the original Saltstone, it is considered that additional testing would be beneficial in understanding the ongoing cement/waste interactions taking place.

The programme does not indicate any timescales for the test period.

The surrogate needs to be prepared in as near as possible the same way as the waste will be produced during future operations.

The programme appears to be focussed upon dealing with a worst case scenario. It may be beneficial to consider a range of formulations to understand any changes occurring as formulations change.

In terms of the actual process, I have assumed that the relevant operating envelopes and equipment deployed and established for the original plant will still be used in the new facility and are therefore outside the scope of these comments.

GH Jonsson
Research and Technology
Sellafield
Seascale
Cumbria.

RESULTS AND DISCUSSION

Processibility, Set Time and Bleed Water

Processibility was evaluated by visual observation. The direct grout slurry was compared to the reference saltstone slurry. The direct grout slurry was easily mixed in the Waring blender. The resulting slurry was fluid and was easily poured into the sample containers. The direct grout gelled (thickened to the extent that it was no longer pourable) in 25 to 30 minutes. The reference saltstone slurry was also very fluid and pourable. However, it gelled in 20 to 25 minutes. Bleed water was not observed on either slurry formulation. Processing results are summarized in Table 3.

Table 3. Processing results for Reference Saltstone and Direct Grout.

Mix Design	Qualitative Flow Properties	Gel Time (minutes)	Bleed Water (volume %)	Set Time (hours)
Reference Saltstone	Very Fluid, Pourable	20-25	0	18-24
Direct Grout	Very Fluid, Pourable	25-30	0	18-24

Compressive Strength

Compressive strength was determined for samples cured for 28 days at 24.5, 45, 70, and 90^0 C. The relative humidity of all of the samples except those cured at 90^0 C was maintained at 100 %. The samples cured at 90^0 C were cured in the presence of excess water/water vapor. However, cracks were observed on these samples when they were removed from the curing chamber. See Figure 1. These samples also appeared dry on the outer surface. This was confirmed when the samples were examined after the compressive strength tests. The outer centimeter of the samples was obviously drier than the inner core.

Consequently the 90^0 C samples experienced some drying. Drying shrinkage is probably not the only explanation for the observed cracks since other samples cured at 90^0 C in sealed containers showed no drying and were also found to be cracked after curing.

Even though the direct grout and reference saltstone 90^0 C samples were cracked prior to the strength determinations the strengths were very high. Given the limited number of samples tested, the strengths of the direct grout and reference saltstone are similar for each curing temperature. Compressive strength results are summarized in Table 4.

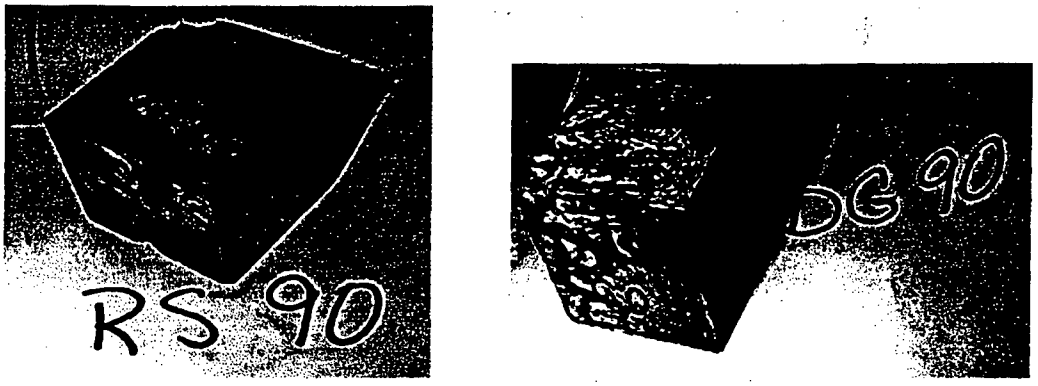

Figure 1. Photographs Illustrating the Crack Patterns Characteristic of Reference and Direct-Grout Sample Cured at 90 °C (No cracking was observed for samples cured Between Room Temp. and 70 °C).

Table 4. Compressive Strength Results for Direct Grout and Reference Saltstone

Mix Design	Curing Temperature (°C)	Compressive Strength (psi)	Average Compressive Strength (psi)
Direct Grout	24.5	2,050	2,212
		2,375	
	45	4,000	4,075
		4,150	
	70	3,250	3,412
		3,575	
	90	4,675	4,562
		4,450	
Reference Saltstone	24.5	2,225	2,325
		2,425	
	45	3,575	3,525
		3,475	
	70	3,875	3,675
		3,475	
	90	4,250	3,925
		3,600	

Leaching

TCLP

Samples were prepared for TCLP testing for Cr and Hg, which are the two potentially hazardous constituents in both the high cesium (direct grout) and reference salt solutions. All samples of reference saltstone and direct grout cured between 24 and 90° C passed the TCLP for Cr and Hg. Consequently, these waste forms qualify to exit RCRA.

The TCLP extract was also analyzed for Cs to give a relative comparison of the Cs leachability for the two formulations. The direct grout samples were spiked with about 20 times more cesium than is actually expected (1.5 Ci/gal Cs-137) to assure detection above the reportable limit in the TCLP extracts since the objective was to evaluate the effect of curing temperature on cesium leachability. Based on the total cesium concentration in the direct grout samples (150 ug/g) between 11 and 16 % of the cesium was leached during the 18 hour TCLP test on crushed samples. This is consistent with the limited retention of cesium in the reference saltstone as modeled in the Z-Area performance assessment ($K_d = 2$ for Cs).[10]

Table 5. TCLP Results for Direct Grout and Reference Saltstone Cured between 24 and 90°C.

Sample Description	Sample ID	Curing Temperature (°C)	TCLP Results		
			Cr (ug/L)	Hg (mg/L)	Cs (ug/L)
Reference Saltstone	980072A	24.5	< 60	< 0.020	< 40
	98L45B	45	< 60	< 0.020	< 40
	980067A	70	< 60	< 0.020	< 40
	980066A	90	< 60	< 0.020	< 40
Direct Grout	980071A	24.5	< 60	< 0.020	1150
	98SL45A	45	< 60	< 0.020	932
	980068A	70	< 60	< 0.020	807
	980069A	90	< 60	< 0.020	882
TCLP Regulatory Limit*			5000 (5 mg/L)	0.2	NA

* Limit for disposal of treated characteristic waste.

Radiolytic Gas Generation

Two samples (approximately 65g each) of direct grout were irradiated in an air sealed systems containing approximately 55 cc of air. Details of the experimental configuration are given elsewhere.[8] Preliminary analysis of the gas collected above the irradiated direct grout samples indicates that hydrogen was produced with a G value of 0.02 to 0.03 molecules per 100 eV. These G values are based on the total mass of grout irradiated

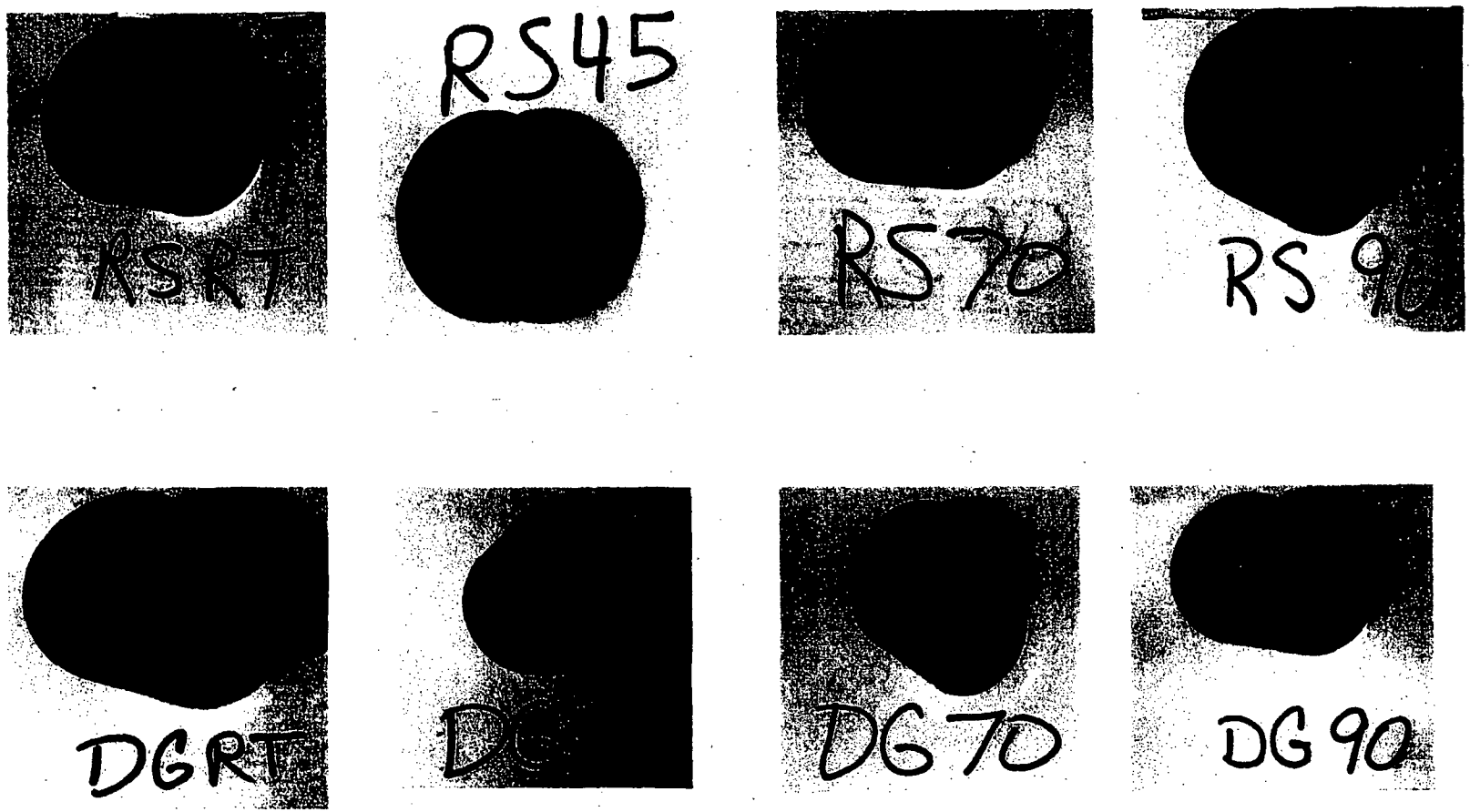

Figure 2. Effect of Curing Temperature on the Reference Saltstone and Direct-Grout Samples Prepared for Immersion Testing (All Samples Were Cured in Sealed Containers). Cracks Were Observed in the 90 C Samples at the Time of De-Molding. No Cracks Were Observed in the Other Samples.

CONCLUSIONS

Salt solution containing up to 6.4 M sodium salts and an average Cs-137 concentration of 1.5 Ci/gal can be stabilized in a saltstone waste form. Based on the results of this feasibility study and the current understanding of the effect of curing temperatures on long term properties, no formulation change is required. This statement assumes that pouring strategies,[1] raw materials temperatures and specifications, and Cs-137 and other radionuclide concentrations will be managed to maintain curing temperatures below 90°C. Based on the data available to date, the temperature threshold for cracking is between 70 and 90° C.

Direct grout made from 6.4 M sodium salt solution containing 1830 and 250 mg/L of Cr and Hg, respectively, were determined to be non hazardous based on the TCLP test. The direct grout saltstone has processing properties similar to those of the current saltstone waste form (except for the additional shielding and remote handling required for the higher activity in the high cesium waste).

Based on results obtained in this feasibility study, hydrogen gas generation due to radiolysis of the free water in the saltstone will not result in the accumulation of hydrogen above the explosive limit since the waste form is monolithic and there is no void space inside the closed vaults. In addition, migration of hydrogen gas through the waste form pore spaces is not expected to damage the microstructure of the saltstone since the pore space is interconnected.

Most of the cracking observed in samples cured at 90°C is attributed to drying shrinkage due to water evaporation. However, at least one other mechanism may be present since samples cured in sealed containers also cracked (too a lesser degree). The compressive strengths of the direct grout and reference saltstone cured at 90°C were high in spite of the cracking observed in the samples. This indicates that although the cracks were formed, they did not open. However, the cracks in the 90°C samples are opening in the immersion test, which requires a 90-day soak in deionized water. Depending on the results of this test, the direct grout and reference saltstone cured at 90°C for long term (28 days) may not pass the immersion test which is intended to indicate structural integrity/durability. In the present analysis, there are two options for addressing the results of the immersion test, 1) cure direct grout and saltstone below 90°C (samples cured at 70°C showed no cracking) or 2) take credit for the structural integrity of the vault (waste form container).

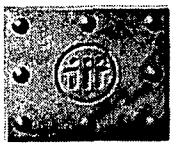

Sterling Robertson/WSRC/Srs

07/12/2005 04:02 PM

To David Chew/WSRC/Srs@srs
cc
bcc
Subject Fw: RAI #38

APPROVED for Release for Unlimited (Release to Public)

----- Forwarded by Sterling Robertson/WSRC/Srs on 07/12/2005 04:02 PM -----

Timothy Chandler/WSRC/Srs

07/12/2005 04:01 PM

To Christine Langton/SRNL/Srs@Srs
cc Sterling Robertson/WSRC/Srs@Srs
Subject RAI #38

Chris,

Based upon a review of the old Operating logs and Engineering calc sheets, the following facts can be discerned:

1. The proportions of the cement, slag, and fly ash (premix) have been essentially constant during the previous operation of the Saltstone Facility. The standard premix composition used in the facility is 10/45/45 cement/slag/fly ash by weight.

2. The variations of this premix composition that were used in actual processing involved reducing or increasing the cement content in the premix by 1 or 2 wt% and making a corresponding adjustment in the Class F fly ash or slag content of the premix in an attempt to optimize the processing properties of the mix.

3. The premix to water ratio was maintained between 0.60 and 0.66, regardless of the salt content of the waste solution.

4. The compressive strength of all grout samples tested at the Saltstone Facility was greater than the minimum requirement of 200 psi.

5. For the table, use the following:

Type II cement = 3 wt% (-1 wt%,+ 2 wt%)
Slag = 25 wt% (+ 1 wt%)
Class F Fly ash = 25 wt% (+ 1 wt%)
Salt solution = 47 wt% (+ 2 wt%)

APPROVED for Release for
Unlimited (Release to Public)
6/6/2005

WSRC-TR-2005-00074 ←
Revision 0

KEY WORDS: **Performance Assessment**
Low-level Radioactive Waste Disposal

SPECIAL ANALYSIS: REVISION OF SALTSTONE VAULT 4 DISPOSAL LIMITS (U)

PREPARED BY:
James R. Cook
Elmer L. Wilhite
Robert A. Hiergesell
Gregory P. Flach

MAY 26, 2005

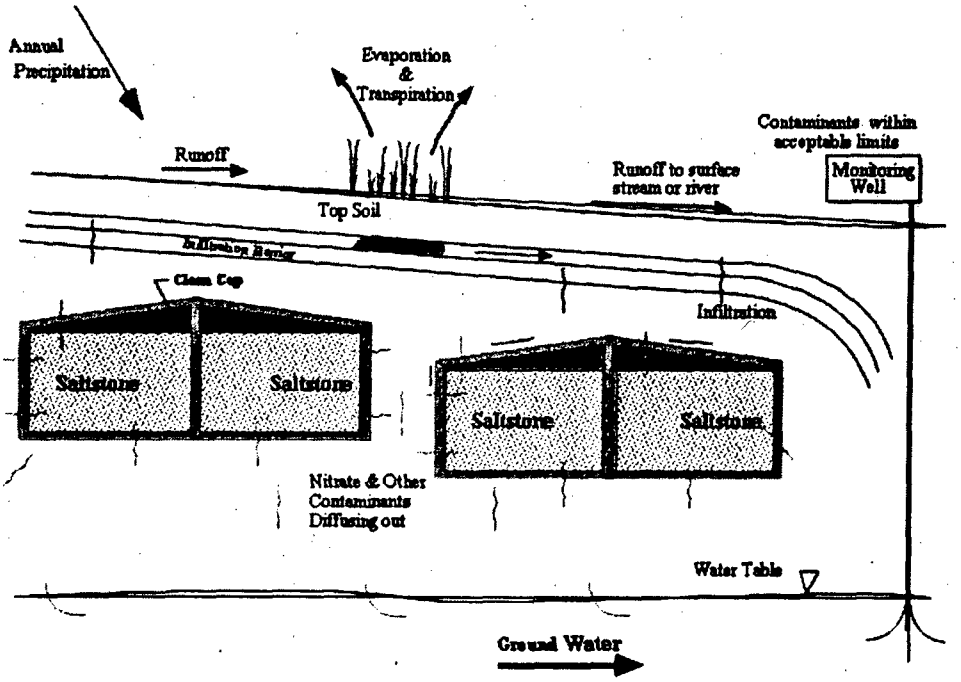

Westinghouse Savannah River Company
Savannah River Site
Aiken, SC 29808

Prepared for the U.S. Department of Energy Under Contract Number DE-AC09-96SR18500

SRNL
SAVANNAH RIVER NATIONAL LABORATORY

A.2.2 Time of Compliance and Simulation Time Intervals

The DOE time of compliance is 1,000 years (Wilhite 2003). However, the total time used for groundwater modeling is extended to 10,000 years to assess the impact of a longer period of compliance. The eight time intervals (Phifer 2004) used for groundwater modeling are shown in Table A-3.

Table A-3. Simulation Time Intervals

INTERVAL	TIME (YEARS)		
TI01	0	to	100
TI02	100	to	300
TI03	300	to	550
TI04	550	to	1,000
TI05	1,000	to	1,800
TI06	1,800	to	3,400
TI07	3,400	to	5,600
TI08	5,600	to	10,000

A.2.3 Flow Modeling

A.2.3.1 Flow Properties

The fundamental concept of the SDF (wasteform and facility features) is controlled contaminant release. Due to the low hydraulic conductivity and low molecular diffusion in cementitious materials, contaminant leaching from the SDF is very slow. This makes transformation into Saltstone an effective method for liquid waste disposal. Among all the factors affecting the SDF performance, the most important factor is hydraulic conductivity. The saturated hydraulic conductivities of the engineered porous media (Saltstone, concrete and gravel drain layers) were measured by Core Lab as described in 1993 (Yu 1993). These intact values are used for the first 100 years of simulation under the column heading TI01 in Table A-4.

Table A-4. Saturated Hydraulic Conductivities (cm/sec)

	TI01	TI02	TI03	TI04	TI05	TI06	TI07	TI08
				Horizontal conductivity:				
Nati/Back	1.00E-04	1.00E-04	1.00E-04	1.00E-04	1.00E-04	1.00E-04	1.00E-04	1.00E-04
Drain Bot	1.00E-01	9.99E-02	9.97E-02	9.90E-02	9.71E-02	9.30E-02	8.63E-02	7.46E-02
Drain Ver	1.00E-01	1.00E-01	1.00E-01	1.00E-01	1.00E-01	1.00E-01	1.00E-01	1.00E-01
Drain Top	1.00E-01	9.99E-02	9.93E-02	9.75E-02	9.28E-02	8.25E-02	6.58E-02	3.66E-02
Concrete	1.00E-12	5.20E-12	1.29E-11	3.16E-11	7.64E-11	1.98E-10	4.19E-10	1.00E-09
Saltstone	1.00E-11	3.00E-11	5.50E-11	1.00E-10	1.80E-10	3.40E-10	5.60E-10	1.00E-09
				Vertical conductivity:				
Drain Bot	9.52E-02	6.45E-02	2.70E-02	8.94E-03	3.34E-03	1.41E-03	7.25E-04	3.93E-04
Drain Top	8.89E-02	4.21E-02	1.29E-02	3.78E-03	1.36E-03	5.69E-04	2.91E-04	1.57E-04

In this SA, it is assumed the hydraulic conductivities of Saltstone and concrete will increase as time proceeds. As a result, water percolation will gradually increase through the vault. It is also assumed that the conductivities of the top and bottom drains will decrease with time due to plugging in the lower part of these drains resulting in the engineered drains becoming less effective in shedding perched water above the concrete roof. It is assumed that the effective

WSRC-TR-2002-00456
Revision 0

KEY WORDS:
Vault
LLW Disposal
Disposal Authorization Statement

SPECIAL ANALYSIS:

REEVALUATION OF THE INADVERTENT INTRUDER, GROUNDWATER, AIR, and RADON ANALYSES FOR THE SALTSTONE DISPOSAL FACILITY

Authors

James R. Cook
Westinghouse Savannah River Company

David C. Kocher
SENES Oak Ridge, Inc.

Laura McDowell-Boyer
Alara Environmental Analysis, Inc.

Elmer L. Wilhite
Westinghouse Savannah River Company

October 23, 2002

Westinghouse Savannah River Company
Savannah River Site
Aiken, SC 29808

Prepared for the U.S. Department of Energy
under Contract No. DE-AC09-96SR18500

1. EXECUTIVE SUMMARY

This Special Analysis updates the inadvertent intruder analysis conducted in 1992 in support of the SDF RPA, extends the groundwater analysis to consider additional radionuclides, and provides an assessment of the air and radon emanation pathways. The results of the RPA were originally published in the WSRC report (WSRC-RP-92-1360) entitled *Radiological Performance Assessment for the Z-Area Saltstone Disposal Facility* (MMES et al., 1992). The present reevaluation considers new requirements and guidance of the USDOE Order 435.1 (USDOE, 1999), expands the list of radionuclides considered, incorporates an increase in design thickness of the roof on a disposal vault, and produces results in terms of interim limits on radionuclide-specific concentration and inventory rather than dose resulting from a projected inventory. The limits derived herein will be updated when the Saltstone PA is revised (currently planned for fiscal years 2003/2004).

The SDF is located within a 650,000 m^2 area of SRS designated as Z Area. The SDF together with the SPF are part of an integrated waste treatment and disposal system at the SRS. Saltstone is a solid waste form that is the product of chemical reactions between a salt solution and a blend of cementitious materials (slag, flyash, and cement). Based on the present projected site layout of the SDF, up to 730-million L (192 million gal) of wastewater can be treated for subsequent disposal as saltstone. The SPF and SDF are regulated by the State of South Carolina, USDOE Orders, and other Federal regulations that are applicable to disposal of solid waste.

As part of the RPA process, USDOE Order 435.1 requires an assessment of the dose to a potential member of the general public to limit doses from all pathways to no more than 25 mrem in a year and, from the air pathway alone, to no more than 10 mrem in a year. The Order also requires an assessment of radon release to ensure that the radon flux does not exceed 20 $pCi/m^2/s$. Additionally, for purposes of establishing limits on concentrations of radionuclides for disposal, the Order requires that an assessment be made of impacts to hypothetical persons assumed to inadvertently intrude into the low-level waste disposal facility and an assessment of the impacts to water resources. For the intruder analysis, the pertinent performance measure specifies that dose to such hypothetical individuals may not exceed 100 mrem EDE per year for chronic exposure, and may not exceed 500 (EDE) mrem from a single event. To meet the assessment requirement addressing impact on water resources in the Order, SRS uses the Safe Drinking Water Act Maximum Contaminant Levels (USEPA, 2000) as the pertinent performance measure.

To limit the number of radionuclides for which analyses are needed, the half-lives of radionuclides and physical processes by which low-level waste destined for the SDF is generated were considered. Such considerations led to selection of 75 radionuclides for analysis. Potentially significant contributions by radioactive decay products of these 75 radionuclides were also assessed.

Two time frames for the analyses are considered in this Special Analysis. The USDOE Order 435.1 specifies a time frame of 1,000 years after facility closure for establishing limits on allowable disposals. Here, both the 1,000-y time frame and a longer time frame of 10,000

years after facility closure are also considered, to be consistent with both the USDOE Order and the Disposal Authorization Statement (DAS) for SRS (Fiori and Frei, 1999).

In the intruder analysis, the only credible scenario within 10,000 years is the resident scenario, based on the current design of the SDF. The 0.4 m of grout directly above the saltstone, 0.1-m concrete roof over the vaults, and 1 m of grout on top of the roof combine to provide at least 0.5-m of shielding up to 10,000 years, assuring that excavation into the waste during this time period is not a credible occurrence (Fig. 1-1). The resident scenario is evaluated at 100, 1,000, and 10,000 years after disposal. In the resident scenario, the intruder is assumed to excavate no more than 3 meters in building a home. Evaluation of the scenario at 100 years, when the engineered barriers (i.e., the grout above the saltstone, the vault roof, and the grout above the roof) are assumed to be intact, resulting in the intruder's home being constructed on top of the uppermost layer of grout, is used to determine limits on allowable disposals of shorter-lived photon-emitting radionuclides in the waste. Evaluation of the resident scenario at 1,000 and 10,000 years, when the engineered barriers are assumed to have failed (i.e., have lost their physical integrity) and are no longer a deterrent to intrusion, resulting in a lesser thickness of shielding above the waste, is used to determine limits on allowable disposals of longer-lived photon-emitting radionuclides. The thickness of uncontaminated material above the waste is the same at these two later times because the upper 0.9 m of the closure has eroded (Fig. 1-1) and the depth of the intruder's excavation is limited to 3 m. The resident scenario at 1,000 years may be important for radionuclides having longer-lived photon-emitting decay products. The resident scenario at 10,000 years is important only when a longer-lived radionuclide has long-lived photon-emitting decay products whose activities increase with time beyond 1,000 years.

For the groundwater, air, and radon emanation pathways, results from the previous SDF PA and applicable portions of the E-Area LLWF PA were used to derive limits on allowable disposals based on analyses for time frames of 1,000 years and 10,000 years after facility closure. For the groundwater pathway, it was necessary to extend the previous analysis in the SDF PA to radionuclides not previously considered, using the PATHRAE code.

The results of this Special Analysis indicate that, for the 10,000-year time frame, 41 radionuclides, of the 75 selected, require limits on disposal. Of the 41 radionuclides for which disposal limits were derived, 34 are limited by the intruder analysis, four by the groundwater pathway analysis, two by the air pathway analysis, and one by the radon emanation analysis. The radionuclide disposal limits were compared with the currently estimated radionuclide concentrations in low curie salt. The greatest fraction of a limit is 0.038 for ^{126}Sn and the total sum-of-fractions of all the limits is 0.084. This provides assurance that low curie salt can be disposed in the saltstone disposal facility without exceeding any of the USDOE performance objectives.

For the 1,000-year time frame, 37 of the 75 radionuclides would require disposal limits. Of these, 35 would be limited by the intruder analysis, none by the groundwater analysis, two by the air pathway analysis, and none by the radon emanation analysis. The greatest fraction of a limit would remain 0.038 for ^{126}Sn and the total sum-of-fractions would decrease to 0.048.

The 10,000-year time frame limits should be used to develop WAC for the SDF.

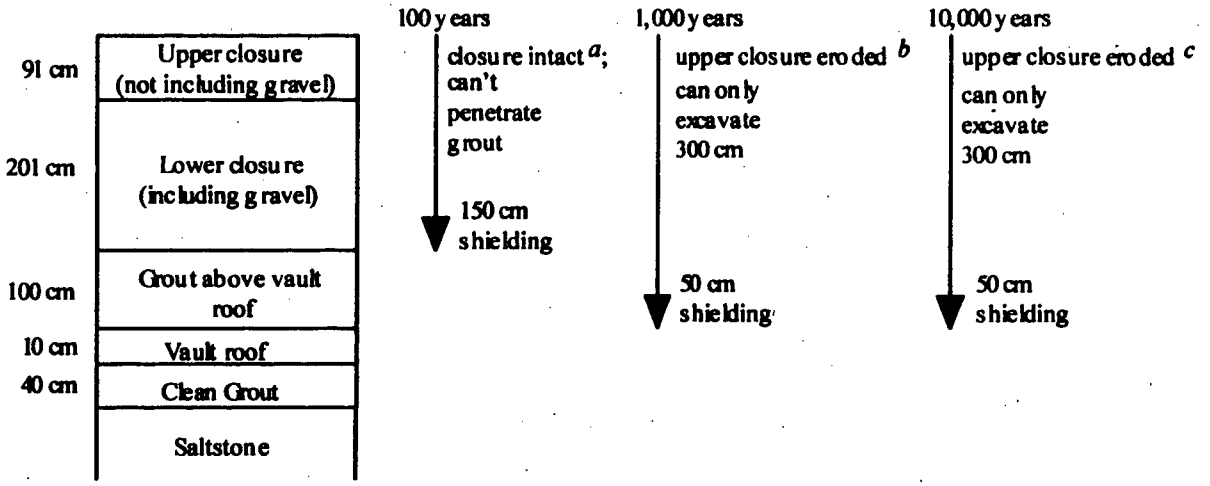

[a] At 100 years after closure, there has been no erosion and the grout and vault roof have not deteriorated so that they effectively prevent excavation. Therefore, the intruder constructs his residence atop the grout above the vault roof, resulting in a total of 150 cm of shielding between the residence and the saltstone.

[b] At 1,000 years after closure, erosion has removed the upper 91 cm of the closure. However, the gravel, which is the uppermost portion of the lower closure, prevents further erosion. The grout and vault roof have deteriorated to soil equivalent material so that they no longer can prevent excavation. Since the intruder's excavation is limited to 300 cm, the residence is constructed on top of the vault roof, resulting in a total of 50 cm of shielding between the residence and the saltstone.

[c] At 10,000 years after closure, erosion has not penetrated further than at 1,000 years (i.e., 91 cm), because of the gravel layer. Since the intruder's excavation is limited to 300 cm, the residence is constructed on top of the vault roof, resulting in a total of 50 cm of shielding between the residence and the saltstone.

Fig. 1-1. Resident Scenario Conceptual Model

TECHNICAL DIVISION
SAVANNAH RIVER LABORATORY

Keywords: Saltstone Durability
Saltstone Diffusion Coefficients
Pennsylvania State University Progress Report

M E M O R A N D U M

DPST-85-528

W. R. Stevens, III, 773-A
E. L. Albenesius, 773-A
E. L. Wilhite, 773-41A
LLW Group (7)
SRL Record Copy (4)

DIFFUSION COEFFICIENTS

Effective diffusion coefficients for Cs^+ were measured for the current reference formulation and 6 other mixes containing DWPF salt solution. Cs^+ was selected as a tracer ion because its mobility through hydrated cement paste is similar to Na^+, NO_3^-, and NO_2^-. The experimental configuration consisted of a Cs^+ sink separated from a Cs^+ source by a thin, 4mm, membrane or wafer of cured saltstone.

The current reference formulation had the lowest diffusion coefficient of about 2×10^{-9} cm/sec. A modified reference mix containing zeolite and a formulation containing slag cement had the next lowest values about 3×10^{-8} and 4.5×10^{-8} cm^2/sec. The other mixes had coefficients between 1 and 4×10^{-7} cm/sec. A report summarizing these experiments is attached.

Recipes for the formulations tested are shown in Table I.

Comparison of Cs^+ diffusion data with permeability, porosity, and median pore radii data indicates that samples with low effective diffusion coefficients have low permeabilities and porosities. They also have the smallest median pore radius. Data are summarized in Table II. Formulations are qualitatively ranked in terms of diffusion coefficients in Table III.

TABLE I

COMPOSITIONS OF MIXTURES EVALUATED FOR DURABILITY

Mix	Cement				Fly Ash			Slag	Extender		Solution
	Lonestar H-10*	Santee II-06	Giant I-12	Blended Z-58	Class C B75	Class F B74 B83	ESP B73	Newcem B63	Attapulgite C86	Chabazite C84	32 wt % E34
84-40 Reference				62.5							37.5
84-41	12.0					38.0 (B74)					50.0
84-42	12.0						38.0				50.0
84-43			15.0			45.0 (B83)					40.0
84-44		15.0				45.0 (B83)					40.0
84-45			7.5			45.0 (B83)		7.5			40.0
84-46	12.0				26.0				2.0		60.0
84-47				58.0						2.0	40.0

*Each starting material was assigned a log number. Each mix was also assigned a log number. Proportions are reported in wt%.

→ TABLE II

CESIUM DIFFUSION COEFFICIENTS FOR Cs^+ IONS THROUGH SALTSTONE WASTE FORMS

PSU Mix #	w/c_{total}*	D_{EFF} Cs^+ (cm^2/sec)	H_2O Permeability K_{H_2O} (Darcy)**	Porosity (%)	Median Pore Radius (nm)
84-40	0.41	2.1×10^{-9}	$<10^{-8}$	40.0	10.8
84-41	2.9	1.1×10^{-7}	1.72×10^{-3}	64.6	125
84-43	1.8	1.5×10^{-7}	2.52×10^{-3}	50.1	26
84-44	1.8	4.1×10^{-7}	5.89×10^{-4}	47.7	18
84-45	1.8	5.3×10^{-8}	$<10^{-8}$	42.5	16
84-46	1.1	3.9×10^{-7}	2.21×10^{-5}	54.9	200
84-47	0.48	4.0×10^{-8}	1.78×10^{-7}	40.6	10.5***

*c_{total} = total cementitious solids; portland cement + granulated blast furnace slag + Class C (high calcium) fly ash.

**1 darcy = 10^{-3} cm/sec

***58 day data are reported for 84-47. 28 day data is reported for the other samples.

→ TABLE III

SALTSTONE TEST MIXES RANKED IN TERMS OF DIFFUSION COEFFICIENTS FOR Cs^+

MIX NUMBER	INGREDIENTS (Solids)	QUALITATIVE RANKING
40	Reference Mix Class H cement Class C fly ash	very good
45	Type I cement Newcem (slag) Class F fly ash	good
47	Ref Mix 2 wt % zeolite (chabazite)	good
44	Type II cement Class F fly ash	average
43	Type I cement Class F fly ash	average
41	Class H cement Class F fly ash	average
46	Class H cement Class C fly ash 2% clay (attapulgite)	bad
42	Class H cement ESP ash	very bad (no samples)

TECHNICAL DIVISION
SAVANNAH RIVER LABORATORY

Keywords: Saltstone Hydraulic Conductivity
Saltstone Permeability

M E M O R A N D U M

DPST-85-982

cc: W. R. Stevens, III, 773-A
E. L. Albenesius, 773-A
E. L. Wilhite, 773-41A
Saltstone Group
SRL Records (4), 773-A

December 10, 1985

TO: H. F. STURM, JR., 773-A

FROM: C. A. LANGTON, 773-41A

SALTSTONE PERMEABILITY (HYDRAULIC CONDUCTIVITY)

SUMMARY

Saturated and unsaturated hydraulic conductivities were measured for the reference saltstone sample cured for about six months. Steady state saturated hydraulic conductivity was 3.3×10^{-8} cm/sec; the partially saturated hydraulic conductivity was 1.1×1^{-8} cm/sec. These values are higher than those previously reported. However, steady state was probably not achieved in previous unsaturated samples.

EXPERIMENTAL PROCEDURE

Saltstone samples containing 42.5 wt% salt solution and 57.5 wt% blended cement were cut into four inch diameter right cylinders and sealed in permeability cells. This material was cured about six months before testing. A constant head method was used in which 4.5 to 20 psi hydraulic pressure was applied. The saturated sample was prepared by pulling a 7 psi vacuum and replacing air with water prior to the permeability measurements.

RESULTS

Results are tabulated in Table 1. Flow was monitored as a function of time since initial values, especially for the unsaturated case do not represent steady state flow through the

saltstone. The unsaturated sample had a hydrualic conductivity of about 1.1×10^{-8} cm/sec after one week of flow. The unsaturated sample had a permeability of about 3.3×10^{-8} cm/sec one week after flow was established through the specimen.

COMPARISON WITH PREVIOUS DATA

Values reported here are about two orders of magnitude lower than those for typical concrete measured at the same laboratory. However, they are higher than values previously reported for saltstone.[1,2,3] Western Company of N. America reported a permeability of $<10^{-11}$ cm/sec for saltstone containing 37.5 rather than 42.5 wt% solution. Also the samples were hydrostatically loaded with 1000 psi during the test. This may have collapsed the fine surface structure and resulted in low values.[2]

Law Engineering also measured permeability on two specimens containing 40 wt% salt solution. Values ranged from an average of 2.9×10^{-9} cm/sec at 20 psi head pressure to 2.55×10^{-10} cm/sec at 100 psi head pressure. Again these specimens contained less solution and therefore less water than the current reference mix.[1]

Personnel at the Materials Research Laboratory, Penn State University, have also measured permeability as a function of curing time. After six months curing a specimen containing 37.5 wt% salt solution had a water permeability of 1×10^{-9} cm/sec.[3] 200 psi hydrostatic pressure was applied during this measurement.

DISCUSSION

Sample size may affect measured permeability. Small samples subjected to high head pressures tend to yield permeabilitiess lower than measured on larger specimens with the same composition. High hydrostatic pressure may collapse some of the gel structure and further reduce the measured permeability.

Small samples have in general smaller imperfections than do larger samples since the small samples can be more carefully screened. This also results in lower measured permeabilities since flow will occur through the largest interconnected pores and through cracks. Very little flow will occur through the bulk matrix if a sample contains zones of higher porosity. (Fine cracks due to surface drying were observed on the specimens tested at the Portland Cement Association.)

CONCLUSIONS

- Hydraulic conductivity of the current reference saltstone (42.5 wt% salt solution; 57.5 wt% blended cement) is about 2×10^{-8} cm/sec.
- Hydraulic conductivities of cement-based waste forms is in part a function of the water to cement ratio. Increased water results in increased porosity and permeability.

REFERENCES

1. R. V. Simmons, Saltstone Field Samples Permeability Results, Memorandum to G. T. Wright, June 19, 1984.
2. A. K. Sarkar, Disposal of Low-Level Radioactive Waste Solution in a Cement Matrixx - Final Report by Western Company of North America, March 1, 1984.
3. P. H. Licastro, personal communication, Penn State Durability Study - Progress Report.

CAL:\tyb
D:IBM

DP-MS-85-9

SLAG CEMENT — LOW-LEVEL WASTE FORMS AT THE SAVANNAH RIVER PLANT

by

R. I. A. Malek, D. M. Roy, and M. W. Barnes

Materials Research Laboratory,
The Pennsylvania State University
University Park, PA 16802

and

C. A. Langton

E. I. du Pont de Nemours and Company
Savannah River Laboratory
Aiken, South Carolina 29808

A paper proposed for presentation at the
87th Annual American Ceramic Society Meeting
Cincinnati, OH
May 5-9, 1985

This paper was prepared in connection with work done under Contract No. DE-AC09-76SR00001 with the U.S. Department of Energy.

Table VIII. Summary of X-Ray Phase Identification - 84-45.

Phase	Age (Days) 7	28	56	90	180
unreacted cement	*	decrease with time ——————>			
unreacted fly ash (quartz + mullite)	*	*	*	*	*
unreacted slag	*	*	*	*	*
lime	**	**	**	**	**
bonding compound	substituted C-S-H	*	*	*	*
$Al(NO_3)_2 \cdot 9H_2O$	large quantity	**	**	**	**
$Ca(NO_3)_2 \cdot 2H_2O$	**	**	*	increase ——>	
Others:					
C_3AH_6, C_3FH_6	**	**	*	*	*
$Na_2CO_3 \cdot 10H_2O$	*	*	*	*	*
$CaCO_3$	**	**	*	increase ——>	

*Identified. **Unidentified.

appreciable reaction of the fly ash spheres and buildup of CSH structure. Some reticular network C-S-H is still apparent at this age. Figure 7 is a micrograph of 84-40 cured for 180 days. Again the overall integrity of the structure is evident. A plerosphere (spheres within fly ash spheres) appears very well reacted externally and bound into the surrounding matrix.

84-41. Figure 8 illustrates the morphology of 84-41 at 7 days. Micrograph 8(a) is a secondary electron image whereas 8(b) is a back-scattered image, which gives better contrast. These images show an area where an agglomerate has occurred (on the right hand side of the micrograph). Figure 8(c,d) are elemental maps for Ca and Si, respectively. It is evident from this series of micrographs that the agglomerated parts are cement (high Ca, low Si). Figures 8(e,f) are successively higher magnifications to the cement

side (right side) of micrographs (a,b). It shows precipitated crystals embedded in the hydrated matrix. EDXA of selected parts of that micrograph are shown. Curve a is for some area outside the crystalline part. It shows the C-S-H structure besides the precipitation of some other salts including Al and Na. Curve b is for a crystalline part. It shows the lime including C-S-H and sulphur-containing compounds. Such agglomerations can lead to a very low early strength (since early strength should be totally dependent on the cement portion) and a very slow strength development. Figure 9 is a series of micrographs at variable magnifications to 84-41 at 90 days. The poor integrity and high porosity of the structure is evident from micrographs 9(a,b). Micrograph 9(c) shows some characteristic features of the dissolution of low-calcium fly ash. Figure 9(c) shows a dissolved glassy surface with residual Fe oxide (magnetite or hematite) (low solubility) remaining attached to the surface of the ash sphere. Figure 10 is a series of micrographs at successively increasing magnifications of 84-41 cured for 180 days. Poor integrity and high porosity despite more gel formation are the common features.

84-45. Figure 11 shows low and high magnifications (backscatter images) of 84-45 cured for 7 days. Integrity and low porosity are apparent with some cenosphere peaks attached to the matrix. Figure 12 gives micrographs of a 28-day-old sample. Features similar to those in Fig. 11 (7 days) are evident. A glassy irregular slag fragmentation seen (left center, b). Figure 13 represents a 56-day-old sample, showing a dense structure. Some of the same common features as in Figs. 11 and 12 are evident, together with the inside of a (hemi-) sphere which remained attached to the matrix after sawing the sample. This indicates a good bond strength between fly ashes and matrix. Analysis of this hemisphere is shown in the EDXA result represented in Fig. 14. Figures 15 and 16 represent backscattered electron images for the mix 84-45 at 90 and 180 days, respectively. The same features of that mix at previous ages are evident; namely, integrity and low porosity. The latter indicates the very high degree of integrity obtained with this composition at 180 days.

4) Contaminant Release Rates

A modified Paige leach test (2) was used in evaluating formulations 84-40, 84-41, and 84-45. The leachant used was a natural spring water

4/10/98

APPROVED for Release for
Unlimited (Release to Public)
6/23/2005

WSRC-RP-92-1360

RADIOLOGICAL PERFORMANCE ASSESSMENT FOR THE Z-AREA SALTSTONE DISPOSAL FACILITY (U)

JRC 2/4/93

Prepared for the
WESTINGHOUSE SAVANNAH RIVER COMPANY
Aiken, South Carolina

by

MARTIN MARIETTA ENERGY SYSTEMS, INC.
EG&G IDAHO, INC.
WESTINGHOUSE HANFORD COMPANY
WESTINGHOUSE SAVANNAH RIVER COMPANY

December 18, 1992

Rev. 0

Table 2.3-1. Weight percent of saltstone components (Heckrotte 1988)

Saltstone Component	Nominal Blend (Wt%)	Range (Wt%)
Lime Source[a]	3	0 to 10
Fly Ash	25	10 to 40
Slag	25	10 to 40
Salt Solution	47	40 to 55

[a] Either Portland Class II cement or $Ca(OH)_2$.

Table 3.3-1 Summary of hydraulic properties assumed in the near-field model

Material	K_s (cm s^{-1})	Effective porosity, θ_s	Residual moisture content, θ_r	α $(cm^{-1})^a$	n^a
Backfill	1.0×10^{-5}	0.44	na[b]	na[b]	na[b]
Clay	7.6×10^{-9}	0.39	0.115	8.2×10^{-4}	1.33
Gravel	0.5	0.38	0.010	8.2×10^{-2}	3.70
Concrete	1.0×10^{-10}	0.08	0.064	7.5×10^{-7}	1.57
Saltstone	1.0×10^{-11}	0.46	0.368	7.4×10^{-6}	4.41

[a] Fitting parameter for van Genuchten and Mualem expressions for moisture characteristic curves.

[b] A Stone's correlation curve was used to describe the moisture characteristic curve for the backfill.

[c] Saltstone, concrete, gravel, and backfill properties not required for fractured saltstone case.

WESTINGHOUSE SAVANNAH RIVER COMPANY
SAVANNAH RIVER TECHNOLOGY CENTER

Keywords: Hydraulic Property
Mechanical Property
Performance Assessment

WSRC-RP-93-894

DATE: JUNE 30, 1993

TO: R. H. HSU, 773-43A
R. S. AYLWARD, 992-4W

FROM: A. D. YU, 773-43A
C. A. LANGTON, 773-43A
M. G. SERRATO, 992-4W

PHYSICAL PROPERTIES MEASUREMENT PROGRAM (U)

SUMMARY

This report summarizes the work performed by Core Laboratories (Carrollton, Texas) under subcontract No. AA46362N for the measurement of hydraulic and mechanical properties of the materials used for Environmental Restoration and Waste Management facilities at the Savannah River Site (SRS). The scope of the work includes the measurement of porosity, permeability to water (saturated hydraulic conductivity), capillary pressure, relative permeability, and mechanical properties of ten field samples. The samples are top soil, gravel, Dixie clay, Grace clay, sand, Burma Road backfill, Turner Road backfill, concrete for E-Area vault, concrete for Saltstone vault, and Saltstone. The Core Lab final report detailing sample preparation, test procedures, results, and QA is attached.

An analysis of the Core Lab results was made by WSRC personnel. The water-air two-phase flow properties (capillary pressure and relative permeability) are curve-fitted to analytical expressions. The calculated versus experimental characteristic curves and the parameters used for the curve fitting and are also included. The analytical expressions are used for groundwater modeling.

File: DRES-92119

SUMMARY OF PERMEABILITY TO LIQUID TEST RESULTS

Westinghouse Savannah River Company

Sample I.D.	Cumulative Test Time, days	Length, cm	Area, cm^2	Viscosity, cp	Delta Pressure, psi	Incremental Flow Rate, cc/sec	Permeability to Liquid, millidarcies	Hydraulic Conductivity, cm/sec (Q/A)	Porosity, percent
Turner Road Backfill - 1	36.8	7.59	11.76	0.988	50.0	1.6e-03	3.1e-01	3.0e-07	45.5
Turner Road Backfill - 2*	35.8	7.59	11.76	0.988	50.0	2.6e-03	4.8e-01	4.7e-07	42.7
Concrete from Saltstone Vault-1B	24.0	6.24	11.05	2.39	50.0	5.3e-07	2.1e-04	1.1e-10	17.4
Concrete from Saltstone Vault-5B	37.7	5.77	11.13	0.988	50.0	1.6e-05	2.4e-03	2.3e-09	18.9
Concrete from Saltst. Vault-7B*	38.0	5.05	11.10	0.988	50.0	9.9e-06	1.3e-03	1.3e-09	16.8
Concrete from E-Area Vault-2E	36.9	5.46	10.76	0.988	50.0	5.0e-09	7.4e-07	7.2e-13	18.1
Concrete from E-Area Vault-4E	37.5	5.35	10.68	0.988	50.0	8.3e-09	1.2e-06	1.2e-12	19.3
Concrete from E-Area Vault-7E*	37.5	4.44	10.72	0.988	50.0	1.0e-08	1.3e-06	1.2e-12	18.6
Saltstone - 1	16.0	4.29	11.07	2.39	50.0	2.4e-08	6.6e-06	3.4e-12	44.6
Saltstone - 3A	16.0	4.35	11.26	2.39	50.0	2.0e-08	5.4e-06	2.8e-12	41.6
Saltstone - 4*	12.0	4.74	11.30	2.39	50.0	1.3e-08	3.7e-06	1.9e-12	40.6

*Sample selected for Gas-Water Relative Permeability Tests

RESPONSE TO RAI COMMENT 39
ROADMAP TO REFERENCES

REFERENCED DOCUMENT	*EXCERPT LOCATION	REMARK
American Concrete Institute (ACI) 2000	Excerpt enclosed following response.	Section 2.1 and 2.2.
Clifton and Knab 1989	Excerpt enclosed following response.	Section 4.
Dixon 2005	Excerpt included in response	Table 39-1 of response
Langmuir 1997	Excerpt enclosed following response.	Pages 28-32.
Ramachandran 2001	Excerpt enclosed following response.	Sections 2.1 and 8.0.
MMES 1992 (Saltstone PA 1992)	Excerpt enclosed following response.	Sections 3.1.3.5, 3.3.1.2 and A-1.3 enclosed (Page 3-60 is excluded since it is a table referenced in section 3.3.1.1 and is not related to section 3.3.1.2.)
Walton et al. 1990	Excerpt enclosed following response.	Abstract of book included for reference.

*Excerpt Locations:

1. Excerpt included in response: The excerpt is included within the text of the response or is appended to the response.
2. Excerpt enclosed following response: The excerpt is enclosed on a separate sheet or sheets following the response.
3. Representative excerpt(s) enclosed following response: Representative excerpts from a document that is wholly or largely applicable are enclosed following the response.
4. Other

ACI 201.2R-01

Guide to Durable Concrete

Reported by ACI Committee 201

american concrete institute
P.O. BOX 9094
FARMINGTON HILLS, MICHIGAN 48333-9094

First Printing, October 2001

Guide to Durable Concrete

Most ACI Standards and committee reports are gathered together in the annually revised ACI Manual of Concrete Practice. The several volumes are arranged to group related material together and may be purchased individually or in sets. The ACI Manual of Concrete Practice is also available on CD-ROM.

ACI Committees prepare standards and reports in the general areas of materials and properties of concrete, construction practices and inspection, pavements and slabs, structural design and analysis, structural specifications, and special products and processes.

A complete catalog of all ACI publications is available without charge.

American Concrete Institute
P.O. Box 9094
Farmington Hills, MI 48333-9094

ACI Certification Programs

The final quality of a concrete structure depends on qualified people to construct it. ACI certification programs identify craftsmen, technicians, and inspectors who have demonstrated their qualifications. The following programs are administered by ACI to fulfill the growing demand in the industry for certified workers:

Concrete Flatwork Finisher

Concrete Flatwork Technician

Concrete Field Testing Technician—Grade I

Concrete Strength Testing Technician

Concrete Laboratory Testing Technician—Grade I

Concrete Laboratory Testing Technician—Grade II

Concrete Construction Inspector-In-Training

Concrete Construction Inspector

Concrete Transportation Construction Inspector-In-Training

Concrete Transportation Construction Inspector

This document may already contain reference to these ACI certification programs, which can be incorporated into project specifications or quality control procedures. If not, suggested guide specifications are available on request from the ACI Certification Department.

Enhancement of ACI Documents

The technical committees responsible for ACI committee reports and standards strive to avoid ambiguities, omissions, and errors in these documents. In spite of these efforts, the users of ACI documents occasionally find information or requirements that may be subject to more than one interpretation or may be incomplete or incorrect.

To assist in the effort for accuracy and clarity, the Technical Activities Committee solicits the help of individuals using ACI reports and standards in identifying and eliminating problems that may be associated with their use.

Users who have suggestions for the improvement of ACI documents are requested to contact the ACI Engineering Department in writing, with the following information:

1. Title and number of the document containing the problem and specific section in the document;
2. Concise description of the problem;
3. If possible, suggested revisions for mitigating the problem.

The Institute's Engineering Staff will review and take appropriate action on all comments and suggestions received. Members as well as nonmembers of the Institute are encouraged to assist in enhancing the accuracy and usefulness of ACI documents.

ISBN 0-87031-053-4

Guide to Durable Concrete

Reported by ACI Committee 201

Robert C. O'Neill Chairman		Russell L. Hill Secretary
W. Barry Butler	Donald J. Janssen	Hannah C. Schell
Joseph G. Cabrera*	Roy H. Keck	James W. Schmitt
Ramon L. Carrasquillo	Mohammad S. Khan	Charles F. Scholer
William E. Ellis, Jr.	Paul Klieger*	Jan P. Skalny
Bernard E. Erlin	Joseph L. Lamond	Peter Smith
Per Fidjestøl	Cameron MacInnis	George W. Teodoru
Stephen W. Forster	Stella L. Marusin	Niels Thaulow
Clifford Gordon	Bryant Mather	Michael D. Thomas
Roy Harrell	Mohamad A. Nagi	J. Derle Thorpe
Harvey H. Haynes	Robert E. Neal	Paul J. Tikalsky
Eugene D. Hill, Jr.	Charles K. Nmai	Claude B. Trusty
Charles J. Hookham	William F. Perenchio	David A. Whiting*
R. Doug Hooton	Robert E. Price*	J. Craig Williams
Allen J. Hulshizer	Jan R. Prusinski	Yoga V. Yogendran

*Deceased.

This guide describes specific types of concrete deterioration. Each chapter contains a discussion of the mechanisms involved and the recommended requirements for individual components of concrete, quality considerations for concrete mixtures, construction procedures, and influences of the exposure environment, all important considerations to ensure concrete durability. Some guidance as to repair techniques is also provided.

This document contains substantial revisions to Section 2.2 (chemical sulfate attack) and also includes a new section on physical salt attack (Section 2.3). The remainder of this document is essentially identical to the previous "Guide to Durable Concrete." However, all remaining sections of this document are in the process of being revised and updated, and these revisions will be incorporated into the next published version of this guide.

Both terms water-cement ratio and water-cementitious materials ratio are used in this document. Water-cement ratio is used (rather than the newer term, water-cementitious materials ratio) when the recommendations are based on data referring to water-cement ratio. If cementitious materials other than portland cement have been included in the concrete, judgment regarding required water-cement ratios have been based on the use of that ratio. This does not imply that new data demonstrating concrete performance developed using portland cement and other cementitious materials should not be referred to in terms of water-cementitious materials. Such information, if available, will be included in future revisions.

Keywords: abrasion resistance; adhesives; admixture; aggregate; air entrainment; alkali-aggregate reaction; bridge deck; carbonation; calcium chloride; cement paste; coating; corrosion; curing; deicer; deterioration; durability; epoxy resins; fly ash; mixture proportion; petrography; plastic; polymer; pozzolan; reinforced concrete; repair; resin; silica fume; skid resistance; spalling; strength; sulfate attack; water-cement ratio; water-cementitious materials ratio.

CONTENTS

ACI 201.2R-01 supersedes ACI 201.2R-92 (Reapproved 1997) and became effective September 6, 2000.

INTRODUCTION

Durability of hydraulic-cement concrete is defined as its ability to resist weathering action, chemical attack, abrasion, or any other process of deterioration. Durable concrete will retain its original form, quality, and serviceability when exposed to its environment. Some excellent general references on the subject are available (Klieger 1982; Woods 1968).

This guide discusses the more important causes of concrete deterioration and gives recommendations on how to prevent such damage. Chapters on freezing and thawing, aggressive chemical exposure, abrasion, corrosion of metals, chemical reactions of aggregates, repair of concrete, and the use of protective-barrier systems to enhance concrete durability are included. Fire resistance of concrete and cracking are not covered, because they are covered in ACI 216, ACI 224R, and ACI 224.1R, respectively.

Freezing and thawing in the temperate regions of the world can cause severe deterioration of concrete. Increased use of concrete in countries with hot climates has drawn attention to the fact that deleterious chemical processes, such as corrosion and alkali-aggregate reactions, are aggravated by high temperatures. Also, the combined effects of cold winter and hot summer exposures should receive attention in proportioning and making of durable concrete.

Water is required for the chemical and most physical processes to take place in concrete, both the desirable ones and the deleterious. Heat provides the activation energy that makes the processes proceed. The integrated effects of water and heat, and other environmental elements are important and should be considered and monitored. Selecting appropriate materials of suitable composition and processing them correctly under existing environmental conditions is essential to achieve concrete that is resistant to deleterious effects of water, aggressive solutions, and extreme temperatures.

Freezing-and-thawing damage is fairly well understood. The damage is accelerated, particularly in pavements by the use of deicing salts, often resulting in severe scaling at the surface. Fortunately, concrete made with quality aggregates, low water-cement ratio (*w/c*), proper air-void system, and allowed to mature before being exposed to severe freezing and thawing is highly resistant to such damage.

Sulfates in soil, groundwater, or seawater are resisted by using suitable cementitious materials and a properly proportioned concrete mixture subjected to proper quality control. Because the topic of delayed ettringite formation (DEF) remains a controversial issue and is the subject of various ongoing research projects, no definitive guidance on DEF is provided in this document. It is expected that future versions of this document will address DEF in significant detail.

It is generally conceded that while these various tests may classify aggregates from excellent to poor in approximately the correct order, they are unable to predict whether a marginal aggregate will give satisfactory performance when used in concrete at a particular moisture content and subjected to cyclic freezing exposure. The ability to make such a determination is of great economic importance in many areas where high-grade aggregates are in short supply, and local marginal aggregates can be permitted. Despite the shortcomings of ASTM C 666, many agencies believe that this is the most reliable indicator of the relative durability of an aggregate (Sturrup et al. 1987).

Because of these objections to ASTM C 666, a dilation test was conceived by Powers (1954) and further developed by others (Harman et al. 1970; Tremper and Spellman 1961). ASTM C 671 requires that air-entrained concrete specimens be initially brought to the moisture condition expected for the concrete at the start of the winter season, with the moisture content preferably having been determined by field tests. The specimens are then immersed in water and periodically frozen at the rate to be expected in the field. The increase in length (dilation) of the specimen during the freezing portion of the cycle is measured. ASTM C 682 assists in interpreting the results.

Excessive length change in this test is an indication that the aggregate has become critically saturated and vulnerable to damage. If the time to reach critical saturation is less than the duration of the freezing season at the job site, the aggregate is judged unsuitable for use in that exposure. If it is more, it is judged that the concrete will not be vulnerable to cyclic freezing.

The time required for conducting a dilation test may be greater than that required to perform a test by ASTM C 666. Also, the test results are very sensitive to the moisture content of the aggregate and concrete. Despite these shortcomings, most reported test results are fairly promising. Although most agencies are continuing to use ASTM C 666, results from ASTM C 671 may turn out to be more useful (Philleo 1986).

When a natural aggregate is found to be unacceptable by service records, tests, or both, it may be improved by removal of lightweight, soft, or otherwise inferior particles.

1.4.4.3 *Admixtures* — Air-entraining admixtures should conform to ASTM C 260. Chemical admixtures should conform to ASTM C 494. Admixtures for flowing concrete should conform to ASTM C 1017.

Some mineral admixtures, including pozzolans, and aggregates containing large amounts of fines may require a larger amount of air-entraining admixture to develop the required amount of entrained air. Detailed guidance on the use of admixtures is provided by ACI 212.3R.

1.4.5 *Maturity*—Air-entrained concrete should withstand the effects of freezing as soon as it attains a compressive strength of about 500 psi (3.45 MPa), provided that there is no external source of moisture. At a temperature of 50 F (10 C), most well-proportioned concrete will reach this strength some time during the second day.

Before being exposed to extended freezing while critically saturated (ASTM C 666), the concrete should attain a compressive strength of about 4000 psi (27.6 MPa). A period of drying following curing is advisable. For moderate exposure conditions, a strength of 3000 psi (20.7 MPa) should be attained (Kleiger 1956).

1.4.6 *Construction practices*—Good construction practices are essential when durable concrete is required. Particular attention should be given to the construction of pavement slabs that will be exposed to deicing chemicals because of the problems inherent in obtaining durable slab finishes and the severity of the exposure. The concrete in such slabs should be adequately consolidated; however, overworking the surface, overfinishing, and the addition of water to aid in finishing must be avoided. These activities bring excessive mortar or water to the surface, and the resulting laitance is particularly vulnerable to the action of deicing chemicals. These practices can also remove entrained air from the surface region. This is of little consequence if only the larger air bubbles are expelled, but durability can be seriously affected if the small bubbles are removed. Timing of finishing is critical (ACI 302.1R).

Before the application of any deicer, pavement concrete should have received some drying, and the strength level specified for the opening of traffic should be considered in the scheduling of late fall paving. In some cases, it may be possible to use methods other than ice-removal agents, such as abrasives, for control of slipperiness when the concrete is not sufficiently mature.

For lightweight concrete, do not wet the aggregate excessively before mixing. Saturation by vacuum or thermal means (for example, where necessary for pumping) can bring lightweight aggregates to a moisture level at which the absorbed water will cause concrete failure when it is cyclically frozen, unless the concrete has the opportunity to dry before freezing. Additional details and recommendations are given in a publication of the California Department of Transportation (1978).

CHAPTER 2—AGGRESSIVE CHEMICAL EXPOSURE

2.1—General

Concrete will perform satisfactorily when exposed to various atmospheric conditions, to most waters and soils containing aggressive chemicals, and to many other kinds of chemical exposure. There are, however, some chemical environments under which the useful life of even the best concrete will be short, unless specific measures are taken. An understanding of these conditions permits measures to be taken to prevent deterioration or reduce the rate at which it takes place.

Concrete is rarely, if ever, attacked by solid, dry chemicals. To produce a significant attack on concrete, aggressive chemicals should be in solution and above some minimum concentration. Concrete that is subjected to aggressive solutions under pressure on one side is more vulnerable than otherwise, because the pressures tend to force the aggressive solution into the concrete.

Table 2.1—Effect of commonly used chemicals on concrete

Rate of attack at ambient temperature	Inorganic acids	Organic acids	Alkaline solutions	Salt solutions	Miscellaneous
Rapid	Hydrochloric Nitric Sulfuric	Acetic Formic Lactic	—	Aluminum chloride	—
Moderate	Phosphoric	Tannic	Sodium hydroxide* > 20%	Ammonium nitrate Ammonium sulfate Sodium sulfate Magnesium sulfate Calcium sulfate	Bromine (gas) Sulfate liquor
Slow	Carbonic	—	Sodium hydroxide* 10 to 20%	Ammonium chloride Magnesium chloride Sodium cyanide	Chlorine (gas) Seawater Soft water
Negligible	—	Oxalic Tartaric	Sodium hydroxide* < 10% Sodium hypochlorite Ammonium hydroxide	Calcium chloride Sodium chloride Zinc nitrate Sodium chromate	Ammonia (liquid)

*The effect of potassium hydroxide is similar to that of sodium hydroxide.

Table 2.2—Factors influencing chemical attack on concrete

Factors that accelerate or aggravate attack	Factors that mitigate or delay attack
1. High porosity due to: i. High water absorption ii. Permeability iii. Voids	1. Dense concrete achieved by: i. Proper mixture proportioning* ii. Reduced unit water content iii. Increased cementitious material content iv. Air entrainment v. Adequate consolidation vi. Effective curing†
2. Cracks and separations due to: i. Stress concentrations ii. Thermal shock	2. Reduced tensile stress in concrete by:‡ i. Using tensile reinforcement of adequate size, correctly located ii. Inclusion of pozzolan (to reduce temperature rise) iii. Provision of adequate contraction joints content
3. Leaching and liquid penetration due to: i. Flowing liquid§ ii. Ponding iii. Hydraulic pressure	3. Structural design: i. To minimize areas of contact and turbulence ii. Provision of membranes and protective-barrier system(s)‖ to reduce penetration

*The mixture proportions and the initial mixing and processing of fresh concrete determine its homogeneity and density.
†Poor curing procedures result in flaws and cracks.
‡Resistance to cracking depends on strength and strain capacity.
§Movement of water-carrying deleterious substances increases reactions that depend on both the quantity and velocity of flow.
‖Concrete that will be frequently exposed to chemicals known to produce rapid deterioration should be protected with a chemically resistant protective-barrier system.

Comprehensive tables have been prepared by ACI Committee 515 (515.1R) and the Portland Cement Association (1968) giving the effect of many chemicals on concrete. Biczok (1972) gives a detailed discussion of the deteriorating effect of chemicals on concrete, including data both from Europe and the U.S.

The effects of some common chemicals on the deterioration of concrete are summarized in Table 2.1. Provided that due care has been taken in selection of the concrete materials and proportioning of the concrete mixture, the most important factors that influence the ability of concrete to resist deterioration are shown in Table 2.2. Therefore, Table 2.1 should be considered as only a preliminary guide.

Major areas of concern are exposure to sulfates, seawater, salt from seawater, acids, and carbonation. These areas of concern are discussed in Sections 2.2 through 2.6.

2.2—Chemical sulfate attack by sulfate from sources external to the concrete

2.2.1 *Occurrence* — Naturally occurring sulfates of sodium, potassium, calcium, or magnesium,[1] that can attack hardened concrete, are sometimes found in soil or dissolved in groundwater adjacent to concrete structures.

Sulfate salts in solution enter the concrete and attack the cementing materials. If evaporation takes place from a surface exposed to air, the sulfate ions can concentrate near that surface and increase the potential for causing deterioration. Sulfate attack has occurred at various locations throughout the world and is a particular problem in arid areas, such as the northern Great Plains and parts of the western United States (Bellport 1968; Harboe 1982; Reading 1975; Reading 1982; USBR 1975; Verbeck 1968); the prairie provinces of Canada (Hamilton and Handegord 1968; Hurst 1968; Price and Peterson 1968); London, England (Bessey and Lea 1953); Oslo, Norway (Bastiansen et al. 1957); and the Middle East (French and Poole 1976).

The water used in concrete cooling towers can also be a potential source of sulfate attack because of the gradual build-up of sulfates due to evaporation, particularly where such systems use relatively small amounts of make-up water. Sulfate ions can also be present in fill containing industrial waste products, such as slags from iron processing, cinders, and groundwater leaching these materials.

[1]Many of these substances occur as minerals, and the mineral names are often used in reports of sulfate attack. The following is a list of such names and their general composition:

anhydrite	$CaSO_4$	thenardite	Na_2SO_4
bassanite	$CaSO_4 \cdot 1/2H_2O$	mirabilite	$Na_2SO_4 \cdot 10H_2O$
gypsum	$CaSO_4 \cdot 2H_2O$	arcanite	K_2SO_4
kieserite	$MgSO_4 \cdot H_2O$	glauberite	$Na_2Ca(SO_4)_2$
epsomite	$MgSO_4 \cdot 7H_2O$	langbeinite	$K_2Mg_2(SO_4)_3$
thaumasite	$Ca_3Si(CO_3)(SO_4)(OH)_1 \cdot 12H_2O$		

Seawater and coastal soil soaked with seawater constitute a special type of exposure. Recommendations for concrete exposed to seawater are in Section 2.3.

2.2.2 *Mechanisms*—The two best recognized chemical consequences of sulfate attack on concrete components are the formation of ettringite (calcium aluminate trisulfate 32-hydrate, $CaO{\cdot}Al_2O_3{\cdot}3CaSO_4{\cdot}32H_2O$) and gypsum (calcium sulfate dihydrate, $CaSO_4{\cdot}2H_2O$). The formation of ettringite can result in an increase in solid volume, leading to expansion and cracking. The formation of gypsum can lead to softening and loss of concrete strength. The presence of ettringite or gypsum in concrete, however, is not in itself an adequate indication of sulfate attack; evidence of sulfate attack should be verified by petrographic and chemical analyses. When the attacking sulfate solution contains magnesium sulfate, brucite ($Mg(OH)_2$, magnesium hydroxide) is produced in addition to ettringite and gypsum. Some of the sulfate-related processes can damage concrete without expansion. For example, concrete subjected to soluble sulfates can suffer softening of the paste matrix or an increase in the overall porosity, either of which diminish durability.

Publications discussing these mechanisms in detail include Lea (1971), Hewlett (1998), Mehta (1976, 1992), DePuy (1994), Taylor (1997), and Skalny et al. (1998). Publications with particular emphasis on permeability and the ability of concrete to resist ingress and movement of water include Reinhardt (1997), Hearn et al. (1994), Hearn and Young (1999), Diamond (1998), and Diamond and Lee (1999).

2.2.3 *Recommendations*—Protection against sulfate attack is obtained by using concrete that retards the ingress and movement of water and concrete-making ingredients appropriate for producing concrete having the needed sulfate resistance. The ingress and movement of water are reduced by lowering the water to cementitious-materials ratio (*w/cm*). Care should be taken to ensure that the concrete is designed and constructed to minimize shrinkage cracking. Air entrainment is beneficial if it is accompanied by a reduction in the *w/cm* (Verbeck 1968). Proper placement, compaction, finishing, and curing of concrete are essential to minimize the ingress and movement of water that is the carrier of the aggressive salts. Recommended procedures for these are found in ACI 304R, ACI 302.1R, ACI 308.1, ACI 305R, and ACI 306R.

The sulfate resistance of portland cement generally decreases with an increase in its calculated tricalcium-aluminate (C_3A) content (Mather 1968). Accordingly, ASTM C 150 includes Type V sulfate-resisting cement for which a maximum of 5% calculated C_3A is permitted and Type II moderately sulfate-resisting cement for which the calculated C_3A is limited to 8%. There is also some evidence that the alumina in the aluminoferrite phase of portland cement can participate in sulfate attack. Therefore, ASTM C 150 provides that in Type V cement the $C_4AF + 2C_3A$ should not exceed 25%, unless the alternate requirement based on the use of the performance test (ASTM C 452) is invoked. In the case of Type V cement, the sulfate-expansion test (ASTM C 452) can be used in lieu of the chemical requirements (Mather 1978b). The use of ASTM C 1012 is discussed by Patzias (1991).

Recommendations for the maximum *w/cm* and the type of cementitious material for concrete that will be exposed to sulfates in soil or groundwater are given in Table 2.3. Both of these recommendations are important. Limiting only the type of cementitious material is not adequate for satisfactory resistance to sulfate attack (Kalousek et al. 1976).

Table 2.3 provides recommendations for various degrees of potential exposure. These recommendations are designed to protect against concrete distress from sulfate from sources external to the concrete, such as adjacent soil and groundwater.

The field conditions of concrete exposed to sulfate are numerous and variable. The aggressiveness of the conditions depends, among others, on soil saturation, water movement, ambient temperature and humidity, concentration of sulfate, and type of sulfate or combination of sulfates involved. Depending on the above variables, solutions containing calcium sulfate are generally less aggressive than solutions of sodium sulfate, which is generally less aggressive than magnesium sulfate. Table 2.3 provides criteria that should maximize the service life of concrete subjected to the more aggressive exposure conditions.

Portland-cement concrete can be also be attacked by acidic solutions, such as sulfuric acid. Information on acid attack is provided in Section 2.5.

2.2.4 *Sampling and testing to determine potential sulfate exposure*—To assess the severity of the potential exposure of concrete to detrimental amounts of sulfate, representative samples should be taken of water that might reach the concrete or of soil that might be leached by water moving to the concrete. A procedure for making a water extract of soil samples for sulfate analysis is given in Appendix A. The extract should be analyzed for sulfate by a method suitable to the concentration of sulfate in the extract solution.[2]

2.2.5 *Material qualification of pozzolans and slag for sulfate-resistance enhancement*—Tests of one year's duration are necessary to establish the ability of pozzolans and slag to enhance sulfate resistance. Once this material property has been established for specific materials, proposed mixtures using them can be evaluated for Class 1 and Class 2 exposures using the 6-month criteria in Sections 2.2.6 and 2.2.7.

Fly ashes, natural pozzolans, silica fumes, and slags may be qualified for sulfate resistance by demonstrating an expansion ≤ 0.10% in one year when tested individually with portland cement by ASTM C 1012 in the following mixtures:

For fly ash or natural pozzolan, the portland-cement portion of the test mixture should consist of a cement with Bogue calculated C_3A[3] of not less than 7%. The fly ash or natural pozzolan proportion should be between 25 and

[2] If the amount of sulfate determined in the first analysis is outside of the optimum concentration range for the analytical procedure used, the extract solution should either be concentrated or diluted to bring the sulfate content within the range appropriate to the analytical method, and the analysis should be repeated on the modified extract solution.

[3] The C_3A should be calculated for the sum of the portland cement plus calcium sulfate in the cement. Some processing additions, if present in sufficient proportions, can distort the calculated Bogue values. Formulas for calculating Bogue compounds may be found in ASTM C 150.

Table 2.3—Requirements to protect against damage to concrete by sulfate attack from external sources of sulfate

Severity of potential exposure	Water-soluble soluble sulfate (SO_4)*	Sulfate (SO_4)* in water, ppm	*w/cm* by mass, max.†‡	Cementitious material requirements
Class 0 exposure	0.00 to 0.10	0 to 150	No special requirements for sulfate resistance	No special requirements for sulfate resistance
Class 1 exposure	> 0.10 and < 0.20	> 150 and < 1500	0.50‡	C 150 Type II or equivalent§
Class 2 exposure	0.20 to < 2.0	1500 to < 10,000	0.45‡	C 150 Type V or equivalent§
Class 3 exposure	2.0 or greater	10,000 or greater	0.40‡	C 150 Type V plus pozzolan or slag§
Seawater exposure	—	—	See Section 2.4	See Section 2.4

*Sulfate expressed as SO_4 is related to sulfate expressed as SO_3, as given in reports of chemical analysis of portland cements as follows: $SO_3\% \times 1.2 = SO_4\%$.

†ACI 318, Chapter 4, includes requirements for special exposure conditions such as steel-reinforced concrete that may be exposed to chlorides. For concrete likely to be subjected to these exposure conditions, the maximum *w/cm* should be that specified in ACI 318, Chapter 4, if it is lower than that stated in Table 2.3.

‡These values are applicable to normalweight concrete. They are also applicable to structural lightweight concrete except that the maximum *w/cm* ratios 0.50, 0.45, and 0.40 should be replaced by specified 28 day compressive strengths of 26, 29, and 33 MPa (3750, 4250, and 4750 psi) respectively.

§For Class 1 exposure, equivalents are described in Sections 2.2.5, 2.2.6, and 2.2.9. For Class 2 exposure, equivalents are described in Sections 2.2.5, 2.2.7, and 2.2.9. For Class 3 exposure, pozzolan and slag recommendations are described in Sections 2.2.5, 2.2.8, and 2.2.9.

35% by mass, calculated as percentage by mass of the total cementitious material.

For silica fume, the portland-cement portion of the test mixture should consist of a cement with Bogue calculated C_3A[3] of not less than 7%. The silica fume proportion should be between 7 and 15% by mass, calculated as percentage by mass of the total cementitious material.

For slag, the portland-cement portion of the test mixture should consist of a cement with Bogue calculated C_3A[3] of not less than 7%. The slag proportion should be between 40 and 70% by mass, calculated as percentage by mass of the total cementitious material.

Material qualification tests should be based on passing results from two samples taken at times a few weeks apart. The qualifying test data should be no older than one year from the date of test completion.

The reported calcium-oxide content[4] of the fly ash used in the project should be no more than 2.0 percentage points greater than that of the fly ash used in qualifying test mixtures. The reported aluminum-oxide content[4] of the slag used in the project should be no more than 2.0 percentage points higher than that of the slag used in qualifying test mixtures.

2.2.6 *Type II Equivalent for Class 1 Exposure*

- A. ASTM C 150 Type III cement with the optional limit of 8% max. C_3A; C 595M Type IS(MS), Type IP(MS), Type IS-A(MS), Type IP-A(MS); C 1157 Type MS; or

B. Any blend of portland cement of any type meeting ASTM C 150 or C 1157 with fly ash or natural pozzolan meeting ASTM C 618, silica fume meeting ASTM C 1240, or slag meeting ASTM C 989, that meets the following requirement when tested in accordance with ASTM C 1012. Any fly ash, natural pozzolan, silica fume, or slag used should have been previously qualified in accordance with Section 2.2.5.

Expansion ≤ 0.10% at 6 months.

2.2.7 *Type V Equivalent for Class 2 Exposure*

A. ASTM C 150 Type III cement with the optional limit of 5% max. C_3A; ASTM C 150 cement of any type having expansion at 14 days no greater than 0.040% when tested by ASTM C 452; ASTM C 1157 Type HS; or

B. Any blend of portland cement of any type meeting ASTM C 150 or C 1157 with fly ash or natural pozzolan meeting ASTM C 618, silica fume meeting ASTM C 1240, or slag meeting ASTM C 989 that meets the following requirement when tested in accordance with ASTM C 1012:

Expansion ≤ 0.05% at 6 months. Any fly ash, natural pozzolan, silica fume, or slag used should have been previously qualified in accordance with Section 2.2.5 in order for a test of only 6 months to be acceptable.

If one or more of the fly ash, natural pozzolan, silica fume, or slag has not been qualified in accordance with Section 2.2.5, then 1-year tests should be performed on the proposed combination and the expansion should comply with the following limit:

Expansion ≤ 0.10% at 1 year.

2.2.8 *Class 3 Exposure*—any blend of portland cement meeting ASTM C 150 Type V or C 1157 Type HS with fly ash or natural pozzolan meeting ASTM C 618, silica fume meeting ASTM C 1240, or slag meeting ASTM C 989, that

[3]The C_3A should be calculated for the sum of the portland cement plus calcium sulfate in the cement. Some processing additions, if present in sufficient proportions, can distort the calculated Bogue values. Formulas for calculating Bogue compounds may be found in ASTM C 150.

[4]Analyzed in accordance with ASTM C 114.

meets the following requirement when tested in accordance with ASTM C 1012:

Expansion ≤ 0.10% at 18 months.

2.2.9 *Proportions and uniformity of pozzolans and slag* — The proportion of fly ash, natural pozzolan, silica fume, or slag used in the project mixture (in relation to the amount of portland cement) should be the same as that used in the test mixture prepared to meet the recommendations of Section 2.2.6, 2.2.7, or 2.2.8. In blends with portland cement containing only one blending material, such as fly ash, natural pozzolan, silica fume, or slag, the proportion of fly ash or natural pozzolan can generally be expected to be in the range of 20 to 50% by mass of the total cementitious material. Similarly, the proportion of silica fume can be expected to be in the range of 7 to 15% by mass of the total cementitious material, and the proportion of slag can be expected to be in the range of 40 to 70% by mass of the total cementitious material. When more than one blending material, such as fly ash, natural pozzolan, silica fume, or slag, or combinations of these, is used in a blend, the individual proportions of the pozzolan, silica fume, or slag, or combinations of these may be less than these values.

The uniformity of the fly ash or slag used in the project should be within the following of that used in the mixtures tested to meet the recommendations of Section 2.2.6, 2.2.7, or 2.2.8:

- *Fly ash*—reported calcium-oxide content[5] no more than 2.0 percentage points higher than that of the fly ash used in the test mixture;
- *Slag*—reported aluminum-oxide content[5] no more than 2.0 percentage points higher than that of the slag used in the test mixture.

The portland cement used in the project should have a Bogue C_3A value no higher than that used in the mixtures tested to meet the recommendations of Section 2.2.6, 2.2.7, or 2.2.8.

Studies have shown that some pozzolans and ground-granulated-iron blast-furnace slags, used either in blended cement or added separately to the concrete in the mixer, considerably increase the life expectancy of concrete in sulfate exposure. Many slags and pozzolans significantly reduce the permeability of concrete (Bakker 1980; Mehta 1981). They also combine with the alkalies and calcium hydroxide released during the hydration of the cement (Vanden Bosch 1980; Roy and Idorn 1982; Idorn and Roy 1986), reducing the potential for gypsum formation (Biczok 1972; Lea 1971; Mehta 1976; Kalousek et al. 1972).

Table 2.3 requires a suitable pozzolan or slag along with Type V cement in Class 3 exposures. Research indicates that some pozzolans and slags are effective in improving the sulfate resistance of concrete made with Type I and Type II cement (ACI 232.2R; ACI 233R; ACI 234R). Some pozzolans, especially some Class C fly ashes, decrease the sulfate resistance of mortars in which they are used (Mather 1981b, 1982). Good results were obtained when the pozzolan was a fly ash meeting the requirements of ASTM C 618 Class F (Dikeou 1975; Dunstan 1976). Slag should meet ASTM C 989.

In concrete made with nonsulfate-resisting cements, calcium chloride reduces resistance to attack by sulfate (USBR 1975), and its use should be prohibited in concrete exposed to sulfate (Class I or greater exposure). If Type V cement is used, however, it is not harmful to use calcium chloride in normally acceptable amounts as an accelerating admixture to mitigate the effects of cold weather (Mather 1992). If corrosion is a concern, calcium chloride should not be added, because it can induce and accelerate corrosion of embedded metal, such as reinforcing steel and aluminum conduit.

2.3—Physical salt attack

Field examples have been cited (Reading 1975; Tuthill 1978; Haynes and O'Neill 1994; Haynes et al. 1996) where deterioration has occurred by physical action of salts from groundwater containing sodium sulfate, sodium carbonate, and sodium chloride. The mechanism of the attack is not fully understood, but discussions of possible mechanisms were presented in Hansen (1963), Folliard and Sandberg (1994), and Haynes and O'Neill (1994), Haynes et al. (1996), and Marchand and Skalny (1999). The mechanism for sodium or magnesium sulfate physical attack may be similar to that used in the Brard test (Schaffer 1932), which is the basis of the ASTM C 88. The damage typically occurs at exposed surfaces of moist concrete that is in contact with soils containing the above salts. Once dissolved, the ions may transport through the concrete, and subsequently concentrate and precipitate at the exposed surface. The distress is surface scaling similar in appearance to freezing-and-thawing damage. Loss of exposed concrete is progressive, and continued exposure, caused by repeated humidity or temperature cycling, can lead to total disintegration of poor-quality concrete. Numerous cycles of dehydration and rehydration of the salts caused by temperature cycling accelerate this deterioration.

The problem can be mitigated with measures that minimize the movement of water in the concrete. While air-entrainment can also be helpful, it is not a substitute for an adequately low *w/cm* concrete for reducing the rate of moisture movement in concrete. Haynes et al. (1996) recommend a maximum *w/cm* of 0.45, along with a pozzolan for improved durability. Adequate curing of the concrete is also an important preventive measure. Vapor barriers and adequate drainage of water away from the concrete are also recommended to reduce moisture ingress into the concrete. This group of measures is considered more effective in protecting concrete from this distress than the use of any specific type of cement or admixture.

2.4—Seawater exposure

2.4.1 Seawater in various locations throughout the world has a range of concentration of total salts, it is less dilute in some areas than in others. The proportions of the constituents of seawater salts, however, are essentially constant.

The concentration is lower in the colder and temperate regions than in the warm seas and is especially high in shallow coastal areas with excessive daily evaporation rates.

[5]Analyzed in accordance with ASTM C 114.

NUREG/CR-5466
NISTIR 89-4086
RW

Service Life of Concrete

'uscript Completed: September 1989
: Published: November 1989

Prepared by
J. R. Clifton, L. I. Knab

National Institute of Standards and Technology
Gaithersburg, MD 20899

Prepared for
Division of Engineering
Office of Nuclear Regulatory Research
U.S. Nuclear Regulatory Commission
Washington, DC 20555
C FIN D2009

in the laboratory on uncracked specimens. Alexander (10) showed that for viscous flow in stone fissures of width b with average spacing of s, the equivalent permeability (k_f) is given by;

$$k_f = b^3/12s. \qquad 3$$

Presuming that this equation is valid for concrete, then cracks with widths of 1 mm, spaced 1 m apart, would give an equivalent permeability of 8×10^{-11} m^2 compared to an intact permeability of around 10^{-16} m^2. The major types of cracks in concrete can be divided into those occurring before hardening and those occurring after hardening (Fig. 5). Those occurring before hardening can be caused by construction movement, plastic shrinkage or drying shrinkage, and early frost damage. The cracks occurring after concrete has hardened involve physical, chemical, thermal and structural processes. Cracks occurring before hardening and most, if not all, of those occurring after hardening (especially those caused by design loads, drying shrinkage, crazing, and early thermal contraction) could be prevented by a proper QA/QC program.

4. SULFATE ATTACK

Probably the most widespread and common attack of concrete in contact with soil involves sulfates. Sulfate attack of concrete can be very deleterious resulting in cracking of concrete and in severe cases its disintegration. Naturally-occurring sulfates of sodium, potassium, calcium, and magnesium are sometimes found in groundwaters and soils, especially when high amounts of clay are present. If the sulfates are in groundwater and concrete is subjected to wetting and drying cycles by the groundwater, then upon evaporation of the groundwater from concrete surfaces the deposited sulfates may accumulate in the concrete at a concentration higher than that in the groundwater. Such processes can significantly accelerate sulfate attack, or also the attack by other aggressive salts such as chlorides. Sulfate attack has occurred in several regions of the United States, and is a particular problem in arid regions, such as the Northern Plains area and in the southwestern states (23). Localized sources of sulfates in groundwater include mine tailings, fills of blast-furnace slag, and deposits of chemical wastes.

The water used in irrigation can be a potential source of sulfate attack because of the gradual accumulation of sulfates as the water evaporates.

4.1 Mechanisms

Sulfate attack of concrete is a complex process and at least three major deleterious reactions can take place depending on the environment (24,25).

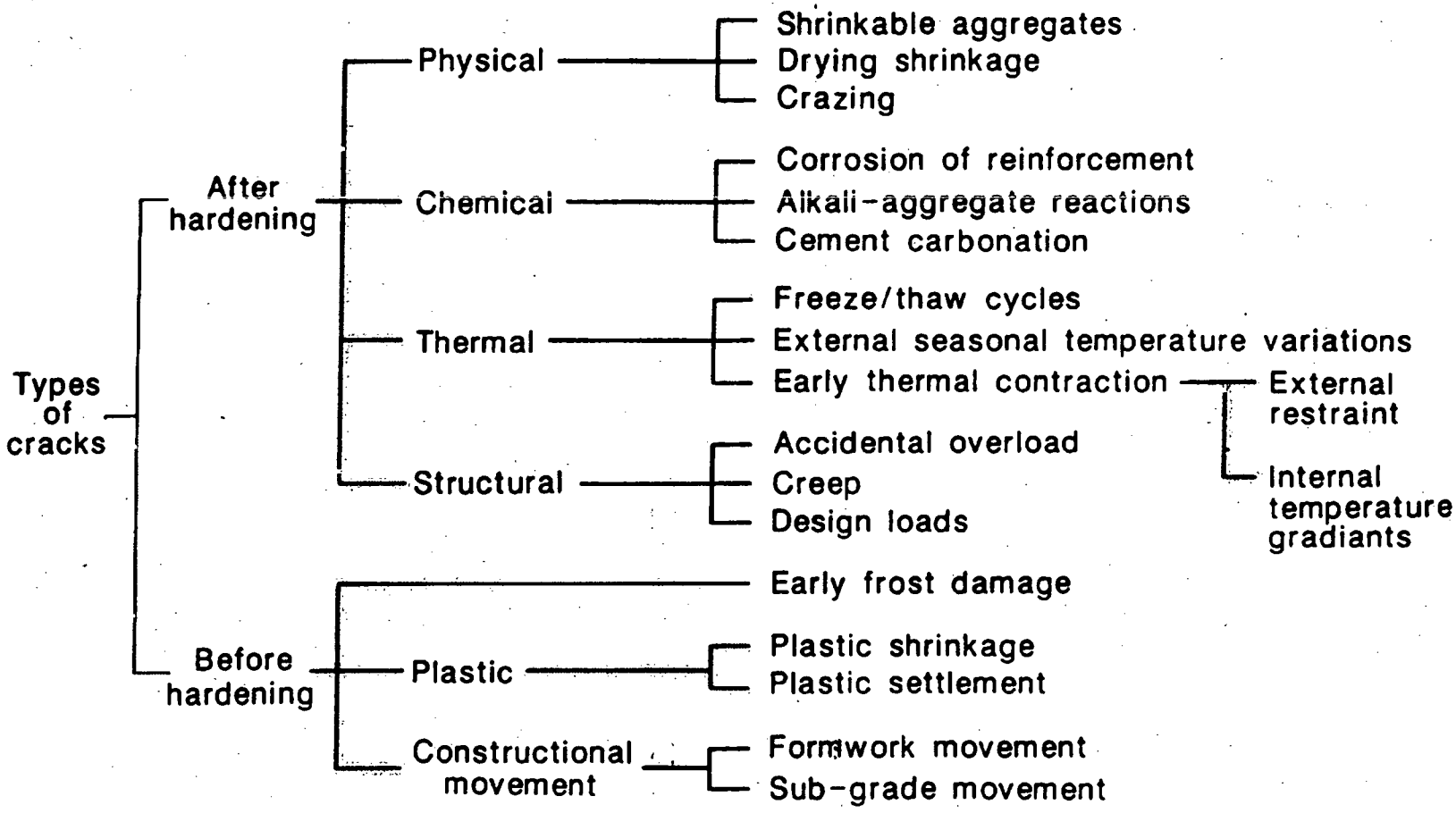

Figure 5. Major causes of cracks in concrete 22).

The first process considered involves the reaction of sulfate ions with calcium aluminate hydrate to form the calcium sulfoaluminate product, ettringite ($3CaO \cdot Al_2O_3 \cdot 3CaSO_4 \cdot 31H_2O$):

$$2(3CaO \cdot Al_2O_3 \cdot 12H_2O) + 3(Na_2SO_4 \cdot 10H_2O) \rightarrow 3CaO \cdot Al_2O_3 \cdot 3CaSO_4 \cdot 31H_2O + 2Al(OH)_3 + 6NaOH + 17H_2O \quad (4$$

Ettringite has a considerably larger volume than the reactants. At low concentrations of sulfate ions, ettringite decomposes to a low sulfate form $3CaO \cdot Al_2O_3 \cdot CaSO_4 \cdot 12H_2O$. The amount of ettringite accumulated and the stress induced, therefore, depends on the availability of sulfate ions. The formation of ettringite appears to be the cause of most of the expansion and deterioration of concrete caused by sulfate solutions (23)

Another process involves the replacement of calcium hydroxide ($Ca(OH)_2$) in concrete by gypsum ($CaSO_4 \cdot 2H_2O$):

$$Ca(OH)_2 + Na_2SO_4 \cdot 10H_2O \rightarrow CaSO_4 \cdot 2H_2O + 2NaOH + 8H_2O \quad (5)$$

Formation of gypsum can lead to the deterioration of concrete by two processes (25). In one process, because gypsum occupies more volume than calcium hydroxide, expansive stresses are produced. In another, gypsum is gradually leached, leaving a porous concrete with a higher permeability. In flowing water and given sufficient time, calcium hydroxide may be essentially completely converted to gypsum; while, in quasi-stagnant water, equilibrium will be attained and only a portion of the calcium hydroxide will be converted.

Similar reactions can occur involving magnesium sulfate. In addition, magnesium sulfate can attack the calcium silicate hydrate ($3CaO \cdot 2SiO_2 \cdot nH_2O$) formed by the hydration of portland cement. The reaction is of the pattern (25):

$$3CaO \cdot 2SiO_2 \cdot 3H_2O + 3MgSO_4 + 6H_2O \rightarrow 3(CaSO_4 \cdot 2H_2O) + 3Mg(OH)_2 + 2SiO_2 \quad (6)$$

This reaction has particularly severe effects. Because of the very low solubility of magnesium hydroxide, the equilibrium is almost completely to the right. The reaction, however, is slow and is of greatest concern when concrete is exposed to sea water.

4.2 Resistance of Concrete to Sulfate Attack

Extensive research has been carried out on the resistance of concretes to sulfate attack. For example, Miller and Manson (26) carried out a 25-year investigation of the sulfate resistance of concrete using more than 75,000 specimens made from 122 commercial cements. Also, the Portland Cement Association (27) has been carrying out a comprehensive study of the resistance of

concretes to sulfate-containing soils. The results of these and numerous other studies have clearly indicated that the tricalcium aluminate content of portland cement greatly affected its sulfate resistance (9, 23, 28). Accordingly, ASTM C 150 includes a Type V (sulfate resistant) cement which sets a maximum of 5%, by mass, on C_3A and a Type II (moderately sulfate-resisting) for which the C_3A is limited to 8%. There is also evidence that the aluminoferrite (C_4AF) phase of portland cement may participate in delayed sulfate attack and, thus, limits have been placed on its contents. The traditional practice of relying on such cements for acceptable sulfate resistance is being replaced with the recent practice of using low-permeability, low $Ca(OH)_2$ containing concrete (28). The sulfate resistance of concrete can be increased either by adding pozzolans or granulated blast-furnace slag to the concrete, or by using blended cements containing a pozzalan or a granulated blast furnace slag. These mineral admixtures react with the $Ca(OH)_2$ produced by the cement hydration to produce additional calcium silicate hydrate which reduces the capillary porosity and thus permeability. Also, decreasing the $Ca(OH)_2$ contents will reduce the amount of concrete expansion caused by the formation of gypsum (equation 5). The US Bureau of Reclamation (29) carried out a 12 year study on the effect of the composition of fly ash on the sulfate durability of concrete. It was found that the effectiveness of a fly ash on improving the sulfate resistance of concrete could be predicted based on its CaO and Fe_2O_3 contents. Based on the ASTM C1012 test method, silica fume has been observed to improved the sulfate resistance of mortar bars (Hooten). Long-term durability tests on the sulfate resistance of concrete containing silica fume, however, have not been reported. The effectiveness of mineral admixtures in preventing sulfate attack depends on their composition and physical properties, and, therefore, they should conform to the appropriate ASTM standards before being used.

Recommendations for selecting cements and mineral admixtures for concretes exposed to sulfates have been given in the ACI Guide for Durable Concrete (23). The recommendations are presented in table 2. Also, they are presented in an expert system form in Durcon (30). Although ASTM Type V portland cement is recommended in the table for severe and very severe exposures, little Type V cement is available in the United States (31). In the case of a severe environment, a Type II portland cement with blast furnace slag or a pozzolan should be an adequate substitute for Type V.

A site with a very severe environment is, undoubtedly, unfit for storing LLW in concrete vaults. Following these recommendations should result in a concrete with acceptable durability for many years, possibly for the 60 to 100 year design life of typical concrete structure. However, they do not provide a basis for predicting the service life of a concrete exposed to a sulfate environment, especially in the case of concrete with a design life of hundreds of years.

Table 2. Recommenations for Sulfate Resistance (23)

Exposure	Water soluble sulfate (a) soil, percent	Soluble (SO_4) in water, ppm	cement	Water-cement ratio, maximum(b)
Mild	0.00-0.10	0-150		
Moderate (Includes Seawater)	0.10-0.20	150-1500	Type II IP (MS) IS (MS) (c)	0.50
Severe	0.20-2.00	1500-10,000	Type V (d)	0.45
Very Severe	Over 2.00	Over 10,000	Type V + Pozzolan or Slag (e)	0.45

(a) Sulfate expressed as SO_4 is related to sulfate expressed as SO_3 as in reports of chemical analysis of cement as SO_3 X 1.2 = SO_4.

(b) A lower water-cement ratio may be necessary to prevent corrosion of embedded steel.

(c) Or a blend of Type I cement and a ground granulated blast-furnac slag or pozzolan that has been determined by tests to give equivalent sulfate resistance.

(d) Or a blend of Type II cement and a ground granulated blast-furnace slag or a pozzolan that has been determined by tests to give equivalent sulfate resistance.

(e) Use a pozzolan or slag that has been determined by tests to improve sulfate resistance when used in concrete containing Type V cement.

4.3 Models and Service Life Predictions

Two major studies have been reported (32, 33) on approaches for estimating the service life of concrete exposed to sulfates. In the first, the US Bureau of Reclamation (32), continously immersed concrete specimens in a 2.1% Na_2SO_4 (sodium sulfate) solution until failure (expansion of 0.5%) or until the investigation was completed. The age of specimens at the completion of the continuous-immersion study was between 18 to 24 years. Companion specimens were subjected to an accelerated test in which they were immersed for 16 hours in a 2.1% Na_2SO_4 solution and then forced air dried at 54°C (130°F) for 8 hours. From a comparison of the times for specimens to reach an expansion of 0.5% in both the accelerated test and the continuous immersion test, it was estimated that 1 year of accelerated testing equalled 8 years of continuous immersion. This was considered to be a conservative ratio as a 1:10 ratio was thought to be more realistic. In many cases, the time for the concretes in the continuous immersion test to expand by 0.5% was estimated by straight-line extrapolation. They concluded that most of the concretes with Types II and V portland cements showed a life expectancy of less than 50 years when exposed to a 2.1% Na_2SO_4 solution. Some concretes containing certain fly ash and ground blast-furnace slag mineral admixtures had estimated service lives of 150 years or more. A 2.1% solution of Na_2SO_4 is a very severe environment (table 2) and if concrete was exposed to a lower level of sulfates the life expectancy would be expected to increase. In addition to providing an approach for service life estimates, the accelerated test results clearly demonstrate the aggressive effect of wetting and drying cycles with sulfate solutions on the durability of concrete.

The above method could be used for predicting the service lives of in-service concretes, in continuous contact with groundwater, if the ratio of 1:8 for the time to attain a equivalent expansion in the accelerated and continuous immersion tests using the 2.1% sulfate solution holds for other sulfate concentrations. Based on the ratio of 1:8, however, to predict if a concrete would have a life expectancy of 500 years may necessitate an unacceptably extended extrapolation of the accelerated test results as follows. Assuming that a concrete with a life of 500 years was actually being tested, then to predict that the concrete would have a life expectancy of 500 years by testing until the 0.5% expansion criterion was reached in the accelerated test would require a testing period of at least 500/8 years, i.e., 63 years. Unfortunately, few durability tests are carried out for 63 years and a 5 to 10 year test is often considered long-termed. If the accelerated test was terminated in 5 years, the expansion for the 500-year-life concrete would be no more than 0.04% and little confidence could be given to predictions based on extrapolating the expansion data to 0.5%.

Another approach to predicting the service life of concrete exposed to groundwater containing sulfate salts was developed by the Building Research Establishment in England (33). In the laboratory, concrete specimens were immersed in a 0.19M sulfate solution (a mixture of alkali and magnesium sulfates) for up to 5 years. The accelerated laboratory tests resulted in a visible deterioration zone, X_s, and the following empirical equation was developed:

$$X_s(cm) = 0.55CA(\%)\ [Mg] + [SO_4]\ t(y \qquad 7)$$

where CA% is the percentage by weight of tricalcium aluminate ($3CaO\cdot Al_2O_3$) in the cement, [Mg] and [SO_4] are the molar concentrations of magnesium and sulfates, respectively, in the test solution, and t(y) is the test time in years. The variability in the depths of attack were around 30% of the average.

Equation no. 7 was found to give satisfactory correlations with the results of field tests (3), in which the depth of penetrations were in the range of 0.8 to 2 cm after 5 years. The equation was used to calculate a range of lifetimes of concrete exposed to groundwater of a known concentration of sulfate salts. Concretes made with ordinary portland cements containing between 5 and 12% C_3A, gave estimated lifetimes of between 180 to 800 years, with a probable lifetime of 400 years. When a sulfate resisting portland cement with 1.2% C_3A was used, the minimum and probable lifetimes were estimated to be 700 years and 2500 years, respectively. These times were estimated based on the loss of one-half of the load-bearing capacity of a 1 m thick concrete section, i.e., X_s of 50 cm. The estimates involve an extrapolation based only on an empirical equation that has been shown to be reasonably predictive only during short-term testing. Atkinson, et al., (3) attempted to verify the equation by determining the extent of deterioration of concretes buried and exposed to the groundwater of a clay for 43 years. An alteration zone of about 1 cm was observed in the concretes which could be caused by several processes. Based on the tricalcium aluminate contents of the cements, equation no. 7 predicts that the thickness of the deteriorated region should be between 1 and 9 cm. Therefore, Atkinson, et al., (3) concluded that the equation either gives a correct estimate or an overestimate of the rate of sulfate attack.

5. CORROSION OF STEEL REINFORCEMENT IN CONCRETE

Portland cement concrete normally provides an internal environment which protects reinforcing steel from corrosion. The high alkaline environment (pH > 12.5) in concrete results in the formation of a tightly adhering film (gamma iron (III) oxide) which passivates the steel and thereby protects it from

Aqueous Environmental Geochemistry

Donald Langmuir
Colorado School of Mines

PRENTICE HALL
Upper Saddle River, New Jersey 07458

Library of Congress Cataloging-in-Publication Data
Langmuir, Donald.
Aqueous environmental geochemistry / by Donald Langmuir.
p. cm.
Includes index.
ISBN 0-02-367412-1
1. Water chemistry. 2. Environmental geochemistry. I. Title.
GB855.L36 1997
551.48--dc21 96-37614
CIP

Executive editor: Robert McConnin
Production: ETP Harrison
Copy editor: ETP Harrison
Cover director: Jayne Conte
Manufacturing manager: Trudy Pisciotti

Printed in the United States of America

10 9 8 7 6 5 4 3 2

ISBN 0-02-367412-1

Prentice-Hall International (UK) Limited, *London*
Prentice-Hall of Australia Pty. Limited, *Sydney*
Prentice-Hall Canada Inc., *Toronto*
Prentice-Hall Hispanoamericana, S.A., *Mexico*
Prentice-Hall of India Private Limited, *New Delhi*
Prentice-Hall of Japan, Inc., *Tokyo*
Simon & Schuster Asia Pte Ltd., *Singapore*
Editora Prentice-Hall do Brasil, Ltda., *Rio de Janeiro*

Co

Preface

1 Therm
1.1 Some I
1.2 Enthal
1.3 Gibbs
the Eq
1.4 Equilil
1.4.1 P
1.4.2 C
1.4.3 S
1.4.4 S
1.5 Summ
Proper
1.6 The E
Pressu
1.6.1 I
1.6.2 I
1.6.3 I
Study
Proble
Chapt

2 Chem
2.1 Chem
Kineti
2.2 Eleme
2.3 Rate l

Example 1.2

The second dissociation step for carbonic acid corresponds to the reaction $HCO_3^- = H^+ + CO_3^{2-}$, for which $K_2 = 10^{-10.33}$ at 25°C. Using thermodynamic data tables we compute ΔH_r° = 3550 cal/mol, and from Shock and Helgeson (1988) we find $\Delta Cp_r^\circ = -61.0$ cal/mol K. Given this information, we ask the question, how does the value of K_2 at 50°C (323.15 K), predicted from the integrated van't Hoff equation, compare to the empirical value at 50°C? The van't Hoff equation is

$$-\log K_2 = 10.33 + \frac{3550}{4.576}\left(\frac{1}{323.15} - \frac{1}{298.15}\right) \qquad .93)$$

from which we find

$$-\log K_2 = 10.33 - 0.20 = 10.13$$

This is in fair agreement with $-\log K_2 = 10.18$ at 50°C computed from the empirical temperature function in Table A1.1. The disagreement reflects the fact that the heat capacity of the reaction is not zero, as assumed in the calculation. If we refine our estimate by including the heat capacity correction term of the expanded integrated van't Hoff equation, the predicted value for K_2 at 50°C is

$$-\log K_2 = 10.33 - 0.20 + 0.04 = 10.17$$

in excellent agreement with the empirical value

Example 1.3

Consider the reaction

$$AgCl(c) = Ag^+ + Cl^- \qquad (1.94)$$

for which $K_{sp} = 10^{-9.75}$ and ΔH_r° = 15,650 cal/mol at 25°C. Silver chloride is also known as the mineral cerargyrite. This reaction takes place in the internal electrolyte of glass pH electrodes. The insolubility of cerargyrite also limits maximum concentrations of silver in many natural waters. We will ask the question, what is K_{sp} at 0°C? The van't Hoff equation leads to

$$-\log K_{sp} = 9.75 - \frac{15{,}650}{4.576}\left(\frac{1}{273.15} - \frac{1}{298.15}\right) \qquad (1.95)$$

and

$$-\log K_{sp} = 9.75 + 1.05 = 10.80$$

This is in exact agreement with the empirical value, indicating that the assumptions inherent in the van't Hoff equation are valid (ΔH_r° is constant and $\Delta Cp_r^\circ = 0$).

1.6.3 Effect of Pressure

Substituting the quantity $(-RT \ln K_{eq})$ for ΔG_r° in the expression

$$\left(\frac{\partial(\Delta G_r^\circ)}{\partial P}\right)_T = \Delta V_r^\circ \qquad (1.96)$$

derived previously, we obtain

$$\left(\frac{\partial \ln K_{eq}}{\partial P}\right)_T = \frac{\Delta V_r^\circ}{RT} \tag{1.97}$$

where ΔV_r° is the molar volume change of the reaction with all reactants and products in their standard states (cf. Millero 1982). Note the similarity of this expression to the van't Hoff equation. Equation (1.97) shows that the effect of a change in pressure on K_{eq} is proportional to the magnitude of the molar volume change for the reaction. Consistent with Le Chatelier's principle, an increase in pressure favors reaction products when ΔV_r° is negative and reactants when ΔV_r° is positive. When a gas is among the reactants or products, the effect of pressure is accounted for by writing the activity of the gas as its partial pressure. For reactions without gases, the effect of pressure can usually be ignored at depths less than 300 m (1000 ft). In following discussion, we will consider the pressure effect on reactions in more detail. Important environmental applications are to reactions in the deep ocean (average deep-ocean pressure is 200 bars (Stumm and Morgan 1981) and to geologic disposal of industrial wastes by deep-well injection. Deep-well injection is typically into saline groundwaters in sedimentary formations at temperatures of 20 to 150°C, with pressures from 50 to 300 bars (Environmental Protection Agency 1990a, 1990b). We will limit discussion in this section to the effect of pressure on reactions, which is usually less important than the coincident temperature effect as discussed previously.

If the molar volume of a reaction is independent of pressure (does not change with pressure in the P range of interest), Eq. (1.97) may be integrated to yield

$$\ln \frac{K_p}{K_1} = -\frac{\Delta V_r^\circ (P - 1)}{RT} \tag{1.98}$$

where K_p and K_1 are the equilibrium constant at P and at the reference pressure, which is usually 1 bar.

If instead ΔV_r° is a function of pressure, we may define the standard partial molar compressibility which for single species i equals

$$\overline{K}_i^\circ = \left(\frac{\partial V}{\partial P}\right)_T \tag{1.99}$$

For a reaction we have

$$\Delta \overline{K}_r^\circ = \left(\frac{\partial \Delta V_r^\circ}{\partial P}\right)_T \tag{1.100}$$

Integration of Eq. (1.97) now leads to

$$\ln \frac{K_p}{K_1} = -\frac{\Delta V_r^\circ (P - 1)}{RT} + \frac{\Delta \overline{K}_r^\circ (P - 1)^2}{2RT} \tag{1.101}$$

in which $\Delta \overline{K}_r^\circ$ is independent of pressure. At elevated pressures (> 100 bars) this simplifies to

$$\ln \frac{K_p}{K_1} = -\frac{\Delta V_r^\circ P}{RT} + \frac{\Delta \overline{K}_r^\circ P^2}{2RT} = -\frac{P}{RT}\left(\Delta V_r^\circ - \frac{\Delta \overline{K}_r^\circ P}{2}\right) \tag{1.102}$$

In these expressions ΔV_r° is in cm^3/mol, R = 83.15 cm^3 bar/mol K, and $\Delta \overline{K}_r^\circ$ is in cm^3/bar mol.

Molar volumes of minerals are proportional to the size of molar formulas and may be computed by dividing a mineral's gram formula weight (g/mol) by its density (g/cm^3). Values for minerals are tabulated by Naumov et al. (1974), Robie et al. (1978), and Helgeson et al. (1978), and may also be found in any edition of the *Handbook of Chemistry and Physics* (CRC Press).

Naumov et al. (1974), Helgeson et al. (1981), Millero (1982), and Tanger and Helgeson (1988) report molar volume data for aqueous species at 25°C. The last two references also give $V°$ data for aqueous species from 0°C up to 50°C and 350°C, respectively. Molar compressibilities of minerals are available in Birch (1966), Mathieson and Conway (1974), and Millero (1982). Millero (1982) also lists values of ΔV_r° and $\Delta \overline{K}_r^\circ$ for aqueous species from 0 to 50°C. Molar volumes and compressibilities vary as a function of temperature and ionic strength (Millero 1982). Such effects may be important for aqueous species and especially for gases.

The molar volume of ions is based on the convention that the molar volume of H^+ ion equals zero at all temperatures. This assumption leads to molar volumes of -0.4 cm^3/mol for Li^+ and 36 cm^3/mol for I^-, for example. Molar volumes of ions increase with increasing temperature. ΔV_r° is negative for most ionization and dissolution reactions so that pressure generally increases the progress of ionization reactions and the solubility of minerals.

Molar compressibilities for minerals range from 0 to -4×10^{-9} cm^3/bar mol and can be assumed equal to zero up to about 1 kb pressure. Values for ions $\overline{K}°$ are generally in the range -5 to -10×10^{-3} cm^3/bar mol. $\Delta \overline{K}_r^\circ$ for completely ionic reactions is small, but for dissolving minerals it may be large.

In a column of freshwater the pressure increases above atmospheric pressure by about 1 bar for every 33.5 ft of depth, or by 30 bars for 1000 ft (305 m) of depth. Pressure gradients are higher in saline than in fresh groundwaters. Pressures measured in groundwater at depth generally range between hydrostatic pressure (that of a column of water) and lithostatic pressure (that of the rock alone). Measured hydrostatic pressure gradients in sediments range from 1 bar/15 ft (roughly equal to the lithostatic pressure gradient) to 1 bar/70 ft of depth. In sediments of the Palo Duro basin of north Texas for example, the pressure gradient is 1 bar/42 to 58 ft to a depth of 5500 ft, where hydrostatic pressure is 130 bars and the temperature 38°C (Langmuir and Melchior 1985).

The effect of pressure on reactions involving only solid phases can be assumed to be negligible. For example, consider the reaction

$$\underset{\text{(corundum)}}{Al_2O_3} + \underset{\text{(quartz)}}{SiO_2} = \underset{\text{(sillimanite)}}{Al_2SiO_5} \qquad (1.103)$$

$V°$ (cm^3/mol)	25.57	22.69	49.92

The molar volumes lead to $(\partial \Delta G_r^\circ / \partial P)_T = \Delta V_r^\circ = 1.66$ cm^3/mol, from which we conclude that an increase in pressure slightly favors corundum and quartz over sillimanite. Given the conversion factor 1 cm^3 bar = 0.02390 cal, we obtain

$$(\partial \Delta G_r^\circ / \partial P)_T = 1.66 \text{ cm}^3\text{/mol} \times 0.02390 \text{ cal/cm}^3 \text{ bar}$$
$$= 0.0397 \text{ cal/mol bar}$$

Thus, an increase in P of 100 bars increases ΔG_r° by only ~4 cal/mol. This is a negligible effect.

When a gas is among the reactants, changes in pressure are generally important. For example, given the reaction at 25°C,

$$\underset{}{CaCO_3\text{(calcite)}} = \underset{}{CaO\text{(lime)}} + \underset{}{CO_2\text{(g)}} \qquad (1.104)$$

$V°$ (cm^3/mol)	36.934	16.764	24,460

TABLE 1.2 Effects of pressure and ionic strength on equilibrium constants for some reactions as a function of the molar volumes of the reactions

Reaction	ΔV_r° (cm³/mol)	K_r/K_1 at 25°C and 1000 bars
H_2O (l) = $H^+ + OH^-$	−22.2	2.36
$CH_3COOH = H^+ + CH_3COO^-$ (K_a acetic acid)	−11.2	1.4
$H_2CO_3 = H^+ + HCO_3^-$ (K_1 carbonic acid)	−27.2	3.2
$HCO_3^- = H^+ + CO_3^{2-}$ (K_2 carbonic acid)	−25.2	2.7
$CaSO_4$ (anhydrite) = $Ca^{2+} + SO_4^{2-}$	−48.9	5.8

Source: Based in part on Stumm and Morgan (1981).

we find ΔV_r° = 24,440 cm³/mol, or 584 cal/mol bar. The (+) sign and large magnitude of ΔV_r° show that increasing pressure strongly favors calcite formation relative to lime and CO_2(g).

The effect of a pressure increase to 1000 bars on some dissociation reactions is shown in Table 1.2. Increased pressure favors dissociation in every case. The effect is proportional to the size of $-\Delta V_r^\circ$. The solubility of calcite increases with increasing pressure as indicated by Table 1.3. The effect is reduced at the ionic strength of seawater.

Pressure generally increases the solubility of minerals. An accurate evaluation of the pressure effect on solubility may require that we consider both molar volumes and compressibilies of reactants and products. In the following problem we compare the solubility of celestite ($SrSO_4$) in a surface water at 1 bar pressure and 25°C to its solubility in groundwater at 6000 ft depth at a temperature of 75°C and pressure of 180 bars. The reaction of interest is $SrSO_4$(celestite) = $Sr^{2+} + SO_4^{2-}$. To solve the problem we need molar volumes and compressibilities for celestite and the ions. We adapt V° (celestite) = 46.25 cm³/mol from Robie et al. (1978). A nearly identical molar volume of 46.27 cm³/mol derives from the molecular weight (183.678 g/mol) divided by the density of celestite (3.97 g cm³; Palache et al. 1951). V°(celestite) can be assumed to be independent of pressure and temperature. Molar volumes for the ions at 75°C are obtained from Tanger and Helgeson (1988). The compressibility of celestite is read from a plot given by Millero (1982). $\bar{K}^\circ$ values for the ions are less readily available. We will use those given by Millero (1982) for 50°C. The comparatively small compressibility of the mineral (about 1% as large as values for the ions) suggests that its value is relatively unimportant in the calculation. The compressibility correction to the solubility will turn out

TABLE 1.3 Effects of increases in pressure and ionic strength at 25°C on the solubility product of calcite ($CaCO_3$) at P versus at 1 bar pressure, expressed as K_P/K_1

P (bar)	Pure water	0.725 M NaCl (seawater)
1	1	1
500	3.2	2.8
1000	8.1	6.7

Note: ΔV_r° = −58.3 cm³/mol for the reaction $CaCO_3 = Ca^{2+} + CO_3^{2-}$ at 25°C.
Source: Based in part on Stumm and Morgan (1981).

to be small, thus our use of 50°C $\bar{K}°$ values for Sr^{2+} and SO_4^{2-} is a good approximation. Chosen $V°$ and $\bar{K}°$ values are given below.

	$SrSO_4$(celestite)	= Sr^{2+}	+ SO_4^{2-}
$V°$ (cm^3/mol)	46.25	−18.27	+14.09
$\bar{K}°$ (cm^3/mol bar)	-0.08×10^{-3}	-8.35×10^{-3}	-6.87×10^{-3}

(1.105)

The $V°$ and $\bar{K}°$ data lead to $\Delta V_r° = -50.43$ cm^3/mol, and $\Delta \bar{K}_r° = -1.514 \times 10^{-3}$ cm^3/mol bar. Substituting into Eq. (1.101) or (1.102), we can determine the effect of pressure on celestite solubility. The result is $\log (K_p/K_1) = 0.1364 - 0.0037 = 0.133$, where the first term in the difference reflects the contribution of $\Delta V_r°$ and the second the small, opposite effect of $\Delta \bar{K}_r°$. At 1 bar pressure and 25°C, K_{sp}(celestite) = 2.32×10^{-7}. For 75°C, K_{sp}(celestite) = 7.45×10^{-7}, computed from the temperature function given by Langmuir and Melchior (1985). Overall results are summarized here.

T(°C)	P (bar)	K_{sp}(celestite)	Overall percent increase above 1 bar and 25°C
25	1	2.32×10^{-7}	0
75	1	7.45×10^{-7}	221%
75	180 ($\Delta V_r°$)	1.02×10^{-6}	340%
75	180 ($\Delta V_r°$ and $\Delta \bar{K}_r°$)	1.01×10^{-6}	335%

As shown, the increase in temperature from 25 to 75°C has more of an effect on solubility (+221%) than does the increase in pressure from 1 to 180 bars, which separately increases solubility by 36%. As evident from this example, and in general, the effect of a temperature increase on solubility greatly exceeds that of the concomitant pressure increase. The example also shows that the pressure correction due to $\Delta \bar{K}_r°$ is minor and usually of an opposite sign to that due to $\Delta V_r°$.

Aggarwal et al. (1990) have proposed a simpler model given by

$$\ln\left(\frac{K_{P,T}}{K_1^\circ}\right) = -\left(\frac{\Delta V_r^\circ}{RT\,\bar{K}_{H_2O}^\circ}\right) \ln\left(\frac{\rho_{H_2O(P,T)}}{\rho_{H_2O}^\circ}\right) \tag{1.106}$$

to estimate the effect of a change in P and T on the equilibrium constant. Their equation requires only $\Delta V_r°$ for the reaction, the compressibility ($\bar{K}_{H_2O}^\circ$) and density ($\rho_{H_2O}^\circ$) of water for reference conditions (usually at 1 bar pressure and 25°C), and water density at P and T ($\rho_{H_2O(P,T)}$). Reactions are written in isocoulombic form so that reaction heat capacity and the term ($\Delta V°/RT\,\bar{K}_{H_2O}^\circ$) are both constant, independent of temperature. The necessary properties of water have been published by Haar et al. (1984). The reader is referred to Aggarwal et al. (1990) for details of this approach.

STUDY QUESTIONS

1. Know the following definitions and how they relate to each other:
   (a) open and closed systems as they relate to mobile and less mobile substances
   (b) phases, components, master species, and the phase rule
   (c) homogeneous, heterogeneous and irreversible, congruent and incongruent reactions
   (d) Gibbs free energy, chemical potential, enthalpy, and entropy, as they relate to components, substances, reactions, and systems

HANDBOOK OF ANALYTICAL TECHNIQUES IN CONCRETE SCIENCE AND TECHNOLOGY

Principles, Techniques, and Applications

Edited by

V. S. Ramachandran

and

James J. Beaudoin

Institute for Research in Construction
National Research Council Canada
Ottawa, Ontario, Canada

NOYES PUBLICATIONS
Park Ridge, New Jersey, U.S.A.

WILLIAM ANDREW PUBLISHING, LLC
Norwich, New York, U.S.A.

Library of Congress Catalog Card Number: 99-29616
ISBN: 0-8155-1437-9
Printed in the United States

Published in the United States of America by
Noyes Publications / William Andrew Publishing, LLC
Norwich, New York, U.S.A.

10 9 8 7 6 5 4 3 2 1

Library of Congress Cataloging-in-Publication Data

Ramachandran, V. S.
Handbook of analytical techniques in concrete science and technology / by V.S. Ramachandran and J.J. Beaudoin.
p. cm.
Includes bibliographical references.
ISBN 0-8155-1437-9
1. Concrete--Testing. 2. Concrete--Analysis. I. Beaudoin, J. J. II. Title.
TA440.R26 1999
624.1'83--dc21 99-29616
CIP

Concrete Science

Vangi S. Ramachandran

INTRODUCTION

Concrete, made from cement, aggregates, chemical admixtures, mineral admixtures, and water, comprises in quantity the largest of all man-made materials. The active constituent of concrete is cement paste and the performance of concrete is largely determined by the cement paste. Admixtures in concrete confer some beneficial effects such as acceleration, retardation, air entrainment, water reduction, plasticity, etc., and they are related to the cement-admixture interaction. Mineral admixtures such as blast furnace slag, fly ash, silica fume, and others, also improve the quality of concrete.

The performance of concrete depends on the quality of the ingredients, their proportions, placement, and exposure conditions. For example, the quality of the raw materials used for the manufacture of clinker, the calcining conditions, the fineness and particle size of the cement, the relative proportions of the phases, and the amount of the mixing water, influence the physicochemical behavior of the hardened cement paste. In the fabrication of concrete, amount and the type of cement, fine and coarse aggregate, water, temperature of mixing, admixture, and the environment to which it is exposed will determine its physical, chemical, and durability behavior. Various analytical techniques are applied to study the effect of

these parameters and for quality control purposes. The development of standards and specifications are, in many instances, directly the result of the work involving the use of analytical techniques. Discussion of the methods employed in standard specifications is beyond the scope of this chapter.

In this chapter, basic aspects of the physical, chemical, durability, and mechanical characteristics of cement paste and concrete are presented because of their relevance to the application of various analytical techniques discussed in other chapters.

2.0 FORMATION OF PORTLAND CEMENT

According to ASTM C-150, *portland cement* is a hydraulic cement produced by pulverizing clinker consisting essentially of hydraulic calcium silicates, usually containing one or more types of calcium sulfate, as an interground addition.

The raw materials for the manufacture of portland cement contain, in suitable proportions, silica, aluminum oxide, calcium oxide, and ferric oxide. The source of lime is provided by calcareous ingredients such as limestone or chalk and the source of silica and aluminum oxide are shales, clays or slates. The iron bearing materials are iron and pyrites. Ferric oxide not only serves as a flux, but also forms compounds with lime and alumina. The raw materials also contain small amounts of other compounds such as magnesia, alkalis, phosphates, fluorine compounds, zinc oxide, and sulfides. The cement clinker is produced by feeding the crushed, ground, and screened raw mix into a rotary kiln and heating to a temperature of about 1300–1450°C. Approximately 1100–1400 kcal/g of energy is consumed in the formation of clinker. The sequence of reactions is as follows: At a temperature of about 100°C (drying zone) free water is expelled. In the preheating zone (750°C) firmly bound water from the clay is lost. In the calcining zone (750–1000°C) calcium carbonate is dissociated. In the burning zone (1000–1450°C) partial fusion of the mix occurs, with the formation of C_3S, C_2S and clinker. In the cooling zone (1450–1300°C) crystallization of melt occurs with the formation of calcium aluminate and calcium aluminoferrite. After firing the raw materials for the required period, the resultant clinker is cooled and ground with about 4–5% gypsum to a specified degree of fineness. Grinding aids, generally polar compounds, are added to facilitate grinding.

2.1 Composition of Portland Cement

The major phases of portland cement are tricalcium silicate ($3CaO \cdot SiO_2$), dicalcium silicate ($2CaO \cdot SiO_2$), tricalcium aluminate ($3CaO \cdot Al_2O_3$), and a ferrite phase of average composition $4CaO \cdot Al_2O_3 \cdot Fe_2O_3$. In a commercial clinker they do not exist in a pure form. The $3CaO \cdot SiO_2$ phase is a solid solution containing Mg and Al and is called *alite*. In the clinker, it consists of monoclinic or trigonal forms whereas synthesized $3CaO \cdot SiO_2$ is triclinic. The $2CaO \cdot SiO_2$ phase occurs in the β form, termed belite, and contains, in addition to Al and Mg, some K_2O. Four forms, α, α', β and γ, of C_2S are known although in clinker only the β form with a monoclinic unit cell exists. The ferrite phase, designated C_4AF, is a solid solution of variable composition from C_2F to C_6A_2F. Potential components of this compound are C_2F, C_6AF_2, C_4AF, and C_6A_2F. In some clinkers small amounts of calcium aluminate of formula NC_8A_3 may also form.

ASTM C-150 describes five major types of portland cement. They are: Normal Type I—when special properties specified for any other type are not required; Type II—moderate sulfate resistant or moderate heat of hydration; Type III—high early strength; Type IV—low heat; and Type V—sulfate resisting. The general composition, fineness, and compressive strength characteristics of these cements are shown in Table 1.[1]

Portland cement may be blended with other ingredients to form blended hydraulic cements. ASTM C-595 covers five kinds of blended hydraulic cements. The portland blast furnace slag cement consists of an intimately ground mixture of portland cement clinker and granulated blast furnace slag or an intimate and uniform blend of portland cement and fine granulated blast furnace slag in which the slag constituent is within specified limits. The portland-pozzolan cement consists of an intimate and uniform blend of portland cement or portland blast furnace slag cement and fine pozzolan. The slag cement consists mostly of granulated blast furnace slag and hydrated lime. The others are pozzolan-modified portland cement (pozzolan < 15%) and slag-modified portland cement (slag < 25%).

Table 1. Compound Composition, Fineness and Compressive Strength Characteristics of Some Commercial U.S. Cements

ASTM Type	ASTM Designation	Composition				Fineness cm^2/g	Compressive Strength % of Type I Cement*		
		C_3S	C_2S	C_3A	C_4AF		1 day	2 days	28 days
	General purpose	50	24	11	8	1800	100	100	100
	Moderate sulfate resistant-moderate heat of hydration	42	33	5	13	1800	75	85	90
III	High early strength	60	13	9	8	2600	190	120	110
IV	Low heat	26	50	5	12	1900	55	55	75
V	Sulfate resisting	40	40	4	9	1900	65	75	85

**All cements attain almost the same strength at 90 days.*

3.0 INDIVIDUAL CEMENT COMPOUNDS

3.1 Tricalcium Silicate

Hydration. A knowledge of the hydration behavior of individual cement compounds and their mixtures forms a basis for interpreting the complex reactions that occur when portland cement is hydrated under various conditions.

Tricalcium silicate and dicalcium silicate together make up 75–80% of portland cement (Table 1). In the presence of a limited amount of water, the reaction of C_3S with water is represented as follows:

$$3CaO{\bullet}SiO_2 + xH_2O \rightarrow yCaO{\bullet}SiO_2{\bullet}(x+y-3)H_2O + (3-y)Ca(OH)_2$$

or typically

$$2[3CaO{\bullet}SiO_2] + 7H_2O \rightarrow 3CaO{\bullet}2SiO_2{\bullet}4H_2O + 3Ca(OH)_2$$

The above chemical equation is somewhat approximate because it is not easy to estimate the composition of C-S-H (the C/S and S/H ratio) and there are also problems associated with the determination of $Ca(OH)_2$. In a fully hydrated cement or C_3S paste, about 60–70% of the solid comprises C-S-H. The C-S-H phase is poorly crystallized containing particles of

and the testing method. This law is valid provided the concrete is fully compacted. This is the reason why, below a certain minimum, further reduction in the w/c ratio does not result in the expected strength gain. At such low w/c ratios, concrete is not workable enough to allow full compaction. Air entrainment reduces concrete strength and this effect should be considered while applying the law.[77]

The strength of concrete depends on the strength of the paste, coarse aggregate, and the paste-aggregate interface. This interface is the weakest region of concrete and is where the failure occurs before its occurrence on the aggregate or the paste. The weakness of this interface is due to weak bonding and the development of cracks which may develop due to bleeding and segregation and volume changes of the cement paste during setting and hydration. The transition zone extends about 50 μm from the surface of the aggregate. The transition zone has a higher porosity and permeability. This space is occupied by oriented, well developed crystals of calcium hydroxide and, in some cases, C-S-H and ettringite. The transition zonal effects are particularly significant with pastes or concrete made at w/c ratios greater than 0.4. The presence of silica fume, however, may modify or even eliminate the transition zone. This is generally attributed to the changes in the viscosity or cohesiveness imparted by silica fume to concrete. The altered transition zone, improved matrix-aggregate bond, and optimal particle packing in the presence of silica fume, result in enhanced strength.

8.0 DURABILITY OF CONCRETE

One of the most important requirements of concrete is that it should be durable under certain conditions of exposure. Deterioration can occur in various forms, such as alkali-aggregate expansion reaction, freeze-thaw expansion, salt scaling by deicing salts, shrinkage and enhanced attack on the reinforcement of steel due to carbonation, sulfate attack on exposure to ground waters containing sulfate ions, sea water attack, and corrosion caused by salts. Addition of admixtures may control these deleterious effects. Air entrainment results in increased protection against freeze-thaw action, corrosion inhibiting admixtures increase the resistance to corrosion, inclusion of silica fume in concrete decreases the permeability

and consequently the rate of ingress of salts, and the addition of slags in concrete increases the resistance to sulfate attack.

8.1 Alkali-Aggregate Expansion

Although all aggregates can be considered reactive, only those that actually cause damage to concrete are cause for concern. Experience has shown that the presence of excessive amount of alkalis enhances the attack on concrete by an expansion reaction. Use of marginal quality aggregate and the production of high strength concrete may also produce this effect.

The alkali-aggregate reaction in concrete may manifest itself as map cracking on the exposed surface, although other reactions may also produce such failures. The alkali-aggregate reaction known as *alkali-silica* type may promote exudation of a water gel which dries to a white deposit. These effects may appear after only a few months or even years.

Three types of alkali-aggregate reactions are mentioned in the literature, viz., alkali-silica reaction,[78]-[80] alkali-carbonate reaction, and alkali-silicate reaction. The alkali-silicate reaction has not received general recognition as a separate entity. Alkali-silica reactions are caused by the presence of opal, vitreous volcanic rocks, and those containing more than 90% silica. The alkali-carbonate reaction is different from the alkali-silica reaction in forming different products.[81]-[83] Expansive dolomite contains more calcium carbonate than the ideal 50% (mole) proportion and frequently also contains illite and chlorite clay minerals. The alkali-silicate reaction was proposed by Gillott.[84] The rocks that produced this reaction were graywackes, argillites, and phyllites containing vermiculites.

The preventive methods to counteract alkali-aggregate expansion include replacement of cement with pozzolans or blast-furnace slag and addition of some chemicals, such as lithium compounds.[85]-[89]

In Fig. 11, the effect of LiOH on the expansion in mortar containing opal, is shown. Mix five, containing opal and high alkali cement, shows the maximum amount of expansion. Mixes one, two, three, and four do not have opal. Mixes six and seven are similar except that mix six has 0.5% LiOH and mix seven 1% LiOH.

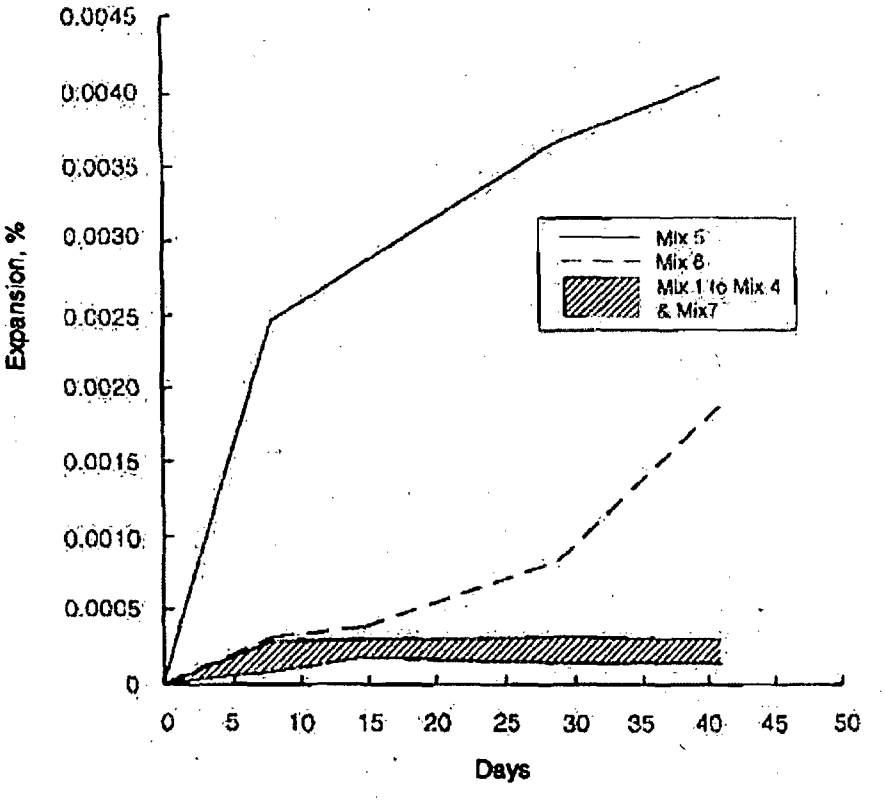

Figure 11. Expansion of mortar containing LiOH.

Frost Action

This is defined as the freezing and thawing of the moisture in materials and the resultant effects on these materials. Essentially three kinds of defects are recognized, viz., spalling, scaling, and cracking. Scaling occurs to a depth of an inch from the surface resulting in local peeling or flaking. Spalling occurs as a definite depression caused by the separation of surface concrete, while cracking occurs as D- or map-cracking and is sometimes related to the aggregate performance. Good resistance to frost expansion can be obtained by proper design and choice of materials and thus durability to frost action is only partly a material behavior. In addition to w/c ratio, quality of aggregate, and proper air entrainment, the frost resistance depends on the exposure conditions. Dry concrete will withstand freezing-thawing whereas highly saturated concrete may be severely damaged by a few cycles of freezing and thawing.

According to many workers, frost damage is not necessarily connected with the expansion of water during freezing although it can contribute to damage. Although many organic compounds, such as benzene and chloroform, contract during freezing, they can cause damage during the freezing transition. When a water-saturated porous material freezes, macroscopic ice crystals form in the coarser pores and water which is unfrozen in the finer pores and migrates to the coarser pores or the surfaces.[90] The large ice crystals can feed on the small ice crystals, even when the larger ones are under constraint.

Length Changes During Freezing of Hydrated Portland Cement. The pore structure of hardened cement paste determines freezing of water contained in the pores. The pore structure depends largely on the initial w/c ratio and the degree of hydration. In general, the pore structure is composed of pores having diameters ranging from 1,000 to 5 nm for non-matured pastes and 100 to 5 nm for mature pastes. The higher the w/c ratio, the greater will be the volume fraction of larger pores. When these pores are saturated with water, a large amount of water will be able to freeze during cooling. A saturated concrete prepared at a higher w/c ratio and with a lower degree of hydration contains a greater amount of water.

Fully saturated samples on cooling at 0.33°C/min show dilations during freezing and residual expansion on thawing. These values are increased in samples made at higher w/c ratios. Thicker samples also exhibit larger expansions. Cooling rates also influence length change values. It has been found that during the slow cooling 30–40% of the evaporable water is lost from the samples. It is apparent that the large dilation is not only due to water freezing in larger pores, but also to water migrating from smaller pores, freezing in limited spaces, and generating stresses. When the rate of cooling is slow, there is enough time for water to vacate the small pores of the sample, causing contraction due to drying shrinkage. Powers and Helmuth[91] added an air-entraining admixture to the paste, producing various amounts of air bubbles of uniform size. With a knowledge of the total volume and average size of the bubbles, the average distance between them (air-void spacing) was calculated. Length change measurements on cooling (0.25°C/min) relatively thick specimens of different air-void spacings, but having similar porosity, are shown in Fig. 12. Shrinkage occurred in specimens with bubble spacings of 0.30 mm or lower. These specimens were saturated (except for the entrained space) and, therefore, the existence of closely-spaced air bubbles provided sites for water to migrate and for ice crystals to grow without the imposition of stress.

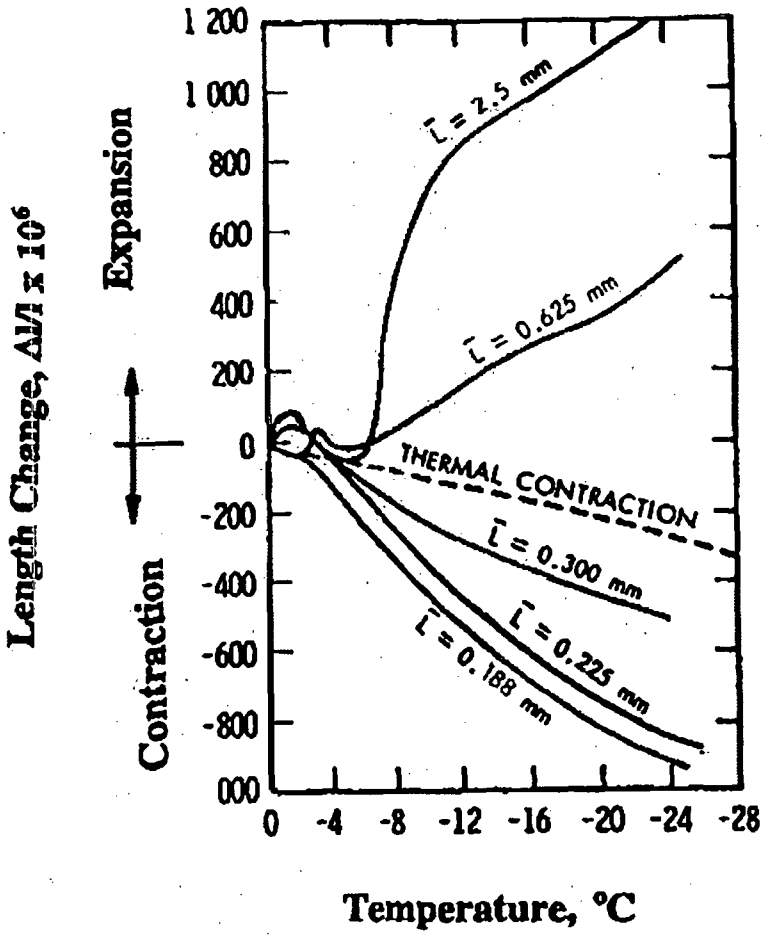

Figure 12. Length changes due to freezing of cement pastes of different air contents. (L is the spacing factor.)

De-Icing Salts—Deterioration of plain concrete due to deicing agents may generally be termed *salt scaling;* it is similar in appearance to frost action, but more severe. Any theory on salt scaling should account for this increased damage.

Length change measurements on freezing and thawing specimens saturated with different concentrations of brine solutions have been conducted by Litvan.[92] Typical results are shown in Fig. 13. The curves are qualitatively similar to those samples containing NaCl, but the magnitude of length changes is different. Maximum dilation effects are observed in solutions containing 5–9% NaCl. The explanation is that the vapor

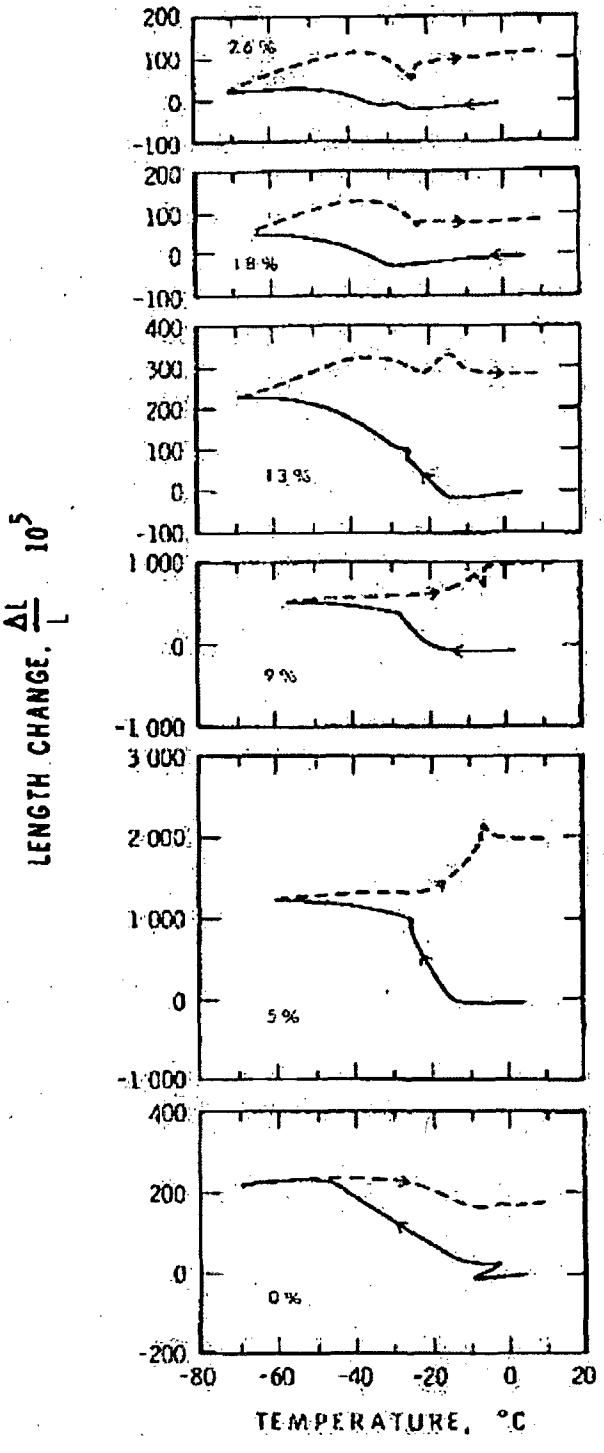

Figure 13. Length changes for air-entrained 0.5 w/c cement paste saturated with brine of various concentrations.

pressure of the saline solution is decreased (with respect to water) and the tendency for the water to migrate from the smaller pores will be lower for the saline solution in comparison with that for pure water. The relative humidity created when bulk ice, $P_{o(Bs)}$, formed in larger pores will be $P_{o(Bs)}/P_{sol}$, which will be larger than $P_{o(Bs)}/P_{o(SL)}$ at any temperature. Consequently, on freezing, greater dilation will occur in the salt-containing specimen than in the salt-free specimen. At high salt concentrations other phenomena, such as a change in the range of freezing temperatures or the effect of high viscosity of the saline solution on the mechanical properties of the body, have to be considered.

In concrete, the pores of the aggregate may be such that the pore water may readily freeze. Larger pores, equivalent to air-entrained bubbles (diameter > 10 nm) may not exist in the aggregates. Thus, the tendency to expand due to freezing of water will either be taken up by elastic expansion of the aggregate or by water flowing out from the aggregate under pressure. For saturated aggregates, there may be a critical size below which no frost action occurs because, during freezing, water will flow out of the specimen.[93]

Tests for Frost Resistance. The most widely used test for assessing the resistance of concrete to freezing and thawing is the ASTM test on "Resistance of Concrete to Rapid Freezing and Thawing" (ASTM C 666). In procedure A, both freezing and thawing occur with the specimens surrounded by water and, in procedure B, the specimens are frozen in air and thawed in water. Procedure A is somewhat more reproducible than Procedure B.

Control of Frost Resistance. The general approach to preventing frost attack in concrete is to use an air-entraining agent. Tiny bubbles of air are entrapped in concrete due to the foaming action developed by the admixture during mixing. Many factors, such as the variability in the materials, impurities, mixing and placing methods, make it difficult to adjust the required amount of air containing the right bubble spacing and size. Trial mixes are often carried out for this purpose.

These problems could largely be avoided if the preformed bubble reservoirs could be added in the form of particles. Two inventions have used this principle; the plastic microspheres[94] and porous particles,[95] which have required air are added to concrete. It has been shown that addition of particles which correspond to less than 2% equivalent air is similar to conventional air-entrained concrete containing 5% air. Control of the right size and spacing of air pockets in these particles can add to the effectiveness to frost action.

8.3 Sea Water Attack

Construction activity has been extending into the oceans and coastal areas because of the increasing number of oil and seabed mining operations. A large portion of these installations will be made from portland cement concrete and great demands will be made on it for increased safety and long term durability.

The deterioration of concrete due to sea water attack is the result of several simultaneous reactions; however, sea water is less severe on concrete than can be predicted from the possible reactions associated with the salts contained in it. Sea water contains 3.5% salts by weight. They include NaCl, $MgCl_2$, $MgSO_4$, $CaSO_4$, and possibly $KHCO_3$.

The deterioration of concrete depends on the exposure conditions. Concrete not immersed, but exposed to marine atmosphere will be subjected to corrosion of reinforcement and frost action. Concrete in the tidal zone, however, will be exposed to the additional problems of chemical decomposition of hydrated products, mechanical erosion, and wetting and drying. Parts of the structure permanently immersed are less vulnerable to frost action and corrosion of the reinforcing steel.

The aggressive components of sea water are CO_2, $MgCl_2$, and $MgSO_4$. Carbon dioxide reacts with $Ca(OH)_2$, finally producing calcium bicarbonate that leads to the removal of $Ca(OH)_2$. Carbon dioxide may also react with calcium aluminate monosulfate and break down the main strength-giving C-S-H component to form aragonite and silica. Even though $MgCl_2$ and sulfate are present only in small amounts they can cause deleterious reactions. These compounds react with $Ca(OH)_2$ to form soluble $CaCl_2$ or gypsum. Sodium chloride in sea water has a strong influence on the solubility of several compounds. Leaching of them makes the concrete weak. Magnesium sulfate may also react with calcium monosulfate aluminate in the presence of $Ca(OH)_2$ to form ettringite; this reaction is slowed down in the presence of NaCl[96] and may not occur if $Ca(OH)_2$ is converted by CO_2 to carbonate.

Calcium chloroaluminate seldom forms in sea water because, in the presence of sulfate, ettringite is the preferred phase. Ettringite formation affects the durability of concrete in seawater in the presence of cements containing $C_3A > 3\%$.[97] Tricalcium aluminate, in combination with high C_3S content, shows an even lower resistance to seawater than C_3A alone (Fig. 14). This is probably also due to the large amount of $Ca(OH)_2$ liberated by the hydration of C_3S. This explains why the addition of blast

furnace slag or fly ash to cement improves the performance in sea water. This is due to the reaction of $Ca(OH)_2$ with the reactive SiO_2 and Al_2O_3 from the fly ash and the low level of $Ca(OH)_2$ that is generally present in good blast furnace slags after the hydration reaction.

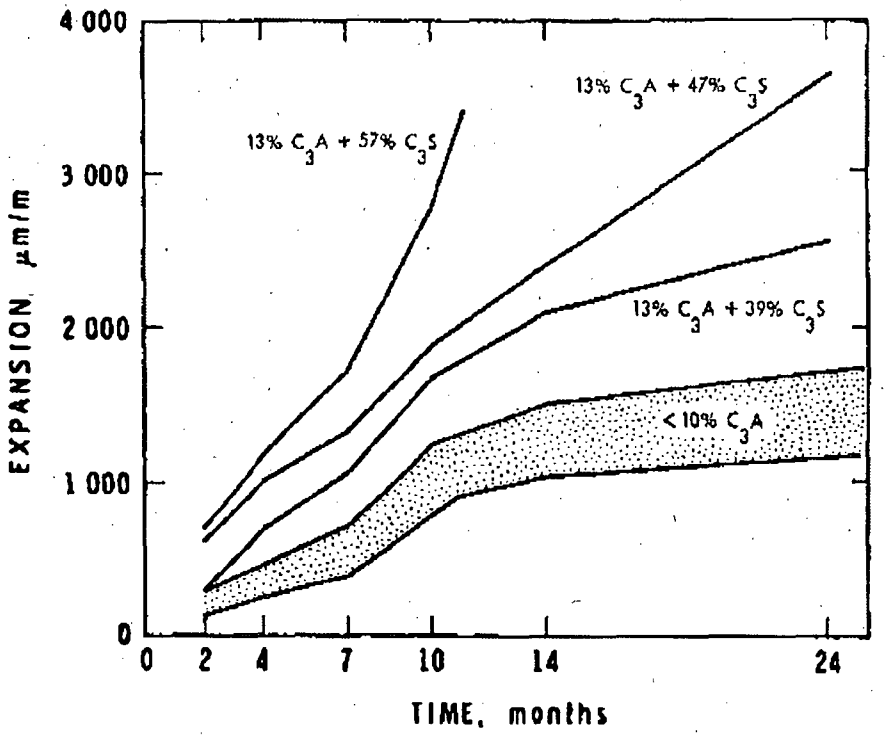

Figure 14. Linear expansion of mortar samples stored in sea water.

8.4 Corrosion of Reinforcement

Corrosion of steel in concrete is probably the most serious durability problem of reinforced concrete in modern times and, therefore, a clear understanding of the phenomenon is of crucial importance. The phenomenon itself is an electrochemical reaction. In its simplest form, corrosion may be described as current flow from anodic to cathodic sites in the presence of oxygen and water. This is represented by the following equations:

$$\text{AT ANODE} \quad Fe \rightarrow Fe^{2+} + 2e^-$$

$$\text{AT CATHODE} \quad \tfrac{1}{2}O_2 + H_2O + 2e^- \rightarrow 2(OH)^-$$

These reactions would result in the formation of oxide at cathodic sites. The high alkalinity of cement paste, however, provides protection for the steel reinforcement. Although it is understandable that the likelihood of corrosion depends on the pH of the solution and the electrical redox potential of the metal, initial observations of diagrams, known as *Pourbaix plots* (showing equilibrium regions where the metal is in a state of immunity or passivity, or where corrosion will occur) for carbon steel or iron show that the redox potential for the hydrogen electrode lies above the region of immunity for iron in both acid and alkaline solutions, suggesting that iron will dissolve with evolution of hydrogen in solutions of all pH values. However, in the pH interval 9.5 to 12.5, a layer of ferrous oxide or hydroxide forms on the metal surface thus conferring immunity from corrosion in these solutions in this range. Some authors[98] refer to this layer, or film, as γ-Fe_2O_3. This protective film is believed to form quite rapidly during the early stages of cement hydration and may grow to a thickness of the order of 10^{-3} to 10^{-1} μm. Only indirect evidence of an oxide film exists and is mainly based on anodic polarization measurements. Much is not known about the conditions of formation, or chemical or mineralogical composition of these passivating layers and it is feasible that the film may consist of several phases.[99]

Chloride depassivation of steel is perhaps better understood than the passivation process and there are several mechanisms proposed.[100][101] One of the mechanisms involves the formation of a complex ion between chloride ion and the ferrous ion in the passive film. It is possible that low Cl ion concentrations enhance Fe solubility[102] even at pHs as high as 12–13 as a result of a chloride complex containing both Fe^{2+} and Fe^{3+}. Migration of this complex destabilizes the passive layer and by this mechanism chloride can rejuvenate the corrosion process. Chloride ions are also responsible for other deleterious effects. They contribute, together with CO_2 ingress, to the depression of the pH of the pore fluid and increase the electrical conductance of the concrete, allowing the corrosion current to increase.

Currently, a limit of 0.2 percent of chloride ion concentration by weight of cement in the concrete is proposed; however, there is no theoretical basis to this value, and it appears possible that this amount of

hydroxyl ion in the cement paste modifies this value. Thus, some researchers have placed a limit on the ratio of chloride to hydroxyl ion[102][103] such that corrosion will occur if the ratio of Cl^- to OH^- is as follows:

$$\frac{Cl}{OH} > 0.6$$

Consequently the chloride ion threshold must also depend upon the alkalis in the cement. The effect of alkalis in aggregates and the removal of chloride ions by aluminate phases further complicate this picture, and it has been pointed out[101] that the fixation of chloride by the latter should not be considered permanent as the chloroaluminate may be unstable in the presence of sulfate or carbon dioxide.

Although the corrosion of the reinforcing steel in concrete is detrimental for the simple fact that the composite will lose strength, the main cause for concern is that this phenomenon causes cracking of the surrounding concrete. Estimates are that as little as 0.1 mil of rust thickness can cause cracking.

Early detection of the corrosion can allow remedial action to be made successfully. One of the more widely used tests is the measurement of the half-cell potential of the reinforcing steel embedded in the concrete (ASTM C876). It is usually understood that corrosion is taking place when half-cell potential values are more negative than -0.35 volts. However, frequently this rule does not strictly apply and it is recommended that corrosion rate values be obtained in questionable areas by measuring polarization resistance.

Generally, it is felt that the rate of corrosion of steel is primarily controlled by the diffusion of oxygen through the concrete cover, followed by the cathodic reaction involving reduction of oxygen.[104] However, there are situations where chloride contents are high and corrosion rates are much higher than would be expected from possible diffusion rates of oxygen. It has been postulated[104] that in these cases there are strong localized reductions in pH in crevices where iron is converted to $Fe(OH)_2$ through the prior conversion to chloride. These reactions involve hydrogen evolution.

Several methods of corrosion prevention have been tried over the years. These include protective coatings, placement of impermeable concrete overlays, cathodic protection, or the use of corrosion resistant steels and galvanized or epoxy coated bars. Recent work has shown[105] that

galvanized steel may be of benefit if used in low chloride bearing concrete (0.3 percent by weight of cement). Epoxy-coated bars have performed well where the concrete contained up to 1.2% chloride, but a breakdown of the coating was detected at a chloride level of 4.8%, indicating finite tolerance limit for chloride. The best durability was exhibited by the stainless clad reinforcing bars.

8.5 Carbonation of Concrete

The corrosion of depassivated steel in reinforced concrete has focused attention to the reactions of acidic gases such as carbon dioxide with hydrated cement and concrete. As a result of the reaction of carbon dioxide, the alkalinity of concrete can be progressively reduced, resulting in a pH value below 10.

The process of carbonation of concrete may be considered to take place in stages. Initially, CO_2 diffusion into the pores takes place, followed by dissolution in the pore solution. Reaction with the very soluble alkali metal hydroxide probably takes place first, reducing the pH and allowing more $Ca(OH)_2$ into the solution. The reaction of $Ca(OH)_2$ with CO_2 takes place by first forming $Ca(HCO_3)_2$ and finally, $CaCO_3$. The product precipitates on the walls and in crevices of the pores. This reduction in pH also leads to the eventual breakdown of the other hydration products, such as the aluminates, CSH gel, and sulfo-aluminates.

The relative humidity at which the pore solution is in equilibrium will greatly affect the rate of carbonation. The relative humidity controls the shape and area of the menisci at the air-water interfaces of the pores; at relative humidities greater than 80 percent, the area of the menisci contacting the air becomes quite small, resulting in a low rate of absorption of CO_2. At relative humidities below 40 percent, no menisci exist and the pore water is predominantly adsorbed water and does not effectively dissolve the CO_2. Consequently, carbonation occurs at a maximum rate between 50 and 70 percent relative humidity. In addition to atmospheric conditions, carbonation rate is also influenced by the permeability of the concrete and the cement content of the concrete. Cement content of approximately 15% produces a concrete relatively resistant to carbonation. An increase over this level produces marginal increases, while below this, results in a precipitous drop in resistance. Generally, it is found that good compaction and curing cause larger improvements in concrete permeability and resistance to carbonation than minor alterations in mix design.

Several workers[106]–[109] have concluded that carbonation depth is proportional to the square root of time. The proportionality constant is a coefficient related to the permeability of the concrete. Factors such as cement content in concrete, CO_2 concentration in the atmosphere, and the relative humidity, in addition to normal factors such as concrete density, affect the value of this coefficient. If the depth of carbonation is measured in mm and the time in years, the average coefficient for precast, prestressed quality concrete is < 1; for high strength concrete used in bridges, an average value of 1 is found, while normal in situ reinforced concrete an average value of 4–5 has been recorded. If the value of 1 is used and reinforced concrete is designed with a cover of 25 mm, predicted time for the carbonated layer to reach the steel would be 625 years. Some doubt may exist with regard to this prediction since some authors[109] have stated that the actual relationship between depth of carbonation and time may be between linear and square root of the time, making the above prediction optimistic. In addition, higher levels of carbonation can lead to densification and blocking of pores, which is beneficial, but carbonation can also lead to carbonation shrinkage and cracking, especially when carbonation occurs at relative humidities between 50 and 75%.

It has been clearly shown[107] that concretes with higher levels of fly ash (≅50%) have increased carbonation, especially when poorly cured. However, the carbonation of concretes containing lower levels of fly ash (15–30%) is generally similar to, or slightly higher than, that of the control concretes. This increased carbonation observed for the 50% fly ash concrete cannot be explained by increased permeability since it has been shown[107] that the permeabilities of these concretes are lower than those of the control. However, the lower permeabilities of these blended cement concretes is due to a discontinuous pore structure. Carbonation and shrinkage cracking may lead to an opening up of the structure, yielding continuous pores and an increase in permeability.

8.6 Delayed/Secondary Ettringite Formation

The potential for concrete deterioration as a consequence of the delayed ettringite formation in the precast industry has recently been recognized. One of the important factors required for this type of reaction is high temperature curing of concrete such as that occurring in the

precast industry.[110] The delayed formation of ettringite is attributed to the transformation of monosulfo-aluminate to ettringite when steam curing is followed by normal curing at later ages. In recent work it was indicated that sulfate may be bound by the C-S-H gel that is released at later ages.[111] Increased temperature is expected to accelerate the absorption of sulfate by the silicate hydrate. It has also been confirmed that the ettringite crystals are usually present in cracks, voids, and transition zone at the aggregate-binder interface, causing expansion and cracking. It has also been observed that ASTM Type III cement is more vulnerable to deterioration due to the delayed ettringite formation than Type I or Type V cement. Thermal drying after high temperature curing intensifies the deterioration. In the secondary ettringite formation, calcium sulfate formed from the decomposition of AFt or AFm phase as a consequence of severe drying, dissolves upon rewetting and migrates into cracks to react with the local Al-bearing materials to cause expansion.[112]

REFERENCES

1. Bresler, B., *Reinforced Concrete Engineering*, Wiley-Interscience, New York (1974)
2. Pressler, E. E., Brunauer, S., Kantro, D. L., and Weise, C. H., Determination of the Free Calcium Hydroxide Contents of Hydrated Portland Cements and Calcium Silicates, *Anal. Chem.*, 33:877–882 (1961)
3. Lehmann, H., Locher, F. W., and Prussog, D., Quantitative Bestimmung des Calcium Hydroxide in Hydratisierten Zementen, *Ton-Ztg.*, 94:230–235 (1970)
4. Ramachandran, V. S., Differential Thermal Method of Estimating Calcium Hydroxide in Calcium Silicate and Cement Pastes, *Cem. Concr. Res.*, 9:677–684 (1979)
5. Midgley, H. G., The Determination of Calcium Hydroxide in Set Portland Cements, *Cem. Concr. Res.*, 9:77–83 (1979)
6. Taylor, H. F. W., Portland Cement: Hydration Products, *J. Edn. Mod. Materials, Sci. & Eng.*, 3:429–449 (1981)
7. Feldman, R. F., and Ramachandran, V. S., Differentiation of Interlayer and absorbed Water in Hydrated Portland Cement of Thermal Analysis, *Cem. Concr. Res.*, 1:607–620 (1971)

4/10980

APPROVED for Release for
Unlimited (Release to Public)
6/23/2005

WSRC-RP-92-1360

RADIOLOGICAL PERFORMANCE ASSESSMENT FOR THE Z-AREA SALTSTONE DISPOSAL FACILITY (U)

JRC 2/4/93

Prepared for the
WESTINGHOUSE SAVANNAH RIVER COMPANY
Aiken, South Carolina

by

MARTIN MARIETTA ENERGY SYSTEMS, INC.
EG&G IDAHO, INC.
WESTINGHOUSE HANFORD COMPANY
WESTINGHOUSE SAVANNAH RIVER COMPANY

December 18, 1992

Rev. 0

A set of parametric simulations were performed to assess the effective permeability as a function of crack width and fraction for the degraded vault and saltstone (Sect. 4.2.1.2). The crack fraction is the total portion of the vault and saltstone which consists of open crack space. At a constant crack fraction there can be many closely-spaced small cracks or fewer widely-spaced large cracks. Maximum flow rates occur at intermediate crack sizes. Note that if the cracks become filled with porous material, the permeability will be much lower than open cracks.

3.1.3.5 Summary of Degradation Scenarios

The discussions above address mechanisms of degradation that may alter the integrity of the cover system, and the permeability of the saltstone monoliths and vaults, but the timing and extent of degradation are not readily predictable due to enormous uncertainties in conditions over thousands of years. In this RPA, cracking of the vaults was chosen to represent the increased permeability of the waste and vaults. Cracking is a complex function of all the processes described above and requires detailed modeling of thermal-mechanical stresses, which is beyond the scope of this analysis. For simplicity, vault cracking was idealized as follows:

- cracks that fully penetrate the vault and saltstone develop at closure,
- the cracks are vertical,
- the crack spacing is 3 m, and
- average crack aperture is .005 cm.

These assumptions were made based on observations of saltstone vault #1. However, they are believed to be conservative largely because: 1) the presence of fully-penetrating cracks has not been established, and 2) the new design incorporates measures to minimize cracking.

The importance of the cover system to the performance of the SDF was also investigated. For this RPA, cover degradation was addressed by considering two scenarios: 1) an intact upper moisture barrier cover over the entire time period of computation; and 2) a completely degraded upper moisture barrier cover over this same time period. These two scenarios were assumed for both the intact vault computations, and the degraded vault computations. The degraded cover was assumed to be of the same permeability as the surrounding soil, and thus the entire 40 cm/year of infiltration was assumed to pass through this zone. The actual case will likely be bounded by these two cases. Initially, (soon after loss of institutional control), the cover will be non-degraded. Erosion is conservatively estimated to remove surface soil at a rate of about 1 mm per year (Sect. 2.8) for predominately crop land. Thus, after about 800 years, the gravel layer would be exposed, assuming the bamboo is removed and the land is used for growing crops. With the upper gravel layer exposed, the underlying clay could possibly become unsaturated, in which case the hydraulic conductivity would increase due to cracking. Under these conditions, the moisture flux would probably be greater than 2 cm/year, but less than 40 cm/year.

In summary, four facility degradation scenarios were addressed in this analysis and are listed below.

1) The intact scenario, where all systems (i.e., cover, vaults, and saltstone) were assumed nondegraded.
2) The degraded cover scenario, where all systems except the upper moisture barrier were assumed to remain intact.
3) The degraded vault/saltstone scenario, where all systems except the vaults and saltstone were assumed to remain intact.
4) The degraded vault/saltstone and cover scenario, where all systems except the clay and gravel drain in contact with the vaults were assumed to be degraded.

These scenarios were shown schematically in Fig. 3.1-2.

3.1.4 Non-Radioactive Constituents

The non-radioactive constituents of the feed have been described in a previous section (Sect. 2.3.1.2). As stated previously, excluding water, the most abundant chemical components in the feed solution are $NaNO_3$, $NaNO_2$, and NaOH. Lesser amounts of Na_2CO_3, $NaAl(OH)_4$, Na_2SO_4, and trace-level compounds (silver, mercury, chromium) are also expected to be in the solution.

In considering the elements and compounds that comprise the chemical component of the saltstone feed solution, sodium stands out as the most ubiquitous. However, its presence would not adversely affect the quality of the water other than adding to its overall salinity (TDS). Sulfate is another compound of minimal concern because it merely adds to the TDS of the water. The most significant inorganic constituents, in terms of impact on water quality, in the list are nitrate and nitrite. Nitrate levels above 45 mg/L (or 10 mg/L as N) are unacceptable, according to U.S.EPA DWS (40 CFR 141), which the State of South Carolina presently plans to use to evaluate groundwater protection compliance at disposal sites. A separate standard for nitrite does not exist, and the nitrate and nitrite concentrations (as nitrogen) were assumed to be additive, with respect to evaluation of compliance.

Leaching studies have been conducted that immerse a saltstone block in water to determine the rate at which various contaminants are released. These tests have been used as a means of measuring the ability of the saltstone to bind these contaminants. Leach tests have been conducted by Brookhaven National Laboratory on 107 L blocks of cured saltstone prepared from decontaminated salt solution from Tank 50H. The ANS 16.1 leach procedure was used on the block to determine the leachability of contaminants. Nitrate, nitrite and sulfate leach rates for these large blocks agreed well with leaching tests on smaller samples. Chromium concentrations were low and only observed in a few of the leachates collected from the reference block. No chromium was found in the leachate from mixes containing slag (Oblath 1986a).

Numerical simulation requires, for practical reasons, averaging of spatial properties. Thus, the conceptual model used to provide a framework for the numerical simulation of the near-field movement of water and contaminants from the SDF relies heavily on such averaging. The subsurface is treated as if it consists of five material types: 1) the backfill or native soil; 2) clay; 3) gravel; 4) concrete; and 5) the saltstone waste form. Each of these materials are treated as if they are homogeneous and isotropic.

Hydraulic properties for each material type are assumed to be adequately described by the following hydraulic parameters: saturated hydraulic conductivity, effective porosity, and moisture characteristic curve. The moisture characteristic curve describes the nonlinear relationship between the matrix potential or pressure head, the moisture content, and the hydraulic conductivity. Details and references for the data and expressions used to quantify the hydraulic properties for each material type in the near-field model are provided in Appendix A.1.2. A summary of hydraulic properties assumed is provided in Table 3.3-1.

In addition to hydraulic properties, assumptions to allow quantification of mass transport are necessary in the near-field model. Specifically, contaminant-specific sorption coefficients, diffusion coefficients, and radioactive decay constants are required. Dispersivities, which determine the spreading of a simulated contaminant plume, are also needed. Tables of these values for contaminants of significance, and references to their source are provided in Appendix A.1.2.1. Solubility considerations are not explicitly addressed in the near-field model, except through the use of media-specific sorption coefficients which do not distinguish surface sorption from precipitation or other processes causing immobilization.

3.3.1.2 Degraded Vault and Saltstone

Two scenarios were addressed for vaults and monoliths assumed to be degraded (i.e., cracks present, Sect. 3.1.3.5): 1) a degraded vault with an intact upper moisture barrier (Sect. 2.4); and 2) a degraded vault with a completely degraded upper moisture barrier, in which the permeability of the degraded cover is that of the backfill soil and the clay layer on top of the vault roof. The only parameter required from Table 3.3-1 for the degraded case is the hydraulic conductivity of the clay on the roof of the vault.

A simplified conceptual model is used to represent the degraded condition of the saltstone and surrounding concrete vault. Two factors contributed to this decision: 1) numerical difficulties associated with modeling fractures in a groundwater computer code and 2) large uncertainty associated with inputs such as the timing, frequency, and size of fractures in the saltstone. Sensitivity analyses are then used to consider a range of possible input values and provide an indication of the impact that changes in the inputs have on the results. Such analyses also provide a set of results that form an envelope around the possible results. Results of sensitivity analyses are discussed in this section and Sect. 4.2.1.

The conceptual model of a degraded vault and saltstone waste form assumes, as discussed in Sect. 3.1.3.5, that: 1) all monoliths and vaults in the facility are fractured, 2) fractures occur every 3 m, 3) all fractures open simultaneously, 4) the fractures are assumed to open at closure of the facility, when remediation of cracks will no longer be routine, 5) transport is assumed to be diffusive (constant diffusion coefficient) out of the intact saltstone matrix and into the fracture where transport is assumed to be dominated by advection (i.e., the fracture case results are independent of the hydraulic conductivity of the saltstone), 6) the clay is assumed to sit immediately on top of the saltstone, and 7) the base of the saltstone is assumed to be adjacent to the backfill soil beneath the vault. Since the majority of the degradation occurs to the vault as opposed to the saltstone, for the vault is conservatively neglected as a barrier to transport. Thus, this case addresses flow and transport through the fractured saltstone. The fractures are assumed to be 0.005 cm in aperture; filling or plugging by soils or precipitates is not considered. Diffusion is assumed to be the only mechanism of transport of radionuclides and nitrate from the saltstone matrix to the fractures, and advection is assumed to be the only means of transporting these potential contaminants from the fractures to the soil beneath the vaults.

This simplified model is considered to be a bounding case on release from fractured vaults because fracturing of the vaults is expected to increase the effective permeability of the vaults, and thus increase radionuclide and nitrate release. The release rate would increase as the number of fractures increases. However, release rates for soluble species would likely decrease with time, as the resident pore water is flushed from the fracture, and diffusion from the saltstone matrix would then control the concentration in the fracture. Therefore, assuming simultaneous opening of all fractures is believed to represent an upper bound on release rates. Remediation of fractures that occur before closure involves filling with epoxy upon discovery. Degradation of the epoxy is likely to be a gradual process rather than immediate. Furthermore, shrinkage cracks in pours may be filled to some extent by subsequent pours. This would also reduce the flow rate through fractures.

Details of the various submodels that were used to adapt a model for flow and transport in fractures, to which semi-analytical solution techniques could be applied, are provided in Appendix A.1.3. Some of the critical assumptions, however, are noted here since they are fundamental to the conceptual approach and the resulting analytical model. One of the primary underlying assumptions is that the fractures remain saturated once they open. Another critical input necessary to evaluate the flow of water through a fracture is the height of water perched on fractured vaults. The intact vault model (Appendix A.1.2.1) was used to predict the depth of the perched water on the vault. Perched water is shown to occur on an intact vault, and the assumption of saturated flow is assumed to be reasonable. These assumptions are discussed in more detail in Appendix A.1.3.

For the fractured saltstone, effective flow rates and subsequent transport were estimated based on the methods described in Appendix A.1.3.

A.1.3 Flow and Mass Transport Through Fractured Vaults

A suite of semi-analytical and analytical models were used to model flow and transport through the degraded vault and waste form. The degradation scenario is defined in Sect. 3.1.3.5. The conceptual models and assumptions for flow and transport for the degraded scenario were briefly discussed in Sect. 3.3.1.2 and 3.4.1.2. This section includes a description of the submodels comprising the conceptualization of the degradation scenario, the two solutions used to analyze these submodels, and discussions of the assumptions and limitations inherent in these models.

As is the case with most analytical models, simplified representations of the system are necessary to fit within the limitations (boundary conditions, etc.) of the mathematical models. These simplified representations are intended to err on the side of conservatism in several areas. This conservatism yields models that overpredict flow and transport rates, providing bounding estimates of release out of the disposal facility. Given the number of uncertainties simply involved in defining the degraded condition of the vault (degradation rates; size, frequency, and alignment of fractures; etc.), this approach is deemed appropriate. The intent is to provide a bounding estimate of performance to provide reasonable assurance that fractures in the saltstone will not cause the releases to exceed acceptable levels.

One positive aspect of the analytical or semi-analytical model is the ease of use when compared to a detailed numerical model. This ease of use enables numerous runs to be made in less than the time it would take to make a single run with a large numerical model. Sensitivity analyses can easily be conducted that test combinations of inputs to identify critical parameters and ranges of critical values. The ability to make numerous runs also allows a wide range of conditions and assumptions to be tested that may not be possible when using a numerical code. In this regard, the "tunnel vision" that sometimes occurs when a limited number of runs are made with a numerical model can be minimized. Sensitivity analyses are discussed in Sect. 4.2.

Two semi-analytical models used to address fracture flow and transport are discussed in the following sections. The first section discusses the model used to estimate the effective flow rate through the fractured saltstone as a function of the height of perched water above the vault, hydraulic conductivity of the clay in the clay/gravel drainage layer above the vault, and fracture characteristics. The second section discusses the model used to estimate the release rate from the vault given the fracture flow rate estimated in the previous solution and initial inventory, distribution coefficients, and diffusion coefficients in the intact saltstone matrix.

Flow and transport through fractures in the saltstone is modeled as if the vault does not exist around the saltstone. Degradation calculations have shown that the majority of changes due to chemical attack and rebar corrosion will be to the vault surrounding the saltstone. Thus, for conservatism, it is assumed that the clay in the clay/gravel drainage layer is placed on top of the saltstone and the base of the saltstone is in direct

contact with the backfill with no credit for any attenuation that may occur as water passes through the vault. The simulations only address flow and transport through fractures in the saltstone.

The first step in the process outlined in Sect. 3.4.1.2 (Demonstrate presence of perched water on vault roof) was accomplished in the intact vault near-field calculations (Appendix A.1.2). The numerical simulations for the intact vault predicted 61 cm of perched water on the roof for infiltration rates of 2 and 40 cm/year. This value is a necessary input for the following flow and transport simulations.

A.1.3.1 Determination of Flow Rate Through Fractures in Saltstone

One approach to determining the permeability of cracked concrete is to use an analogy of parallel plates to provide an estimate. However, for the case of underground vaults, permeability of the soil surrounding the vault can also have an impact on flow rate of the vault. This is due to the relatively large permeability of a fracture relative to the soil. Furthermore, entrance and exit head losses can also affect flow through the fractures when perched water is present above the vault. Thus, effective flow rate through fractured saltstone reflects the physical properties of the soil and characteristics of the cracks in the saltstone, while being independent of the hydraulic conductivity of the intact saltstone matrix. The approach adopted for this assessment accounts for the effects of the material around the vault and entrance and exit head losses. A brief summary of the approach is provided below with further details regarding the approach in Walton and Seitz (1991, pp. 5-4 to 5-6).

For the case of steady-state saturated flow through a crack, a simplified case of an analytical model by Yates (1988) can be applied. Figure A.1-12 is a comparison of the modeled system with the more realistic condition of the degraded vault. The backfill refers to the clay layer above the vault in this figure. The basic assumptions governing the simplified representation are: 1) steady-state saturated flow; 2) constant head at the top of the perched water and at the entrance to the crack; 3) head losses through the crack and at the crack exit are small compared to head losses at the entrance (if the additional losses are considered, the flow rate would be slightly less); 4) symmetry boundaries apply at the center of the crack and half the distance between cracks; and 5) the cracks in different pours are open and directly aligned.

Inputs required for the modified analytical model are: 1) the distance between the cracks; 2) the crack half-width (one-half of the aperture); and 3) the depth of perched water (distance to constant head boundary). The solution provides a dimensionless flow rate; that is, the ratio of the flow through the crack to the flow through the backfill. An estimate of the maximum flow rate (i.e, saturated flow rate) can be approximated by multiplying the result from the semianalytic model by the saturated hydraulic conductivity of the clay in the clay/gravel drainage layer (see Sect. A.1.2) above the vault (assuming a unit gradient through the backfill).

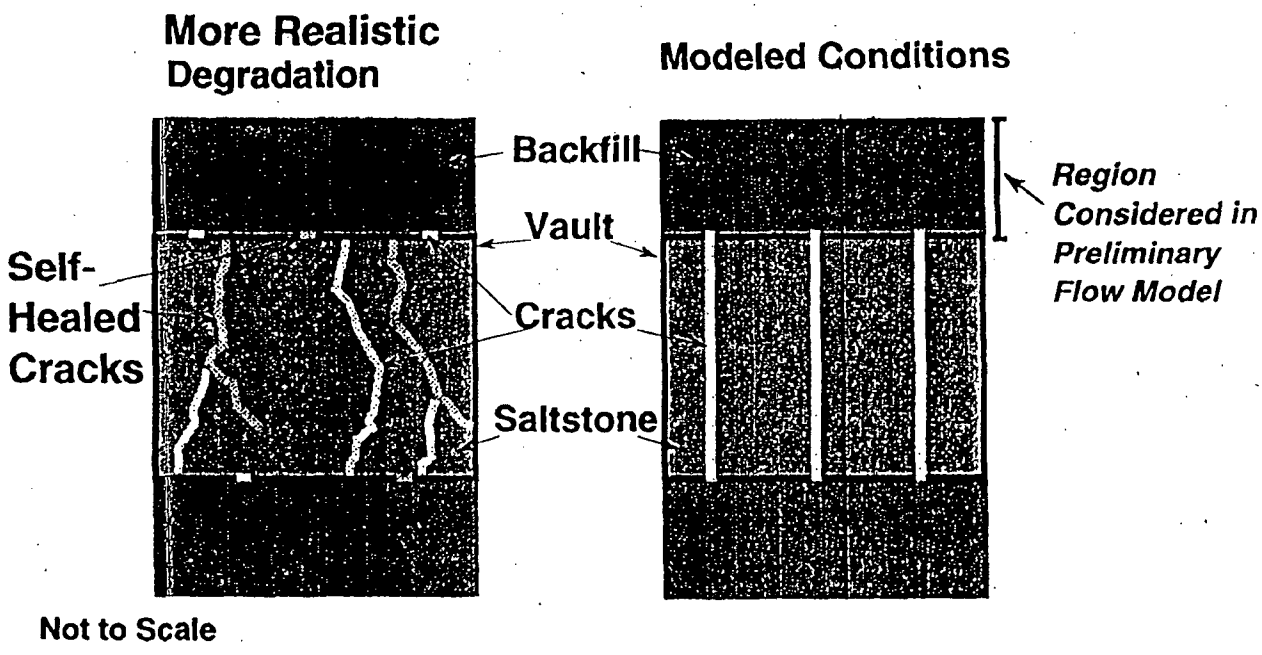

Fig. A.1-12. Comparison of more realistic system and modeled representation of flow rate through backfill (clay in this case) and fractured vault.

After normalizing variables and applying the appropriate simplifications (i.e., homogeneous soil, equally-spaced fractures) to Yate's solution, the dimensionless flow rate, ζ_3, is calculated using

$$\zeta_3 = \frac{-z_o}{x_o\left[\left(\sum_{n=1}^{\infty} V_n\right) - z_o\right]}$$

where

$$z_o = \frac{Z_o}{\Psi},$$

$$x_o = \frac{X_o}{\Psi},$$

$$V_n = \frac{\lambda_j (2p_{1j} + 2p_{1j}^2 p_{2j})}{\cosh[\tau_j]\,\beta j},$$

Ψ = the half-width of the crack,
z_o = the depth of perched water, and
x_o = half the distance between the fracture center lines.

The coefficients for V_n are defined as follows:

$$\lambda_j = \frac{2}{Z_o \tau_j^2}$$

$$p_{1j} = \tanh[\tau_j (x_o - 1)]$$

$$p_{2j} = \tanh[\tau_j]$$

$$j = 2n - 1$$

$$\tau_j = \frac{\pi j}{2 z_o}$$

$$\beta_j = 2p_{1j}(1 + p_{2j}^2) + 2p_{2j}(1 + p_{1j}^2).$$

Flow through fractured concrete vaults and saltstone was predicted based on the parameter values listed in Table A.1-4. The predicted velocity in each fracture (assuming all flow occurs through the fracture) based on the values in Table A.1-4 was 780 cm/year (darcy velocity divided by the ratio of crack width to crack spacing). Contributions from the intact matrix are considered separately in Appendix A.1.2. This value is subsequently used as an input to the transport simulations. Test cases comparing flow results from the analytical solution with results from the PORFLO-2D (Kline et al. 1983) finite difference code have demonstrated excellent agreement (Walton and Seitz 1991).

Table A.1-4. Input values assumed for flow calculations

Parameter	Assumed Value
Crack width	0.005 cm[a]
Crack spacing	300 cm[a]
Depth of perched Water on roof	61 cm[b]
Saturated hydraulic Conductivity of clay	0.24 cm/year[b]

[a] Sect. 3.1.3.5
[b] Appendix A.1.2

Note that the assumption of saturated flow is conservative for predicting contaminant flux because flow rates through the fracture would be largest when it is saturated. The predicted build-up of perched water on intact vaults, based on PORFLOW-3D simulations, suggests saturated flow is likely to occur. However, neglecting the vault around the saltstone and the assumption of aligned fractures in the different layers of saltstone is likely to result in inflated flow rates. Reduced flow would be expected in the case where fractures are not aligned. Flow rates will also be reduced if cracks in lower pours of saltstone are filled by a subsequent pour. Although flow rates are the greatest source of uncertainty in these degraded vault calculations, it is assumed that neglecting the vault and considering open, aligned fractures in the saltstone represents an upper bound of the flow rate through fractures.

A.1.3.3 Determination of Release Rate from Vault

A number of semi-analytical models have been developed for transport through fractured porous media. Of available methods, the solution of Rasmuson and Neretnieks (1981) is perhaps most appropriate for application to release rates from massive concrete waste forms. This solution allows a decaying source term, which is required for leaching, and the solution is given in terms of dimensionless parameters, which can be used to interpret and generalize the results from the analysis. Note that their published model estimates transport from a decaying source of radionuclides into a fractured porous medium and is the complement of the desired solution for release from a fractured concrete monolith, where contaminants are leached from (rather than into) a fractured porous medium.

The saltstone is envisioned as a large fractured monolith, with blocks of intact concrete separated by fractures. Advection dominates mass transport in the fractures, while diffusion controls mass transport laterally from the porous matrix to the fractures. Figure A.1-13 illustrates this conceptual model in a schematic form. Partitioning of compounds between solid and liquid phases is also considered. The velocity through the saltstone fractures is determined using the methods described in Sect. A.1.3.2. Since the crack is significantly more permeable than the adjacent saltstone matrix, all flow is assumed to occur through the fractures. Thus, this solution is also independent of the hydraulic conductivity of the intact saltstone matrix. Contributions from the intact saltstone are considered in the intact modeling (Appendix A.1.2).

This assessment is limited to the case of no dispersion in the fractures in the concrete. This is a conservative case (in terms of concentration) for radionuclide release rates from concrete waste forms. In reality, fractures are likely to be in the form of a tortuous network, with a significant, but unknown, amount of dispersion resulting. Thus, conservative assumptions are made to account for the uncertainty in accurately representing a fractured vault.

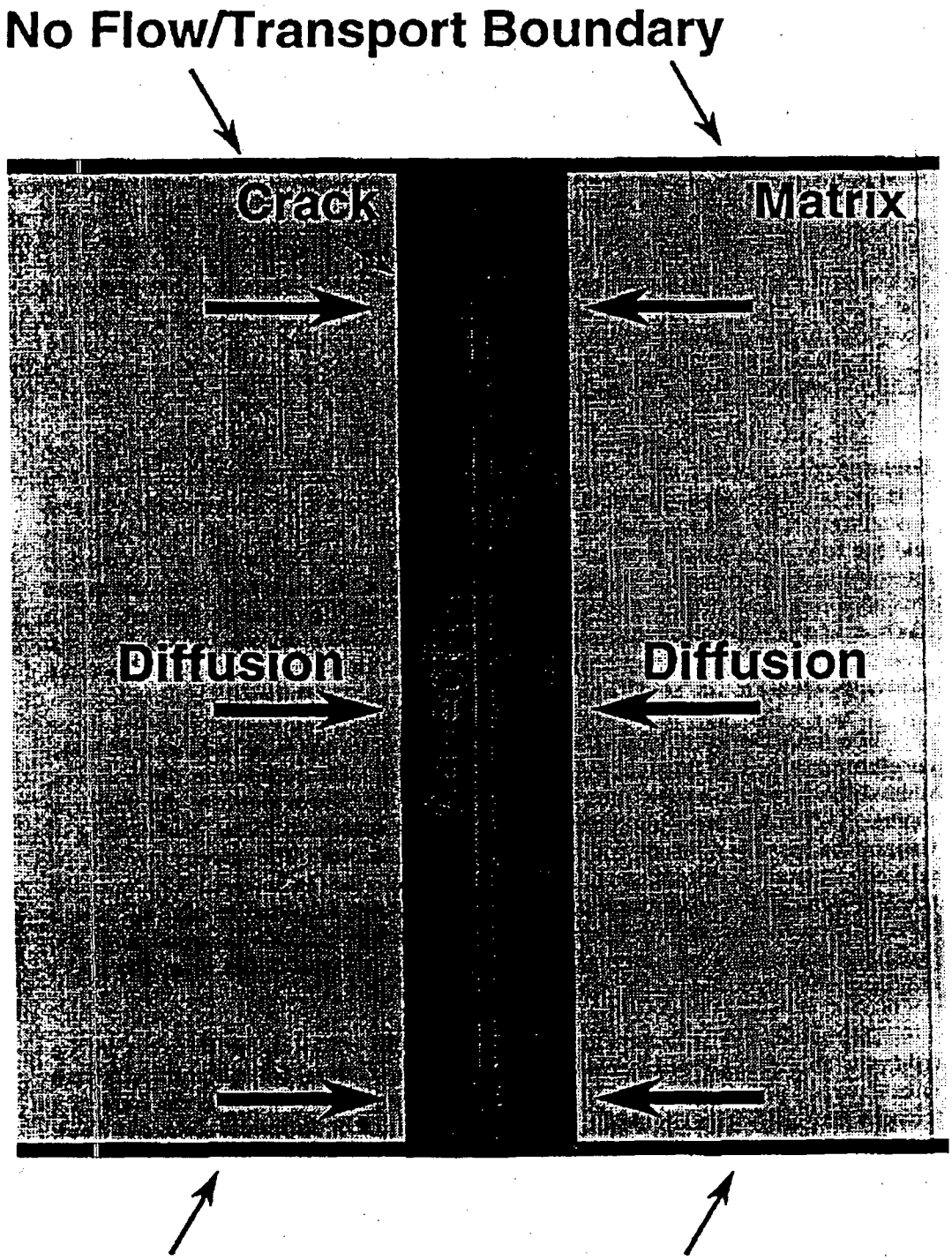

Fig. A.1-13. Schematic of conceptual model of release from fractured vault.

The analytical solution used for this assessment is, with slight modification, (i.e., by ignoring dispersion) from Rasmuson and Neretnieks (1981).

$$H_1(\lambda) = \lambda\left(\frac{(sinh2\lambda + sin2\lambda)}{cosh2\lambda - cos2\lambda}\right) - 1$$

$$H_2(\lambda) = \lambda\left(\frac{sinh2\lambda + sin2\lambda)}{cosh2\lambda - cos2\lambda}\right)$$

If $\zeta > 0$ then,

$$\frac{\alpha C_f}{C_{t_o}} = (1 - Y)\,[\exp(-\beta)]$$

$$Y = \frac{1}{2} + \frac{2}{\pi}\int_0^{\infty} \exp(-\delta H_1)\sin(\zeta\lambda^2 - \delta H_2)\,\frac{d\lambda}{\lambda}$$

If $\zeta < 0$ then,

$$\frac{aC_f}{C_{t_o}} = \exp(-\beta)$$

where the solution depends upon these dimensionless variables that follow:

$\zeta = (2D_a\theta)/r_o^2$ = dimensionless contact time,
$\alpha C_f/C_{to}$ = dimensionless concentration,
$\beta = \lambda_d t$ = dimensionless radioactive decay, and
$\delta = (\gamma z)/(mU_f)$ = bed length parameter.

The above variables are derived in turn from these variables

θ = t-z/U_p,
C_f = concentration in fractures,
α = volumetric distribution coefficient (moisture content * retardation factor),
λ_d = decay rate = ln $2/t^{1/2}$,
r_o = effective radius of spherical blocks (= 0.5 S for cubic blocks and 1.5 S for slabs),
S = fracture spacing,
U_f = velocity in fractures,
D_a = apparent diffusion coefficient,
z = thickness of vault,

z_o = total distance along fracture from top or upgradient portion of vault,
ϕ_f = fracture porosity,
ϕ_m = matrix porosity,
$m = \phi_f/(1-\phi_f)$,
$\gamma = (3D_a\alpha)/r_o^2$, and
t = time.

Values for the independent variables are listed in Table A.1-5. The velocity in the fracture, U_p was predicted using the approach discussed in Appendix A.1.3.2. The crack spacing, S, is discussed in Sect. 3.1.3.5. The apparent diffusion coefficient, D_a, is simply the effective diffusion coefficient from Sect. 2.4 (5×10^{-9} cm^2/s) divided by the radionuclide-specific retardation coefficient for saltstone. The porosity values for the fracture and saltstone, ϕ_f and ϕ_m, assume an open crack and the porosity of saltstone specified in Sect. 2.4.

The analytical solution was derived for the case of a semi-infinite medium, whereas, the application of concern is for a concrete vault of finite dimensions. If dispersion is ignored, this is not a limitation. Ignoring dispersion is required because of the lack of information concerning dispersion in cracks. Because dispersion in cracks is likely due to variation in aperture, sensitivity analyses addressing changes in crack width can be used to help account for this phenomenon (Sect. 4.2).

The fracture flow solution provides concentrations as a function of time in the fracture. These concentrations, in conjunction with the Darcy velocities predicted, are then used to calculate flux from the fractures of a degraded vault. The total flux of a degraded vault must also consider the flux from the intact portions between fractures. This was accomplished by adding the releases predicted from the intact modeling (Appendix A.1.2) to the releases predicted from this analysis.

A.2 GROUNDWATER FLOW AND MASS TRANSPORT MODEL AND SIMULATIONS

This section of Appendix A provides details of the conceptual model adopted for simulating flow and mass transport through the saturated hydrologic zones beneath the Z-Area SDF (Sect. A.2.1), and details related to simulation of the model using the PORFLOW-3D computer code (Sect. A.2.2).

A.2.1 Conceptual Saturated Flow and Transport Model

Based on the piezometric data at Z-Area (Sect. 2.1.7), it is apparent that the groundwater flow field is highly variable within and among the hydrologic units in the vicinity of Z-Area. A three-dimensional representation of the groundwater flow system was chosen to allow the divergent lateral flow to be simulated (Fig. A.2-1).

NUREG/CR-5542
EGG-2597
RW, CC

Models for Estimation of Service Life of Concrete Barriers in Low-Level Radioactive Waste Disposal

Manuscript Completed: July 1990
Date Published: September 1990

Prepared by
J. C. Walton, L. E. Plansky, R. W. Smith

Idaho National Engineering Laboratory
Managed by the U.S. Department of Energy

EG&G Idaho, Inc.
P.O. Box 1625
Idaho Falls, ID 83415

Prepared for
Division of Engineering
Office of Nuclear Regulatory Research
U.S. Nuclear Regulatory Commission
Washington, DC 20555
NRC FIN A6858

Abstract

Concrete barriers will be used as intimate parts of systems for isolation of low-level radioactive wastes subsequent to disposal. This work reviews mathematical models for estimating the degradation rate of concrete in typical service environments. The models considered cover sulfate attack, reinforcement corrosion, calcium hydroxide leaching, carbonation, freeze/thaw, and cracking. Additionally, fluid flow, mass transport, and geochemical properties of concrete are briefly reviewed. Example calculations included illustrate the types of predictions expected of the models.

FIN No. A6858 - Performance of Concrete Barriers in Low-Level Waste Disposal

RESPONSE TO RAI COMMENT 40
ROADMAP TO REFERENCES

REFERENCED DOCUMENT	*EXCERPT LOCATION	REMARK
Dicke 1992	Entire document enclosed following response	
MMES 1992 (Saltstone PA 1992)	Excerpts enclosed following response.	Sections 3.2.3.5, 3.3.1.2, A.1.3 and Appendix B.3.

*Excerpt Locations:

1. Excerpt included in response: The excerpt is included within the text of the response or is appended to the response.
2. Excerpt enclosed following response: The excerpt is enclosed on a separate sheet or sheets following the response.
3. Representative excerpt(s) enclosed following response: Representative excerpts from a document that is wholly or largely applicable are enclosed following the response.
4. Other

4/10980

APPROVED for Release for
Unlimited (Release to Public)
6/23/2005

WSRC-RP-92-1360 ←

RADIOLOGICAL PERFORMANCE ASSESSMENT FOR THE Z-AREA SALTSTONE DISPOSAL FACILITY (U)

RC 2/4/93

Prepared for the
WESTINGHOUSE SAVANNAH RIVER COMPANY
Aiken, South Carolina

by

MARTIN MARIETTA ENERGY SYSTEMS, INC.
EG&G IDAHO, INC.
WESTINGHOUSE HANFORD COMPANY
WESTINGHOUSE SAVANNAH RIVER COMPANY

December 18, 1992

Rev. 0

A set of parametric simulations were performed to assess the effective permeability as a function of crack width and fraction for the degraded vault and saltstone (Sect. 4.2.1.2). The crack fraction is the total portion of the vault and saltstone which consists of open crack space. At a constant crack fraction there can be many closely-spaced small cracks or fewer widely-spaced large cracks. Maximum flow rates occur at intermediate crack sizes. Note that if the cracks become filled with porous material, the permeability will be much lower than open cracks.

3.1.3.5 Summary of Degradation Scenarios

The discussions above address mechanisms of degradation that may alter the integrity of the cover system, and the permeability of the saltstone monoliths and vaults, but the timing and extent of degradation are not readily predictable due to enormous uncertainties in conditions over thousands of years. In this RPA, cracking of the vaults was chosen to represent the increased permeability of the waste and vaults. Cracking is a complex function of all the processes described above and requires detailed modeling of thermal-mechanical stresses, which is beyond the scope of this analysis. For simplicity, vault cracking was idealized as follows:

- cracks that fully penetrate the vault and saltstone develop at closure,
- the cracks are vertical,
- the crack spacing is 3 m, and
- average crack aperture is .005 cm.

These assumptions were made based on observations of saltstone vault #1. However, they are believed to be conservative largely because: 1) the presence of fully-penetrating cracks has not been established, and 2) the new design incorporates measures to minimize cracking.

The importance of the cover system to the performance of the SDF was also investigated. For this RPA, cover degradation was addressed by considering two scenarios: 1) an intact upper moisture barrier cover over the entire time period of computation; and 2) a completely degraded upper moisture barrier cover over this same time period. These two scenarios were assumed for both the intact vault computations, and the degraded vault computations. The degraded cover was assumed to be of the same permeability as the surrounding soil, and thus the entire 40 cm/year of infiltration was assumed to pass through this zone. The actual case will likely be bounded by these two cases. Initially, (soon after loss of institutional control), the cover will be non-degraded. Erosion is conservatively estimated to remove surface soil at a rate of about 1 mm per year (Sect. 2.8) for predominately crop land. Thus, after about 800 years, the gravel layer would be exposed, assuming the bamboo is removed and the land is used for growing crops. With the upper gravel layer exposed, the underlying clay could possibly become unsaturated, in which case the hydraulic conductivity would increase due to cracking. Under these conditions, the moisture flux would probably be greater than 2 cm/year, but less than 40 cm/year.

In summary, four facility degradation scenarios were addressed in this analysis and are listed below.

1) The intact scenario, where all systems (i.e., cover, vaults, and saltstone) were assumed nondegraded.
2) The degraded cover scenario, where all systems except the upper moisture barrier were assumed to remain intact.
3) The degraded vault/saltstone scenario, where all systems except the vaults and saltstone were assumed to remain intact.
4) The degraded vault/saltstone and cover scenario, where all systems except the clay and gravel drain in contact with the vaults were assumed to be degraded.

These scenarios were shown schematically in Fig. 3.1-2.

3.1.4 Non-Radioactive Constituents

The non-radioactive constituents of the feed have been described in a previous section (Sect. 2.3.1.2). As stated previously, excluding water, the most abundant chemical components in the feed solution are $NaNO_3$, $NaNO_2$, and NaOH. Lesser amounts of Na_2CO_3, $NaAl(OH)_4$, Na_2SO_4, and trace-level compounds (silver, mercury, chromium) are also expected to be in the solution.

In considering the elements and compounds that comprise the chemical component of the saltstone feed solution, sodium stands out as the most ubiquitous. However, its presence would not adversely affect the quality of the water other than adding to its overall salinity (TDS). Sulfate is another compound of minimal concern because it merely adds to the TDS of the water. The most significant inorganic constituents, in terms of impact on water quality, in the list are nitrate and nitrite. Nitrate levels above 45 mg/L (or 10 mg/L as N) are unacceptable, according to U.S.EPA DWS (40 CFR 141), which the State of South Carolina presently plans to use to evaluate groundwater protection compliance at disposal sites. A separate standard for nitrite does not exist, and the nitrate and nitrite concentrations (as nitrogen) were assumed to be additive, with respect to evaluation of compliance.

Leaching studies have been conducted that immerse a saltstone block in water to determine the rate at which various contaminants are released. These tests have been used as a means of measuring the ability of the saltstone to bind these contaminants. Leach tests have been conducted by Brookhaven National Laboratory on 107 L blocks of cured saltstone prepared from decontaminated salt solution from Tank 50H. The ANS 16.1 leach procedure was used on the block to determine the leachability of contaminants. Nitrate, nitrite and sulfate leach rates for these large blocks agreed well with leaching tests on smaller samples. Chromium concentrations were low and only observed in a few of the leachates collected from the reference block. No chromium was found in the leachate from mixes containing slag (Oblath 1986a).

Numerical simulation requires, for practical reasons, averaging of spatial properties. Thus, the conceptual model used to provide a framework for the numerical simulation of the near-field movement of water and contaminants from the SDF relies heavily on such averaging. The subsurface is treated as if it consists of five material types: 1) the backfill or native soil; 2) clay; 3) gravel; 4) concrete; and 5) the saltstone waste form. Each of these materials are treated as if they are homogeneous and isotropic.

Hydraulic properties for each material type are assumed to be adequately described by the following hydraulic parameters: saturated hydraulic conductivity, effective porosity, and moisture characteristic curve. The moisture characteristic curve describes the nonlinear relationship between the matrix potential or pressure head, the moisture content, and the hydraulic conductivity. Details and references for the data and expressions used to quantify the hydraulic properties for each material type in the near-field model are provided in Appendix A.1.2. A summary of hydraulic properties assumed is provided in Table 3.3-1.

In addition to hydraulic properties, assumptions to allow quantification of mass transport are necessary in the near-field model. Specifically, contaminant-specific sorption coefficients, diffusion coefficients, and radioactive decay constants are required. Dispersivities, which determine the spreading of a simulated contaminant plume, are also needed. Tables of these values for contaminants of significance, and references to their source are provided in Appendix A.1.2.1. Solubility considerations are not explicitly addressed in the near-field model, except through the use of media-specific sorption coefficients which do not distinguish surface sorption from precipitation or other processes causing immobilization.

3.3.1.2 Degraded Vault and Saltstone

Two scenarios were addressed for vaults and monoliths assumed to be degraded (i.e., cracks present, Sect. 3.1.3.5): 1) a degraded vault with an intact upper moisture barrier (Sect. 2.4); and 2) a degraded vault with a completely degraded upper moisture barrier, in which the permeability of the degraded cover is that of the backfill soil and the clay layer on top of the vault roof. The only parameter required from Table 3.3-1 for the degraded case is the hydraulic conductivity of the clay on the roof of the vault.

A simplified conceptual model is used to represent the degraded condition of the saltstone and surrounding concrete vault. Two factors contributed to this decision: 1) numerical difficulties associated with modeling fractures in a groundwater computer code and 2) large uncertainty associated with inputs such as the timing, frequency, and size of fractures in the saltstone. Sensitivity analyses are then used to consider a range of possible input values and provide an indication of the impact that changes in the inputs have on the results. Such analyses also provide a set of results that form an envelope around the possible results. Results of sensitivity analyses are discussed in this section and Sect. 4.2.1.

The conceptual model of a degraded vault and saltstone waste form assumes, as discussed in Sect. 3.1.3.5, that: 1) all monoliths and vaults in the facility are fractured, 2) fractures occur every 3 m, 3) all fractures open simultaneously, 4) the fractures are assumed to open at closure of the facility, when remediation of cracks will no longer be routine, 5) transport is assumed to be diffusive (constant diffusion coefficient) out of the intact saltstone matrix and into the fracture where transport is assumed to be dominated by advection (i.e., the fracture case results are independent of the hydraulic conductivity of the saltstone), 6) the clay is assumed to sit immediately on top of the saltstone, and 7) the base of the saltstone is assumed to be adjacent to the backfill soil beneath the vault. Since the majority of the degradation occurs to the vault as opposed to the saltstone, for the vault is conservatively neglected as a barrier to transport. Thus, this case addresses flow and transport through the fractured saltstone. The fractures are assumed to be 0.005 cm in aperture; filling or plugging by soils or precipitates is not considered. Diffusion is assumed to be the only mechanism of transport of radionuclides and nitrate from the saltstone matrix to the fractures, and advection is assumed to be the only means of transporting these potential contaminants from the fractures to the soil beneath the vaults.

This simplified model is considered to be a bounding case on release from fractured vaults because fracturing of the vaults is expected to increase the effective permeability of the vaults, and thus increase radionuclide and nitrate release. The release rate would increase as the number of fractures increases. However, release rates for soluble species would likely decrease with time, as the resident pore water is flushed from the fracture, and diffusion from the saltstone matrix would then control the concentration in the fracture. Therefore, assuming simultaneous opening of all fractures is believed to represent an upper bound on release rates. Remediation of fractures that occur before closure involves filling with epoxy upon discovery. Degradation of the epoxy is likely to be a gradual process rather than immediate. Furthermore, shrinkage cracks in pours may be filled to some extent by subsequent pours. This would also reduce the flow rate through fractures.

Details of the various submodels that were used to adapt a model for flow and transport in fractures, to which semi-analytical solution techniques could be applied, are provided in Appendix A.1.3. Some of the critical assumptions, however, are noted here since they are fundamental to the conceptual approach and the resulting analytical model. One of the primary underlying assumptions is that the fractures remain saturated once they open. Another critical input necessary to evaluate the flow of water through a fracture is the height of water perched on fractured vaults. The intact vault model (Appendix A.1.2.1) was used to predict the depth of the perched water on the vault. Perched water is shown to occur on an intact vault, and the assumption of saturated flow is assumed to be reasonable. These assumptions are discussed in more detail in Appendix A.1.3.

For the fractured saltstone, effective flow rates and subsequent transport were estimated based on the methods described in Appendix A.1.3.

A.1.3 Flow and Mass Transport Through Fractured Vaults

A suite of semi-analytical and analytical models were used to model flow and transport through the degraded vault and waste form. The degradation scenario is defined in Sect. 3.1.3.5. The conceptual models and assumptions for flow and transport for the degraded scenario were briefly discussed in Sect. 3.3.1.2 and 3.4.1.2. This section includes a description of the submodels comprising the conceptualization of the degradation scenario, the two solutions used to analyze these submodels, and discussions of the assumptions and limitations inherent in these models.

As is the case with most analytical models, simplified representations of the system are necessary to fit within the limitations (boundary conditions, etc.) of the mathematical models. These simplified representations are intended to err on the side of conservatism in several areas. This conservatism yields models that overpredict flow and transport rates, providing bounding estimates of release out of the disposal facility. Given the number of uncertainties simply involved in defining the degraded condition of the vault (degradation rates; size, frequency, and alignment of fractures; etc.), this approach is deemed appropriate. The intent is to provide a bounding estimate of performance to provide reasonable assurance that fractures in the saltstone will not cause the releases to exceed acceptable levels.

One positive aspect of the analytical or semi-analytical model is the ease of use when compared to a detailed numerical model. This ease of use enables numerous runs to be made in less than the time it would take to make a single run with a large numerical model. Sensitivity analyses can easily be conducted that test combinations of inputs to identify critical parameters and ranges of critical values. The ability to make numerous runs also allows a wide range of conditions and assumptions to be tested that may not be possible when using a numerical code. In this regard, the "tunnel vision" that sometimes occurs when a limited number of runs are made with a numerical model can be minimized. Sensitivity analyses are discussed in Sect. 4.2.

Two semi-analytical models used to address fracture flow and transport are discussed in the following sections. The first section discusses the model used to estimate the effective flow rate through the fractured saltstone as a function of the height of perched water above the vault, hydraulic conductivity of the clay in the clay/gravel drainage layer above the vault, and fracture characteristics. The second section discusses the model used to estimate the release rate from the vault given the fracture flow rate estimated in the previous solution and initial inventory, distribution coefficients, and diffusion coefficients in the intact saltstone matrix.

Flow and transport through fractures in the saltstone is modeled as if the vault does not exist around the saltstone. Degradation calculations have shown that the majority of changes due to chemical attack and rebar corrosion will be to the vault surrounding the saltstone. Thus, for conservatism, it is assumed that the clay in the clay/gravel drainage layer is placed on top of the saltstone and the base of the saltstone is in direct

contact with the backfill with no credit for any attenuation that may occur as water passes through the vault. The simulations only address flow and transport through fractures in the saltstone.

The first step in the process outlined in Sect. 3.4.1.2 (Demonstrate presence of perched water on vault roof) was accomplished in the intact vault near-field calculations (Appendix A.1.2). The numerical simulations for the intact vault predicted 61 cm of perched water on the roof for infiltration rates of 2 and 40 cm/year. This value is a necessary input for the following flow and transport simulations.

A.1.3.1 Determination of Flow Rate Through Fractures in Saltstone

One approach to determining the permeability of cracked concrete is to use an analogy of parallel plates to provide an estimate. However, for the case of underground vaults, permeability of the soil surrounding the vault can also have an impact on flow rate of the vault. This is due to the relatively large permeability of a fracture relative to the soil. Furthermore, entrance and exit head losses can also affect flow through the fractures when perched water is present above the vault. Thus, effective flow rate through fractured saltstone reflects the physical properties of the soil and characteristics of the cracks in the saltstone, while being independent of the hydraulic conductivity of the intact saltstone matrix. The approach adopted for this assessment accounts for the effects of the material around the vault and entrance and exit head losses. A brief summary of the approach is provided below with further details regarding the approach in Walton and Seitz (1991, pp. 5-4 to 5-6).

For the case of steady-state saturated flow through a crack, a simplified case of an analytical model by Yates (1988) can be applied. Figure A.1-12 is a comparison of the modeled system with the more realistic condition of the degraded vault. The backfill refers to the clay layer above the vault in this figure. The basic assumptions governing the simplified representation are: 1) steady-state saturated flow; 2) constant head at the top of the perched water and at the entrance to the crack; 3) head losses through the crack and at the crack exit are small compared to head losses at the entrance (if the additional losses are considered, the flow rate would be slightly less); 4) symmetry boundaries apply at the center of the crack and half the distance between cracks; and 5) the cracks in different pours are open and directly aligned.

Inputs required for the modified analytical model are: 1) the distance between the cracks; 2) the crack half-width (one-half of the aperture); and 3) the depth of perched water (distance to constant head boundary). The solution provides a dimensionless flow rate; that is, the ratio of the flow through the crack to the flow through the backfill. An estimate of the maximum flow rate (i.e, saturated flow rate) can be approximated by multiplying the result from the semianalytic model by the saturated hydraulic conductivity of the clay in the clay/gravel drainage layer (see Sect. A.1.2) above the vault (assuming a unit gradient through the backfill).

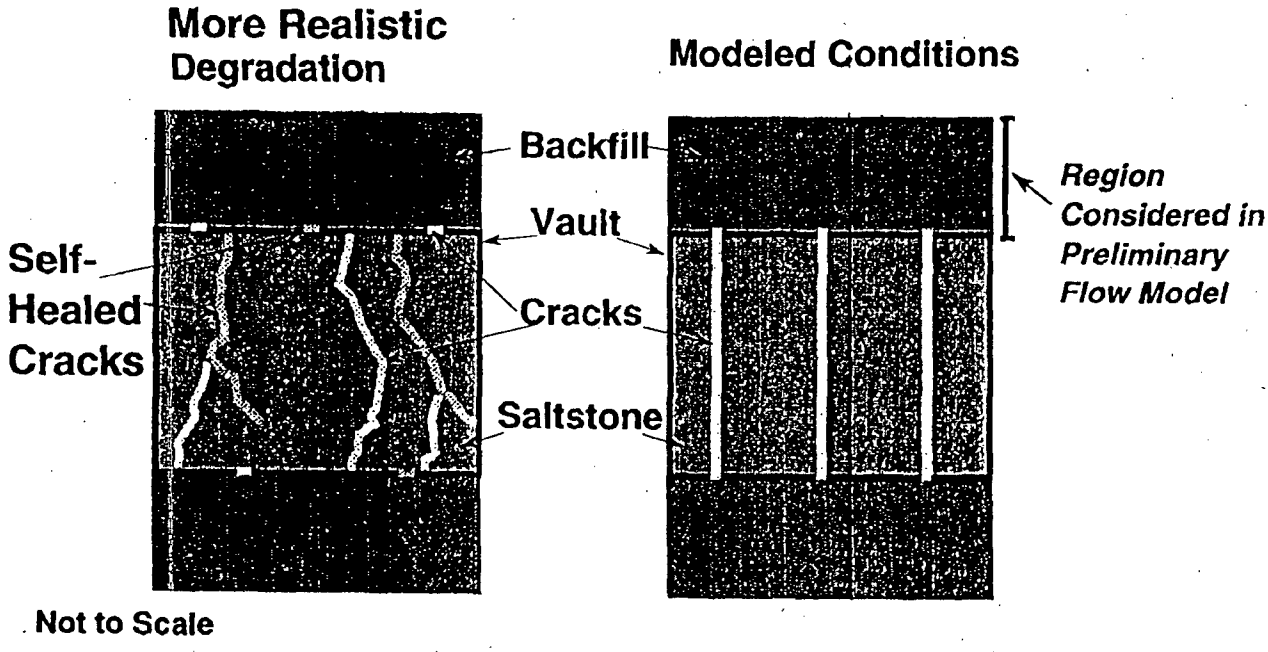

Fig. A.1-12. Comparison of more realistic system and modeled representation of flow rate through backfill (clay in this case) and fractured vault.

After normalizing variables and applying the appropriate simplifications (i.e., homogeneous soil, equally-spaced fractures) to Yate's solution, the dimensionless flow rate, ζ_3, is calculated using

$$\zeta_3 = \frac{-z_o}{x_o\left[\left(\sum_{n=1}^{\infty} V_n\right) - z_o\right]}$$

where

$$z_o = \frac{Z_o}{\Psi},$$

$$x_o = \frac{X_o}{\Psi},$$

$$V_n = \frac{\lambda_j (2p_{1j} + 2p_{1j}^2 p_{2j})}{\cosh[\tau_j]\,\beta_j},$$

Ψ = the half-width of the crack,
z_o = the depth of perched water, and
x_o = half the distance between the fracture center lines.

The coefficients for V_n are defined as follows:

$$\lambda_j = \frac{2}{Z_o \tau_j^2}$$

$$p_{1j} = \tanh[\tau_j(x_o - 1)]$$

$$p_{2j} = \tanh[\tau_j]$$

$$j = 2n-1$$

$$\tau_j = \frac{\pi j}{2 z_o}$$

$$\beta_j = 2p_{1j}(1 + p_{2j}^2) + 2p_{2j}(1 + p_{1j}^2).$$

Flow through fractured concrete vaults and saltstone was predicted based on the parameter values listed in Table A.1-4. The predicted velocity in each fracture (assuming all flow occurs through the fracture) based on the values in Table A.1-4 was 780 cm/year (darcy velocity divided by the ratio of crack width to crack spacing). Contributions from the intact matrix are considered separately in Appendix A.1.2. This value is subsequently used as an input to the transport simulations. Test cases comparing flow results from the analytical solution with results from the PORFLO-2D (Kline et al. 1983) finite difference code have demonstrated excellent agreement (Walton and Seitz 1991).

Table A.1-4. Input values assumed for flow calculations

Parameter	Assumed Value
Crack width	0.005 cm[a]
Crack spacing	300 cm[a]
Depth of perched Water on roof	61 cm[b]
Saturated hydraulic Conductivity of clay	0.24 cm/year[b]

[a] Sect. 3.1.3.5
[b] Appendix A.1.2

Note that the assumption of saturated flow is conservative for predicting contaminant flux because flow rates through the fracture would be largest when it is saturated. The predicted build-up of perched water on intact vaults, based on PORFLOW-3D simulations, suggests saturated flow is likely to occur. However, neglecting the vault around the saltstone and the assumption of aligned fractures in the different layers of saltstone is likely to result in inflated flow rates. Reduced flow would be expected in the case where fractures are not aligned. Flow rates will also be reduced if cracks in lower pours of saltstone are filled by a subsequent pour. Although flow rates are the greatest source of uncertainty in these degraded vault calculations, it is assumed that neglecting the vault and considering open, aligned fractures in the saltstone represents an upper bound of the flow rate through fractures.

A.1.3.3 Determination of Release Rate from Vault

A number of semi-analytical models have been developed for transport through fractured porous media. Of available methods, the solution of Rasmuson and Neretnieks (1981) is perhaps most appropriate for application to release rates from massive concrete waste forms. This solution allows a decaying source term, which is required for leaching, and the solution is given in terms of dimensionless parameters, which can be used to interpret and generalize the results from the analysis. Note that their published model estimates transport from a decaying source of radionuclides into a fractured porous medium and is the complement of the desired solution for release from a fractured concrete monolith, where contaminants are leached from (rather than into) a fractured porous medium.

The saltstone is envisioned as a large fractured monolith, with blocks of intact concrete separated by fractures. Advection dominates mass transport in the fractures, while diffusion controls mass transport laterally from the porous matrix to the fractures. Figure A.1-13 illustrates this conceptual model in a schematic form. Partitioning of compounds between solid and liquid phases is also considered. The velocity through the saltstone fractures is determined using the methods described in Sect. A.1.3.2. Since the crack is significantly more permeable than the adjacent saltstone matrix, all flow is assumed to occur through the fractures. Thus, this solution is also independent of the hydraulic conductivity of the intact saltstone matrix. Contributions from the intact saltstone are considered in the intact modeling (Appendix A.1.2).

This assessment is limited to the case of no dispersion in the fractures in the concrete. This is a conservative case (in terms of concentration) for radionuclide release rates from concrete waste forms. In reality, fractures are likely to be in the form of a tortuous network, with a significant, but unknown, amount of dispersion resulting. Thus, conservative assumptions are made to account for the uncertainty in accurately representing a fractured vault.

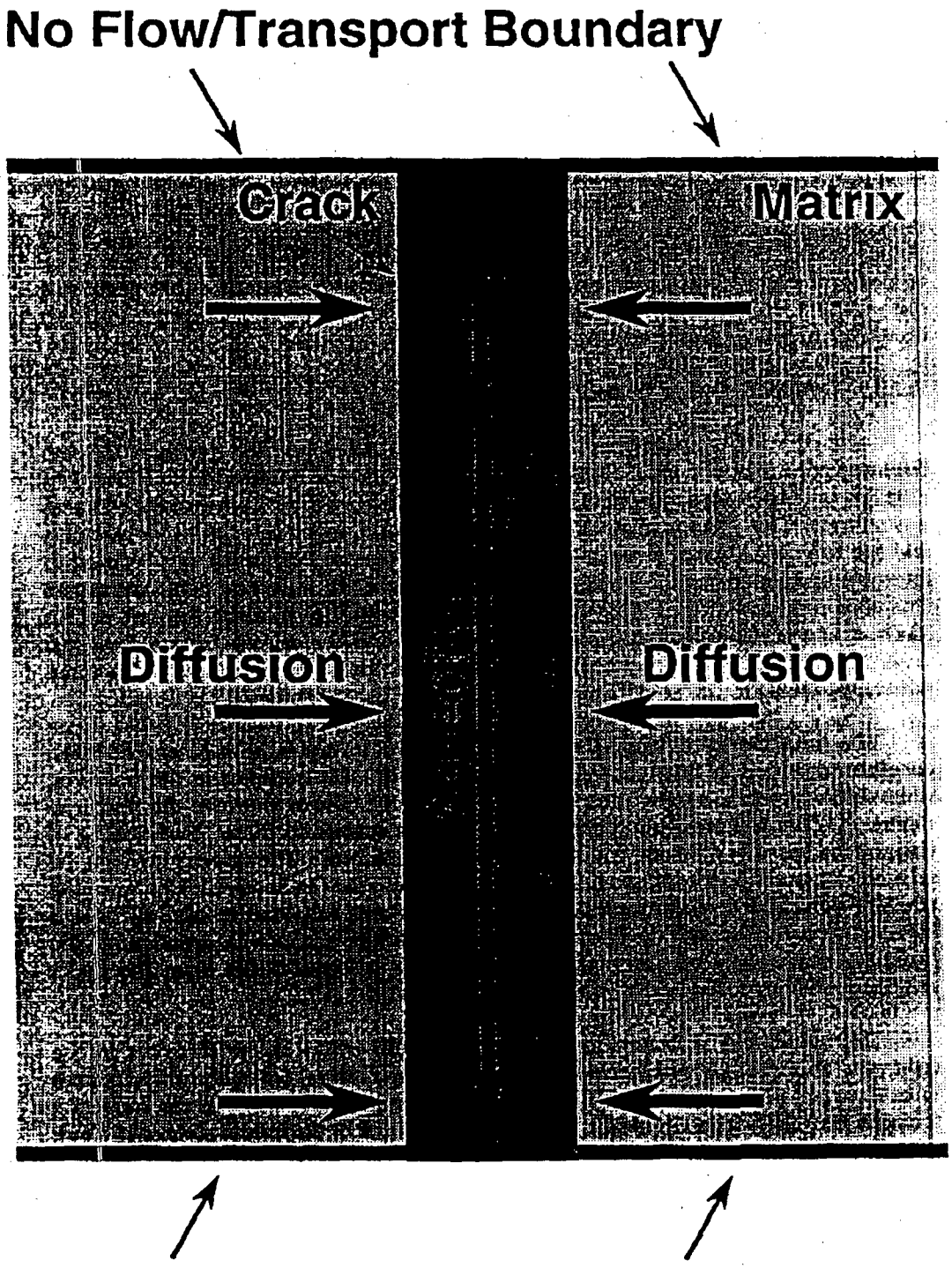

Fig. A.1-13. Schematic of conceptual model of release from fractured vault.

The analytical solution used for this assessment is, with slight modification, (i.e., by ignoring dispersion) from Rasmuson and Neretnieks (1981).

$$H_1(\lambda) = \lambda\left(\frac{(sinh2\lambda + sin2\lambda)}{cosh2\lambda - cos2\lambda}\right) - 1$$

$$H_2(\lambda) = \lambda\left(\frac{sinh2\lambda + sin2\lambda)}{cosh2\lambda - cos2\lambda}\right)$$

If $\zeta > 0$ then,

$$\frac{\alpha C_f}{C_{t_o}} = (1 - Y)\,[\exp(-\beta)]$$

$$Y = \frac{1}{2} + \frac{2}{\pi}\int_0^{\infty} \exp(-\delta H_1)\sin(\zeta\lambda^2 - \delta H_2)\,\frac{d\lambda}{\lambda}$$

If $\zeta < 0$ then,

$$\frac{\alpha C_f}{C_{t_o}} = \exp(-\beta)$$

where the solution depends upon these dimensionless variables that follow:

$\zeta = (2D_a\theta)/r_o^2$ = dimensionless contact time,
$\alpha C_f/C_{to}$ = dimensionless concentration,
$\beta = \lambda_d t$ = dimensionless radioactive decay, and
$\delta = (\gamma z)/(mU_f)$ = bed length parameter.

The above variables are derived in turn from these variables

θ = $t\text{-}z/U_p$
C_f = concentration in fractures,
α = volumetric distribution coefficient (moisture content * retardation factor),
λ_d = decay rate = $\ln 2/t^{1/2}$,
r_o = effective radius of spherical blocks (= 0.5 S for cubic blocks and 1.5 S for slabs),
S = fracture spacing,
U_f = velocity in fractures,
D_a = apparent diffusion coefficient,
z = thickness of vault,

z_o = total distance along fracture from top or upgradient portion of vault,
ϕ_f = fracture porosity,
ϕ_m = matrix porosity,
m = $\phi_f/(1-\phi_f)$,
γ = $(3D_a\alpha)/r_o^2$, and
t = time.

Values for the independent variables are listed in Table A.1-5. The velocity in the fracture, U_f, was predicted using the approach discussed in Appendix A.1.3.2. The crack spacing, S, is discussed in Sect. 3.1.3.5. The apparent diffusion coefficient, D_a, is simply the effective diffusion coefficient from Sect. 2.4 (5×10^{-9} cm^2/s) divided by the radionuclide-specific retardation coefficient for saltstone. The porosity values for the fracture and saltstone, ϕ_f and ϕ_m, assume an open crack and the porosity of saltstone specified in Sect. 2.4.

The analytical solution was derived for the case of a semi-infinite medium, whereas, the application of concern is for a concrete vault of finite dimensions. If dispersion is ignored, this is not a limitation. Ignoring dispersion is required because of the lack of information concerning dispersion in cracks. Because dispersion in cracks is likely due to variation in aperture, sensitivity analyses addressing changes in crack width can be used to help account for this phenomenon (Sect. 4.2).

The fracture flow solution provides concentrations as a function of time in the fracture. These concentrations, in conjunction with the Darcy velocities predicted, are then used to calculate flux from the fractures of a degraded vault. The total flux of a degraded vault must also consider the flux from the intact portions between fractures. This was accomplished by adding the releases predicted from the intact modeling (Appendix A.1.2) to the releases predicted from this analysis.

A.2 GROUNDWATER FLOW AND MASS TRANSPORT MODEL AND SIMULATIONS

This section of Appendix A provides details of the conceptual model adopted for simulating flow and mass transport through the saturated hydrologic zones beneath the Z-Area SDF (Sect. A.2.1), and details related to simulation of the model using the PORFLOW-3D computer code (Sect. A.2.2).

A.2.1 Conceptual Saturated Flow and Transport Model

Based on the piezometric data at Z-Area (Sect. 2.1.7), it is apparent that the groundwater flow field is highly variable within and among the hydrologic units in the vicinity of Z-Area. A three-dimensional representation of the groundwater flow system was chosen to allow the divergent lateral flow to be simulated (Fig. A.2-1).

Output Options: The MINTEQ code outputs the following:

- Echo of the data file input
- progress of the Newton-Raphson iterations
- full speciation of the input water composition
- charge balance and ionic strength for the aqueous composition
- saturation state of the water with respect to minerals in the data base

The user can also specify that the thermodynamic data base be printed. Debugging printing options are supported.

B.3 VAULT DEGRADATION COMPUTER CODE

I. Code Description - Concrete Degradation and Steel Reinforcement Corrosion

Purpose and Scope: The code used to estimate concrete degradation and rebar corrosion is designed to model the important degradation processes that can affect the long-term performance of concrete barriers. The processes modeled include: (1 concrete attack by sulfate and magnesium, 2) concrete leaching (both concrete and geologically controlled), 3) carbonation, and 4) rebar corrosion.

Development History: The current model consists of analytical solutions for concrete degradation processes. These solutions were selected as the best available means of predicting long-term concrete barrier performance.

Code Attributes: The code is written in Mathematica programming language (Wolfram 1988) and consists of four separate modules. Three of the modules are used to estimate concrete degradation and one is used to predict corrosion of steel reinforcement.

Sulfate and magnesium attack on concrete is described by an empirical relationship determined by Atkinson and Hearne (1984). Leaching of concrete components is described by a shrinking core model, in the case of concrete-controlled leaching, and by diffusional mass transport for geologic-controlled leaching (Atkinson and Hearne 1984). Walton et al. (1990) derived a shrinking core model to describe concrete carbonation. Rebar corrosion is described by an empirical correlation to determine time to onset of corrosion from chloride attack (Clear 1976) and a one dimensional diffusion calculation for actual corrosion (Walton et al. 1990).

Computer Requirements: The code was developed on an Apple Macintosh IIcx and has also been run using a NEXT workstation. The code will run on any workstation, mainframe or PC that runs Mathematica. The degradation code will run on any system running the Mathematica software package. The Macintosh version 1.2.2 recommends a minimum of 4 megabytes of RAM.

Restrictions: The code has been developed in the Mathematica software package and is therefore restricted by the purchase of the software.

II. Code Selection Basis

General Critique: The code is a compilation of analytical solutions for important concrete degradation processes (Clear 1976; Atkinson and Hearne 1984; Walton et al. 1990) selected based on the work of Walton et al. (1990). These analytical solutions are considered to be the best available means of predicting concrete degradation. The equations that are used to represent the degradation processes are based on observed conditions (i.e., sulfate, magnesium, chloride and dissolved oxygen concentrations in groundwater, etc.). However, in some cases the conditions encountered in a performance assessment are very different from the conditions on which the empirical relationships are based. Also, the observations that form the basis of the equation are for much shorter periods of time (tens of years) than is needed for performance assessments (thousands of years).

Code Verification: The Mathematica version of the code has been verified against the results of Walton et al. 1990.

Code Benchmarking: The code is made up of analytical solutions, therefore the benchmarking process does not apply.

Code Validation: The code is made up of analytical solutions, therefore the validation process does not apply.

III. Theoretical Framework

Governing Equation and Assumptions:

Sulfate and Magnesium Attack. The equations that form the basis for the calculations are based on chemical reactions between concrete and rebar with chemical constituents from the monolith and/or the geologic media surrounding the vault. Sulfate attack on concrete is the result of reactions of sulfate with hydrated tricalcium aluminate (C_3A) and portlandite [$Ca(OH)_2$] to form compounds of larger volume leading to expansion and disruption of the concrete. The reactions between sulfate and cement

compounds can be written as

Gypsum:

$$Ca(OH)_2 + SO_4^{2-} + 2H_2O \Longrightarrow CaSO_4 \cdot 2H_2O + 2OH^-$$

Monosulphoaluminate:

$$3CaO \cdot Al_2O_3 \cdot 6H_2O + CaSO_4 + 6H_2O \Longrightarrow 3CaO \cdot Al_2O_3(CaSO_4) \cdot 12H_2O$$

Ettringite:

$$3CaO \cdot Al_2O_3(CaSO_4) \cdot 12H_2O + 2CaSO_4 + 20H_2O \Longrightarrow 3CaO \cdot Al_2O_3 \cdot 3(CaSO_4) \cdot 32H_2O$$

An example of a reaction between cement paste and magnesium sulfate is

Brucite:

$$3CaO \cdot 2SiO_2 + 3MgSO_4 \cdot 7H_2O \Longrightarrow 3CaSO_4 \cdot 2H_2O + 3Mg(OH)_2 + 2SiO_2 + 2H_2O$$

The low solubility of $Mg(OH)_2$ causes the reaction to proceed to completion, making the attack more severe.

The depth of sulfate and magnesium attack is described by the equation

$$x = 0.55\ C_a\ (Mg^{2+} + SO_4^{2-})t$$

where

x = depth of deterioration (cm),
C_a = weight percent of C_3A in non-hydrated cement,
Mg^{2+} = concentration of magnesium in the bulk solution (mol/L),
SO_4^{2-} = concentration of sulfate in the bulk solution (mol/L), and
t = time (years).

Assumptions: The rate of attack is proportional to sulfate and magnesium concentration in the solution and C_3A content of the cement.

Limitations: Correlations are only valid over the time/system parameters tested. Application outside this range is highly questionable.

The empirical correlation does not include the impacts of advective transport and/or the known importance of water cement ratio (WCR) on durability. Application of the model is not clearly conservative.

Concrete-Controlled Leaching of Calcium Hydroxide. Cement components will be leached from concrete in environments in contact with water and have significant percolation rates. The alkalis are the first components to be leached followed by calcium hydroxide. The leaching of calcium hydroxide from the cement is described by

$$Ca(OH)_2 ==> Ca^{2+} + 2OH^-$$

The equation that describes concrete controlled leaching is

$$x = [2D_i \{(C_l - C_{gw})/C_s\}t]^{1/2}$$

where

- x = depth of leaching (cm),
- D_i = intrinsic diffusion coefficient of Ca^{2+} in concrete solid (mol/cm^3),
- C_l = concentration of Ca^{2+} in concrete pore water (mol/cm^3),
- C_{gw} = concentration of Ca^{2+} in the groundwater or soil moisture (mol/cm^3),
- C_s = bulk concentration of Ca^{2+} in the concrete solid (mol/cm^3), and
- t = time (s).

Assumptions: The rate of calcium removal from the exterior of the concrete is assumed to be rapid relative to the movement of calcium ions through the concrete. Therefore, diffusion controls the transport rate of the calcium.

Limitations: Diffusional mass transport is considered, but advection through and around the concrete is not considered.

D_i for the leached portion of the concrete will be substantially higher than D_i for intact concrete. Permeability of the concrete will increase as leaching proceeds leading to greater flow rates through the leached area. Diffusional control may no longer be valid under these conditions.

Geology-Controlled Leaching of Calcium Hydroxide. Geology-controlled leaching occurs as a result of the diffusion being controlled by the geologic material surrounding the concrete. The resulting equation is

$$x = 2 \text{ phi } [(C_l - C_{gw} / C_b] [(R_d D_E t) / pi]^{1/2}$$

where

- x = depth of leaching (cm),
- phi = porosity of the geologic material (cm^3 voids/cm^3 total),
- C_l = concentration of Ca^{2+} in concrete pore water (mol/cm^3),
- C_{gw} = concentration of Ca^{2+} in the groundwater or soil moisture (mol/cm^3),
- C_b = concentration of Ca^{2+} in the bulk concrete (solid+pore) (mol/cm^3),

R_d = retardation factor for Ca^{2+} in the geologic material,
D_E = effective dispersivity/diffusivity of Ca^{2+} in geologic material (cm^2/s), and
t = time (s).

Assumptions: Diffusion into the surrounding geologic material controls leaching. Leaching is highest in low calcium concentration environments.

Limitations: Parameters for geologic material are needed (R_d, D_E, phi).

Concrete Carbonation. Carbonation is typically thought of as the reaction between calcium hydroxide and carbon dioxide as represented by

$$Ca(OH)_2 + CO_2 ==> CaCO_3 + H_2O$$

Carbonation can occur only as rapidly as dissolved carbonate can diffuse through the concrete. Carbonation rate is dependent on the moisture content of the concrete and the relative humidity of the ambient medium and the concentration of CO_2 in the ambient medium. If diffusion in the concrete is too slow, an equilibrium is reached where the diffusion of CO_2 and carbonation are stopped or severely reduced.

Carbonation rate is dependent on the moisture content of the concrete. As relative humidity changes from 0 to 100%, the rate of carbonation passes through a maximum.

Because the pH in concrete is high (>12), the carbonation reaction actually occurs as

$$Ca(OH)_2 + CO_3^{2-} ==> CaCO_3 + 2OH^-$$

The relationship between carbonation depth and groundwater concentration, portlandite in the concrete, and intrinsic diffusion coefficient of calcium is:

$$x = [2D_i (C_{gw}/C_s) t]^{1/2}$$

where

x = depth of carbonation (cm),
D_i = intrinsic diffusion coefficient of Ca^{2+} in concrete (cm^2/s),
C_{gw} = concentration of total inorganic carbon in the groundwater (mol/cm^3),
C_s = bulk concentration of $Ca(OH)_2$ in the concrete solid (mol/cm^3), and
t = time (s).

Assumptions: Concrete is saturated with water.

Limitations: The type of cement ultimately affects the depth of carbonation. This relationship becomes increasingly invalid as the relative humidity of the concrete decreases from 100% to 50%; below this level, the reaction rates decline rapidly resulting in a reduction in carbonation rate.

Reinforcement Corrosion/Chloride Attack. The alkaline environment of the concrete and the isolation it provides from external corrosive agents protects the steel reinforcement from corrosion by forming a protective oxide layer on the metal surface. The passive oxide layer may undergo attack by corrosive agents as the concrete deteriorates. Historically, aqueous chloride is the corrosive agent associated with the break up of the passive layer.

Reinforcement corrosion may also be associated with reduction of concrete alkalinity in the absence of elevated chloride levels. Carbonation and leaching can cause a decrease in the concrete pH with eventual loss of passivity.

Chloride attack is modeled in two stages (a) time to breakup of the passive layer and initiation of corrosion and (b) corrosion rate subsequent to breakup of the passive layer. An empirical correlation for the time to passive layer breakup is

$$t_c = (129\, x_c^{1.22})/(WCR\ Cl^{0.42})$$

where

t_c = time to onset of corrosion (years),
x_c = thickness of concrete over the rebar (in.),
WCR = water to cement ration (by mass), and
Cl = chloride ion concentration in groundwater (ppm).

Assumptions: The time to onset of corrosion is related to the water to cement ratio, depth of cement cover, and chloride concentration in groundwater.

Limitations: Applicability to conditions outside the observed chloride concentrations on which the equation is based is questionable.

The simplest method of estimating the corrosion rate subsequent to initiation of corrosion is a one dimensional diffusion calculation assuming limitation of the corrosion rate by oxygen diffusion. The percent of reinforcement remaining at any time is given by

$$\%\ remaining = 100[(4*9.4\ \ sD_iC_{gw}t)/(pi\ d^2\ delta\ x)]$$

where

s = spacing between reinforcement bars (cm),
D_i = intrinsic diffusion coefficient of O_2 in concrete (cm^2/s),
C_{gw} = concentration of oxygen in the groundwater (mol/cm^3),
delta x = depth of reinforcement below surface (cm), and
t = time (s).

Assumptions: The corrosion rate is limited by oxygen diffusion.

Limitations: Applicable only if oxygen diffusion controls corrosion.

Initial Conditions: Not applicable.

Numerical Techniques: Not applicable.

IV. Code Inputs and Outputs

Input Data Structure: Input for the calculations is contained in the Mathematica file for degradation calculations. The values may be changed from within Mathematica and the file is evaluated as needed.

Output Options: Output can be in the form of numeric values, tables, two- or three-dimensional plots, and contour plots. Mathematica allows many forms of output to be displayed within the package and exported for use in other graphics packages.

B.4 SATURATED/UNSATURATED FLOW AND TRANSPORT CODE

I. General Code Description

Purpose and Scope. The PORFLOW-3D computer code was selected and applied to predict the isolation performance of the saltstone vaults in the vadose zone, to predict transport of radionuclides released to the underlying aquifer, and to predict contaminant transport in the aquifer. Specifically, the computer code was used to model water flow through the backfill, gravel-clay barrier, vault structure, and saltstone waste form. The code was then used to model the release of contaminants from the waste form, migration through the vault structure, surrounding soils and underlying formations. The simulation results generated by the PORFLOW-3D code were then post-processed to obtain predictions of

- water pathlines and travel times to the aquifer,
- contaminant plume distributions in the vadose zone,
- contaminant fluxes to the aquifer, and
- contaminant plume distributions in the aquifer's saturated zone.

EG&G Idaho, Inc.
FORM EG&G-2631 (Rev. 12-88)

Project File Number SALT-92-002

EDF Serial Number SALT-92-003

Functional File Number

Date 04/12/92

ENGINEERING DESIGN FILE

Project/Task SAVANNAH RIVER SITE Z-AREA P.A.

Subtask CONCRETE DEGRADATION CALCULATIONS

Subject: CONCRETE DEGRADATION CALCULATIONS FOR Z-AREA VAULTS

Abstract:

A set of calculations have been made to determine the most important degradation processes that may influence vault integrety. Processes selected for determinations include: 1) Sulfate and Magnesium attack, 2) Calcium Leaching, 3) Carbonation, and 4) Rebar Corrosion.

A Mathematica notebook was used to document the input parameters used in the calculations.

Distribution (complete package)

C.A. Dicke, MS 2110; S.O. Magnuson, MS 2110; S.J. Maheras, MS 2110;
R.R. Seitz, MS 2110; B.W. Smith, MS 2110; C.S. Smith, MS 2107,
J.C. Walton, 13507 Circle A Trail, Helotes, TX 78023; SEM Project File

Distribution (cover sheet only): Project EDF file log, EDF serial no. log

Author	Dept.	Reviewed	Date	Approved	Date
Cam ADicke	4/12/92				
C. A. Dicke	SEM	R. R. Seitz	SEM	S. J. Maheras	SEM

Concrete Degradation Notebook

The following information was taken from "Properties of Concrete" (3rd edition), A. M. Neville, 1981, J. Wiley and Sons, Inc., NY, 779 p.

APPROXIMATE COMPOSITION LIMITS OF PORTLAND CEMENT

Species	%	Typical %
CaO	60-67	63
SiO2	17-25	20
Al2O3	3-8	6
Fe3O3	0.5-6	3
MgO	0.1-4	1.5
Alkalis	0.2-1.3	1
SO3	1-3	2

MgO, TiO2, Mn2O3, K2O and Na2O are minor compounds and usually amount to no more than a few percent of cement by weight. The term alkalis refers to Na2O and K2O although other alkaline metals are present.

The Bogue's Equation is often used to calculate the percentage of C3S, C2S, C3A and C4AF in the cement based on composition. This technique tends to underestimate the C3S content and overestimate C2S because other oxides replace some of the CaO in C3S. This will not be a concern in this task because C3A is the only compound needed.

MAIN COMPOUNDS OF PORTLAND CEMENT

Tricalcium Silicate	3CaO SiO2	C3S
Dicalcium Silicate	3 CaO SiO2	C2S
Tricalcium Aluminate	3 CaO Al2O3	C3A
Tetracalcium Aluminoferrite	4CaO Al2O3 Fe2O3	C4AF

BOGUE'S EQUATION

C3S = 4.07(CaO) - 7.60(SiO2) - 6.72(Al2O3) - 1.43(Fe2O3) - 2.85(SO3)
C2S = 2.87(SiO2) - 0.754(C3S)
C3A = 2.65(Al2O3) - 1.69(Fe2O3)
C4AF = 3.04(Fe2O3)

Calculated Composition from Bogue's Equation Based on Typical Cement Composition
C3S = 54.1 C2S = 16.6 C3A = 10.8 C4AF = 9.1

cao = 63; sio2 = 20; al2o3 = 6; fe2o3 = 3; mgo = 1.5; alk = 1; so3 = 2

c3s = 4.07(cao) - 7.60(sio2) - 6.72(al2o3) - 1.43(fe2o3) - 2.85(so3)
c2s = 2.87(sio2) - 0.754(c3s)
c3a = 2.65(al2o3) - 1.69(fe2o3)
c4af = 3.04(fe2o3)

Type II Concrete has the following compound percentages

	C3S	C2S	C3A	C4AF	CaSO4	Free CaO	MgO
Maximum	55	39	8	16	3.4	1.8	4.4
Minimum	37	19	4	6	2.1	0.1	1.5
Mean	46	21	6	12	2.8	0.6	3.0

The cement used will be Type II with C3S + C3A not exceeding 0.58 (58%). The cement will contain a pozzolan, an air-entrained admixture, and a water reducing admixture. The air content will be between 3 and 6% by volume. Water used in the mixing of the concrete will contain no greater than 250 ppm chloride and will not exceed 2000 pprn TDS. These specifications are listed in the Furnishing and Delivery of Concrete specifications for the Z-Area Saltstone project.

Water cement ratios (WCR) range from 0.43 to 0.60 over all types of cements (A, B, C, ...) according to the "Concrete Manual" (8th edition) US Dept. of Interior, Bureau of Reclamation, 627 p. Type C cement, covered by backfill, has a WCR of 0.58+-0.02.
This is the value that is expected to be used. Another value may be substituted at a later date if needed.
The description of the concrete to be used as stated in the functional design specifications is as follows: Blast furnace slag for 40-50% of cement (Grade 120), Air-entrained concrete, hydraulic conductivity of < 10^-7 cm/sec, and a distibution coefficient for soluble anions (nitrate, chloride, iodine, etc) of < 10^-8 cm^2/sec. Walls, roof, and base mat will be 18", 24", and 24", respectively.

The following section contains the variables and variable values used in the calculation of corrosion and degradation for the Saltstone Vaults. This is a master list and a change in these variables will be carried through all calculations containing the variable upon evaluation of the notebook. It should be noted that sections can be calculated without evaluating the entire notebook.

INPUT Parameters

```
Needs["/me/Library/MathPackages`graphics`"]

vcms = 0.55        (* constant for mg/so4 attack equation [(cm/yr)/(M)] *)
wtca = 8           (* weight percent C3A in cement [unitless] *)
mgson = 5.75 10^-6  (* sum of minimum mg/so4 in groundwater [mole/L or M] *)
mgsod = 1.50 10^-4  (* sum of median mg/so4 in groundwater [mole/L or M] *)
mgsox = 9.26 10^-4  (* sum of maximum mg/so4 in groundwater [mole/L or M] *)

vcin = 129         (* constant for onset of rebar corrosion equation [129 yr inch/ppm] *)
corw = 5.08        (* thickness of concrete coverage over rebar in walls [cm] *)
corf = 7.62        (* thickness of concrete coverage over rebar in floor [cm] *)
corc = 7.62        (* thickness of concrete coverage over rebar in roof [cm] *)
wcr = 0.43         (* water to cement ratio [kg/kg] *)
clgwn = 1.41 10^-5  (* minimum chloride concentration in groundwater [mole/L or M] *)
clgwd = 5.08 10^-5  (* median chloride concentration in groundwater [mole/L or M] *)
clgwx = 1.49 10^-4  (* maximum chloride concentration in groundwater [mole/L or M] *)

vcpr = 37.6        (* constant for % rebar remaining equation [37.6 cm^3/mole] *)
sr = 30.5          (* rebar spacing in concrete [cm] *)
diox =1 10^-7      (* intrinsic diffusion coefficient for oxygen in concrete [cm^2/sec] *)
dion = 2 10^-6     (* intrinsic diffusion coefficient for oxygen in concrete [cm^2/sec] *)
ogw = 3.125 10^-4   (* oxygen concentration in groundwater [mole/L or M] *)
dr = 2.54          (* rebar diameter [cm] *)

capw = 2.7 10^-3    (* calcium concentration in concrete pore water [mole/L or M] *)
cagwn = 2.75 10^-6  (* minimum calcium concentration in groundwater [mole/L or M] *)
cacsn = 1.875      (* minimum calcium concentration in bulk concrete solid [mole/L] *)
cacsx = 2.250      (* maximum calcium concentration in bulk concrete solid [mole/L] *)
dica= 10^-6        (* intrinsic diffusion coefficient of calcium in concrete solid [cm^2/sec
```

```
dico3 = 10^-7      (* carbonate diffusion coefficient [cm^2/sec]  *)
phix = 0.30        (* maximum porosity of geologic material [unitless] *)
rdn = 2            (* minimum retardation factor of Ca in geologic material [ml/cm^3] *)
rdx = 5            (* maximum retardation factor of Ca in geologic material [ml/cm^3] *)
decan = 1 10^-6    (* minimum effective dispersivity/diffusivity of Ca in geo. mat. [cm^2
decax = 3 10^-6    (* maximum effective dispersivity/diffusivity of Ca in geo. mat. [cm^2

ticgwn = 1.64 10^-5 (* minimum total inorganic carbon in groundwater [mole/L or M] *)
ticgwx =2.00 10^-3  (* maximum total inorganic carbon in groundwater [mole/L or M] *)
chbcn = 0.72       (* minimum bulk concentration of Ca(OH)2 in concrete [mole/L or M] *
chbcx = 2.25       (* maximum bulk concentration of Ca(OH)2 in concrete [mole/L or M] *

vcmi = 0.3937      (* converts cm to inches [0.3937 inch/cm] *)
vcic = 0.001       (* converts mole/L or M to mole/cm^3 [0.001 L/cm^3] *)
vcfm = 35453       (* converts Cl from moles/L or M to ppm [35453 ppm/M] *)
vcsy = 31536000    (* converts x/second to x/year [31536000 second/year] *)

t = .              (* Time  {cleared for plotting with time} [years] *)
tmin = 0           (*  minimum Time [years] *)
tmax = 10000       (* maximum Time [years] *)
```

The following calculation is for Degradation of Saltstone Vault due to Magnesium and Sulfate Attack on Concrete.

Summary for Empirical Model for Loss Degradation

The model is based on Norwick Park study based on observed loss of cement at block corners after 5 years in 0.19 M Na2SO4 solution. The depth of attack on the block was 42mm and indicates a linear relationship with time. Rate of attack is assumed to be proportional to sulfate concentration in the solution and tricalciumaluminate (C3A) content in the cement. Depth of attack in a MgSO4 solution is approximately twice that of Na2SO4.

Concentrations of magnesium and sulfate are based on surface and ground water compositions from Marine (1976). The data for surface waters and groundwaters from Coastal Plains Formations were selected as most representative of the soil waters at the Savannah River Site. Soil water concentrations may be added to the plots at a later date if they become available. A table containing minimum, median, and maximum values of combined Mg and SO4 concentrations (M) is provided below. Concentrations were added after conversion from mg/L to moles/L for each available sample. The data were sorted and pertanent values were selected.

Water from several formations and surface waters have been collected and analyzed for chemical composition. The water compositions that will be applied in this study are the surface waters and waters from the Coastal Plains Sediments. The surface waters and those in the shallow Coastal Plain Formations are not separate and distinct, but part of the same system. Surface water, especially in dry weather, has passed through the ground for some time and distance (Marine, 1976).

The water analyses reported in Marine (1976) have been used to determine concentrations for needed parameters. Some analyses were removed from the data used to define parameter values. Values for Savannah River at Highway 301, Hollow Creek at Highway 125, and Lower Three Runs at Highway 125 on 11/30/71 were removed due to possible sample contamination with respect to Mg (values on this date are an order of magnitude higher than other analyses).

Well 905-72G penetrates most of the Tuscaloosa Formation and may be contaminated by waters contacting the metamorphic rock below. Single analyses have been eliminated for wells DRB 4WW, DRB 6WW, 13G, 54P, and 55R because they offer no means of comparison for verification.

Magnesium concentrations range from 0.14 to 8 ppm (5.76E-6 to 3.29E-4 moles/Liter) with a mean and median of 2.28 and 1.5 ppm (9.37E-5 and 6.17E-5 mole/Liter), respectively. Sulfate has a range of 0.27 to 15 ppm (2.81E-6 to 1.56E-04 mole/Liter) with a mean and median of 3.66 and 2 ppm (3.81E-5 and 2.08E-5 mole/Liter), respectively. The sums of Mg and SO4 range from 0.57 to 18.5 ppm (1.51E-5 to 3.77E-4 mole/Liter) with a mean and median of 5.94 and 4.95 ppm (1.32E-4 and 1.08E-4 mole/Liter), respectively.

Values to be used in the calculations are:
3.77E-4 mole/Liter MgSO4*
1.08E-4 mole/Liter MgSO4
1.51E-5 mole/Liter MgSO4

The cement specified by the Technical Specifications for Furnishing and Delivery of Concrete for the Defense Processing Facility is Portland Cement conforming to ASTM C 150, Type II. This specifies that C3A be at or below 8%. This value will be used in the calculations to follow.

8 % tricalcium aluminate (* Worse case scenario)

```
        ldmsn = vcms wtca mgson t
        ldmsd = vcms wtca mgsod t
        ldmsx = vcms wtca mgsox t
tt = 10^ttt
Plot3D[vcms wtca mgso tt,{ttt,2,4},{mgso,mgson,mgsox},
    Ticks->{LogScale[2,4,3],Automatic,Automatic},
    Lighting->False,Shading->False,Epilog->
  {Text[ColumnForm[{"Time","(yrs)"}],{0.25,0.03}],
  Text[ColumnForm[{"SO4+Mg",""}],{0.93,0.21}],
  Text[ColumnForm[{"Loss","(cm)"}],{0.01,0.60}]},
  PlotRange->All]
```

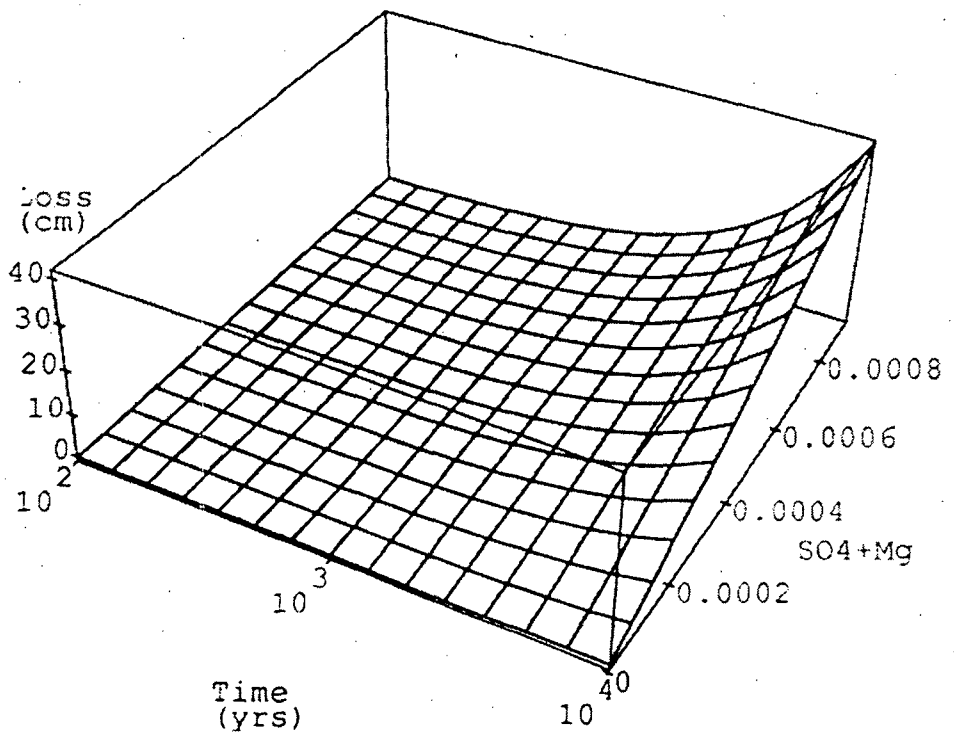

The following calculation is for Degradation of Saltstone Vault due to Chloride Attack on Steel Reinforcement.

Chloride attack is modeled as a two stage process (a) time to breakup of the passive layer and initiation of corrosion and (b) corrosion rate subsequent to breakup of the passive layer. An empirical model for initiation of corrosion and a corrosion rate model are used to calculate these processes.

A protective oxide layer forms on the steel reinforcement due to the alkaline environment inside the concrete and isolation from external corrosive agents. Deterioration of the concrete with time leads to ingression of corrosive agents. These corrosive agents can now attack the oxide layer on the steel and may lead to active metal corrosion. Metal corrosion is an important factor not only in the structural integrity of the vault, but also in the containment of the waste due to increased cracking and infiltration into the vault.

Cracks development is due in part to the increase in volume due to the formation of corrosion products that have higher molar volumes. Steel expansion leads to spalling and disruption of the concrete. Steel strength is also reduced by corrosion and may lead to structural instabilities. Loss of steel will increase the strain from physical load and cracking over steel will occur when the internal pressure generated by corrosion products exceeds the tensile strength of the concrete.

The following equation is based on the correlation for time to depassivation developed by Stratful and modified by Clear (1976). The equation shows the impact of cement cover over the steel and WCR on steel corrosion. This model has several drawbacks (a) it was derived from work conducted on bridge decks and the range of chloride concentrations found in soils is outside the range for which the equation is intended and (b) the model contains no provision for chloride threshold (thought to be conservative limitation).

Passive layer breakup has historically been associated with chloride ion ingress into the concrete (ACI, 1985). Destruction of the passive layer may occur by direct attack by elevated levels of Cl or by Cl serving as a supporting electrolyte in the solution. The start of reinforcement corrosion is thought to be linked with a threshold chloride level.

Lower concentrations of Cl may lead to corrosion of steel reinforcement when the alkalinity of the concrete is reduced making the passive layer less stable. Carbonation and leaching are processes that will lead to gradual lowering of pH and eventual loss of passivity. Depassivity of steel reinforcement can occur when the pH near the rebar drops below 9 (Papadakis et al., 1989). In low chloride environments carbonation and leaching may be important processes in depassivation. Time until depassivation has been clearly linked to the depth of cover over the reinforcement and the water cement ratio in studies of steel corrosion in concrete slabs (Clear, 1976).
The thickness of concrete coverage over the rebar in the walls, ceiling, and floor is 5.08 cm (2 inches), not available, and 7.63 cm (3 inches) on bottom bars.

The water to cement ratio is 0.43 kg/kg as required by specifications.

Chloride concentration in the soil/groundwater ranges from 1.24E-5 moles/Liter (0.44 ppm) to 1.49E-4 moles/Liter (5.3 ppm) with a mean and median of 4.46E-5 and 3.67E-5 moles/Liter (1.58 and 1.3 ppm), respectively.
A value of 1.50E-4 moles/Liter will be used as a worse case scenario.

clinwn = (vcin (corw vcmi)^1.22) / (wcr (vcfm clgwn)^0.42)

935.084

clinwd = (vcin (corw vcmi)^1.22) / (wcr (vcfm clgwd)^0.42)

545.833

clinwx = (vcin (corw vcmi)^1.22) / (wcr (vcfm clgwx)^0.42)

347.364

clincfn = (vcin (corf vcmi)^1.22) / (wcr (vcfm clgwn)^0.42)

1533.49

clincfd = (vcin (corf vcmi)^1.22) (wcr (vcfm clgwd)^0.42)

895.14

clincfx = (vcin (corf vcmi)^1.22) / (wcr (vcfm clgwx)^0.42)

569.66

clinwn = (vcin (corw vcmi)^1.22) / (wcr (vcfm clgwn)^0.42)

935.084

clinwd = (vcin (corw vcmi)^1.22) / (wcr (vcfm clgwd)^0.42)

545.833

clinwx = (vcin (corw vcmi)^1.22) / (wcr (vcfm clgwx)^0.42)

347.364

clincfn = (vcin (corf vcmi)^1.22) / (wcr (vcfm clgwn)^0.42)

1533.49

clincfd = (vcin (corf vcmi)^1.22) / (wcr (vcfm clgwd)^0.42)

895.14

clincfx = (vcin (corf vcmi)^1.22) / (wcr (vcfm clgwx)^0.42)

569.66

clgw=.
wcr=.
clinw = (vcin (corw vcmi)^1.22) / (wcr (vcfm clgw)^0.42)

```
pltld8 = Plot3D [{clinw, GrayLevel [0.8]} , {wcr,.4,.5},
{clgw,clgwn,clgwx},
AxesLabel->{ColumnForm[{"  Water/Cement"}],
ColumnForm[{"      Cl in ", "    groundwater"}],
ColumnForm[{"   Time to  "," Onset of "," Corrosion  "}] } ]
```

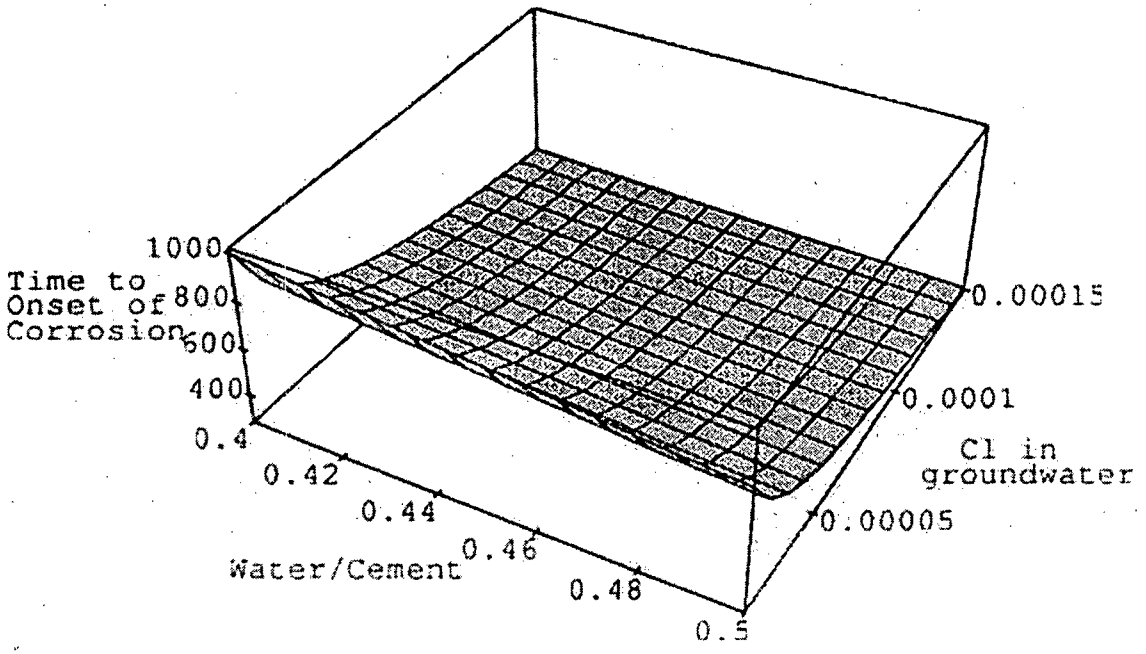

The following calculations are for Degradation of Saltstone Vault Steel Reinforcement Limited by Oxygen Diffusion.

The rebar spacing varies for the walls and foundation, and the final design of the ceiling has not been confirmed and can only be estimated at this time. Rebar in the walls will be spaced at 30.48 cm (12 inches) horizontal with 20.32 cm (8 inches) vertical for the bottom 487.68 cm (16 feet) of the wall and 40.64 cm (16 inches) vertical for the top 274.32 cm (9 feet) of the wall for each face.

The intrinsic diffusion coefficient for oxygen in the concrete used in these calculations is 2E-8 cm^2/sec was taken from the Walton et al. (1990).

The range of oxygen found in the soil/groundwater in the Savannah River Plant area range from 1.25E-4 to 3.125E-4 moles/Liter (4 to 10.1 ppm) with a mean and median value of 2.41E-4 and 2.47E-4 moles/Liter (7.7 and 7.9 ppm), respectively. The concentration of oxygen in the soil/groundwater to be used in this calculation will be 3.13E-4 moles/Liter (10 ppm) to give a conservative estimate. Marine (1976) notes that groundwaters to a depth of 800 feet have shown values as high as 10 ppm depending on the concentration of sulfate (low sulfate <13 ppm allows higher oxygen concentrations to exist).

Rebar diameter used in the vault foundation is #7 for top and bottom each way. The diameter used for the horizontal reinforcement of the walls is also #7, but the vertical reinforcement is #9. The actual diameters in centimeters is yet to be determined.

The thickness of concrete coverage over the rebar in the walls, ceiling, and floor is 5.08 cm (2 inches), not available, and 7.63 cm (3 inches) on bottom bars.

```
peremwx=100*(1-((vcpr sr diox vcsy ogw vcic t)/(Pi dr^2 corw)))
peremwn= 100*(1-((vcpr sr dion vcsy ogw vcic t)/(Pi dr^2 corw)))
peremfx=100*(1-((vcpr sr diox vcsy ogw vcic t)/(Pi dr^2 corf)))
peremfn=100*(1-((vcpr sr dion vcsy ogw vcic t)/(Pi dr^2 corf)))
peremcx=100*(1-((vcpr sr diox vcsy ogw vcic t)/(Pi dr^2 corc)))
peremcn=100*(1-((vcpr sr dion vcsy ogw vcic t)/(Pi dr^2 corc)))

prplt1 = Plot[{peremwx,peremwn}, {t,tmin,tmax},  PlotStyle->{{RGBColor[1,0,0]},{RGBCol
PlotRange->{0,100},Axes->{0,99.4},AxesLabel->{ColumnForm[{"    Time","    (yrs)"}],
ColumnForm[{" Percent","Remaining","  (%)","  "}]}]

prplt2 = Plot[{peremfx,peremfn}, {t,tmin,tmax},  PlotStyle->{{RGBColor[1,0,0]},{RGBColor
PlotRange->{85,100},Axes->{0,99.4},AxesLabel->{ColumnForm[{"    Time","    (yrs)"}],
ColumnForm[{" Percent","Remaining","  (%)","  "}]}]
```

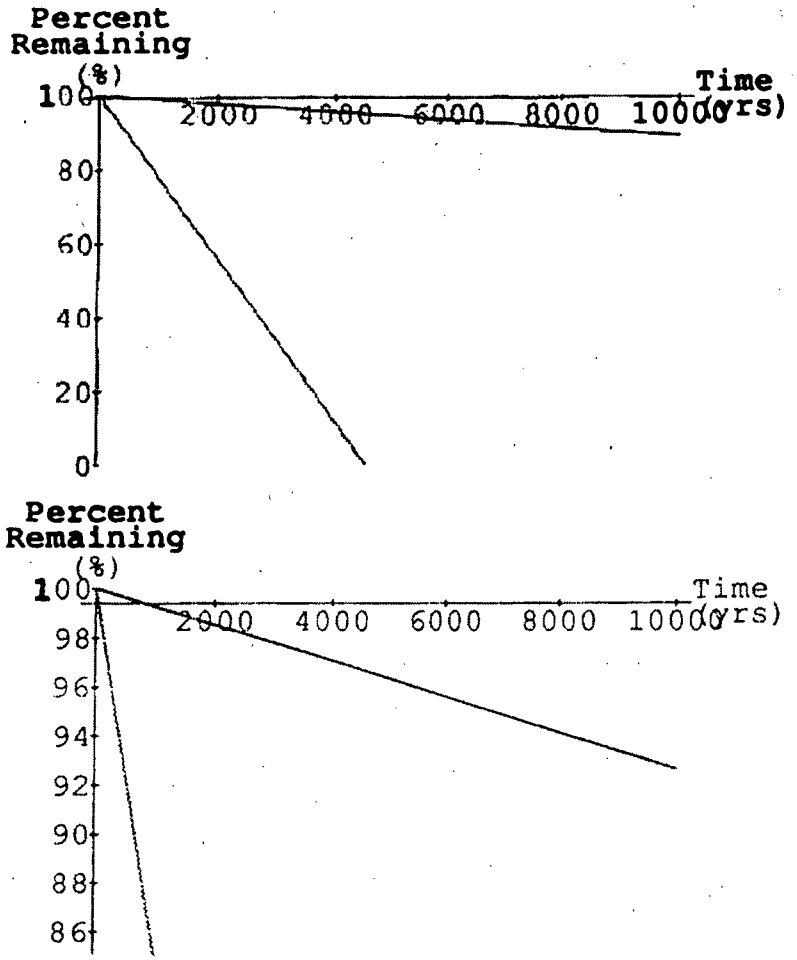


```
Clear[diox]
peremw=100*(1-((vcpr sr diox vcsy ogw vclc t)/(Pi dr^2 corw)))//N
diox = 10^tmp
Clear[tt]
t = 10^tt

pltld3 = Plot3D [peremw , {tt, 2, 4},  {tmp, -8, -6},
Epilog->{Text[ColumnForm[{"Time","(yrs)"}],{0.25,0.025}],
Text[ColumnForm[{"Diff.","Coef.","(sq cm/s)"}],{0.93,0.15}],
Text[ColumnForm[{"%","Rebar","Left"}],{0.03,0.65}]}, Shading->
False, Ticks->{LogScale[2,4,3],LogScale[-8,-6,2],Automatic},
PlotRange->{100,50}]
```

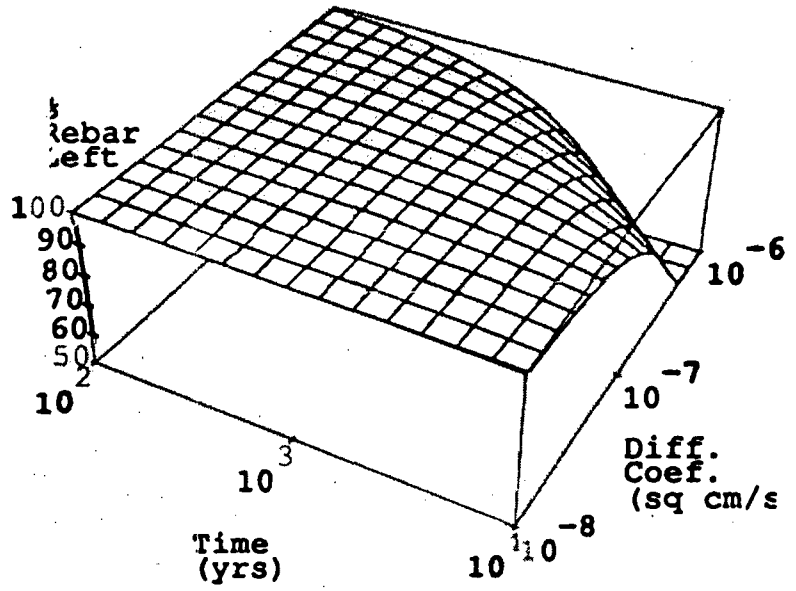


```
rebar=Table[{N[t],N[diox],peremw},{tt,2,4,0.1},{tmp,-8,-6,0.1}];

OpenWrite["/Projects/SR/Sept91/rebar"]
Do[Write["/Projects/SR/Sept91/rebar",
FortranForm[rebar[[i,j,1]]],OutputForm[" "]
,FortranForm[rebar[[i,j,2]]],OutputForm[" "]
,FortranForm[rebar[[i,j,3]]]],{i,1,20},{j,1,20}]
Close["/Projects/SR/Sept91/rebar"]
```

/Projects/SR/Sept91/rebar

The following calculations are for Degradation of Saltstone Vault due to Concrete Controlled (CaOH) Leaching of Concrete.

Cement components will be leached from concrete in environments that are in contact with water and have significant water percolation rates. Atkinson (1985) and Atkinson et al. (1988) describe for stages of leaching based on modeling and experimental results.

1) pH is approximately 13 due to presence of alkali metal oxides and hydroxides These are the first components to be leached.

2) pH is 12.5 and is controlled by the solid Ca(OH)2 following leaching of alkali metals.

3) pH slowly moves to 10.5 as calcium silicate hydrate gel phases begin to dissolve
incongruently following loss of calcium hydroxide. Calcium:Silicon ratio drops to 0.85.

4) pH held at 10.5 by congruent dissolution of calcium silicate hydrate gel.

Leaching of calcium hydroxide tends to lower the strength of the cement.
Concrete Controlled Leaching Summary (Shrinking Core Model)
The Shrinking Core Model (Atkinson and Hearne, 1984) assumes that removal of Ca from the exterior of the concrete is rapid relative to the movement through the concrete (controlled by diffusion). Because the concrete is much less permeable than the surrounding geologic materials, water tends to flow laterally around the concrete structure. The intrinsic diffusion coeffient (Di) used in the Shrinking Core Model is for leached portion of the concrete and is therefore higher than Di for intact concrete. Permeablility and subsequently flow rate in the leached concrete will also be greater than for intact concrete. This may lead to conditions such that diffusion is no longer the dominant mode of transport.

The calcium concentration of the pore water in the concrete was taken from Walton et al. (1990) is 2.7E-3 moles/Liter (2.7E-6 mole/cm^3).

The calcium concentration in the surface/groundwater ranges from 2.50E-6 to 4.82E-4 moles/Liter (0.1 to 19.3 ppm) with mean and median values of 5.74E-5 and 2.35E-5 moles/Liter (2.3 and 0.94 ppm), respectively.

The following information was taken from "Properties of Concrete" (3rd edition), A. M. Neville, 1981, J. Wiley and Sons, Inc., NY, 779 p.

APPROXIMATE COMPOSITION LIMITS OF PORTLAND CEMENT

Species	%	Typical %
CaO	60-67	63
SiO2	17-25	20
Al2O3	3-8	6
Fe3O3	0.5-6	3
MgO	0.1-4	1.5
Alkalis	0.2-1.3	
SO3	1-3	2

MgO, TiO2, Mn2O3, K2O and Na2O are minor compounds and usually amount to no more than a few percent of cement by weight. The term alkalis refers to Na2O and K2O although other alkaline metals are present.

```
lchdcx = (2 dica vcsy (((capw vclc)-(cagwn vclc))/(cacsn vclc)) t)^0.5


      0.5 (tmp + tt)
301.216 10

Clear[dica]
t=10^tt
dica = 10^tmp
lchdcx = (2 dica vcsy (((capw vclc)-(cagwn vclc))/(cacsn vclc)) t)^0.5

Plot3D [lchdcx , {tt,2,4},{tmp,-7,-5},
Epilog->{
Text[ColumnForm[{"Time (yrs)"}],{0.15,0.1}],
Text[ColumnForm[{"D (sq cm/s)"}],{0.92,0.16}],
Text[ColumnForm[{"Leach","Pene.","(cm)"}],{0.03,0.65}]},
Shading->False ,PlotRange->All,
Ticks->{LogScale[2,4,3],LogScale[-7,-5,3],Automatic}]
```

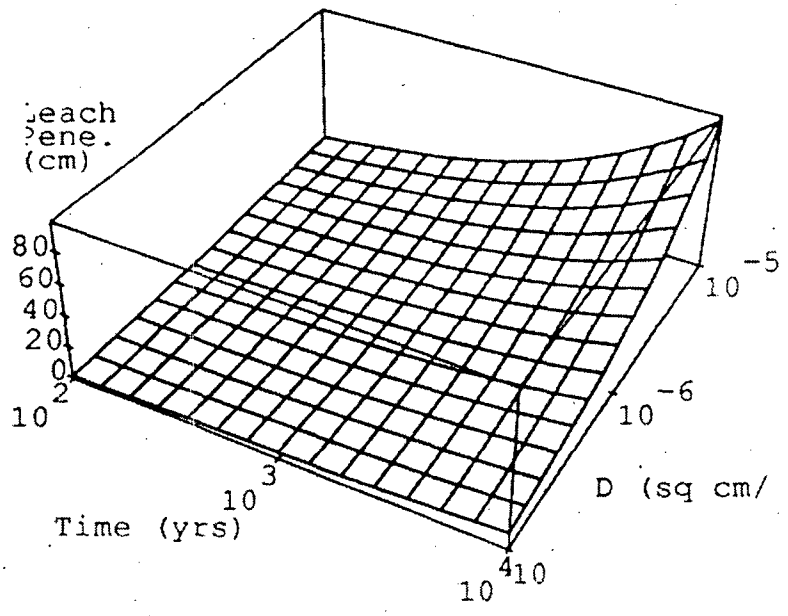


```
ccleach=Table[{lchdcx,N[t],N[dica]},{tt,2,4,0.1},{tmp,-7,-5,0.1}];


OpenWrite["/Projects/SR/Sept91/ccleach"]
Do[Write["/Projects/SR/Sept91/ccleach",
FortranForm[ccleach[[i,j,1]]],OutputForm[" "]
,FortranForm[ccleach[[i,j,2]]],OutputForm[" "]
,FortranForm[ccleach[[i,j,3]]]],{i,1,20},{j,1,20}]
Close["/Projects/SR/Sept91/ccleach"]
```

/Projects/SR/Sept91/ccleach

The following calculations are for Degradation of Saltstone Vault due to Geologic Controlled Leaching of Concrete.

An alternative to the Shrinking Core Model is also given by Atkinson and Hearne (1984) to be used when diffusion into the surrounding media is controlling the leaching. The equation describing Geology Controlled Leaching is

```
Clear[t]
lchdgx = 2 phix (((capw vclc)-(cagwn vclc))/((capw vclc)+(cacsn vclc)))*
(((rdx decax vcsy t)/Pi)^0.5)

ldgplt1 = Plot[{lchdgx},{t,tmin,tmax},PlotRange->{0.0001,1.5},
PlotStyle->{{RGBColor[1,0,0]}},
AxesLabel->{" Time (yr)",
ColumnForm[{" Leaching","Penetration","  (cm)"}]}]
```

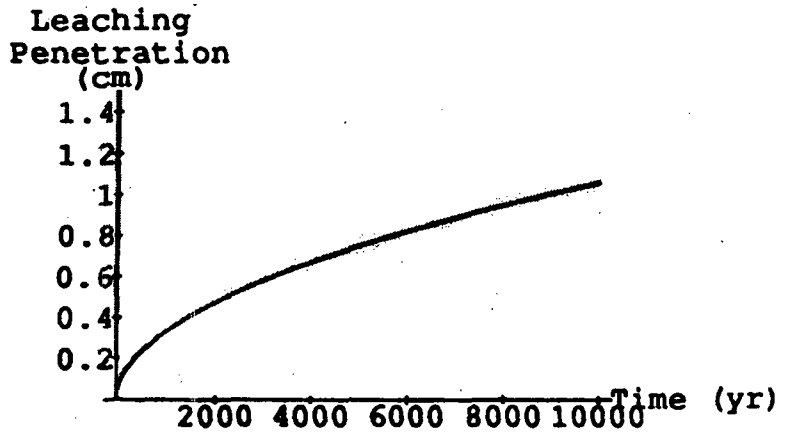


```
gcleach=Table[{N[lchdgx],N[t]},{tt,2,4,0.1}]

{{0.10576, 100.}, {0.118664, 125.893}, {0.133144, 158.489},

 {0.14939, 199.526}, {0.167618, 251.189}, {0.18807, 316.228},

 {0.211018, 398.107}, {0.236766, 501.187}, {0.265656, 630.957},

 {0.298071, 794.328}, {0.334442, 1000.}, {0.37525, 1258.93}

 {0.421037, 1584.89}, {0.472411, 1995.26}, {0.530054, 2511.89},

 {0.594731, 3162.28}, {0.667299, 3981.07}, {0.748721, 5011.87},

 {0.840079, 6309.57}, {0.942584, 7943.28}, {1.0576, 10000.}}

OpenWrite["/Projects/SR/Sept91/gcleach"]
```

/Projects/SR/Sept91/gcleach

```
Do[Write["/Projects/SR/Sept91/gcleach",
FortranForm[gcleach[[i,1]]],OutputForm[" "]
,FortranForm[gcleach[[i,2]]]]
,{i,1,21}]

Close["/Projects/SR/Sept91/gcleach"]
```

/Projects/SR/Sept91/gcleach

The following calculations are for Degradation of Saltstone Vault due to Carbonation of Concrete.

Carbonation refers to the process that forms carbonates when cement components react with carbon dioxide. The carbonation rate depends on the moisture content of the concrete and the relative humidity of the ambient medium. Slow diffusion in the concrete will allow equilibrium to be reached where the diffusion of carbon dioxide and carbonation are stopped or severly reduced. The type of cement ultimately affects the depth of carbonation.

The long term durability of the concrete is not adversely effected by carbonation. Carbonation does not cause general disruption or increased permeability of the concrete matrix. Calcium carbonate formation may increase retardation through solid solution reactions.

Shrinkage due to carbonation is thought to occur as minerals are removed from the areas of compressive stress and redeposited in regions of lower stress. The strength of concrete generally increases under carbonation with the exception of high sulfate concretes. The excess shrinkage may result in increased cracking cracking and/or joint permeability. Carbonation forces the local pH toward neutral, going from over 12 to abou 8, thereby removing some chemical barrier benefits of the concrete and providing a potentially corrosive environment for steel reinforcements if water, moisture and oxygen can penetrate.

The rate of carbonation is dependent upon water saturation or relative humidity of the environment. As relative humidity increases from 0 to 100%, the rate of carbonation passes through a maximum. The maximum rate of carbonation occurs because water is required in the reaction of carbon dioxide and calcium hydroxide to form calcium carbonate, but increasing water contents slow the diffusion rate of carbon dioxide through the concrete.

Summary of Shrinking Core Model for Carbonation
Carbonation can occur only as rapidly as dissolved carbonate can diffuse through teh concrete. Transport of carbonate through the concrete can occur either as carbonate in the aqueous phase or carbon dioxide in the vapor phase. Vapor phase diffusion is approximately four orders of magnitude more rapid than aqueous diffusion, therefore carbonation rates to increase as teh saturation level of the concrete decreases - at least until the water required for the reaction becomes in short supply. Carbonation rates have been found to peak at 50% relative humidity (Verbeck, 1958).

A shrinking core model for carbonation can be formulated by evaluating the migration rate of carbon dioxide into the concrete in relation to the initial amount of calcium hydroxide. Aqueous phase diffusion generally controls the transport of carbon dioxide in concrete even in the vadose zone due because the concrete tends to stay saturated due to small pore sizes relative to surrounding material.

Neville (1981) states "White cement has a slightly lower specific gravity than ordinary Portland Cement, generally between 3.05 to 3.10 g/cm^3 (dry cement)." If a porosity of 30% is used the density is 2.135 to 2.17 g/cm^3. The upper value will be considered to be 3.15 g/cm^3 based on this statement. This compares favorably with the values found in the specification document.

The cement is specified to be 144 to 147 PCF (lbs/ft^3) in specification document. This equates to a density of 2.33 to 2.38 g/cm^3 for the cement. The density of cement paste is approximately 2.35 g/cm^3. The range of calcium hydroxide is then 2.5e-2 to 3.0e-2 moles/cm3 with a typical value of 2.75e-2 moles/cm3. The assumption that all CaO is hydrated (Ca(OH)2) has been used in the following calculations. This is overestimating the degree of hydration as complete hydration seldom occurs. The range of CaO for Porland Cement ranges from 60 to 67% with a typical value of 63%.

The model used in this evaluation is valid only for water saturated concrete

```
dcarbn = (2 dico3 vcsy ((ticgwn vclc)/(chbcx vclc)) t)^0.5
dcarbx = (2 dico3 vcsy ((ticgwx vclc)/(chbcn vclc)) t)^0.5

crbplt1 = Plot[{dcarbn,dcarbx},{t,tmin,tmax},PlotRange->{0,15.0},
PlotStyle->{{RGBColor[1,0,0]},{RGBColor[0,1,0]}},
AxesLabel->{ColumnForm[{"  Time","  (yrs)"}],
ColumnForm[{" Depth of","Carbonation","  Attack","  (cm)"," "}]}]
```

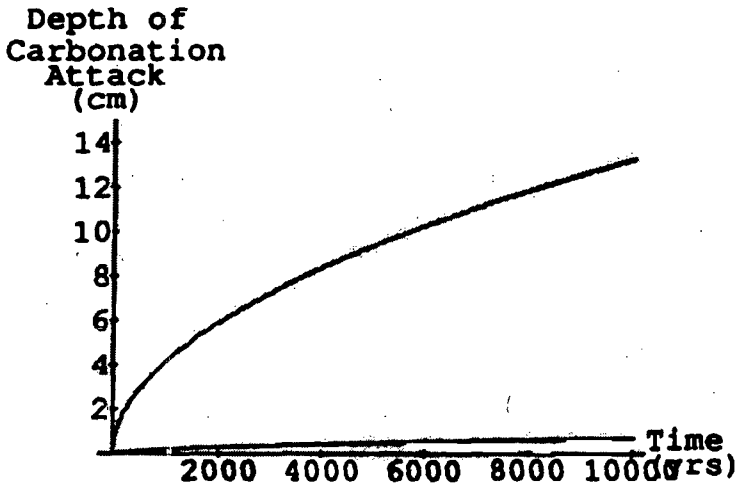


```
Clear[dico3]
dico3 = 10^tmp
t = 10^tt
 dcarbx = (2 dico3 vcsy ((ticgwx vclc)/(chbcn vclc)) t)^0.5

Plot3D [dcarbx, {tt, 2,4},{tmp,-8,-5},
AxesLabel->{ColumnForm[{"Time","(yrs)"}],
ColumnForm[{"D (sq cm/s)"}],
ColumnForm[{"Depth","(cm)"}]},Ticks->
{LogScale[2,4,3],LogScale[-8,-5,4],Automatic},Shading->False,
PlotRange->All ]
```

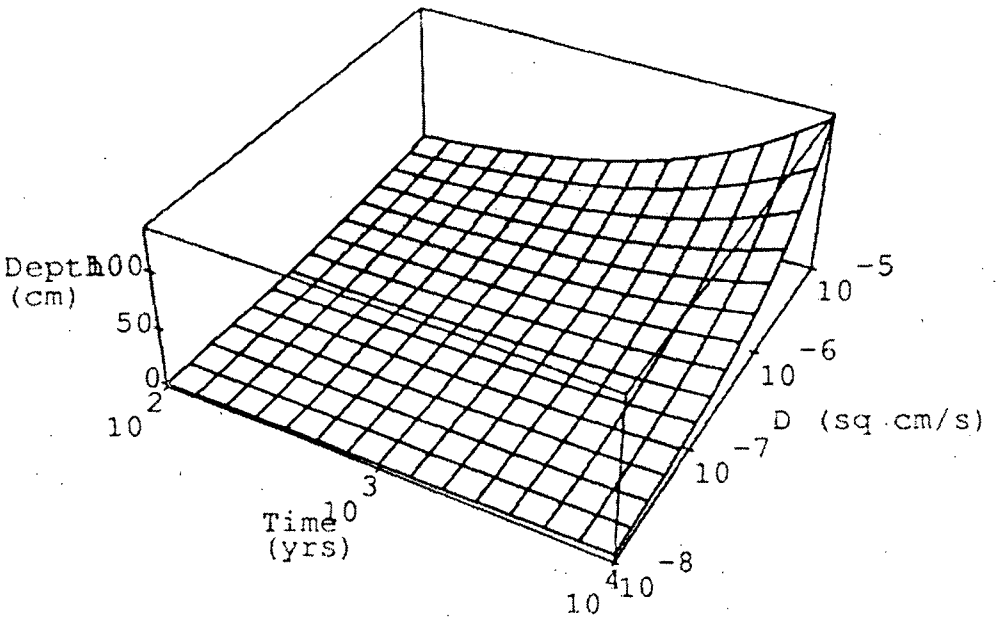


```
carbo=Table[{dcarbx,N[t],N[dico3]},{tt,2,4,0.1},{tmp,-8,-5,0.1}];

OpenWrite["/Projects/SR/Sept91/carbo"]
Do[Write["/Projects/SR/Sept91/carbo",
FortranForm[carbo[[i,j,1]]],OutputForm[" "]
,FortranForm[carbo[[i,j,2]]],OutputForm[" "]
,FortranForm[carbo[[i,j,3]]]],{i,1,20},{j,1,20}]
Close["/Projects/SR/Sept91/carbo"]
"/Projects/SR/Sept91/carbo"
```

/Projects/SR/Sept91/carbo

RESPONSE TO RAI COMMENT #41
ROADMAP TO REFERENCES

REFERENCED DOCUMENT	*EXCERPT LOCATION	REMARK
Bradbury and Sarott (1995)	Page 251 = Excerpt included	Additional details are provided in Table 50-2, in response to Comment 50.
Cook et al 2005 (WSRC-TR-2005-00074)	Page 248 = Representative excerpt enclosed	This reference is included in its entirety for information.
Kaplan and Hang 2003 (WSRC-RP-2003-00362)	Page 248, 250 = Excerpt included in response	
Lukens et al. 2005	Page 249, 250, 251 = Excerpt included in response	
Saltstone PA (WSRC-RP-92-1360)	Page 248 = Representative excerpt enclosed Page 249 = Excerpt enclosed	This reference is included in its entirety for information. Attach Appendix D
Smith and Walton 1993 (ref. 16)	Page 249, 251 = Excerpt enclosed following response	This reference is included in its entirety for information.

*Excerpt Locations:

1. Excerpt included in response: The excerpt is included within the text of the response or is appended to the response.
2. Excerpt enclosed following response: The excerpt is enclosed on a separate sheet or sheets following the response.
3. Representative excerpt(s) enclosed following response: Representative excerpts from a document that is wholly or largely applicable are enclosed following the response.
4. Other

7/14/2005

Evolution of Technetium Speciation in Reducing Grout

Wayne W. Lukens, Jerome J. Bucher, David K. Shuh, and Norman M. Edelstein*

Actinide Chemistry Group

Chemical Sciences Division

Lawrence Berkeley National Laboratory

Berkeley, CA 94720

wwlukens@lbl.gov, phone: (510) 486-4305, FAX: (510) 486-5596

RECEIVED DATE (to be automatically inserted after your manuscript is accepted if required according to the journal that you are submitting your paper to)

ABSTRACT Cementitious waste forms (CWFs) are an important component of the strategy to stabilize high-level nuclear waste resulting from plutonium production by the U.S. Department of Energy (DOE). Technetium (^{99}Tc) is an abundant fission product of particular concern in CWFs because of the high solubility and mobility of Tc(VII), pertechnetate (TcO_4^-) the stable form of technetium in aerobic environments. CWFs can more effectively immobilize ^{99}Tc if they contain additives that reduce mobile TcO_4^- to immobile Tc(IV) species. The ^{99}Tc leach rate of reducing CWFs that contain Tc(IV) is much lower than for CWFs that contain TcO_4^-. Previous X-ray absorption fine structure (XAFS) studies showed that Tc(IV) species were oxidized to TcO_4^- in reducing grout samples prepared on a laboratory scale. Whether the oxidizer was atmospheric O_2 or NO_3^- in the waste simulant was not determined. In actual CWFs, rapid oxidation of Tc(IV) by NO_3^- would be of concern, whereas oxidation by atmospheric O_2 would be of less concern due to the slow diffusion and reaction of O_2 with the reducing CWF. To address this uncertainty, two series of reducing grouts were prepared using TcO_4^- containing

waste simulants with and without NO_3^-. In the first series of samples, referred to as "permeable samples", the TcO_4^- was completely reduced using Na_2S, and the samples were sealed in cuvettes made of polystyrene, which has a relatively large O_2 diffusion coefficient. In these samples, all of the technetium was initially present as a Tc(IV) sulfide compound, TcS_x, which was characterized by extended X-ray absorption fine structure (EXAFS) spectroscopy. The EXAFS data is consistent with a structure consisting of triangular clusters of Tc(IV) centers linked together through a combination of disulfide and sulfide bridges as in MoS_3. From the EXAFS model, the stoichiometry of TcS_x is Tc_3S_{10}, and TcS_x is presumably the compound generally referred to as Tc_2S_7. The TcS_x initially present in the permeable samples was steadily oxidized over 4 years. In the second series of samples, called "impermeable samples", the TcO_4^- was not completely reduced initially, and the grout samples were sealed in cuvettes made of poly(methyl methacrylate), which has a small O_2 diffusion coefficient. In the impermeable samples, the remaining TcO_4^- continued to be reduced, presumably by blast furnace slag in the grout, as the samples aged. When the impermeable samples were opened and exposed to atmosphere, the lower-valent technetium species were rapidly oxidized to TcO_4^-.

MANUSCRIPT TEXT

Introduction Remediation of the sites used by the U. S. Department of Energy (DOE) for plutonium production is one of the most expensive and complex remediation projects in the U. S.[1,2] An important component of this effort is the use of grout based cementitious waste forms (CWFs) at the Savannah River Site to solidify and stabilize the low-activity waste stream and to stabilize the waste residues in high-level tanks.[3-6] The long-term effectiveness of these measures to prevent the migration of radionuclides is described by performance assessments that depend on the leach rates of the radionuclides.[3,5,7,8] ^{99}Tc is one of the radionuclides of greatest concern for leaching from CWFs because of the high mobility and lack of sorption of Tc(VII), pertechnetate (TcO_4^-), the most stable form of technetium under aerobic conditions.[8,9]

For soluble contaminants such as TcO_4^- or NO_3^-, leach rates from CWFs can be modeled using an effective diffusion coefficient, $D_{eff} = D_m/N_m$, where D_m is the molar diffusion coefficient of the contaminant in water and N_m is the MacMullin number, a characteristic of the porous solid that is identical for solutes such as gases or anions that are highly soluble and not adsorbed by the matrix.[10,11] Among potential CWFs, the effective diffusion coefficient of nitrate, $D_{eff(NO3-)}$, varies from 1.3×10^{-9} cm^2 s^{-1} to 6.2×10^{-8} cm^2 s^{-1}.[5,9,12] The D_{eff} values for NO_3^- and TcO_4^- are similar since their molar diffusion coefficients are almost identical: 1.53×10^{-5} cm^2 s^{-1} and 1.48×10^{-5} cm^2 s^{-1}, respectively.[13,14] The leachability of technetium can be greatly decreased by reducing soluble TcO_4^- to relatively insoluble Tc(IV) by the addition of blast furnace slag (BFS) or other reductants to the grout. The $D_{eff(99Tc)}$ values of reducing grouts are much smaller than in ordinary CWFs, 3×10^{-11} cm^2 s^{-1} to 4×10^{-12} cm^2 s^{-1}, because Tc(IV) has low solubility and is readily adsorbed by the grout matrix.[9,12] Reducing conditions are used in actual CWFs to take advantage of this decreased leachability and create a more effective waste form.[6,12]

A previous research study showed that although TcO_4^- is reduced to Tc(IV) in reducing grouts, the degree of reduction varied with experimental conditions.[15] In some cases, TcO_4^- was initially reduced to Tc(IV) but was later oxidized. Two species, NO_3^- and O_2, are present in large quantities in or around CWFs and are potentially capable of oxidizing Tc(IV) to TcO_4^-. Whether NO_3^- or O_2 is responsible for oxidizing Tc(IV) has a profound effect on the behavior of technetium in CWFs. If NO_3^- is chiefly responsible for the oxidation, Tc(IV) would be oxidized throughout the entire CWF, increasing the leachability of ^{99}Tc in the entire volume of the waste. In this scenario, the rate of oxidation of Tc(IV) to TcO_4^- would depend only on the reaction rate and the concentration of the reactants.

The scenario involving oxidation by O_2 is more complicated. In this case, diffusion of O_2 into the CWF would result in the formation of an oxidized surface region in the grout in contact with oxygenated

surface water. This surface region would have greater technetium leachability that would be similar to that of CWFs that do not contain reducing agents. However, the leachability of technetium in the bulk of the waste would be unchanged since it would remain Tc(IV). As shown by Smith and Walton, the thickness of the oxidized region depends mainly upon the rate of oxygen diffusion and the reductive capacity of the CWF.[16] Using typical parameters for reducing CWFs, the thickness of the oxidized region is small compared to the dimensions of the CWF at times comparable to the half-life of ^{99}Tc, so oxidation by O_2 is of less concern than oxidation by NO_3^-.

Therefore, the primary concern raised by the rapid oxidation of Tc(IV) observed in the previous study was the possibility that NO_3^- rather than O_2 was responsible for the oxidation. Rapid oxidation of Tc(IV) by NO_3^- would mean that all of the initially reduced technetium in actual CWFs would be quickly oxidized back to TcO_4^-. In this paper, the evolution of ^{99}Tc speciation in a series of grout samples in containers with very different O_2 permeabilities and with and without NO_3^- was followed for an extended period, using X-ray absorption fine structure (XAFS), to determine whether NO_3^- or O_2 was responsible for oxidizing Tc(IV) species in these grout samples.

Experimental Section

Procedures. *Caution: ^{99}Tc is a β-emitter (E_{max} = 294 keV, $\tau_{1/2} = 2 \times 10^5$ years).* All operations were carried out in a radiochemical laboratory equipped for handling this isotope. Technetium, as $NH_4^{99}TcO_4$, was obtained from Oak Ridge National Laboratory and was purified as previously described.[17] Where available, the standard deviation of measured and calculated values are included in parentheses following the value and are in the same units as the last digit.

All operations were carried out in air. Water was deionized, passed through an activated carbon cartridge to remove organic material and then distilled. All other chemicals were used as received. The grout samples are similar to those previously used for the study of chromium reduction in reducing

grout samples and are similar to Saltstone, the CWF used to immobilize low activity waste at the Savannah River Site.[12,18] The dry grout components consisted of 46% Type F fly ash, 46% BFS, and 8% Portland cement.[18] The fly ash, BFS, and Portland cement are those used by the Savannah River Saltstone facility, and were provided by C. A. Langton. Two series of grout samples were prepared and were assumed to have a density of 1.7 g cm^{-3}.[19] The cuvettes were standard semi-micro cuvettes with interior dimensions of 1.0 × 0.4 × 4.5 cm.

The first series of samples was prepared using waste simulants with and without NO_3^- and NO_2^- as shown in Table 1. To the waste simulant was added TcO_4^- (0.02 mmol, 0.1 mL, 0.2 M NH_4TcO_4), which was then reduced with Na_2S (0.29 mmol, 0.1 mL, 2.9 M) in 1 M LiOH forming a very dark solution with a black precipitate. The dry grout components were added forming a slurry that was placed in a polystyrene (PS) cuvette, which was capped and closed with vinyl tape then sealed inside two 0.05 mm polyethylene (PE) bags. This first series of samples will be referred to as "permeable samples" since O_2 has a high diffusion coefficient of 2.3×10^{-7} cm^2 s^{-1} in PS.[20,21] The final composition of the waste solution after addition of the TcO_4^- and Na_2S solutions is listed in Table 1.

The second series of samples was prepared analogously to the first. To the waste simulant was added TcO_4^- (0.012 mmol, 0.30 mL, 0.039 M $NaTcO_4$) and Na_2S (0.05 mmol, 0.065 mL, 0.8 M) in 1 M LiOH (same solution as above, which had oxidized from air exposure), forming a dark solution with a black precipitate. The dry grout components were added, forming a slurry that was placed in a poly-(methyl methacrylate) (PMMA) cuvette that was sealed with a plug of epoxy and further sealed inside two 0.1 mm (PE) bags. This second series of samples will be referred to as "impermeable samples" since O_2 has a very low diffusion coefficient of 2.3×10^{-9} cm^2 s^{-1} in PMMA.[22] The final composition of the waste solution after addition of the TcO_4^- and Na_2S solutions is also listed in Table 1. Samples A and C were opened after 26 months and placed in loosely capped jars that were fully opened weekly. The grout

samples removed from the cuvettes and used for XAFS studies measured 1.0 × 0.4 × ~1.0 cm, and retained the flat surfaces of the cuvette. Sample B remained sealed.

Table 1: Composition of cement samples

Sample	Tc (mg)	Solution (mL)	Final Solution Composition	Dry grout mixture (g)
			Permeable Samples	
1	2	1.5	1.85 M $NaNO_3$, 1.07 M NaOH, 0.57 M $NaNO_2$, 0.23 M $NaAl(OH)_4$, 0.16 M Na_2CO_3, 0.14 M Na_2SO_4, 0.02 M NaCl, 0.02 M $Na_2C_2O_4$, 0.008 M Na_3PO_4, 0.13 M Na_2S	3
2	2	1.5	As Sample 1, but no $NaNO_3$, $NaNO_2$	3
3	2	0.95	As Sample 1, but 0.05 M Na_3PO_4	1.5
4	2	0.95	As Sample 2, but 0.05 M Na_3PO_4	1.5
			Impermeable Samples	
A	1.2	0.66	2 M NaOH, 2 M NaCl	1.0
B	1.2	0.66	2 M NaOH, 2 M $NaNO_3$	1.0
C	1.2	0.66	2 M NaOH, 2 M $NaNO_2$	1.0

The reductive capacity of the BFS was determined using a slightly modified version of the Angus and Glasser method.[23] The BFS (~0.5 g) was slurried in 5-10 mL of water to which was added 25.0 mL of 0.059 M $(NH_4)_4Ce(SO_4)_4 \cdot 2H_2O$ in 2 M sulfuric acid. After 1 hour, the solution was titrated with freshly prepared 0.050 M $(NH_4)_2Fe(SO_4)_2 \cdot 6H_2O$ in 0.75 M sulfuric acid. The end point was determined using 0.25 mL of 0.025 M Fe(II) tris-(1,10-phenanthroline) complex.[24,25] The reductive capacity of the BFS sample was 0.82(1) meq g^{-1} as determined from the difference in the volume of Fe(II) solution needed to titrate 25.0 mL of the Ce(IV) solution alone and with the BFS. Analysis of the sulfide content of

Na_2S in 1 M LiOH, which was used to reduce the TcO_4^- in the grout samples, was performed analogously by comparison with a sample of freshly recrystallized $Na_2S \cdot 9H_2O$. Determination of the reductive capacity of BFS using Cr(VI) as the oxidizer has also been reported and gives much smaller values than the Angus and Glasser method.[19]

XAFS spectra were acquired at the Stanford Synchrotron Radiation Laboratory (SSRL) at Beamline 4-1 using a Si(220) double crystal monochromator detuned 50% to reduce the higher order harmonic content of the beam. All ^{99}Tc samples were triply contained. X-ray absorption spectra were obtained in fluorescence yield mode using a multi-pixel Ge-detector system.[26] In all cases, the grout samples were oriented at 45° relative to both the photon beam and the fluorescence detector. The cuvettes were positioned horizontally as illustrated in Figure 1. The spectra were energy calibrated using the first inflection point of the Tc K-edge spectrum of TcO_4^- adsorbed on Reillex-HPQ™ anion exchange resin defined as 21044 eV.

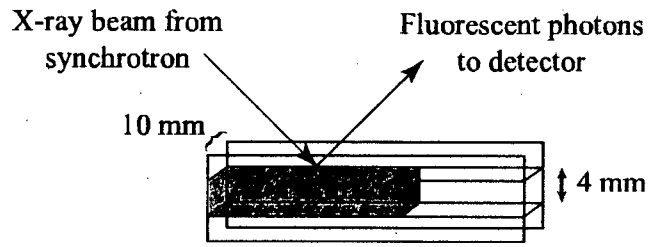

Figure 1: Geometry of a grout sample in semi-micro cuvette used in XAFS experiments.

Extended X-ray absorption fine structure (EXAFS) data analysis was performed by standard procedures[27] using the programs ifeffit,[28] and Athena/Artemis;[29] theoretical EXAFS phases and amplitudes were calculated using FEFF7[30]. All fitting was performed in R-space (R range: 1 to 4.5 Å; k range: 2 to 13.3 $Å^{-1}$; 27 independent points[31]) on k^3 weighted data. Kaiser-Bessel windows were applied to both the R-space and k-space data, with widths of 0.1 Å and 1 $Å^{-1}$, respectively. The EXAFS data for these samples were analyzed with three different models. Model one had only two shells of

neighboring atoms: ~7 S neighbors at 2.38 Å and ~2 Tc neighbors at 2.77 Å. Model two had an additional shell of 6-11 S neighbors with a large static disorder at 4.5 Å. Model three was similar to the second model with an additional Tc neighbor at either 3.8 Å (~1/3 occupancy) or 4.3 Å (~2/3 occupancy). The model chosen as most appropriate was the one whose fit gave the lowest reduced chi-squared, χ^2/ν, where ν is the number of degrees of freedom of the fit: 20, 17, and 13 for models one, two, and three, respectively. For samples 2, 3, and 4, the best model was model three, and for sample 1, model two was slightly better than model three. In addition, all four data sets were fit simultaneously to a single set of parameters for a given model. In this case, the numbers of degrees of freedom were 101, 98, and 94 for models one, two, and three, respectively, and model three gave the best fit.

The X-ray absorption near edge structure (XANES) spectra of the samples were fit using a linear combination the XANES spectra of TcS_x, TcO_4^-, and $TcO_2 \cdot 2H_2O$ as standards, and only the energy calibration of the samples were allowed to vary. This procedure required the careful energy calibration of the XANES spectra of the standards. The fitting was done using the code "fites" developed by C. H. Booth.[32] The fit used 4 parameters (amplitudes of each standard and the energy shift of the sample spectrum), and the XANES spectra had 19 independent data points (150 eV spectra with 8 eV spectral resolution due to a combination of core hole lifetime and instrumental resolution).

The X-ray absorption coefficients for Sample A were determined using Eq 1 where ρ is the sample density (1.7 g cm^{-3}),[19] w_i is the wt. % of element i in the sample, and μ_i is the absorption coefficient of element i (in $cm^2\ g^{-1}$).[33,34] The elemental composition of sample A was determined from the fraction of waste solution, BFS, fly ash, and Portland cement used to prepare the sample, and the elemental compositions of BFS, fly ash, and Portland cement reported by Serne, et al. were used.[5] The X-ray absorption coefficients of sample A at the incident and fluorescent photon energies, $\mu_{tot}(E)$ and $\mu_{tot}(E_f)$, are 5.2 cm^{-1} and 7.5 cm^{-1}, respectively.

$$\mu_{tot} = \rho \sum w_i \mu_i \qquad (1)$$

Results and Discussion

EXAFS studies of initial technetium speciation. A prerequisite for investigating the long-term behavior of technetium in grout is identifying which technetium species are present. While it is obvious that TcO_4^- will be present under oxidizing conditions,[35] the species present under reducing conditions are less obvious. The hydrous Tc(IV) oxide, $TcO_2 \cdot 2H_2O$, results from the reduction of TcO_4^- in the absence of other ligands both in solution and in grout samples.[15,36] In addition, sulfide, either BFS or added to the grout as Na_2S, reduces TcO_4^- to a lower-valent technetium sulfide species thought to be similar to TcS_2.[15] Interestingly, the reaction of sulfide with TcO_4^- in alkaline solution is a known route to Tc_2S_7,[37] which is generally believed to be the technetium species present in reducing CWFs.[16,37] While these results appear to be contradictory, the inconsistency is largely due to the Tc(VII) oxidation state implied by the stoichiometry of Tc_2S_7. If Tc_2S_7 is not actually a Tc(VII) sulfide complex but a lower-valent disulfide complex, no contradiction exists between these previous studies. Although Tc_2S_7 is generally assumed to be a Tc(VII) compound, this assumption has never been examined.[14]

To identify the technetium sulfide species present in reducing grouts, the Tc K-edge EXAFS spectra of the permeable samples were examined shortly after they were prepared. Only these samples contained a single technetium species. All other samples, including these samples at later times, contained more than one species. The permeable samples initially had identical Tc K-edge EXAFS spectra, as shown in Figure 2. The parameters derived by fitting the spectra are listed in Table 2. Therefore, in addition to containing only one technetium species, all of these samples contain the same technetium species, which will be referred to as TcS_x.

Table 2: Initial technetium coordination environment in the permeable samples[a]

Scattering Atom		Sample 1[b]	2	3	4	All data[c]
	N[d]	7.3(5)	7.6(6)	7.0(5)	7.4(6)	7.4(2)
S	R(Å)[e]	2.379(5)	2.376(6)	2.381(5)	2.380(5)	2.378(2)
	σ^2(Å^2)[f]	0.0111(7)	0.0118(9)	0.0113(7)	0.0121(8)	0.0117(3)
	N[d]	1.9(4)	1.8(5)	1.6(4)	1.7(4)	1.8(2)
Tc	R(Å)[e]	2.771(4)	2.771(5)	2.779(5)	2.776(5)	2.774(2)
	σ^2(Å^2)[f]	0.007(1)	0.007(1)	0.007(1)	0.007(1)	0.0071(5)
	N[d]	0.3[g]	0.4[g]	0.3[g]	0.3[g]	0.4[g]
Tc	R(Å)[e]	3.80(4)	3.83(3)	3.83(3)	3.86(3)	3.84(1)
	σ^2(Å^2)[f]	0.007[g]	0.005[g]	0.004[g]	0.004[g]	0.006[g]
	N[d]	0.7(2)	0.6(2)	0.7(2)	0.7(1)	0.6(1)
Tc	R(Å)[e]	4.30(3)	4.28(2)	4.29(2)	4.30(3)	4.30(1)
	σ^2(Å^2)[f]	0.006(2)	0.005(2)	0.004(1)	0.004(2)	0.006(1)
	N[d]	11(11)	6(6)	6(6)	6(5)	5(2)
S	R(Å)[e]	4.48(3)	4.47(3)	4.48(3)	4.49(3)	4.47(1)
	σ^2(Å^2)[f]	0.02(1)	0.02(1)	0.01(1)	0.01(1)	0.012(4)
	ΔE_0	0.4(7)	0.8(8)	0.6(7)	0.5(8)	0.7(3)
	R[h]	0.078	0.096	0.082	0.085	0.102

a) The number in parentheses is the standard deviation of the parameter obtained by fitting the EXAFS data. In comparison to crystallographic data, N differs by up to 25%, and in R by 0.5%.

b) The best model for the EXAFS spectrum of sample 1 did not include the Tc shells at 3.82 and 4.31 Å, but this model is included for comparison with the other samples.

c) All data fit simultaneously using a single set of parameters.

d) N: number of neighboring atoms.

e) R: distance from the scattering atom to the technetium center.

f) σ^2: Debye-Waller parameter, the amount of disorder in the distance to the neighboring atoms.

g) Parameter determined from the corresponding parameter in the following shell.

h) $\text{R-factor} = \left(\sum(y_i(\text{data}) - y_i(\text{fit}))^2 / \sum(y_i(\text{data}))^2\right)^{1/2}$.

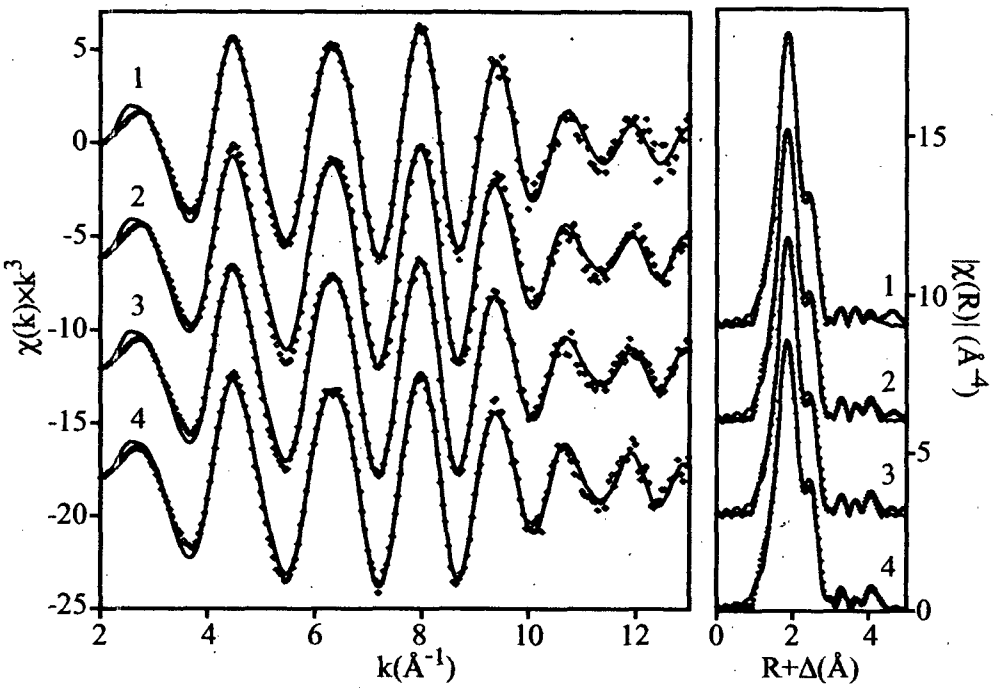

Figure 2: Tc K-edge EXAFS spectra (left) and their Fourier transforms (right) of the technetium species initially present in grout samples prepared by reducing the TcO_4^- with excess sodium sulfide. Data is shown as dots and the fits are shown as lines (Fit range: k = 2 to 13.3 $Å^{-1}$; R = 1 to 4.5 Å). Sample numbers are indicated next to the traces.

The coordination environment of TcS_x can be described by considering the first two and last three coordination shells separately. The first two coordination shells, which comprise the largest features in the Fourier transforms, consist of ~7 sulfur neighbors at 2.37 Å and 2 technetium nearest neighbors at 2.77 Å. These distances and coordination numbers are similar to those of the molybdenum sulfide complex, $Mo_3(\mu^3\text{-}S)(S_2)_6^{2-}$, shown in Figure 3, in which each molybdenum center has 7 sulfur and 2 molybdenum neighbors at 2.44 and 2.72 Å, respectively.[38] The $Mo_3(\mu^3\text{-}S)(\mu\text{-}S_2)_3$ core of this complex, without the triply bridging sulfide, forms the building block of the MoS_3 structure,[39] which has an EXAFS spectrum similar to that of TcS_x.[40,41] The nearest neighbor environments in both compounds are analogous; in MoS_3, each molybdenum center has ~6 sulfur neighbors at 2.44 Å and 2 molybdenum neighbors at 2.75 Å. The similarities of the distances and coordination numbers of the first two

coordination shells of MoS_3, $Mo_3S(S_2)_6^{2-}$ and TcS_x strongly suggest that the TcS_x structure contains the same triangular core, $Tc_3(\mu^3\text{-}S)(\mu\text{-}S_2)_3S_6$ as shown in Figure 3. Furthermore, the 2.77 Å Tc-Tc distance is typical for such a triangular complex composed of seven-coordinate metal centers; analogous triangular complexes with six-coordinate metal centers have substantially shorter metal-metal distances.[42]

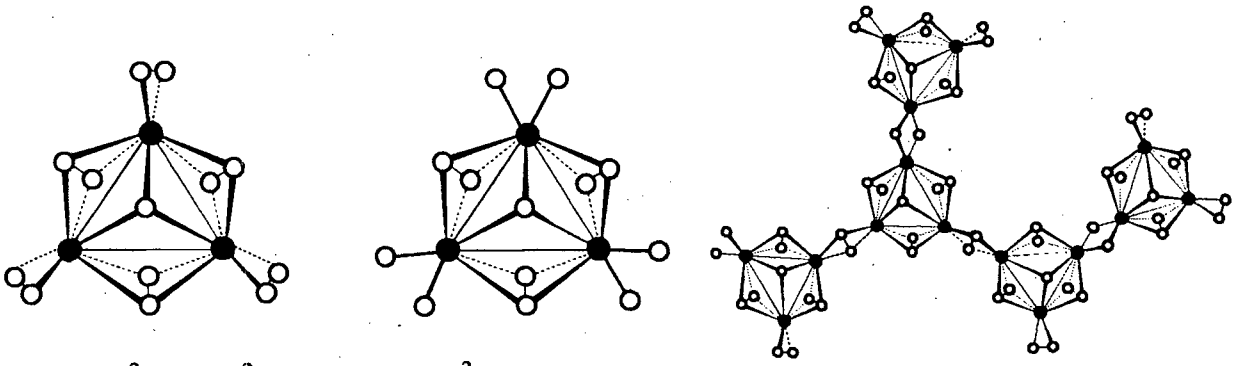

$Mo_3(\mu^3\text{-}S)(S_2)_6^{2-}$ $Tc_3(\mu^3\text{-}S)(S_2)_3S_6$ core $Tc_3S_2(S_2)_4$ ("TcS_x")

Figure 3: Structures of $Mo_3(\mu^3\text{-}S)(S_2)_6^{2-}$, the proposed structure of the analogous $Tc_3(\mu^3\text{-}S)(S_2)_3S_6$ core that forms the building block of TcS_x, and the proposed structure of TcS_x (only a portion of the extended structure is illustrated). Metal atoms are illustrated by solid circles, sulfur atoms are depicted by open circles.

The last three coordination shells give rise to the small features at higher R in the Fourier Transform. The uncertainty in the assignments of these last shells is much greater than for the first two shells except for the additional sulfur atoms at 4.5 Å, which much be present in the $Tc_3(\mu^3\text{-}S)(S_2)_3S_6$ core. In addition to the additional sulfur atoms, each technetium has a next-nearest technetium neighbor at either 3.8 Å (~1/3 of the technetium centers) or 4.3 Å (~2/3 of the technetium centers). The two different Tc-Tc distances suggest that different ligands bridge the technetium centers. Since the presence of 7 first shell sulfur neighbors requires that each technetium center has two sulfur atoms capable of bridging adjacent technetium centers, possible identities of the bridging ligands are two bridging sulfide (or hydrosulfide) ligands or an edge-bound disulfide similar to the bridging disulfide of the $Tc_3(\mu^3\text{-}S)(\mu\text{-}S_2)_3$ cluster

without the Tc-Tc bond. The Tc-Tc distance of two technetium centers symmetrically bridged by an edge-bound disulfide ligand would be close to 4.3 Å. In a similar copper complex,[43] two Cu centers are separated by 4.03 Å, but the Tc-S bonds in TcS_x are 0.1 Å longer than the Cu-S bonds. Moreover, the S-S distance of the disulfide bridge, determined from the Tc-Tc and Tc-S distances, must be 2.0 Å, typical for a bridging disulfide.[38,43] For these reasons, the 4.3 Å Tc-Tc distance is assigned to two Tc centers symmetrically bridged by a disulfide ligand.

The 3.8 Å Tc-Tc distance could be due to either two bridging sulfide or hydrosulfide ligands. If the Tc and S atoms are coplanar, the Tc-Tc and Tc-S distances produce a Tc-S-Tc angle of 109°. Although few families of complexes exist in which the parameters for bridging sulfide and hydrosulfide ligands can be compared directly, a M-S-M angle of 109° is more typical of a bridging sulfide than of a hydrosulfide, which generally have M-(SH)-M angles of ~100°.[44-46] For this reason, the 3.8 Å Tc-Tc distance is assigned to two Tc centers symmetrically bridged by two sulfide ligands. Overall, the EXAFS data is consistent with a TcS_x structure composed of triangular $Tc_3(\mu^3\text{-}S)(\mu\text{-}S_2)_3$ clusters linked by either bridging disulfide or by two bridging sulfide ligands as shown in Figure 3.

Although the assignments of the last two technetium scattering shells in the EXAFS spectrum of TcS_x is much less certain than the assignments of the other three shells, the resulting model provides the best fit to the data as judged by the reduced χ^2 value. In addition, the resulting bond distances can be interpreted in a chemically meaningful and reasonable manner. For these reasons, the model that best describes the EXAFS spectrum of TcS_x is the one given in Table 2 and shown in Figure 3.

The structure of TcS_x has a stoichiometry of $Tc_3S_2(S_2)_4$ or Tc_3S_{10}, which is almost identical to the stoichiometry of $TcS_{3.2}$ determined for "Tc_2S_7" prepared under similar conditions.[37] Since the conditions used to prepare grout samples are analogous to those used to prepare Tc_2S_7, it seems likely

that TcS_x and Tc_2S_7 are the same compound. However, the technetium centers in TcS_x are clearly not heptavalent. From the EXAFS model, TcS_x would be a Tc(IV) compound, which is consistent with its Tc-K edge absorption energy, 6.5 eV below that of TcO_4^-. For comparison, the energies of the Tc-K edges of Tc(IV) complexes with oxygen coordination shells occur at ~5.5 eV below that of TcO_4^-.[17] Consequently, the technetium sulfide species present in reducing containing grouts, TcS_x, appears to be Tc_2S_7 as previously suggested;[16,37] however, the technetium centers in TcS_x are most likely tetravalent in agreement with the previous XAFS study.[15]

Evolution of technetium speciation determined by XANES spectroscopy. The speciation of technetium in the grout samples was determined by least squares fitting of the XANES spectra using the XANES spectra of $TcO_2 \cdot 2H_2O$, TcO_4^-, and TcS_x as components. This method is analogous to those previously described by Ressler et al. and Panak et al., which have been shown to yield quantitative speciation information assuming that appropriate, correctly calibrated standards are employed.[47,48] The results for the evolution of technetium speciation in the permeable and impermeable samples is addressed separately.

Permeable samples. As described in the previous section, the technetium speciation of all the permeable samples was initially identical since all samples contained only TcS_x. However, as the samples aged, their XANES spectra changed as shown in Figure 4, which also shows the deconvolution of the XANES spectrum of a 45-month-old sample. The mole fraction of TcO_4^- in these samples is shown in Figure 5 as a function of the age of the sample. The scatter of the data shown in Figure 5 is much greater than the standard deviation of the measurement and will be discussed below. Unfortunately, this large degree of scatter results in a correspondingly large uncertainty in the rate of oxidation of Tc(IV) in these samples. However, Figure 5 shows that NO_3^- does not play a major role in the oxidation of Tc(IV) in these samples since the degree of oxidation of all samples is approximately equivalent despite the fact that samples 2 and 4 do not contain NO_3^-.

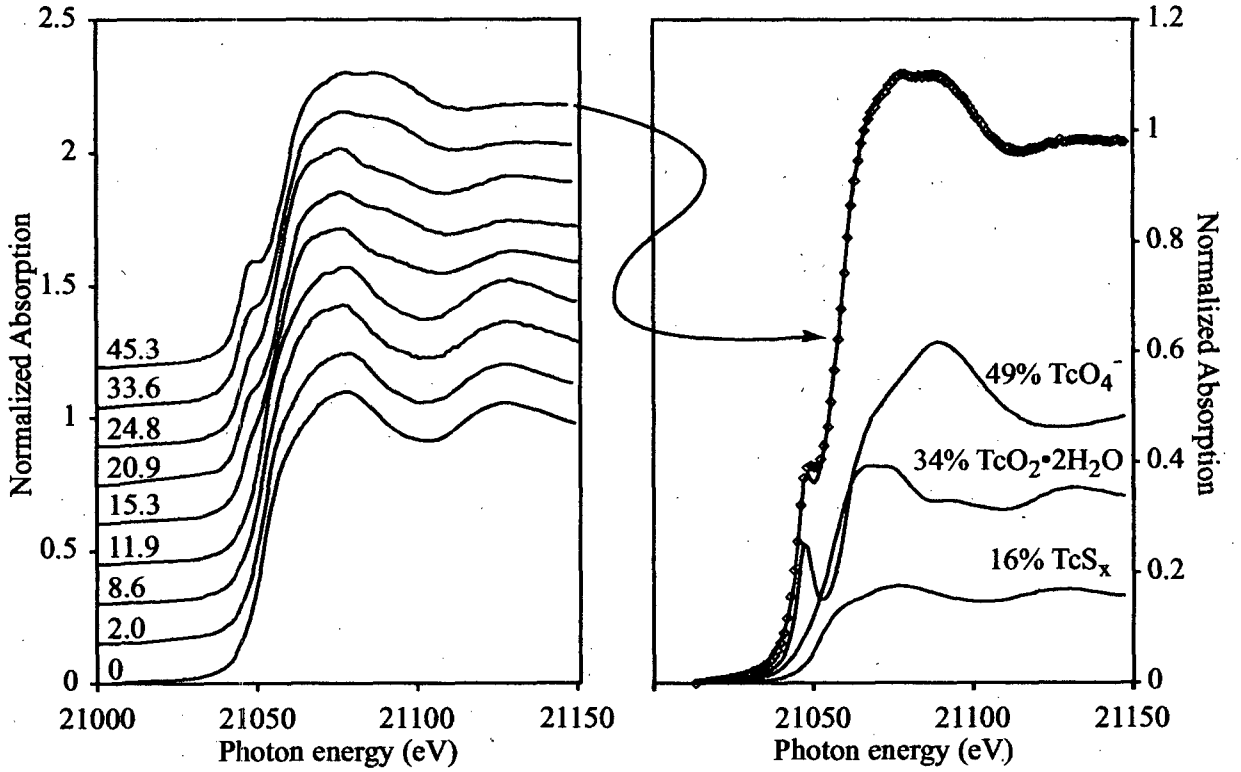

Figure 4: (left) Evolution of the Tc-K edge XANES spectra of sample 4 as a function of age. The age of cement (in months) is given next to the corresponding spectrum. (right) Deconvolution of the XANES spectrum of a 45 month old sample. Data are shown as dots and the least squares fit is shown as a line.

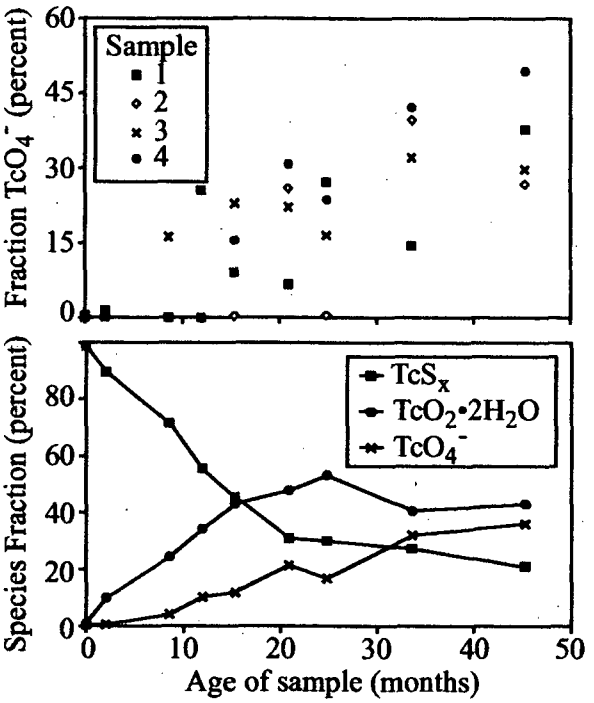

Figure 5: (upper) Evolution of the fraction of technetium present as TcO_4^- in the permeable samples as a function of age. (lower) Evolution of technetium speciation in the permeable samples averaged over all samples.

Permeable samples. In contrast to the permeable samples, ~20% of the TcO_4^- in the impermeable samples was not reduced to Tc(IV) at the beginning of the experiment. However, as the samples aged, the amount of TcO_4^- decreased, as shown in Figure 6, presumably from its reaction with the BFS in the grout.[15] The large increase in the amount of TcO_4^- observed in samples A and C at 26 months is due to exposure of these samples to atmosphere; sample B remained sealed. Based on the assumption that the fraction of TcO_4^- in these samples is the same at 26 months as when it was previously determined at 18 months, the fraction of TcO_4^- present in Samples A and C increased by 34% and 46%, respectively, during the 4 months that they were exposed to air. In comparison to the permeable samples, less scatter is present in the fraction of TcO_4^- in these samples and the fraction of TcO_4^- varies little among the samples until samples A and C were exposed to air. As in the permeable samples, the presence of NO_3^- has no observable effect on the speciation of technetium.

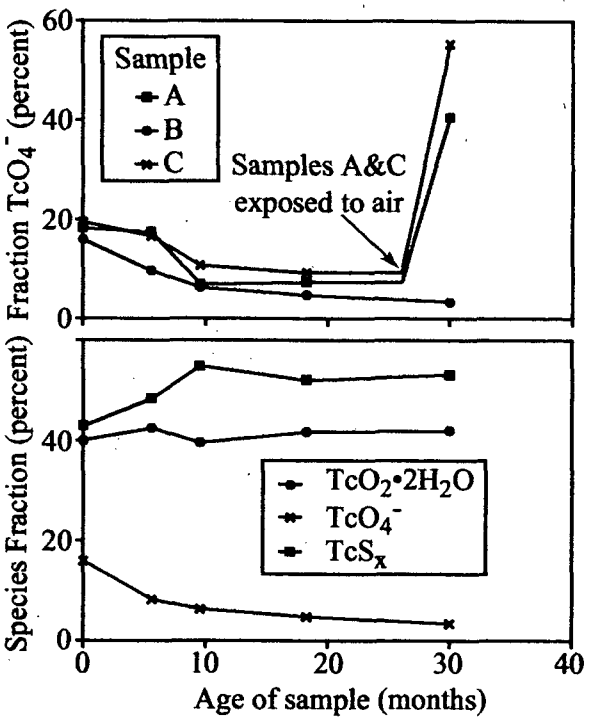

Figure 6: (upper) Evolution of the fraction of technetium present as TcO_4^- in the impermeable samples as a function of age. Arrow indicates that samples A and C were opened at 26 months (the fraction TcO_4^- at that point is assumed to be the same as previously determined at 18 months). (lower) Evolution of technetium speciation in sample B, which remained sealed throughout the experiment.

Discussion

The data from both series of samples show that TcS_x in grout is unstable towards oxidation. As noted previously, both NO_3^- and O_2 could oxidize the lower-valent technetium species present in these samples. Since the presence of NO_3^- had no significant effect on the rate of oxidation of technetium in these samples, atmospheric O_2 is the likely oxidizing agent. In addition, oxidation by O_2 rather than by NO_3^- helps explain the scatter in the speciation data observed in the permeable samples.

The scatter in the data in Figure 5 is believed to result from a variation in the amount of O_2 diffusing into the samples, which produces different amounts of oxidized TcS_x in different areas of the samples. Since the regions probed by the X-ray beam were chosen arbitrarily, such spatial inhomogeneity of the Tc speciation would result in the sort of scatter observed in Figure 5. Although the O_2 diffusion into the samples was originally thought to result from air leaking through the caps of the PS cuvettes, XANES spectra obtained at intervals from the top of the samples to the bottom show that this is not the case; instead, the technetium speciation varies somewhat along the length of the cuvette (Figure 7). Interestingly, O_2 is diffusing into the impermeable samples through the ~1 cm thick epoxy plug, but not through the ~2 mm thick PMMA cuvette, as indicated by the presence of TcO_4^- at the top of the cuvette (Figure 7). In the case of the permeable samples, the variation in the rate of O_2 diffusion is believed to be caused by the ridged walls of the cuvette through which the XAFS spectra were obtained since O_2 would diffuse more quickly through the thinner areas between the ridges.

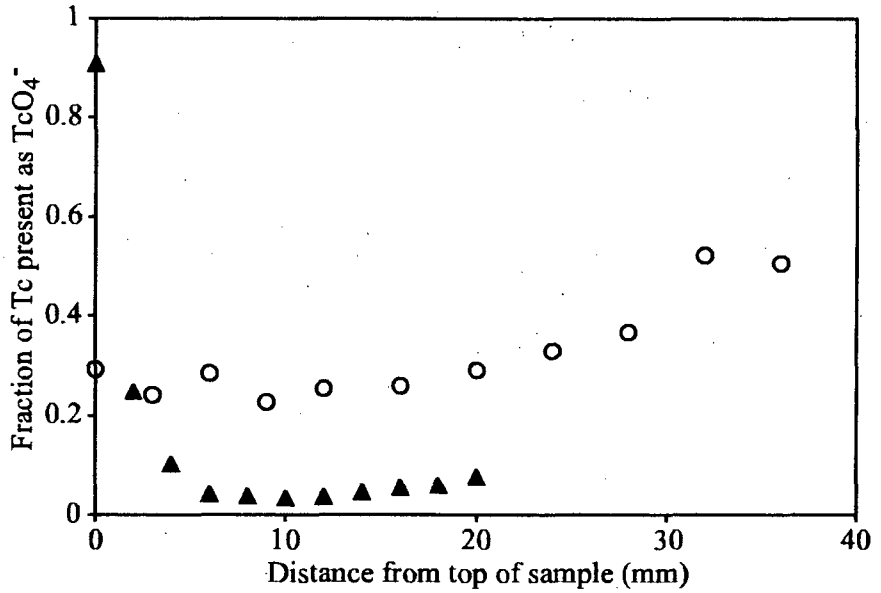

Figure 7: Technetium speciation as a function of position within permeable sample 1 (circles) and impermeable sample B (triangles). Age of sample 1, 73 months; sample B, 59 months.

The premise that O_2 is the actual oxidizer is strongly supported by the results from the impermeable

samples shown in Figure 6. Although ~20% of the TcO_4^- in these samples was not reduced to TcS_x, the amount of TcO_4^- in these samples declined at later times, presumably due to reduction by BFS. Furthermore, the technetium speciation in the impermeable samples is relatively homogeneous (except near the top). Although the technetium speciation evolved and the portions of the samples probed by XANES were arbitrarily chosen, little scatter exists in the technetium speciation among the different samples. Since, atmospheric O_2 cannot readily diffuse into these samples, technetium speciation should not vary with position. However, the most dramatic evidence for O_2 oxidation is the 40% increase in the amount of TcO_4^- observed in the initially sealed impermeable samples after 4 months exposure to atmosphere.

One unexpected result is the appearance of $TcO_2 \cdot 2H_2O$ in the permeable samples as they aged. Formation of $TcO_2 \cdot 2H_2O$ cannot result from the hydrolysis of TcS_x since it is stable to hydrolysis under the conditions present in the grout samples. Rather, the observation of $TcO_2 \cdot 2H_2O$ implies that the oxidation of TcS_x proceeds by initial oxidation to $TcO_2 \cdot 2H_2O$, which is then oxidized to TcO_4^- as shown in Eqs 2 and 3. This hypothesis is also supported by the evolution of the technetium speciation shown in the lower panel of Figure 5. Initial oxidation of TcS_x to $TcO_2 \cdot 2H_2O$ is consistent with the potentials for the reduction of SO_4^{2-} to S^{2-} (-0.67 V) and of TcO_4^- to $TcO_2 \cdot 2H_2O$ (-0.28 V) at pH 13. Although the detailed mechanism is certainly more complex than this simple picture, the observation of $TcO_2 \cdot 2H_2O$ in the permeable samples is consistent with the premise that oxidation of TcS_x to TcO_4^- proceeds with $TcO_2 \cdot 2H_2O$ as an intermediate.

$$Tc_3S_{10} + 18\,O_2 + 20\,HO^- \rightarrow 3\,TcO_2 \cdot 2H_2O + 10\,SO_4^{2-} + 4\,H_2O \qquad (2)$$

$$4\,TcO_2 \cdot 2H_2O + 4\,HO^- + 3\,O_2 \rightarrow 4\,TcO_4^- + 10\,H_2O \qquad (3)$$

The oxidation of the impermeable samples that have been removed from their cuvettes should occur at all of surfaces of the grout sample as illustrated in Figure 8. Consequently, the XAFS experiment examines a layer of oxidized grout on the surface of a sample consisting mainly of reduced grout, based on the reasonable assumption that oxidation of reducing grout proceeds by the shrinking core mechanism as proposed by Smith and Walton.[16] The thickness of the oxidized region formed in the initially sealed samples after exposure to atmosphere can be determined from the fraction of technetium that is oxidized using the formula for the fluorescence yield from a sample of a given thickness.[49,50] For a sample of thickness d, the fluorescence yield is given by Eq 4, where A is the area of the detector, r is the distance from the sample to the detector, ε_{Tc} is the fluorescence yield from the technetium K-shell, μ_{Tc} is the technetium absorption coefficient at the incident photon energy, $\mu_{tot}(E)$ and $\mu_{tot}(E_f)$ are the total absorption coefficients of the sample at the incident and fluorescent photon energies, and θ, ϕ, and d are defined in Figure 8. Since the total fluorescence yield for a thick sample is given by Eq 5, the contribution of a surface layer of thickness, d, to the total fluorescence signal is given by Eq 6, where I_d is the fluorescence from a surface layer of thickness, d, and I_{tot} is the total fluorescence from the sample. For the impermeable samples exposed to air, the average increase in pertechnetate content of 40 %, or $I_d/I_{tot}=0.4$ in Eq 5, corresponds to a 0.28 mm thick oxidized layer, using $\mu_{tot}(E)$ and $\mu_{tot}(E_F)$ calculated for sample A. Because 99% of the fluorescence from this sample comes from the upper 2.6 mm of the 4 mm thick sample, the sample can be considered thick and the contribution to the fluorescence of the oxidized layer on the opposite side of the sample can be ignored.

$$I_d/I_0(E) \propto \frac{A}{r^2}\varepsilon_{Tc}\frac{\mu_{Tc}(E)}{\mu_{tot}(E)+\mu_{tot}(E_f)\frac{\sin\phi}{\sin\theta}}\left\{1-\exp\left[-\left(\frac{\mu_{tot}(E)}{\sin\phi}+\frac{\mu_{tot}(E_f)}{\sin\theta}\right)d\right]\right\} \qquad (4)$$

$$I_{tot}/I_0(E) \propto \frac{A}{r^2}\varepsilon_{Tc}\frac{\mu_{Tc}(E)}{\mu_{tot}(E)+\mu_{tot}(E_f)\frac{\sin\phi}{\sin\theta}} \qquad (5)$$

$$\frac{I_d}{I_{tot}} = 1 - \exp\left[-\left(\frac{\mu_{tot}(E)}{\sin\phi} + \frac{\mu_{tot}(E_f)}{\sin\theta}\right)d\right] \qquad (6)$$

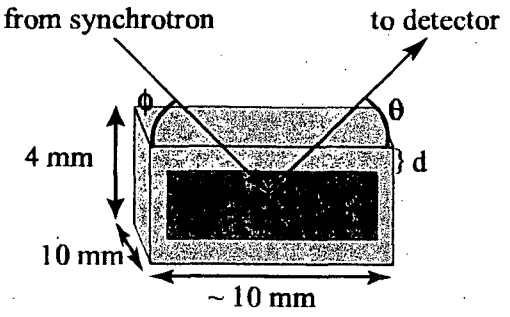

Figure 8: Illustration of the XAFS experiment on an initially sealed, impermeable sample that has been exposed to air. The oxidized layer of thickness d is illustrated by the lighter colored region and is on the surface of the darker colored reducing grout.

The thickness of the oxidized layer calculated from the fraction of TcO_4^- present in the sample can be compared with the thickness of the oxidized region determined analogously using the shrinking core model of Smith and Walton.[16] The difference between the model employed here and the Smith and Walton model is that here the effective diffusion coefficient of oxygen, $D_{eff(O2)}$, is determined from the MacMullin number and the diffusion coefficient of oxygen in water: $D_{eff(O2)} = D_{m(O2)}/N_m$ as described earlier. The rate of growth of the oxidized layer of thickness d is given by Eq 7 where t is time (in seconds), C_{O2} is the concentration of oxygen in water at the surface of the grout (3.7×10^{-7} mol cm^{-3}), $D_{m(O2)}$ is the diffusion coefficient of oxygen in water (2.0×10^{-5} cm^2 s^{-1}), and C_{red} is the concentration of reducing equivalents in the CWF in moles of electrons (3.7×10^{-4} mol cm^{-3} for a CWF with a density of 1.7 g cm^{-3} composed of 27% BFS with a measured reducing capacity of 0.81 meq g^{-1}, all other grout

components are assumed to have a negligible reducing capacity). Using Eq 7, the thickness of the oxidized region determined from the XANES experiment, 0.28 mm, in grout samples exposed to air for 120 days corresponds to a N_m of 1.6×10^3 or a $D_{eff(NO3-)}$ of 9.5×10^{-9} cm^2 s^{-1}, which is within the range of $D_{eff(NO3-)}$ reported for CWFs. The thickness of the oxidized layer determined from the XANES experiment is consistent with the thickness of the oxidized layer anticipated from the shrinking core model of Smith and Walton.

$$d = \sqrt{\frac{8C_{O_2}tD_{m(O_2)}}{N_m C_{red}}} \qquad (7)$$

The effect of oxidation by O_2 on an actual waste form, Saltstone, also can be examined using this model to illustrate the difference between oxidation of reduced technetium species by O_2 and NO_3^-. In comparison to sample A, Saltstone has smaller $D_{eff(NO3-)}$, ranging from 1.3×10^{-9} cm^2 s^{-1} to 5×10^{-9} cm^2 s^{-1}, but a similar C_{red} since Saltstone is prepared from the same BFS in similar proportions to those used to prepare Sample A. Using a $D_{eff(NO3-)}$ of 5×10^{-9} cm^2 s^{-1}, the thickness of the oxidized region would be 17 cm after one ^{99}Tc half-life (213,000 yr), and after ten half-lives, the oxidized region would be 53 cm thick. For comparison, the dimensions of a Savannah River Saltstone monolith are 30.5 m × 30.5 m × 7.5 m.[7] Therefore, approximately 6% of the technetium in the waste form would be oxidized after one ^{99}Tc half-life, and approximately 20% would be oxidized after ten half-lives based on the assumption that oxidation occurs at all sides of the Saltstone cell. This simple estimate ignores the presence of concrete vault surrounding the Saltstone and the layer of reducing grout without technetium at the top of the Saltstone vault, both of which would decrease the rate of ^{99}Tc leaching. Cracking and flow of surface water through the CWF could greatly increase the rate of oxidation and the leaching of TcO_4^- by effectively decreasing the size of the Saltstone cell to the intercrack spacing,[7,8] so this discussion is intended only to illustrate the difference between oxidation by O_2, which produces an oxidized surface region with an increased $D_{eff(99Tc)}$, and oxidation by NO_3^-, which would result in an increased

$D_{eff(^{99}Tc)}$ throughout the entire volume of the waste. The results in this study indicate that the oxidation of Tc(IV) species in these grout samples is due solely to O_2, and that NO_3^- has no observable effect on the speciation of technetium in these samples. While these results do not show that NO_3^- is unreactive towards Tc(IV) in reducing grouts, this reaction occurs too slowly to be observed in this study.

ACKNOWLEDGMENT. The authors thank Corwin Booth for helpful discussions about least squares fitting of the XANES and EXAFS data and for the use of the code "fites". The authors thank Christine Langton for providing the pulverized fly ash, BFS, and Portland cement. This work was supported by the Environmental Management Science Program of the U.S. DOE Office of Science, Biological and Environmental Research, Environmental Remediation Sciences Division and was performed at the Lawrence Berkeley National Laboratory, which is operated by the U. S. DOE under Contract No. DE-AC03-76SF00098. Portions of this research were carried out at the Stanford Synchrotron Radiation Laboratory, a national user facility operated by Stanford University on behalf of the U.S. Department of Energy, Office of Basic Energy Sciences.

SUPPORTING INFORMATION AVAILABLE: Detailed description of EXAFS model selection criteria; composition of Sample A used to determine the X-ray absorption coefficients; Tables of the data shown in Fig. 5 and 6; plots of the evolution of the XANES spectra of Sample B and an example of a XANES fit for Sample B; derivation of the shrinking core model used to obtain Eq 7. This information is available free of charge via the Internet at http://pubs.acs.org.

REFERENCES

(1) Gray, R. H.; Becker, C. D. *Environ. Manage.* **1993**, *17*, 461.
(2) "Response to Requirement for Report to Congress Under Floyd D. Spence National Defense Authorization Act for Fiscal Year 2001," Office of River Protection, 2000.
(3) Oblath, S. B. "Relative Release Rates of Nitrate, Tc, Cs, and Sr from Saltstone," DPST-84-620, Savannah River Laboratory, 1984.
(4) Oblath, S. B. *Environ. Sci. Technol.* **1989**, *23*, 1098.
(5) Serne, R. J.; Lokken, R. O.; Criscenti, L. J. *Waste Manage.* **1992**, *12*, 271.

(6) National Research Council. *Research Needs for High-Level Waste Stored in Tanks and Bins at U.S. Department of Energy Sites*; National Academy Press: Washington, D.C., 2001.
(7) Seitz, R. R.; Walton, J. C.; Dicke, C. A.; Cook, J. R. *Mat. Res. Soc. Symp. Proc.* **1993**, *294*, 731.
(8) Kaplan, D. I.; Serne, R. J. *Radiochim. Acta* **1998**, *81*, 117.
(9) Gilliam, T. M.; Spence, R. D.; Bostick, W. D.; Shoemaker, J. L. *J. Hazard. Mater.* **1990**, *24*, 189.
(10) MacMullin, R.; Muccini, G. *Am. Inst. of Chem. Engin., J.* **1956**, *2*, 393.
(11) Taffinder, G. G.; Batchelor, B. *J. Environ. Eng.* **1993**, *119*, 17.
(12) Langton, C. A. "Challenging Applications for Hydrated and Chemically Reacted Ceramics," DP-MS--88-163, Savannah River Laboratory, 1988.
(13) Yeh, B. S.; Wills, G. B. *J. Chem. Engin. Data* **1970**, *15*, 187.
(14) Rard, J. A.; Rand, M. H.; Anderegg, G.; Wanner, H. *Chemical Thermodynamics of Technetium*; Elsevier Science: Amsterdam, 1999.
(15) Allen, P. G.; Siemering, G. S.; Shuh, D. K.; Bucher, J. J.; Edelstein, N. M.; Langton, C. A.; Clark, S. B.; Reich, T.; Denecke, M. A. *Radiochim. Acta* **1997**, *76*, 77.
(16) Smith, R. W.; Walton, J. C. *Mat. Res. Soc. Symp. Proc.* **1993**, *294*, 247.
(17) Lukens, W. W.; Bucher, J. J.; Edelstein, N. M.; Shuh, D. K. *Environ. Sci. Technol.* **2002**, *36*, 1124.
(18) Bajt, S.; Clark, S. B.; Sutton, S. R.; Rivers, M. L.; Smith, J. V. *Anal. Chem.* **1993**, *65*, 1800.
(19) Kaplan, D. I. "Estimated Duration of the Subsurface Reducing Environment Produced by the Z-Area Saltstone Disposal Facility (U)," WSRC-RP-2003-00362, Westinghouse Savannah River Company, 2003.
(20) Kneas, K. A.; Demas, J. N.; Nguyen, B.; Lockhart, A.; Xu, W.; DeGraff, B. A. *Anal. Chem.* **2002**, *74*, 1111.
(21) Gao, Y.; Ogilby, P. R. *Macromolecules* **1992**, *25*, 4962.
(22) Hormats, E. I.; Unterleitner, F. C. *J. Phys. Chem.* **1965**, *69*, 3677.
(23) Angus, M. J.; Glasser, F. P. *Mat. Res. Soc. Symp. Proc.* **1985**, *50*, 547.
(24) Walden, G. H.; Hammett, L. P.; Chapman, R. P. *J. Am. Chem. Soc.* **1931**, *53*, 3908.
(25) Smeller, J. A. *Amer. Lab. News* **1999**, *October*, 6.
(26) Bucher, J. J.; Allen, P. G.; Edelstein, N. M.; Shuh, D. K.; Madden, N. W.; Cork, C.; Luke, P.; Pehl, D.; Malone, D. *Rev. Sci. Instrum.* **1996**, *67*, 4.
(27) Koningsberger, D. C.; Prins, R. *X-Ray Absorption: Principles, Applications, Techniques of EXAFS, SEXAFS, and XANES*; John Wiley & Sons: New York, 1988.
(28) Newville, M. *J. Synchrotron Rad.* **2001**, *8*, 322.
(29) Ravel, B. *Physica Scripta* **2003**, *in press*.
(30) Rehr, J. J.; Albers, R. C.; Zabinsky, S. I. *Phys. Rev. Lett.* **1992**, *69*, 3397.
(31) Stern, E. *Phys. Rev. B* **1993**, *48*, 9825.
(32) Sarrao, J. L.; Immer, C. D.; Fisk, Z.; Booth, C. H.; Figueroa, E.; Lawrence, J. M.; Modler, R.; Cornelius, A. L.; Hundley, M. F.; Kwei, G. H.; Thompson, J. D.; Bridges, F. *Phys. Rev. B* **1999**, *59*, 6855.
(33) McMaster, W.; Kerr Del Grande, N.; Mallett, J.; Hubbell, J. "Compilation of X-ray Cross Sections," UCRL-50174, Lawrence Livermore National Laboratory, 1969.
(34) Bandyopadhyay, B., "Mucal on the web," http://www.csrri.iit.edu/mucal.html.
(35) Colton, R. *The Chemistry of Technetium and Rhenium*; Interscience Publishers: New York, 1965.
(36) Cartledge, G. H. *J. Electrochem. Soc.* **1971**, *118*, 231.
(37) Lee, S. Y.; Bondietti, E. A. *Mat. Res. Soc. Symp. Proc.* **1983**, *15*, 315.
(38) Müller, A.; Pohl, S.; M., D.; Cohen, J. P.; Bennett, J. M.; Kirchner, R. M. *Z. Naturforsh.* **1979**, *34b*, 434.
(39) Weber, T.; Muijsers, J. C.; Niemantsverdriet, J. W. *J. Phys. Chem.* **1995**, *99*, 9194.
(40) Hibble, S. J.; Rice, D. A.; Pickup, D. M.; Beer, M. P. *Inorg. Chem.* **1995**, *34*, 5109.

(41) Cramer, S. P.; Liang, K. S.; Jacobson, A. J.; Chang, C. H.; Chianelli, R. R. *Inorg. Chem.* **1984**, *23*, 1215.
(42) Müller, A.; Jostes, R.; Cotton, F. A. *Angew. Chem. Int. Ed. Engl.* **1980**, *19*, 875.
(43) Fujisawa, K.; Moro-oka, Y.; Kitajima, N. *J. Chem. Soc., Chem. Commun.* **1994**, 623.
(44) Mueting, A. M.; Boyle, P.; Pignolet, L. H. *Inorg. Chem.* **1984**, *23*, 44.
(45) Bianchini, C.; Mealli, C.; Meli, A.; Sabat, M. *Inorg. Chem.* **1986**, *25*, 4617.
(46) Pleus, R. J.; Waden, H.; Saak, W.; Haase, D.; Pohl, S. *J. Chem. Soc., Dalton Trans.* **1999**, 2601.
(47) Ressler, T.; Wong, J.; Roos, J.; Smith, I. L. *Environ. Sci. Technol.* **2000**, *34*, 950.
(48) Panak, P.; Booth, C.; Caulder, D.; Bucher, J.; Shuh, D.; Nitsche, H. *Radiochim. Acta* **2002**, *90*, 315.
(49) Goulon, J.; Goulon-Ginet, C.; Cortes, R.; Dubois, J. M. *J. Physique* **1982**, *43*, 539.
(50) Tröger, L.; Arvanitis, D.; Baberschke, K.; Michaelis, H.; Grimm, U.; Zschech, E. *Phys. Rev. B* **1992**, *46*, 3283.

KEYWORDS technetium, cement, grout, nuclear waste

BRIEF The speciation of technetium in reducing grout samples was examined using X-ray absorption fine structure spectroscopy; the reduced technetium species were oxidized by atmospheric oxygen.

Scientific Basis for Nuclear Waste Management XVI

Symposium held November 30–December 4, 1992,
Boston, Massachusetts, U.S.A.

EDITORS:

C.G. Interrante
U.S. Nuclear Regulatory Commission
Washington, DC, U.S.A.

R.T. Pabalan
CNWRA, Southwest Research Institute
San Antonio, Texas, U.S.A

MRS
MATERIALS RESEARCH SOCIETY
Pittsburgh, Pennsylvania

A substantial portion of the funding for this symposium was provided by the United States Department of Energy and the United States Nuclear Regulatory Commission, Award No. NRC-02-93-002. However, the views and findings of the various papers are solely those of the authors, and do not necessarily represent the policy of either agency. The agencies encourage wide dissemination of the technical information contained herein, with due respect for the Publisher's rights regarding the complete volume.

Single article reprints from this publication are available through University Microfilms Inc., 300 North Zeeb Road, Ann Arbor, Michigan 48106

CODEN: MRSPDH

Published by:

Materials Research Society
9800 McKnight Road
Pittsburgh, Pennsylvania 15237
Telephone (412) 367-3003
Fax (412) 367-4373

Library of Congress Cataloging in Publication Data

Scientific basis for nuclear waste management XVI: symposium held November 30 December 4, 1992, Boston, Massachusetts, U.S.A./editors, C.G. Interrante, R.T. Pabalan

p. cm.—(Materials Research Society symposium proceedings, ISSN 0275-0112; vol. 294)
Bibliography: p.
ISBN 1-55899-189-1
1. Radioactive waste disposal Congresses. 2. Glass waste—Congresses.
I. Interrante, C.G. II. Pabalan, R.T. III. Title: Scientific basis for nuclear waste management sixteen IV. Series.
TD 898.S424 1991 88-5323
621.4838—dc19 CIP

Manufactured in the United States of America

THE ROLE OF OXYGEN DIFFUSION IN THE RELEASE OF TECHNETIUM FROM REDUCING CEMENTITIOUS WASTE FORMS

ROBERT W. SMITH* AND JOHN C. WALTON**
*Idaho National Engineering Laboratory, P.O. Box 1625, Idaho Falls, ID 83415
**Center for Nuclear Waste Regulatory Analyses, Southwest Research Institute, 6220 Culebra Road, San Antonio, TX 78023

ABSTRACT

Cementitious materials provide an ideal geochemical environment (e.g., high pH pore fluids and large surface areas for sorption) for immobilizing nuclear waste. The inclusion of reducing agents, such as blast furnace slag (BFS) can immobilize radionuclides by forming of solid sulfide phases. Thermodynamic calculations using the MINTEQ geochemical computer code indicate that elemental sulfur present in BFS reacts with the highly mobile pertechnetate anion (TcO_4^-) anion to form an insoluble technetium sulfide phase ($Tc_2S_{7(s)}$). Initially, the waste form very effectively immobilizes technetium. However, as oxygen diffuses into the waste form, an outer zone of oxidized concrete and a shrinking core of reduced intact concrete develops. Oxidation of sulfur in the outer zone results in increased technetium concentrations in the pore fluid because $Tc_2S_{7(s)}$ oxidizes to the mobile TcO_4^- anion. The TcO_4^- anion can then diffuse from the waste form into the environment.

A mathematical model that accounts for diffusion of oxygen into concrete coupled with oxidation of sulfur and sulfide to sulfate has been developed. This model assumes the existence of an oxidized outer layer of concrete surrounding a shrinking core of reducing intact concrete. A sharp boundary between the two zones moves slowly inward resulting in oxidation of $Tc_2S_{7(s)}$ and subsequent release of TcO_4^- via aqueous diffusion in the concrete pore fluids. The model indicates that this mechanism results in a linear dependance of release with the square root of time, similar to pure diffusion. In addition, the release of technetium is related to the inverse of the square root of the concentration of BFS, indicating that performance will significantly increase with the addition of approximately 20 percent BFS to the cement mix.

INTRODUCTION

In the United States and other countries cementitious materials are used to immobilize low-level radioactive waste. Although concrete waste forms are used primarily for their physical properties, such as low permeability, cementitious materials can provide an ideal geochemical environment (e.g., high pH pore fluids and large surface areas for sorption) for immobilizing nuclear waste. Including reducing agents can immobilize radionuclides, such as ^{99}Tc by forming of solid sulfide phases and reducing multivalent radionuclides to lower oxidation states that are less mobile. Blast furnace slag (BFS), which is a widely available glassy by product of pig iron production, is a commonly used reducing agent in cement mixes.

Under oxidizing conditions, aqueous technetium occurs in the heptavalent oxidation state as the pertechnetate anion (TcO_4^-). Heptavalent technetium solids have high solubilities leading to potentially elevated aqueous concentrations. In addition, as a monovalent anion, TcO_4^- is only weakly sorbed by cementitious solids. The combination of high solubility and low sorption can result in the release of significant amounts of technetium from cementitious waste forms. Furthermore, the long half-life (213,000 y) of ^{99}Tc makes the physical isolation of technetium impractical; therefore, greater reliance on chemical isolation is required. To decrease the mobility and release of technetium, a reducing agent, such as BFS, is added to the concrete formulation to immobilize TcO_4^- as a precipitated solid. This may occur by the reaction of pertechnetate with reduced sulfur in the BFS to form a technetium sulfide phase ($Tc_2S_{7(s)}$).

The placement of low-level waste disposal facilities in the vadose zone requires that the diffusion of diatomic oxygen into and the reaction of oxygen with reduced chemical species in barriers and waste forms be considered in evaluating radionuclide releases from disposal facilities. Initially, the BFS is very effective in reducing the release rate of technetium. However,

Mat. Res. Soc. Symp. Proc. Vol. 294. © 1993 Materials Research Society

4/10980

WSRC-RP-92-1360

RADIOLOGICAL PERFORMANCE ASSESSMENT FOR THE Z-AREA SALTSTONE DISPOSAL FACILITY (U)

RC 2/4/93

Prepared for the
WESTINGHOUSE SAVANNAH RIVER COMPANY
Aiken, South Carolina

by

MARTIN MARIETTA ENERGY SYSTEMS, INC.
EG&G IDAHO, INC.
WESTINGHOUSE HANFORD COMPANY
WESTINGHOUSE SAVANNAH RIVER COMPANY

December 18, 1992

Rev. 0

APPENDIX D

GEOCHEMICAL INTERACTIONS

D.1 INTRODUCTION

One of the most important input parameters to the flow models used to simulate transport of contaminants from the Saltstone Production and Disposal Facility (Z-Area) vaults to the nearest point of compliance is the determination of a representative pollutant source term. The most representative source term for this purpose is the resultant concentration of pollutants in the pore fluid within the saltstone grout matrix following the geochemical interactions that occur after the wastewater feed solution and the cementitious materials (cement, slag, and fly-ash) are mixed together. The predominant transport pathway from the saltstone to the nearest point of compliance is downward migration via fluids which have passed through the waste form and concrete vaults and through the vadose zone into the saturated zone. The most representative source term for this transport pathway is the concentration of pollutants in the interstitial fluids within the vadose zone immediately surrounding the saltstone vaults. This latter source term estimate is based on the geochemical interactions that occur between the saltstone pore fluid and the soil (sediments) immediately surrounding the Z-Area vaults.

This appendix provides an estimate of selected pollutant concentrations in the saltstone pore fluid obtained by using the MINTEQ computer code. Pollutant concentration in interstitial fluids within the vadose zone are also estimated using the MINTEQ code.

The MINTEQ code was selected for this geochemical evaluation because it is well documented and generally accepted within the technical community. The MINTEQ code was installed and tested on computers at both EG&G Idaho, Inc. and Westinghouse Hanford Company. EG&G Idaho, Inc. studied the evolution of the pollutant contamination within the saltstone pore fluid while Westinghouse Hanford Company studied the pollutant contamination within the interstitial fluids in the vadose zone. The same thermodynamic properties of chemical compounds and mineral species, published saltstone properties, and sediment composition at the Savannah River Site were used as the data base for calculations conducted by both contractors.

Kaolinite, quartz, and iron compounds were assumed to be the major constituents in the sediments surrounding the Z-Area vaults with which the saltstone pore fluid will react.

The pollutants selected for the initial source term evaluation are technetium-99, tritium, and nitrate ion. There are other pollutants of interest present in the feed solution which are candidates for future evaluation. These are iodine-129, tin-126, selenium-79, americium-241, and carbon-14.

D.1.2 Background

The large concentration of dissolved solids in the feed solution (>300,000 mg/L) are beyond solution concentrations normally used when the MINTEQ code is used to calculate appropriate activity coefficients and solubilities. Initial test runs were made to evaluate the sensitivity of the MINTEQ code to these high concentrations. The code was used to calculate appropriate activity coefficients and solubilities of the pore fluid in the saltstone grout matrix at the time the feed solution and the dry additives were mixed. Results from the test runs showed that the MINTEQ code could be used with reliability to determine the composition of pore fluids. Further, that activity coefficients and solubility data are not as sensitive as previously thought to the high concentrations of dissolved solids.

Movement of pore fluids through the saltstone matrix is controlled by advection and diffusion. Leaching occurs both at the outermost surface of the saltstone matrix and along the surface of cracks and fractures within the saltstone matrix. The data indicate that the most significant leach rates will occur along the cracks and fractures in the saltstone where the influx of water has the shortest residence time.

D.2 SUMMARY AND CONCLUSION

The nominal concentration of technetium-99 in the waste form is projected to be 25,000 pCi/g. Upon mixing with the cementitious materials a significant portion of the technetium is partitioned between the solid matrix (40,700 pCi/g) and the pore fluid (46.3 pCi/mL). An estimated Kd of 880 mL/g was calculated for technetium in the saltstone. The reaction of pore fluids with the sediments did not influence the technetium concentration.

Results show that elemental sulfur present in blast furnace slag will react to form sulfide species during the hydration of the saltstone. the sulfide is available to react with technetium to form insoluble technetium sulfide (Tc_2S_7) which significantly reduces the technetium concentrations in the pore fluid from 46,300 pCi/L to 2.4×10^{-3} pCi/L. For each 10 fold increase of HS^- in the pore fluid the technetium concentration decreases by a factor of 3,200. Results also show that a decrease of 1 unit in pH results in an decrease in technetium in the pore fluid by a factor of 32,000.

Initial tritium concentration in the waste form is projected to be 7,000 pCi/g. Upon mixing with the cementitious materials the concentration of water in the pore fluid is 0.825 g/mL and the concentration of water in the hydrated cement is 0.177 g/g which gives a calculated K_d of 0.2 for tritium in the saltstone. The tritium concentration in the pore fluid is 16,000,000 pCi/L. The tritium concentration in the interstitial fluid within the vadose zone was reduced slightly because some of the insoluble minerals that are precipitated from solution are hydrated.

The total nitrogen (as NO_3^-) in the waste water feed solution exceeds 150,000 mg/L. The loss of water into the saltstone from hydration causes the nitrate concentration in the pore fluid to increase to more than 200,000 mg/L. The nitrate concentration in the interstitial fluid within the vadose zone will decrease primarily due to the dilution of the interstitial fluid by naturally occurring waters present in the vadose zone.

D.3 PORE FLUID COMPOSITION WITHIN SALTSTONE

The partitioning of contaminants between the aqueous phase (pore fluid) and solid matrix (hydrated cement) must be understood in order to understand the release of contaminants from a saltstone waste form. The term sorption describes the partitioning processes and is mathematically represented by the use of a distribution coefficient (K_d). However, sorption does not occur by a single mechanism. The three mechanisms important to calculating the hydration and pore fluid composition for saltstone are

1) Adsorption - The contaminant is partitioned between the solid surface and the pore fluid. At low concentrations this adsorption can be linear and reversible allowing the use of a K_d to represent partitioning.

2) Precipitation - The contaminant forms a separate solid phase or coprecipitates into an existing solid phase. The aqueous concentration is controlled by the solubility of this solid phase (i.e., the pore fluid concentration is independent of the solid concentration). Typically the solid phase has a very low solubility; therefore, the contaminants are effectively immobilized in the solid waste form. The relationship between aqueous and solid concentration for coprecipitated contaminants are related by kinetic and thermodynamic considerations (Murphy and Smith 1989). However, at low contaminant concentrations multiphase thermodynamic equilibrium can be mathematically represented by a K_d (Smith and Walton 1992).

3) Absorption - This mechanism is important when calculating a source term for tritium. During the hydration of cement water is taken up into the cement paste, removing tritium from solution in proportion to the total amount of water transferred into the solid phase.

In addition to contaminants, the release of ions such as sulfate from the saltstone waste form may lead to the degradation of the concrete vault. These releases need to be understood in order to evaluate long-term contaminant release performance. To quantify the saltstone pore fluid composition, hydration calculations have been conducted to 1) determine the distribution of water between pore fluid and hydrated cement and 2) estimate the composition of the pore fluid. In addition, the distribution of water between pore fluid and solid matrix can be used to estimate a distribution coefficient

(K_d) for tritium. The results of hydration calculations are summarized below.

D.3.1 Hydration Calculation

The saltstone mix is composed of 3% Class II cement, 25% blast furnace slag, 25% Class F fly ash , and 47% Nominal Blend Salt Solution Feed (Heckrotte 1988). The compositions of the four components of saltstone are given in Table D.3-1. As the concrete waste form cures, water is taken up from the salt solution feed and incorporated into the cement mix by hydration, forming the solid matrix of the waste form. A portion of the initial free water is incorporated into the solid matrix of the waste form; the remaining water occurs as pore fluid. Ions that are not incorporated into the solid matrix (e.g., nitrate, nitrite), are concentrated in the pore fluids. Table D.3-2 documents the hydration of 100 g of the cement mixture. The compositions of the solid phases were taken from Table 4 of Malek et al. (1985). The maximum extent of hydration was estimated by assuming that

- SiO_2 and TiO_2 do not consume water during hydration,
- Al_2O_3 and Fe_2O_3 consume 3 mol of water per mol of oxide,
- SO_3 reduces hydration by 1 mol of water per mol of oxide,
- Na_2O and K_2O dissolve into the pore fluid, and
- All other oxides consume 1 mol of water per mol of oxide.

The hydration process results in a 15.8 g (16%) increase in the mass of the solid matrix. This value is consistent with the range given in Neville (1981). The total amount of salt feed solution per 100 g of cement mixture is 88.7 g (28.4% total dissolved solids), of which 63.5 g are free water and 25.2 g are salt. The hydration process results in the transfer of 15.8 g of the free water into the solid matrix leaving 47.7 g of free water in the pore fluid. The loss of free water results in an increase in the salt concentration in the pore fluid to 34.6% (25.2 g/72.9 g) total dissolved solids. The final distribution of water is as follows: 47.7 g of free water in the pore fluids and 20.5 g of hydration water in the solid matrix (4.7 g initially in the cement mixture plus 15.8 g from the salt feed solution).

The density of the pore fluid is estimated to be 1.26 g/mL (34% sodium nitrate, CRC Press (1987). Using this density the total volume of pore fluid per 100 g of cement mixture (115.8 g hydrated cement) is calculated to be 57.8 mL (72.9 g/1.26 g/mL). The concentration of water in the pore fluid is 0.825 g/mL (47.7 g/57.8 mL). The concentration of water in the hydrated cement is 0.177 g/g (20.5 g/ 115.8 g). A distribution coefficient (K_d) of 0.2 mL/g [(0.177 g/g)/(0.825 g/mL)] was estimated for tritium based on the hydration calculations and the assumptions that tritium occurs as tritiated water and that the isotope fractionation effects (i.e., exchange of ^1H for ^3H) are small.

Table D.3-1. Composition of starting material for saltstone formation in weight percent[a]

	Hydration factor	Formula[b] weight	Slag	Fly ash	Portland Cement	Salt Feed Solution
SiO_2	0	60.09	34.70	52.17	21.10	
$A_{l2}O_3$	3	101.96	10.70	27.60	4.66	
TiO_2	0	79.90	0.51	1.98	0.23	
Fe_2O_3	3	159.69	0.41	4.36	4.23	
MgO	1	40.30	11.90	0.61	1.21	
CaO	1	56.08	39.37	0.96	64.55	
MnO	1	70.94	0.54	0.01	0.16	
BaO	1	153.34	0.05	0.10	0.02	
Na_2O		61.98	0.25	0.26	0.11	
K_2O		94.20	0.55	1.53	0.34	
So_3	-1	80.06		0.33	2.50	
S		32.06	1.34			
LOI(H_2O)	-1	18.02		9.92	0.86	71.60
Salt						28.40
Total			100.32	99.83	99.97	100.00

[a] Composition of solids for Malek et al. (1985). Composition of salt feed solution for Heckrotte (1988). Hydration factor and formula weights were used to calculate hydration as described in text.

[b] g/mol.

Table D.3-2. Summary of saltstone hydration calculations for a mixture of 47% salt feed and 53% cement mix. Composed of 47.17% each of slag and fly ash and 5.66% of Portland cement. Normalized to 100 g of cement mix[a]

	Salt feed solution	Cement mix	Hydrated cement	Pore fluid
SiO_2		42.14	42.14	
Al_2O_3		18.32	28.03	
TiO_2		1.19	1.19	
Fe_2O_3		2.49	3.33	
MgO		5.97	8.63	
CaO		22.66	29.94	
MnO		0.27	0.34	
BaO		0.07	0.08	
Na_2O		0.25	0.25	
K_2O		1.00	1.00	
SO_3		0.30	0.23	
S		0.63	0.63	
LOI(H_2O)	63.49	4.72		47.71
Salt	25.18			25.18
Total	88.68	100.00	115.79	72.89
	47%	53%	61.4%	38.6%

[a] Compositions are from Table D-1.

Given that the initial tritium loading of the saltstone is 7,000 pCi/g, the concentration of ^3H in the solid matrix and the pore fluid can be calculated. A total of 1,320,000 pCi of ^3H occur in 188.7 g of saltstone (115.8 g hydrated cement + 72.9 g pore fluid). The partitioning of ^3H is given by:

$$\begin{aligned}
\text{Total} &= M_s \times C_s + V_l \times C_l, \\
C_s &= C_l \times K_d, \\
\text{Total} &= C_l (K_d \times M_s + V_l), \\
C_l &= \text{Total} / (K_d \times M_s + V_l), \\
C_l &= 16{,}000 \text{ pCi/mL} = 16{,}000{,}000 \text{ pCi/L, and} \\
C_s &= 3{,}300 \text{ pCi/g.}
\end{aligned}$$

where

Total is the total ^3H (1,320,000 pCi),
M_s is that mass of the hydrated cement (115.8 g),
C_s is the concentration of ^3H in the hydrated cement (pCi/g),
V_l is the volume of pore fluid (57.8 ml), and
C_l is the concentration of ^3H in the pore fluid (pCi/mL).

D.3.2 Concentration of Technetium-99 and Nitrate in Saltstone Pore Fluids

Previous screening suggested that technetium and nitrate are the two contaminants most likely to determine the overall performance of saltstone. For this reason, geochemical calculations were conducted to estimate the pore fluid concentrations of technetium, nitrate, and nitrite. The computer code MINTEQ was used to calculate an equilibrium solution speciation and to evaluate degree of saturation with respect to concrete minerals. Activity coefficients for aqueous species were calculated using the B-dot method documented in Helgeson (1969). Thermodynamic data for complexes of nitrate were taken from Smith and Martell (1976). Thermodynamic data for cement phases were obtained from the compilation of Crisentia and Serne (1990). Modified salt feed solution composition was calculated from the salt feed solution composition (Heckrotte 1988) and the hydration calculations described above. The modified salt feed solution composition was used as input for MINTEQ to calculate pore fluid composition. Additionally, the aqueous $NaAl(OH)_4$ was allowed to react via:

$$NaAl(OH)_{4,aq} = Al(OH)_{3,s} + NaOH_{aq} \quad (1)$$

$Al(OH)_{3,s}$ refers to fully hydrated Al_2O_3 in the solid matrix and not to a particular pure phase aluminum hydroxide. This adjustment to the pore fluid is based on the very low aluminum concentration in saltstone pore fluids reported by Malek et al. (1987).

Equilibrium between the pore fluid and calcite, C_3AH_6, C-S-H gel, and C_3FH_6 was assumed in the MINTEQ calculations.

where

C = CaO,
A = Al_2O_3,
H = H_2O,
S = SiO_2, and
F = Fe_2O_3 (standard cement nomenclature).

The solid phases chosen for these calculations were identified by x-ray diffraction in the slag containing cement mixes (Malek et al. 1987). The pH value was determined from the hydroxide concentration and charge balance.

Calculations showed the pore fluid to be undersaturated with any aluminum sulfate phase and with portlandite, and significantly undersaturated with aluminum and calcium nitrates. Furthermore, hydration calculations similar to those described above conducted for the 84-48 saltstone mix of Malek et al. (1987) indicate that, within experimental uncertainties, all nitrate and nitrite in saltstone occurs within the pore fluids. These calculations differ from the x-ray diffraction analysis of Malek et al. (1987) who found solid hydrated aluminum and calcium nitrates. A possible explanation for the difference between the calculated results and the observations of Malek et al. (1987) may be in their preparation of saltstone samples for x-ray diffraction. If the saltstone samples were dried before analysis, the precipitation of soluble nitrate salts in the saltstone would be expected.

The aluminum concentration of the pore fluid was buffered at extremely low concentrations by equilibrium with the solid phases. As a result, the pore fluids are essentially NaOH-$NaNO_3$-$NaNO_2$ mixtures with a very high pH of 13.8 to 14.0 (see reaction 1). The resulting composition for the pore fluid is presented in Table D.3-3. Additionally, a NO_3^- concentration is reported based on the stoichiometric oxidation of NO_2^- to NO_3^-.

Under oxidizing conditions, aqueous technetium occurs in the heptavalent oxidation state as the pertechnetate ion (TcO_4^-). Many heptavalent technetium solids have high solubilities leading to potentially elevated aqueous concentrations. In addition, as a monovalent anion, TcO_4^- is only weakly sorbed by cementitious solids. The combination of high solubility and low sorption can result in the release of significant amounts of technetium from cementitious waste forms. To decrease release, a reducing agent, blast furnace slag, was added to the saltstone formulation to immobilize TcO_4^- as a precipitated solid. Thermodynamic calculations using the MINTEQ code indicate that in slag cement, technetium is immobilized as a Tc (VII) sulfide. During the hydration of blast furnace slag-cement, elemental sulfur in the slag (Angus and Glasser 1985) reacts to form reduced aqueous sulfur species such as sulfide. The aqueous sulfide reacts with $TcO4^-$ to form $Tc_2S_{7(s)}$. The over all reaction is given by

$$6TcO_4^- + 28S_s + 8\,OH^- = 3Tc_2S_{7,s} + 7SO_4^{2-} + 4H_2O \quad (2)$$

Table D.3-3. Calculated saltstone pore fluid composition using MINTEQ, the results of the hydration calculations and equilibrium with calcite, C_3AH_6, C-S-H gel, and C_3FH_6. ^{99}Tc is calculated by assuming equilibrium with $Tc_2S_{7,\beta}$ as described in the text

Species	mg/L	HS (mg/L)	^{99}Tc (pCi/L)
Na^+	139,000		
CO_3^{2-}	12,800		
SO_4^{2-}	15,000		
NO_2^-	36,800		
NO_3^-	159,000		
OH^-	32,900		
Ca^{2+}	1		
$SiO_{2,aq}$	1		
Al^{3+}	11		
K^+	9,800		
NH^{4+}	400		
pH	13.97		
Total N as NO_3^-	209,000		
Density	1.26		
High sulfide		10	2.4×10^{-8}
Stoichiometric		0.003	46,300

The $Tc_2S_{7,s}$ phase is very insoluble, limiting the TcO_4^- concentration in pore fluids to very low concentrations. To calculate the concentration of TcO_4^- in the pore fluid, the concentration of HS^- is needed. Angus and Glasser (1985) report aqueous sulfide concentration for slag cement ore fluids of up to 1100 mg/L for a mixture containing 97.5% slag. For a mixture containing 50% slag (similar to the saltstone mix) 12 mg/L sulfide was reported (Angus and Glasser 1985). This value was used in conjunction with the pore fluid to calculate concentrations of technetium. Additionally, a technetium concentration was calculated by assuming that technetium and sulfide occurred in solution in stoichiometric proportions (i.e., 2:7). The second concentration of technetium is higher, and the total sulfide concentration is much lower. The resulting concentrations of sulfide and technetium are presented in Table D.3-3.

Using the higher TcO_4^- concentration from Table D.3-3, K_d values for technetium can be calculated. The total loading of ^{99}Tc in saltstone is 25,000 pCi/g. From the hydration calculations the volume of pore fluid per gram of saltstone is 0.306 mL (57.8 mL/188.7 g). A total of 14 pCi (46,000 pCi/L × 0.000306 L) of technetium occurs in the 0.306 mL of pore fluid. The remaining 24,986 pCi occurs in the 0.614 g of the solid matrix, with a concentration of 40,700 pCi/g. Although the technetium concentration is limited by the solubility of $Tc_2S_{7,s}$ the solid and aqueous concentration can be used to estimate a K_d of 880 mL/g [(40,700 pCi/g)/(46.3 pCi/mL)] for ^{99}Tc in saltstone.

Technetium concentrations are insensitive to the variations in the total salt concentration or to the selection of solid cement phases used in the equilibrium calculations. The sensitivity of technetium concentration to pH and sulfide concentration can be evaluated by examining the stoichiometry of the dissolution reaction

$$Tc_2S_{7,s} + 8H_2O = 2TcO_4^- + 7HS^- + 9H^+ \quad (3)$$

$$\log [TcO_4^-] = 0.5 \log Q - 3.5 \log [HS^-] + 4.5 \text{ pH} \quad (4)$$

where log Q is a conditional equilibrium quotient (constant at constant ionic strength) and brackets denote molal concentration. Examination of the coefficients in equation (4) indicates that the concentration of TcO_4^- decreases by a factor of 3,200 for each 10 fold increase in HS^- concentration. An increase of pH by 1 unit results in an increase in TcO_4^- concentration by a factor of 32,000.

For the case in which technetium and sulfur are related by stoichiometry, log $[TcO_4^-]$ is directly proportional to pH. Because the aqueous concentration of TcO_4^- is proportional to pH, the value of K_d for ^{99}Tc in saltstone calculated above will also be dependent on pH. The dependency is calculated using this proportional relationship and the K_d of 880 in mL/g and is given by:

$$\log Kd = 16.94 - \text{pH} \quad (5)$$

Hence, the K_d of 880 mL/g is conservative because the pore fluid pH will decrease over time as NaOH is leached from the saltstone. In response to decreasing pH the K_d will become larger.

The results of these calculations for technetium indicate that the concentration of technetium in the pore fluid, and hence the release, is very sensitive to the presence of aqueous sulfide. Because no direct measurements of sulfide are available for saltstone pore fluids, these calculations are subject to a great amount of uncertainty. In addition, the thermodynamic solubility data for $Tc_2S_{7,s}$ are highly uncertain. If credit is to be taken for formation of technetium sulfide, measurements should be made of sulfur speciation in saltstone pore fluids; if possible, the solubility of $Tc_2S_{7,s}$ should be measured in strongly alkaline solutions. However, the tentative results presented here indicate that even in the more conservative case, greater than 99.9% of the technetium in the saltstone waste form is initially present in the solid matrix.

D.4 FLUID COMPOSITIONS IN SEDIMENTS OUTSIDE THE VAULT

The behavior of the saltstone fluid composition outside the vault was evaluated using the MINTEQ geochemical code. Pore fluid compositions were reacted with the unsaturated sediments surrounding the saltstone vaults. This model considers only equilibrium geochemical reactions, not transport and flow of the saltstone fluids.

D.4.1 Modeling Steps

Geochemical modeling was carried out by simulating the reactions between the pore fluid calculated above and the unsaturated sediments surrounding the saltstone vaults. All modeling was done at a temperature of 25°C; pertinent details of the modeling conditions follow.

1) Solution is reacted with CO_2 gas at atmospheric pressure ($10^{-3.5}$ atm.). This is the only gas likely to be present in this environment, because of the reducing environment created in sediments by organic activity.

2) React solution with a sediment representative of that found in the Savannah River Z-Area. Individual sediment components used were quartz, kaolinite, gibbsite, and an iron oxide phase.

3) Fine-tune results by eliminating saturated phases which are geologically unreasonable. This last step should not bias the results if a competent geologist or mineralogist evaluates the phases with respect to the probability of formation at surface conditions.

Results from the final solutions using the steps outlined above are shown below..

D.4.2 Interactions with the Sediment

The composition of the pore fluid in equilibrium with the grout phases, as described in Sect. D.3, was reacted with mineral phases in the unsaturated zone. Reaction of the evolved pore solution (Table D.3-3) with CO_2 in the unsaturated zone reduces the pH from 13.78 to 7.32.

The pore fluid changed very little after reacting with the soil minerals. A small amount of diaspore was precipitated, reducing the aluminum concentration in the interstitial fluid. Presence of an iron oxide or iron hydroxide phase has very little effect on the precipitated phases or intensive parameters (i.e., pH, Eh). Further, the specific composition of the iron phase did not substantially change the composition of the reacted solution or the composition or quantity of the precipitated minerals. A small amount of the iron phase dissolved, adding iron to the reacted solution. This is present almost totally as ferric iron. The amount of dissolved iron varies according to what iron phase is chosen.

The composition of the pore solution after reacting with unsaturated zone minerals and CO_2 is presented in Table D.4-1, along with the amount of the precipitated phase. Speciation of the pore solution is presented in Table D.4-2.

In summary, reaction with iron minerals increased the concentration of iron in solution from nearly zero to 3 ppb. The concentration of the three primary pollutants, ^{99}Tc, tritium, and nitrate do not substantially change in the interstitial fluid during communication with the unsaturated zone minerals. The precipitation of diaspore ($AlO^{\bullet}OH$), would attenuate tritium to a small degree, but the amount is insignificant. The concentration of all three pollutants will decrease in the interstitial fluid due to the dilution by naturally occurring water present in the vadose zone.

Table D.4-1. Composition of interstitual fluid after reaction with unsaturated zone minerals, and type and amount of precipitated solids

Species	mg/L	HS^- (mg/L)	^{99}Tc (pCi/L)
Na^+	139,000		
CO_3^{2-}	12,800		
SO_4^{2-}	15,000		
NO_2^-	36,800		
NO_3^-	159,000		
OH^-	32,900		
Ca^{2+}	1		
$SiO_{2,aq}$	1		
Al^{3+}	4.4 × 10 E-04		
K^+	9,800		
NH^{4+}	400		
pH	7.32		
Total N as NO_3^-	209,000		
Density	1.26		
High sulfide		10	2.4×10^{-8}
Stoichiometric		0.003	46,300

Precipitate	Concentration (mg/L)
Diaspore	25

Table D.4-2. Percentage distribution of components in reacted interstitial fluid

Component	Percentage	Species	Component	Percentage	Species
Na	89.5	Na^+	S	100	S^{0}
	7.8	$NaNO_3$			
	2.6	$NaSO_4^-$	Al	100	$Al(OH)_4^-$
K	98.1	K^+	NO_3	83.4	NO_3^-
	1.9	KSO_4^-		16.6	$NaNO_{3,aq}$
H_4SiO_4	98.3	H_4SiO_4	CO_3	60.3	$NaHCO_{3,aq}$
	1.7	$H_3SiO_4^-$		37.9	HCO_3^-
SO_4^{2-}	32.4	SO_4^{2-}	Ca	97	$CaCO_{3,aq}$
	65.5	$NaSO_4^-$		1.6	$CaSO_{4,aq}$
	1.9	KSO_4^-			
NH_4	97.1	NH_4^+	Fe^{+3}	1.4	$FeOH_4^+$
	2.7	$NH_4SO_4^-$		33.1	$FeOH_2^{+2}$
				65.5	$FeOH_3^{+}$
NO_2	100	NO_2^-	Fe^{+2}	97.5	Fe^{+2}
				2.4	$FeSO_{4,aq}$

APPENDIX D REFERENCES

Angus, M. J., and F. P. Glasser. 1985. The chemical environment in cement matrices. *Mat. Res. Soc. Symp. Proc.*, 50:547-556.

CRC Press, Inc. 1987. *CRC Handbook of Chemistry and Physics.* 68th Edition, R. C. Weast, M. J. Astle, W. H. Beyer, Eds. CRC Press, Inc., Boca Raton, Florida.

Crisentia, L., and R. J. Serne. 1990. Thermodynamic modeling of cement/groundwater interaction as a tool for long term performance assessment. *Mat. Res. Soc. Symp. Proc.* 176:81-89.

Heckrotte, R. W. 1988. Project-1780-Savannah River Plant-200-S-area Defense Waste Processing Facility - sludge plant request to Modify the DWPF Saltstone Industrial Solid Waste Permit. memo PP-001183 (January).

Helgeson, H. C. 1969. Thermodynamics of hydrothermal systems at elevated temperatures and pressures. *Am. J. Sci.*, 267:729-804.

Malek, R. I. A., P. H. Liscastro, and C. A. Langton. 1985. *Saltstone Starting Materials Characterization.* E. I. du Pont de Nemours & Co., Inc.

Malek, R. I. A, P. H. Liscastro, and D. M. Roy. 1987. *Saltstone Pore Solution Analyses.* Materials Research Laboratory, The Pennsylvania State University, University Park, Penn.

Murphy, W. M., and R. W. Smith. 1989. Irreversible dissolution of solids solutions: a kinetic and stoichiometric model. *Radiochim. Acta,* 44/45:395-401.

Neville, A. M. 1981. *Properties of Concrete.* 3rd Edition, John Wiley & Sons, New York, NY.

Smith, R. M., and A. E. Martell. 1976. *Critical Stability Constants Volume 4: Inorganic Complexes.* Plenum Press, New York, NY.

Smith, R. W., and J. C. Walton. 1992. The effects of calcite solid solution formation on the transient release of radionuclides from concrete barriers. *Mat. Res. Soc. Symp. Proc.* 212:547-556.